

## Copyright Undertaking

This thesis is protected by copyright, with all rights reserved.

**By reading and using the thesis, the reader understands and agrees to the following terms:**

1. The reader will abide by the rules and legal ordinances governing copyright regarding the use of the thesis.
2. The reader will use the thesis for the purpose of research or private study only and not for distribution or further reproduction or any other purpose.
3. The reader agrees to indemnify and hold the University harmless from and against any loss, damage, cost, liability or expenses arising from copyright infringement or unauthorized usage.

### IMPORTANT

If you have reasons to believe that any materials in this thesis are deemed not suitable to be distributed in this form, or a copyright owner having difficulty with the material being included in our database, please contact [lbsys@polyu.edu.hk](mailto:lbsys@polyu.edu.hk) providing details. The Library will look into your claim and consider taking remedial action upon receipt of the written requests.

# A STUDY OF NANOCHITOSANS AND THEIR APPLICATIONS

LIU LIWEI

Ph.D

The Hong Kong Polytechnic University

2011

# A STUDY OF NANOCHITOSANS AND THEIR APPLICATIONS

By LIU Liwei

(A thesis submitted in partial fulfillment of the requirements for  
the degree of Doctor of Philosophy)

December 2010

---

## **CERTIFICATE OF ORIGINALITY**

I hereby declare that this thesis is my own work and that, to the best of my knowledge and belief, it reproduces no material previously published or written, nor material that has been accepted for the award of any other degree or diploma, except where due acknowledgement has been made in the text.

\_\_\_\_\_ (Signed)

LIU Liwei (Name of student)

---

## ABSTRACT

This project provided a simple and fast method for the preparation of nanochitosan emulsions and studied the applications of nanochitosan emulsions. First, a novel ultrasound method was developed for the preparation of nanochitosan without any chemicals except water. The nanochitosan was characterized using laser scanning, FT-IR,  $^1\text{H}$  NMR, X-ray, SEM, TEM, and AFM.

The prepared nanochitosan emulsion was then used for dye sorption studies and dyeability enhancement of nylon. The capacities of the nanochitosan as an adsorbent for 5 anionic dyes including Acid Orange 7, Acid Red 1, Acid Red 18, Direct Red 84, and Direct Red 80, were studied. The sorption behaviors of microchitosan were also studied for comparison. It was found that the nanochitosan had higher sorption capacities than those of the microchitosan, especially for the dyes with large molecular sizes. The sorption mechanism, sorption kinetics and equilibrium isotherm were also investigated.

The nanochitosan was also applied to nylon fabrics and the corresponding dyeing properties were studied. The nanochitosan-treated and control nylon were dyed with 8 anionic dyes. The results showed that the dyeing depths of the chitosan-treated fabrics were higher and the fastness was not affected.

---

## **ACKNOWLEDGEMENTS**

I would like to express my deep and sincere gratitude to my supervisor, Dr. Szeto Yau-shan, associate professor at the Institute of Textiles and Clothing of the Hong Kong Polytechnic University. His constant guidance, invaluable advice, and sustained encouragement and understanding helped me a lot during the study. He taught me to think and to work like a scientist. His precise academic discipline and study attitude will affect my whole life.

Here I would also like to express my sincere thanks to Dr Chan Wing Lai, assistant professor at the Department of Applied Biology and Chemical Technology. He was not my official co-supervisor, but he provided me with great help during my study and research. Without his support, I could never finish much of the work in the study.

I also thank those who helped me during the study and research, the colleagues, the laboratory technicians at the Institute of Textiles and Clothing, Department of Applied Biology and Chemical Technology, Department of Applied Physics, and Material Research Center. During all the three-year study, there were so many people who offered me a lot of help and I would like to show my deep appreciation here to every one of them.

I am forever indebted to my loving father and mother. They sacrificed a lot for my study. Without all the love, encouragement and understanding of them, I will never have the chance to finish my study here.

Also, the financial support of the Hong Kong Polytechnic University is gratefully acknowledged.

## Table of Contents

<b>Chapter 1 Introduction.....</b>	<b>1</b>
1.1 Introduction of chitosan .....	1
1.2 Physical and chemical characters of chitosan .....	3
1.3 Applications of chitosan .....	5
1.3.1 Applications of chitosan in water treatments.....	5
1.3.2 Applications of chitosan in textile finishing.....	6
1.4 Scope of research .....	7
1.4.1 Preparation and characterization of nanochitosan .....	7
1.4.2 Applications of nanochitosan emulsion on dye sorption .....	8
1.4.3 Dyeability enhancement of nylon using nanochitosan emulsion.....	8
1.5 Project significance and value .....	9
<b>Chapter 2 Literature Review .....</b>	<b>11</b>
2.1 Introduction of chitosan .....	11
2.1.1 Solubility of chitosan .....	12
2.1.2 Degree of deacetylation .....	13
2.1.3 Molecular weight of chitosan and distribution of acetyl groups.....	17
2.2 Preparation of chitosan-based nanoparticles.....	18
2.2.1 Methods for the preparation of chitosan nanoparticles.....	18
2.2.2 Core-shell nanoparticles based on chitosan .....	20
2.3 Ultrasonic method for the preparation of nanomaterials .....	23
2.3.1 Sonochemical synthesis .....	23

2.3.1.1	Nanostructured metals prepared by sonochemical synthesis.....	24
2.3.1.2	Nanostructured metal oxides prepared by sonochemical synthesis.....	26
2.3.1.3	Nanostructured carbons prepared by sonochemical synthesis.....	27
2.3.1.4	Protein and polymer nano- and microstructures prepared by sonochemical synthesis.....	28
2.3.2	Ultrasonic spray pyrolysis (USP).....	29
2.3.2.1	Metal salt-based nanocomposites prepared by USP .....	30
2.3.2.2	Polymer-based nanocomposites prepared by USP.....	31
2.3.3	Ultrasonic method for the preparation of nanochitosans .....	32
2.4	Applications of chitosan on dye sorption.....	33
2.4.1	Dye wastewaters .....	33
2.4.2	Overview of various adsorbents.....	36
2.4.2.1	Activated carbon and other low cost alternatives in dyes sorption.....	36
2.4.2.2	Chitosan in dyes sorption.....	37
2.4.3	Sorption mechanisms of dyes onto chitosan.....	38
2.4.3.1	Electrostatic interactions.....	41
2.4.3.2	Physical surface adsorption.....	42
2.4.3.3	Aggregation.....	42
2.4.3.4	Hydrogen bonding .....	43
2.4.3.5	Hydrophilic and hydrophobic interactions.....	43
2.4.4	Parameters affecting sorption.....	44
2.4.4.1	Particle sizes.....	44



2.4.4.2	Initial dye concentrations .....	44
2.4.4.3	pH values .....	45
2.4.4.4	Temperature .....	45
2.4.4.5	Molecular mechanisms .....	46
2.4.5	Equilibrium isotherm models.....	46
2.4.6	Kinetic models .....	48
2.5	Applications of chitosan on dyeing.....	49
2.5.1	Applications of chitosan on cotton dyeing.....	51
2.5.2	Applications of chitosan on wool dyeing.....	52
2.5.3	Applications of chitosan on silk dyeing.....	53
2.5.4	Applications of chitosan on nylon dyeing .....	54
2.5.4.1	Interactions between acid dyes and nylon .....	55
2.5.4.1.1	Electrostatic forces between nylon and acid dyes.....	55
2.5.4.1.2	Hydrophobic interaction .....	56
2.5.4.2	Applications of chitosan on nylon for dyeing enhancement.....	57
<b>Chapter 3 Preparation and Characterization of Nanochitosan Emulsions.....</b>		<b>58</b>
3.1	Research background .....	58
3.2	Materials .....	59
3.3	Preparation of nanochitosan emulsions .....	59
3.3.1	Using factorial design to study experiment conditions for nanochitosan .....	60
3.3.2	Uniformity optimization with central composite design .....	66
3.4	Characterization of nanochitosan emulsions .....	73

3.4.1	The pH value, zeta potential of nanochitosan emulsions.....	74
3.4.2	Particle size and molecular weight ( $m_v$ ) of chitosan nanoparticles .....	74
3.4.3	Degree of deacetylation (DD) measurement.....	75
3.4.3.1	FT-IR method for DD measurement.....	75
3.4.3.2	$^1\text{H}$ NMR method for DD measurement .....	76
3.4.3.3	Elemental analysis for DD measurement.....	78
3.4.4	Powder x-ray diffraction (XRD) .....	79
3.4.5	Morphological characterization .....	79
3.5	Results and discussion .....	80
3.5.1	Nanochitosan emulsions images and stability .....	80
3.5.2	The pH value and zeta potential of nanochitosan emulsions.....	82
3.5.3	Particle size and molecular weight of nanochitosan .....	84
3.5.4	DD of the nanochitosan .....	85
3.5.5	Crystallinity of the nanochitosan .....	85
3.5.6	Morphological characterization .....	87
3.5.6.1	SEM images.....	87
3.5.6.2	TEM images.....	89
3.5.6.3	AFM images.....	89
3.6	Conclusions.....	91
<b>Chapter 4</b>	<b>Applications of Nanochitosan Emulsion on Dye Sorption .....</b>	<b>92</b>
4.1	Research background.....	92
4.2	Materials .....	95

---

4.3 Experimental .....	95
4.3.1 Preparation of nanochitosan emulsion (CsNano) .....	95
4.3.2 Preparation of 180 $\mu\text{m}$ chitosan (CsMicro) .....	97
4.3.3 Sorption kinetics experiments .....	97
4.3.4 Sorption equilibrium experiments .....	97
4.3.5 Desorption experiments .....	98
4.4 Characterization .....	98
4.4.1 Particle size of chitosan nanoparticles .....	98
4.4.2 Morphology of chitosan nanoparticles .....	99
4.4.3 Concentration of dye solutions .....	99
4.4.4 Hydrophobic/hydrophilic ratio of dyes .....	99
4.4.5 Sorption ability .....	100
4.4.6 Desorption efficiency .....	100
4.5 Results and discussion .....	101
4.5.1 Particle size of chitosan nanoparticles .....	101
4.5.2 Morphology of chitosan nanoparticles .....	101
4.5.3 Sorption kinetic results .....	102
4.5.4 Sorption kinetics study .....	110
4.5.4.1 The pseudo-first-order kinetic model .....	110
4.5.4.2 The pseudo-second-order kinetic model .....	112
4.5.5 Sorption isotherms results .....	118
4.5.6 Equilibrium isotherms .....	121

4.5.6.1	Langmuir equilibrium isotherms.....	121
4.5.6.2	Freundlich equilibrium isotherms .....	125
4.5.7	Sorption mechanisms .....	128
4.5.8	Effect factors in sorption.....	130
4.5.8.1	Effect of sorbent particle size.....	130
4.5.8.2	Effect of sorbates molecules .....	131
4.5.8.2.1	Dimensions of dye molecules .....	131
4.5.8.2.2	Hydrophobic/hydrophilic ratio of dyes.....	131
4.5.8.3	Effect of temperature .....	133
4.5.9	Thermodynamic parameters.....	136
4.5.10	Desorption and regeneration studies.....	138
4.6	Conclusions.....	139
<b>Chapter 5</b>	<b>Application of Nanochitosan Emulsion on Dyeing .....</b>	<b>141</b>
5.1	Research background .....	141
5.2	Materials and instruments .....	143
5.2.1	Fabric .....	143
5.2.2	Dyestuffs .....	143
5.2.3	Chemicals.....	143
5.3	Experimental and characterization.....	144
5.3.1	Washing of the nylon fabric .....	144
5.3.2	Preparation and characterization of chitosan-treated nylon fabric samples	144
5.3.2.1	Preparation of nanochitosan emulsion .....	144

---

5.3.2.2	Pad-dry-cure of chitosan on fabric samples .....	144
5.3.2.3	FT-IR spectroscopy .....	145
5.3.2.4	Scanning electron microscopy (SEM) .....	145
5.3.2.5	Measurement of the coefficient of friction .....	145
5.3.2.6	Amine group analysis of nylon fabric.....	146
5.3.3	Dyeing of fabric .....	146
5.3.3.1	Recipe of dyeing .....	146
5.3.3.2	Dyeing profile .....	147
5.3.4	Study of the dyeing exhaustion rate.....	148
5.3.4.1	Concentration measurement and calibration.....	148
5.3.4.2	Evaluation of exhaustion.....	149
5.3.5	Evaluation of un-dyed fabrics .....	150
5.3.5.1	CIE Whiteness Index .....	150
5.3.5.2	Yellowness Index (ASTM E 313).....	151
5.3.6	Evaluation of dyed fabrics .....	151
5.3.6.1	Visual assessment under daylight D <sub>65</sub> .....	151
5.3.6.2	CIE L*a*b* .....	152
5.3.6.3	K/S values of the dyed fabrics .....	153
5.3.6.4	Colorfastness test .....	153
5.3.6.4.1	Colorfastness to water (ISO 105-E01:1996).....	153
5.3.6.4.2	Colorfastness to washing (ISO 105-C01:1989) .....	153
5.4	Results and discussion .....	154

5.4.1	FT-IR spectroscopy .....	154
5.4.2	Melting point.....	156
5.4.3	Scanning electron microscopy (SEM) .....	156
5.4.4	Coefficient of friction.....	158
5.4.5	Determination of amine end group in nylon fabric.....	159
5.4.6	Determination of number of amino dyesites in chitosan-treated fabric.....	160
5.4.7	Estimation of depths of dyeing .....	161
5.4.7.1	Mono-sulphonated dyes: Acid Orange 7.....	163
5.4.7.2	Di-sulphonated dye: Acid Red 1 .....	163
5.4.7.3	Tri-sulphonated dye: Acid Red 18 .....	163
5.4.7.4	Tetra-sulphonated dye and other multi-sulphonated dyes .....	164
5.4.8	Exhaustion of dyeing .....	164
5.4.9	Comparisons between dyes exhaustion of chitosan-treated and control fabrics.....	177
5.4.9.1	Final exhaustion .....	177
5.4.9.2	Time to achieve equilibrium exhaustion .....	177
5.4.9.3	Time of half dyeing ( $T_{1/2}$ ) .....	178
5.4.10	Evaluation of un-dyed fabrics .....	180
5.4.11	Visual assessment under $D_{65}$ of dyed fabrics.....	181
5.4.12	CIE $L^*a^*b^*$ of dyed fabrics .....	190
5.4.12.1	Acid Orange 7 .....	190
5.4.12.2	Acid Red 1 .....	192

5.4.12.3 Acid Red 18 .....	193
5.4.12.4 Sirius Brown 3RL .....	195
5.4.12.5 Sirius Red F3B .....	196
5.4.12.6 Telon Red M-BL .....	197
5.4.12.7 Telon Yellow M-4GL .....	199
5.4.12.8 Telon Blue M-RLW .....	200
5.4.13 K/S measurement of dyed fabrics .....	201
5.4.14 Colorfastness .....	206
5.4.14.1 Colorfastness to water (ISO E05-C01:1996) .....	206
5.4.14.2 Colorfastness to washing (ISO 105-C01:1989) .....	209
5.5 Conclusions .....	212
<b>Chapter 6 Conclusions and Suggestions for Future Research .....</b>	<b>214</b>
6.1 Preparation and characterization of nanochitosan emulsions .....	215
6.1.1 Conclusions .....	215
6.1.2 Future research .....	215
6.2 Application of nanochitosan emulsion on dye sorption .....	216
6.2.1 Conclusions .....	216
6.2.2 Future research .....	217
6.3 Application of nanochitosan emulsion on dyeing .....	217
6.3.1 Conclusions .....	217
6.3.2 Future research .....	218
<b>References .....</b>	<b>219</b>

**List of Figures**

<b>Figure 1.1</b> Chemical structures of chitin and chitosan .....	1
<b>Figure 1.2</b> Advantages and applications of chitosan .....	2
<b>Figure 1.3</b> Workflow of chitosan production.....	3
<b>Figure 1.4</b> Reactive groups of chitosan .....	4
<b>Figure 2.1</b> Structures of cellulose, chitin and chitosan.....	11
<b>Figure 2.2</b> $^1\text{H}$ NMR spectrum of chitosan at 70°C .....	14
<b>Figure 2.3</b> IR spectrum of chitosan and representation of different baselines .....	15
<b>Figure 2.4</b> Preparation of chitosan nanoparticles with TPP .....	19
<b>Figure 2.5</b> Zones of the nanoparticles (left) and their TEM micrograph (right) .....	19
<b>Figure 2.6</b> Flow chart for the preparation of cross-linked chitosan nanoparticles .....	20
<b>Figure 2.7</b> SEM micrographs of (a) chitosan particles (10,000 $\times$ ) and (b)-(d) AP loaded chitosan particles with different chitosan to AP weight ratios: (b) 1:1.00 (1000 $\times$ ), (c) 1:1.00 (10,000 $\times$ ) and (d) 1:1.50 (10,000 $\times$ ) .....	22
<b>Figure 2.8</b> Reaction in the sonolysis of water .....	24
<b>Figure 2.9</b> Sonochemically prepared gold nanobelts .....	25
<b>Figure 2.10</b> Tilt-view SEM images of vertically aligned ZnO rods produced using sonochemical-induced anisotropic growth of ZnO along the (0001) .....	26
<b>Figure 2.11</b> a) Schematic of the intercalation/exfoliation process. TEM images of b) a thin plate of graphitic sheets in the process of scrolling, c) an isolated carbon nanoscroll with open ends, and d) a mass of scrolled material, representative of the bulk of the sample.....	28
<b>Figure 2.12</b> Mechanism of anionic dye adsorption by chitosan in acidic condition .....	41



<b>Figure 2.13</b> Main interactions between dyes and chitosan in an alkaline solution.....	43
<b>Figure 2.14</b> The grafting mechanism between degummed silk and chitosan using succinic anhydride as a bridge .....	53
<b>Figure 2.15</b> Electrostatic forces between nylon and an acid dye.....	55
<b>Figure 3.1</b> Main effects plot for size .....	63
<b>Figure 3.2</b> Interaction plot for size .....	63
<b>Figure 3.3a</b> Surface plot of size versus concentration, time.....	64
<b>Figure 3.3b</b> Surface plot of size versus concentration, time .....	64
<b>Figure 3.4a</b> Contour plot of size versus concentration, time.....	65
<b>Figure 3.4b</b> Contour plot of size versus concentration, time.....	65
<b>Figure 3.5a</b> Surface plot of uniformity versus concentration, time.....	68
<b>Figure 3.5b</b> Surface plot of uniformity versus concentration, time.....	68
<b>Figure 3.5c</b> Surface plot of uniformity versus concentration, time .....	69
<b>Figure 3.6a</b> Contour plot of uniformity versus concentration, time .....	69
<b>Figure 3.6b</b> Contour plot of uniformity versus concentration, time.....	70
<b>Figure 3.6c</b> Contour plot of uniformity versus concentration, time .....	70
<b>Figure 3.7a</b> Surface plot of uniformity versus power, concentration .....	71
<b>Figure 3.7b</b> Surface plot of uniformity versus power, concentration. ....	71
<b>Figure 3.7c</b> Surface plot of uniformity versus power, concentration. ....	72
<b>Figure 3.8a</b> Contour plot of uniformity versus power, concentration .....	72
<b>Figure 3.8b</b> Contour plot of uniformity versus power, concentration .....	73
<b>Figure 3.8c</b> Contour plot of uniformity versus power, concentration.. ....	73

<b>Figure 3.9</b> FTIR spectrum of chitosan showing the baselines for calculating the amide-I band	
absorbance and hydroxyl band absorbance .....	76
<b>Figure 3.10</b> Reaction scheme .....	77
<b>Figure 3.11</b> Three kinds of units in the $^1\text{H}$ NMR sample solution. ....	78
<b>Figure 3.12</b> $^1\text{H}$ -NMR spectrum of chitosan with signal assignments.....	78
<b>Figure 3.13</b> Newly prepared chitosan emulsions with different ultrasonic duration.....	80
<b>Figure 3.14</b> Chitosan emulsions with different ultrasonic duration after 10 days of preparation.....	80
<b>Figure 3.15</b> Particle size of nanochitosan with different ultrasonic duration in 30 days.....	81
<b>Figure 3.16</b> A laser through samples CS0 and CS180.....	81
<b>Figure 3.17</b> Chitosan film.....	82
<b>Figure 3.18</b> Effect of pH on zeta potential of nanochitosan emulsion (CS30).....	82
<b>Figure 3.19</b> The relationships among pH, zeta potential and ultrasonic duration.. ....	83
<b>Figure 3.20</b> Relationships among particle size, $M_v$ and ultrasonic duration.....	84
<b>Figure 3.21</b> XRD patterns of the chitosan nanoparticles with different ultrasonic duration. ....	86
<b>Figure 3.22</b> The relationship between the crystallinity and ultrasonic duration.....	86
<b>Figure 3.23</b> SEM image of the nanochitosan using vacuum-dry (CS60).....	87
<b>Figure 3.24</b> SEM image of the freeze-dried nanochitosan .....	88
<b>Figure 3.25</b> SEM image of the nanochitosan using freeze-dry process (CS60).....	88
<b>Figure 3.26</b> TEM images of the nanochitosan (CS60) .....	89
<b>Figure 3.27</b> AFM images of nanochitosan (CS60).....	90
<b>Figure 3.28</b> Particle sizes of the nanochitosan .....	90
<b>Figure 3.29</b> AFM images of a nanochitosan film(CS60) .....	90

<b>Figure 4.1</b> Relationship between particle size and ultrasonic duration .....	101
<b>Figure 4.2</b> SEM images of the nanochitosan particles with ultrasonic duration of 60 minutes .....	102
<b>Figure 4.3</b> Plots of sorption ability of nanochitosan and microchitosan for Acid Orang 7 at different temperatures .....	104
<b>Figure 4.4</b> Plots of sorption ability of nanochitosan and microchitosan for Acid Red 1 at different temperatures .....	106
<b>Figure 4.5</b> Plots of sorption ability of nanochitosan and microchitosan for Acid Red 18 at different temperatures .....	107
<b>Figure 4.6</b> Plots of sorption ability of nanochitosan and microchitosan for Direct Red 84 at different temperatures .....	108
<b>Figure 4.7</b> Plots of sorption ability of nanochitosan and microchitosan for Direct red 80 at different temperatures .....	109
<b>Figure 4.8</b> Pseudo-first-order kinetics for the sorption of Acid Orange 7 at 30°C .....	113
<b>Figure 4.9</b> Pseudo-second-order kinetics for the sorption of Acid Orange 7 at 30°C .....	114
<b>Figure 4.10</b> Pseudo-second-order model for sorption kinetics of Acid Orange 7 onto nanochitosan and microchitosan at different temperatures .....	116
<b>Figure 4.11</b> Pseudo-second-order model for sorption kinetics of Acid Red 1 onto nanochitosan and microchitosan at different temperatures .....	116
<b>Figure 4.12</b> Pseudo-second-order model for sorption kinetics of Acid Red 18 onto nanochitosan and microchitosan at different temperatures .....	117
<b>Figure 4.13</b> Pseudo-second-order model for sorption kinetics of Direct Red 84 onto nanochitosan and microchitosan at different temperatures .....	117

<b>Figure 4.14</b> Pseudo-second-order model for sorption kinetics of Direct Red 80 onto nanochitosan and microchitosan at different temperatures .....	118
<b>Figure 4.15</b> Sorption capacities of nanochitosan and microchitosan for Acid Orange 7 at different temperatures, pH=5.5 .....	119
<b>Figure 4.16</b> Sorption capacities of nanochitosan and microchitosan for Acid Red 1 at different temperature, pH=5.5 .....	119
<b>Figure 4.17</b> Sorption capacities of nanochitosan and microchitosan for Acid Red 18 at different temperatures, pH=5.5 .....	120
<b>Figure 4.18</b> Sorption capacities of nanochitosan and microchitosan for Direct Red 84 at different temperatures, pH=5.5 .....	120
<b>Figure 4.19</b> Sorption capacities of nanochitosan and microchitosan for Direct Red 80 at different temperatures, pH=5.5 .....	121
<b>Figure 4.20</b> Langmuir isotherm linear plots (a: Direct Red 80 onto nanochitosan at 30°C b: Direct Red 80 onto microchitosan at 30°C) .....	122
<b>Figure 4.21</b> Langmuir isotherm model for Direct Red 80 onto nanochitosan and microchitosan at 30°C .....	123
<b>Figure 4.22</b> Freundlich isotherm model for: Direct Red 80 onto nanochitosan and microchitosan at 30°C .....	126
<b>Figure 4.23</b> Freundlich isotherm data for: Acid Red 1 onto nanochitosan and microchitosan at 30°C .....	127
<b>Figure 4.24</b> Dye-chitosan interactions (a) ionic attraction between anionic sulphonate group(s) of dissolved dye molecules and the cationic amino groupsof protonated chitosan, (b)	

dipole-dipole hydrogen bonding interactions between chitosan hydroxyl groups and electronegative residues in the dye molecule; (c) Yoshida H-bonding between chitosan hydroxyl groups and aromatic residues in dye .....	128
<b>Figure 4.25</b> The dimensions of Acid Orange 7, Acid Red 1, Acid Red 18, Direct Red 84, Direct Red 80 .....	132
<b>Figure 4.26</b> Sorption capacities of nanochitosan for Acid Orange 7 (AO 7), Acid Red 1 (AR 1), Acid Red 18 (AR 18), Direct Red 84 (DR 84) and Direct Red 80 (DR 80) at 30°C, pH=5.5 .....	133
<b>Figure 5.1</b> Measuring frictional properties and geometrical surface roughness.....	145
<b>Figure 5.2</b> Dyeing profile for nylon dyeing .....	148
<b>Figure 5.3</b> Extraction of dye liquor from dye bath.....	150
<b>Figure 5.4</b> Viewing geometry in color visual assessment.....	152
<b>Figure 5.5</b> The IR spectrum of nylon fabric .....	155
<b>Figure 5.6</b> The IR spectrum of nanochitosan-emulsion-treated nylon fabric.....	155
<b>Figure 5.7</b> Surface of control and chitosan-treated nylon fabrics.....	157
<b>Figure 5.8</b> Repeat unit of 95% DD chitosan polymer chain.....	160
<b>Figure 5.9</b> Exhaustion curves of Acid Orange 7 at different depths: a (1.05% depth), b (2.10% depth), and c (4.20% depth) .....	165
<b>Figure 5.10</b> Exhaustion curves of Acid Red 1 at different depths: a (1.02% depth), b (2.04% depth), and c (4.08% depth) .....	166
<b>Figure 5.11</b> Exhaustion curves of Acid Red 18 at different depths: a (0.60% depth), b (1.21% depth), and c (2.42% depth) .....	167

<b>Figure 5.12</b> Exhaustion curves of Sirius Brown 3RL at different depths: a (2.27% depth), b (4.55% depth), and c (9.10% depth).....	168
<b>Figure 5.13</b> Exhaustion curves of Sirius Red F3B at different depths: a (1.37% depth), b (2.75% depth), and c (5.50% depth) .....	169
<b>Figure 5.14</b> Exhaustion curves of Telon Red M-BL at different depths: a (2% depth), b (4% depth), and c (8% depth) .....	170
<b>Figure 5.15</b> Exhaustion curves of Telon Yellow M-4GL at different depths: a (2% depth), b (4% depth), and c (8% depth) .....	171
<b>Figure 5.16</b> Exhaustion curves of Telon Blue M-RLW at different depths: a (2% depth), b (4% depth), and c (8% depth) .....	172
<b>Figure 5.17</b> Fabric samples dyed by Acid Orange 7 .....	182
<b>Figure 5.18</b> Fabric samples dyed by Acid Red 1 .....	183
<b>Figure 5.19</b> Fabric samples dyed by Acid Red 18.....	184
<b>Figure 5.20</b> Fabric samples dyed by Sirius Brown 3RL .....	185
<b>Figure 5.21</b> Fabric samples dyed by Sirius Red F3B .....	186
<b>Figure 5.22</b> Fabric samples dyed by Telon Red M-BL .....	187
<b>Figure 5.23</b> Fabric samples dyed by Telon Yellow M-4GL .....	188
<b>Figure 5.24</b> Fabric samples dyed by Telon Blue M-RLW .....	189
<b>Figure 5.25</b> K/S curves of fabrics dyed by Acid Orange 7.....	202
<b>Figure 5.26</b> K/S curves of fabrics dyed by Acid Red 1 .....	202
<b>Figure 5.27</b> K/S curves of fabrics dyed by Acid Red 18 .....	203
<b>Figure 5.28</b> K/S curves of fabrics dyed by Sirius Brown 3RL.....	203

<b>Figure 5.29</b> K/S curves of fabrics dyed by Sirius Red F3B .....	204
<b>Figure 5.30</b> K/S curves of fabrics dyed by Telon Red M-BL.....	204
<b>Figure 5.31</b> K/S curves of fabrics dyed by Telon Yellow M-4GL.....	205
<b>Figure 5.32</b> K/S curves of fabrics dyed by Telon Blue M-RLW .....	205

**List of Tables**

<b>Table 2.1</b>	Characteristics of methods to analyze infrared spectra of chitin or chitosan.....	16
<b>Table 2.2</b>	Mark–Houwink constants for chitosan in various solvents .....	17
<b>Table 2.3</b>	The preparation of protein and polymer nano and micromaterials by ultrasound .....	29
<b>Table 2.4</b>	Recent batch studies on sorption of various dyes onto chitosan.....	39
<b>Table 2.5</b>	The Langmuir model and the Freundlich model equations .....	47
<b>Table 2.6</b>	The kinetic models and their linear forms .....	49
<b>Table 2.7</b>	The applications of chitosan on fabrics dyeing.....	50
<b>Table 3.1</b>	Factors for the factorial design experiment .....	60
<b>Table 3.2</b>	Factorial design, with four factors, and four replicates.....	62
<b>Table 3.3</b>	Factors for uniformity optimization.....	67
<b>Table 3.4</b>	Central composite design for nanochitosan preparation .....	67
<b>Table 3.5</b>	Samples with different ultrasonic duration .....	74
<b>Table 3.6</b>	DD of chitosan calculated by different methods.....	85
<b>Table 3.7</b>	Crystalline index (CrI; %) of the chitosan nanoparticles.....	87
<b>Table 4.1</b>	Characteristics of acid dyes .....	96
<b>Table 4.2</b>	Pseudo-first order rate constants for the anionic dyes .....	111
<b>Table 4.3</b>	Pseudo-second order rate constants for the anionic dyes.....	115
<b>Table 4.4</b>	Langmuire sorption isotherm constants for the anionic dyes .....	124
<b>Table 4.5</b>	Hydrophobic/hydrophilic ratio of AO 7, AR1, AR 18, DR 84, and DR 80 .....	133
<b>Table 4.6</b>	Thermodynamic parameters of sorption onto microchitosan and nanochitosan.....	137
<b>Table 4.7</b>	Desorption efficiency of microchitosan and nanochitosan .....	138



<b>Table 5.1</b> Dyeing recipe of AO 7, AR 1, AR 18, SB 3RL, SR F3B, TR, TY and TB at different depths .....	147
<b>Table 5.2</b> Detailed information on extraction of dye liquor from dye-bath .....	150
<b>Table 5.3</b> Coefficients of friction of the chitosan-treated and control fabrics .....	158
<b>Table 5.4</b> Data of amine end group analysis.....	159
<b>Table 5.5</b> No. of sulphonate groups in the dyeing solution of Acid Orange 7, Acid Red 1, Acid Red 18, Sirius Brown 3RL and Sirius Red F3B at different depths .....	162
<b>Table 5.6</b> Exhaustion data of the anionic dyes .....	174
<b>Table 5.7</b> Comparing of actual dyeing data and theoretical data obtained from sorption study.....	176
<b>Table 5.8</b> Initial ratios of the number of amino group dyesites to the number of sulphonate groups in the dye solution .....	179
<b>Table 5.9</b> Whiteness and Yellowness of chitosan-treated and control fabrics in various curing conditions .....	181
<b>Table 5.10</b> The color difference of the chitosan-treated and the control fabrics (grey scales) .....	190
<b>Table 5.11</b> CIE $L^*a^*b^*$ of the chitosan-treated and control fabrics dyed by Acid Orange 7.....	191
<b>Table 5.12</b> Color difference between the chitosan-treated and control fabrics dyed by Acid Orange 7.....	191
<b>Table 5.13</b> CIE $L^*a^*b^*$ of the chitosan-treated and control fabrics dyed by Acid Red 1 .....	192
<b>Table 5.14</b> Color difference between the chitosan-treated and control fabrics dyed by Acid Red 1 ..	193
<b>Table 5.15</b> CIE $L^*a^*b^*$ of the chitosan-treated and control fabrics dyed by Acid Red 18.....	194
<b>Table 5.16</b> Color difference between the chitosan-treated and control fabrics dyed by Acid Red 1 ..	194
<b>Table 5.17</b> CIE $L^*a^*b^*$ of the chitosan-treated and control fabrics dyed by Sirius Brown 3RL .....	195

<b>Table 5.18</b> Color difference between the chitosan-treated and control fabrics dyed by Sirius	
Brown 3RL.....	195
<b>Table 5.19</b> CIE L*a*b* of the chitosan-treated and control fabrics dyed by Sirius Red F3B .....	197
<b>Table 5.20</b> Color difference between the chitosan-treated and control fabrics dyed by Sirius Red	
F3B.....	197
<b>Table 5.21</b> CIE L*a*b* of the chitosan-treated and control fabrics dyed by Telon Red M-BL .....	198
<b>Table 5.22</b> Color difference between the chitosan-treated and control fabrics dyed by Telon Red	
M-BL.....	198
<b>Table 5.23</b> CIE L*a*b* of the chitosan-treated and control fabrics dyed by Telon Yellow M-4GL ..	199
<b>Table 5.24</b> Color difference between the chitosan-treated and control fabrics dyed by Telon	
Yellow M-4GL .....	199
<b>Table 5.25</b> CIE L*a*b* of the chitosan-treated and control fabrics dyed by Telon Blue M-RLW .....	200
<b>Table 5.26</b> Color difference between the chitosan-treated and control fabrics dyed by Telon Blue	
M-RLW .....	200
<b>Table 5.27</b> K/S differences of fabrics at $\lambda_{\max}$ of different depths.....	206
<b>Table 5.28</b> Colorfastness to water of fabrics dyed by Acid Orange 7, Acid Red 1, and Acid Red 18..	207
<b>Table 5.29</b> Colorfastness to water of fabrics dyed by Sirius Brown 3RL, Sirius Red F3B, Telon	
Red M-BL, Telon Yellow M-4GL and Telon Blue M-RLW .....	208
<b>Table 5.30</b> Colorfastness to washing of fabrics dyed by Acid Orange 7, Acid Red 1, and Acid Red	
18.....	210
<b>Table 5.31</b> Colorfastness to washing of fabrics dyed by Sirius Brown 3RL, Sirius Red F3B, Telon	
Red M-BL, Telon Yellow M-4GL and Telon Blue M-RLW.....	211

**List of Abbreviations**

AFM	Atomic Force Microscopy
ASTM	American Society for Testing and Materials
DD	Degree of deacetylation
DSC	Differential scanning calorimetry
FT-IR	Fourier transform infrared spectroscopy
GPC	Gel permeation chromatography
$^1\text{H}$ NMR	Hydrogen nuclear magnetic resonance
HPLC	High performance liquid chromatography
HPSEC	High-performance size exclusion chromatography
NIR	Near infrared
SEM	Scanning electron microscopy
TEM	Transmission Electron Microscopy
UV-vis	Ultraviolet-visible
XRD	X-ray diffraction
DD	Degree of deacetylation
DSC	Differential scanning calorimetry
FT-IR	Fourier transform infrared spectroscopy

## Chapter 1 Introduction

### 1.1 Introduction of chitosan

Chitosan is the deacetylated derivative of chitin that is the second most abundant polysaccharide next to cellulose on the earth. It is the N-deacetylated derivative of chitin, and most of its glucopyranose residues are 2-deoxy- $\beta$ -D-glucopyranose. Figure 1.1 shows the chemical structures of chitin and chitosan.

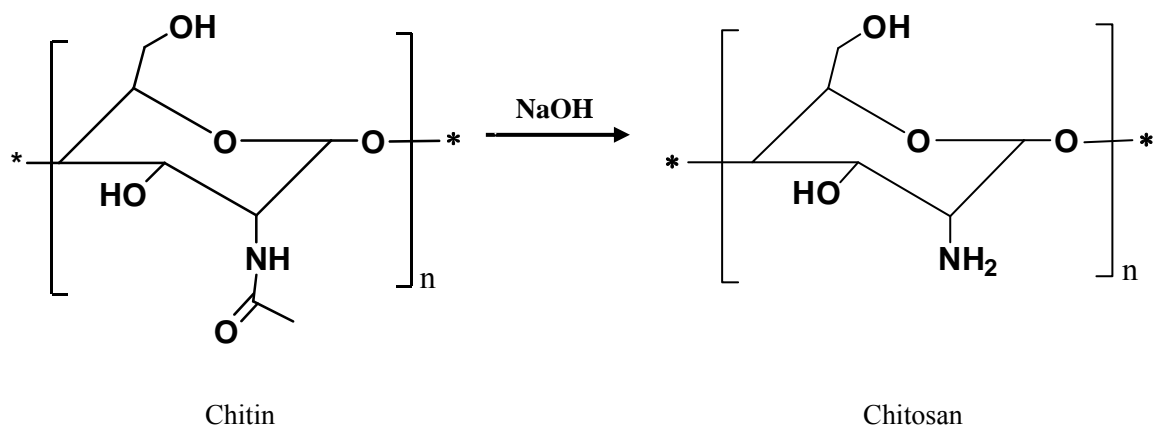


**Figure 1.1** Chemical structures of chitin and chitosan

Generally, chitosan is produced through the deacetylation reaction of chitin using a sodium hydroxide solution with a concentration over 40% [1]. The degree of deacetylation (DD) is the proportion of glucosamine monomer residues in chitin, and has a striking effect on the solubility and solution properties of chitosan. There are several methods for the measurement of DD, including infrared resonance spectroscopy (IR), UV-vis spectroscopy, circular dichroism, proton nuclear magnetic resonance (<sup>1</sup>H NMR) spectroscopy, solid-state NMR spectroscopy, elemental analysis, gel permeation chromatography, and titration methods [2].

Chitin is the main component in the shells of crustaceans such as shrimps, crabs, and

lobsters; it is also found in the exoskeletons of mollusks and insects and the cell walls of some fungi [1, 3-4]. Every year, an enormous quantity of crabs and shrimp shells is abandoned as wastes by seafood companies worldwide and the utilization of chitosan (chitin) in these renewable wastes has aroused considerable scientific and technological interests. In the past 30 years, a number of researchers have demonstrated that chitosan had a great potential for a wide range of uses due to its good biodegradability, high biocompatibility, effective antibacterial activity, low toxicity, and versatile chemical and physical properties [3]. The applications of chitosan cover a variety of fields, such as pharmaceutical and medical applications, paper productions, textiles, wastewater treatments, biotechnologies, cosmetics, food processing, and agriculture [5-6]. Figure 1.2 summarizes its advantages and applications.

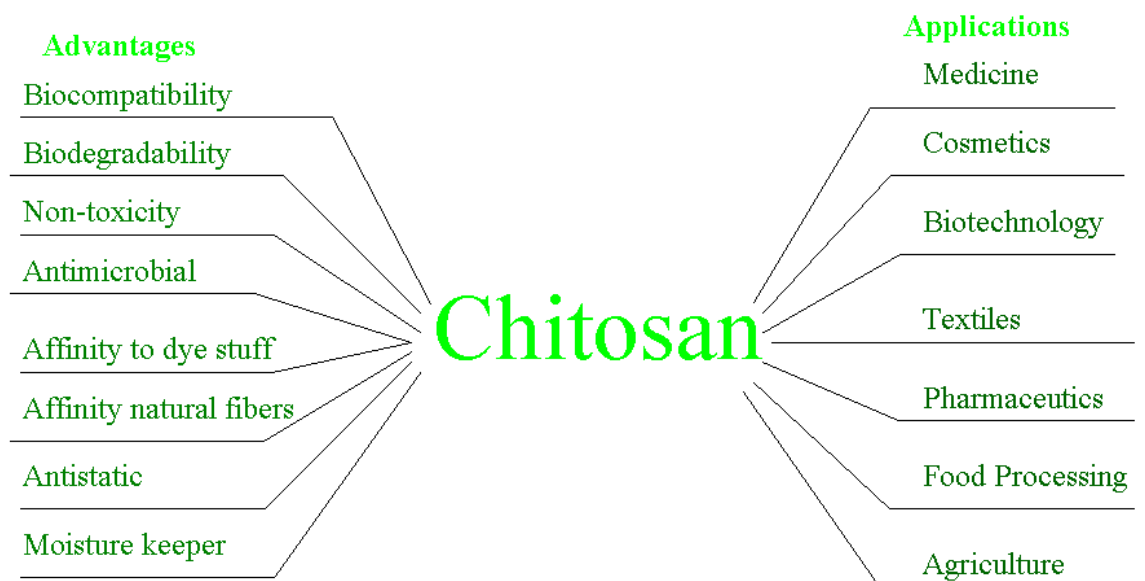


**Figure 1.2** Advantages and applications of chitosan

## 1.2 Physical and chemical characters of chitosan

Commercial chitosan for food or medicine is usually white powder with a DD higher than 80%. In the solid state, chitosan is a semi-crystalline polymer. Single crystals of chitosan were obtained using fully deacetylated chitin of low molecular weights. The electron diffraction diagram can be indexed in an orthorhombic unit cell ( $P2_12_12_1$ ) with  $a=0.807$  nm,  $b=0.844$  nm,  $c=1.034$  nm; the unit cell contains two antiparallel chitosan chains and no water molecules [7-9].

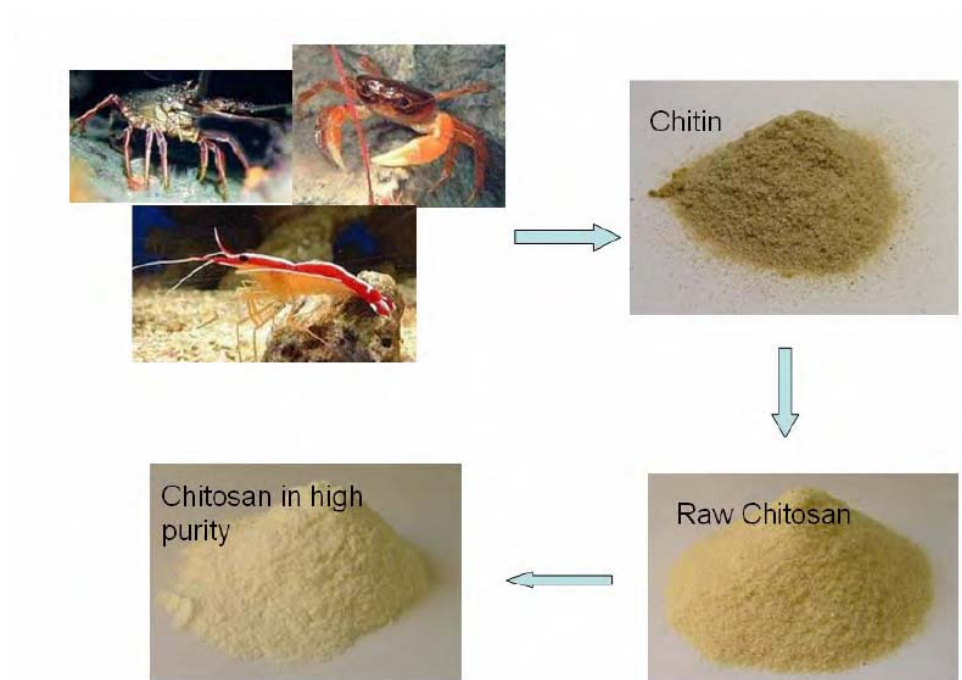


**Figure 1.3** Workflow of chitosan production

The molecular weight, crystallinity, solubility and DD of chitosan are affected by the conditions of production from chitin. The production process is illustrated in Figure 1.3. There is no widely agreed nomenclature on the DD defined between chitin and chitosan [10-11]. Among the physical and chemical properties of chitosan, its solubility and chemical activities are of the most concerns because they are the main factors affecting its

applications.

Both chitin and chitosan are insoluble in water at pH 7. Although many solvents have been developed, most of them are not applicable due to their toxic, corrosive, or mutagenic properties [5]. Chitosan is easier to control than chitin because it readily dissolves in dilute mineral or organic acids due to the protonation of free amino groups at low pH [1]. The solubilization occurs by protonation of the  $\text{-NH}_2$  function group on the C-2 position of the D-glucosamine repeat unit, whereby the polysaccharide is converted to a polyelectrolyte in acidic media. In fact, the solubility is a very difficult parameter to control: it is related to the DD, the ionic concentration, the pH, the nature of the acid used for protonation, and the distribution of acetyl groups along the chain, as well as the conditions of isolation and drying of the polysaccharide. Chitosan is the only pseudo-natural cationic polymer and thus, it finds many applications.

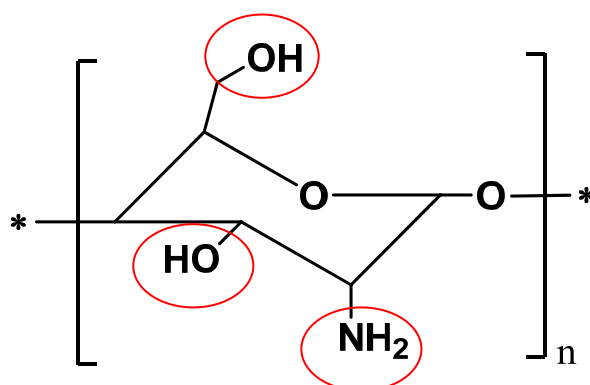


**Figure 1.4** Reactive groups of chitosan

With three reactive groups, chitosan is more chemically active than chitin. The reactive groups are the primary and secondary hydroxyl groups in each repeat unit, and the amino group on each deacetylated unit, as shown in Figure 1.4. Positively charged amino groups can bind to other negatively charged materials, resulting in many different kinds of applications such as adsorption, antibacterial, and other applications which involve the protonated amino groups in chitosan [12-15].

## 1.3 Applications of chitosan

A wide variety of applications of chitosan covering many kinds of fields including biotechnologies [16-18], pharmaceutical and medical applications [19-29], wastewater treatments [12, 30-32], textiles [33-38], cosmetics [39-40], food processing [41-42], agriculture and solid-state batteries [5-6] have been reported over the last four decades. Nowadays as the development of nanotechnology which provides versatile tools to modify the properties of materials, chitosan in both nanofiber and nanoparticle forms are widely studied [15].

### 1.3.1 Applications of chitosan in water treatment

Due to its unique molecular structure, chitosan has an extremely high affinity to many classes of dyes, including disperse dyes, direct dyes, reactive dyes, acid dyes, vat dyes, sulfur and naphthol dyes. Chitosan also has a high affinity to metals and surfactants which are usually present in the dyeing of textiles.

There are many published reports on the of adsorption performance of chitosan, especially on its adsorption capacity. Generally, the adsorption performance of chitosan-based materials depends on the following factors [31]:

- (i) the origin and nature of chitosan, such as its physical structure, chemical nature and functional groups;
- (ii) the activation conditions of the raw polymer, such as physical treatments and chemical modifications;
- (iii) the influence of process variables such as contact time, initial dye concentration, polymer dosage and stirring rate;
- (iv) the chemistry of the dye including its  $pK_a$ , polarity,  $M_w$  and functional groups etc.;



(v) the solution conditions, including its pH, ionic strength, temperature and presence of impurities.

There were many reports on the preparation of chitosan nanoparticles which were used to improve the sorption ability of chitosan. Two methods have been commonly used. They are the ionotropic gelation method, and the water-oil-reversed-phase micro-emulsion method [43-48]. However, the chitosan prepared was not pure, while the surfactants are difficult to remove.

### **1.3.2 Applications of chitosan in textile finishing**

Chitosan can easily adsorb anionic dyes, such as direct dyes, acid dyes and reactive dyes, by electrostatic attractions because of the cationic nature of chitosan in acidic media. As an environmentally friendly material, chitosan is used as a finishing agent for textiles to improve the dyeing ability and other functional properties such as antibacterial performance. A number of studies showed that the treatment of cotton and polyester with chitosan before dyeing significantly improved the color intensity and fastness properties; the capillary and sorption properties of the fabrics were also improved [33].

It was postulated that the affinity of chitosan to cotton would be van der Waals forces. Another possibility for the bonding of chitosan to cellulose was a cross-link by the formation of the Schiff base between the reducing end ( $-\text{CO}-\text{H}$ ) of cellulose and the amino group of chitosan. Hydrogen bonds also played an important role. It was reported that chitosan pretreatment increased the exhaustion of reactive dyes on cotton and the highest dye up-take was achieved using a pad-dry method [34]. Thus, the application of chitosan to cotton could reduce the amount of dye used and the residual dyes in wastewaters due to better dye exhaustion. In addition, the use of chitosan could decrease

the amount of salt required when using direct and reactive dyes by about 50% to produce a comparable shade to that of the untreated fabric [35].

Besides the improvement on dyeing ability of fabrics, chitosan is also used as an additive in spinning to provide antimicrobial properties for textiles [36-37]. Some studies also showed that chitosan could provide shrink-resist properties for the fabrics [38].

## **1.4 Scope of research**

The applications of chitosan in textiles were focused in this study. First, the preparation of nanochitosan was investigated. Second, the sorption behaviors of the nanoparticles and microparticles were studied and compared. Third, the nanoparticles were coated on the surface of nylon fabrics and their dyeing behaviors were investigated.

### **1.4.1 Preparation and characterization of nanochitosan**

In this study, nanochitosan emulsions with different particle sizes were prepared using a novel sonolysis method. The emulsions had zeta potential values ranging from +25 mV to +40 mV at pH 6.5 and remained stable for a month. The optimal conditions for preparing the nanochitosan emulsions with uniform sizes were studied using a factorial design. Laser scanning, scanning electron microscopy (SEM), transmission electron microscopy (TEM), and atomic force microscopy (AFM) analyses were performed on the samples to obtain the particle sizes and images. Generally, the particle size and molecule weight decreased with the ultrasonic duration. The DD of chitosan had no obvious change during the ultrasound treatment. The crystallinity of chitosan nanoparticles was investigated using X-ray diffraction.

### **1.4.2 Application of nanochitosan emulsion on dye sorption**

The effectiveness of the nanochitosan as an adsorbent for five selected anionic dyes including Acid Orange 7, Acid Red 1, Acid Red 18, Direct Red 84 (Sirius Brown 3RL) and Direct Red 80 (Sirius Red F3B) were thoroughly studied at temperatures from 30°C to 90°C. The sorption behaviors of microchitosan were also studied for comparison. The sorption kinetics of the dyes onto nanochitosan and microchitosan were analyzed. The sorption of the dyes onto the nanochitosan fit the pseudo-second-order model. The Langmuir equilibrium isotherms were then used to analyze the equilibrium data. The sorption mechanisms were then discussed. The desorption and regeneration studies were also investigated and the desorption efficiency was the highest at pH 10, ranging from 70%-88%. The recycled chitosan could be used repeatedly.

### **1.4.3 Dyeability enhancement of nylon using nanochitosan emulsion**

The enhancement in dyeability of nylon fabrics with the nanochitosan emulsion was studied. The emulsions were applied on the nylon fabrics using a pad-dry-cure method. The surface of the treated nylon was studied by SEM. Both the nanochitosan-treated and control fabrics were then dyed with eight anionic dyes. The dyes were Acid Orange 7, Acid Red 1, Acid Red 18, Sirius Brown 3RL (Direct Red 84), Sirius Red F3B (Direct Red 80), Telon Red M-BL, Telon Yellow M-4GL and Telon Blue M-RLW. The exhaustion data of dyeing were recorded and analyzed. The color evaluations of the dyed fabrics were performed using grey scales and VIS spectroscopic techniques. The durability of the treatment was assessed using color fastness to water (ISO 105 E01:1996) and color fastness to washing (ISO 105 C01:1989) methods.

## 1.5 Project significance and value

The dyeing industry generates a large quantity of wastewaters in production. Pollution prevention is becoming important in both product design and manufacture. Using chitosan which is derived from wastes can help to reduce pollution and improve both the wastewater treatment and dyeing efficiencies.

The objectives of this study are:

- a.** To develop a new method to prepare nanochitosan emulsions;
- b.** To optimize the preparation method for the nanochitosan emulsions;
- c.** To study the sorption ability of the nanochitosan on selected anionic dyes;
- d.** To improve the dyeing depths of nylon using the nanochitosans.

Many reports were published on the preparation of chitosan nanoparticles by using organic solvents, supernatants or cross-linking agents. However, it was difficult to determine the particle contents in the emulsions and to avoid the effect of dissolving chitosan. The chemicals used in the preparation were generally difficult to remove from the system, and could cause negative effects on the end uses, eg, the organic solvents used could damage protein resulting in limited applications in the biological fields.

In order to overcome the disadvantages of the existing preparation methods, we have developed a novel sonolysis method to prepare pure and stable emulsions containing only chitosan and water. It is envisaged that the applications can be widened.

Although the sorption of dyes using chitosan has been widely studied, however, the sorption behaviors of nanochitosan were rarely reported. We have investigated the dye

sorption of nanochitosan and compared the results with that of microchitosan. The nanochitosan has been found to have much higher sorption capacities than those of the microchitosan and the sorption equilibrium of dyes onto nanochitosan could be achieved at much shorter duration.

The nanochitosan was then applied to nylon fabrics to improve their depths of dyeing. nylon has only a small number of dyesites (50 mmol/kg) when compared with wool (820 mmol/kg). Deep dyeing is always a challenge to dyers. The vast number of dyesites in chitosan could increase the dyeing depths of the polymer. Also, more dyes could be exhausted by the fibres, thus the quantity of the dyes in the effluent could be reduced.

## Chapter 2 Literature Review

### 2.1 Introduction of chitosan

Chitosan is a linear polysaccharide composed of randomly distributed  $\beta$ -(1-4)-linked D-glucosamine (deacetylated unit) and N-acetyl-D-glucosamine (acetylated unit). Usually, chitosan is prepared by deacetylation of chitin with alkaline [10-11, 50]. Chitosan is more chemically versatile than cellulose and chitin due to the presence of free amino groups. The structures of cellulose, chitin and chitosan are shown in Figure 2.1.

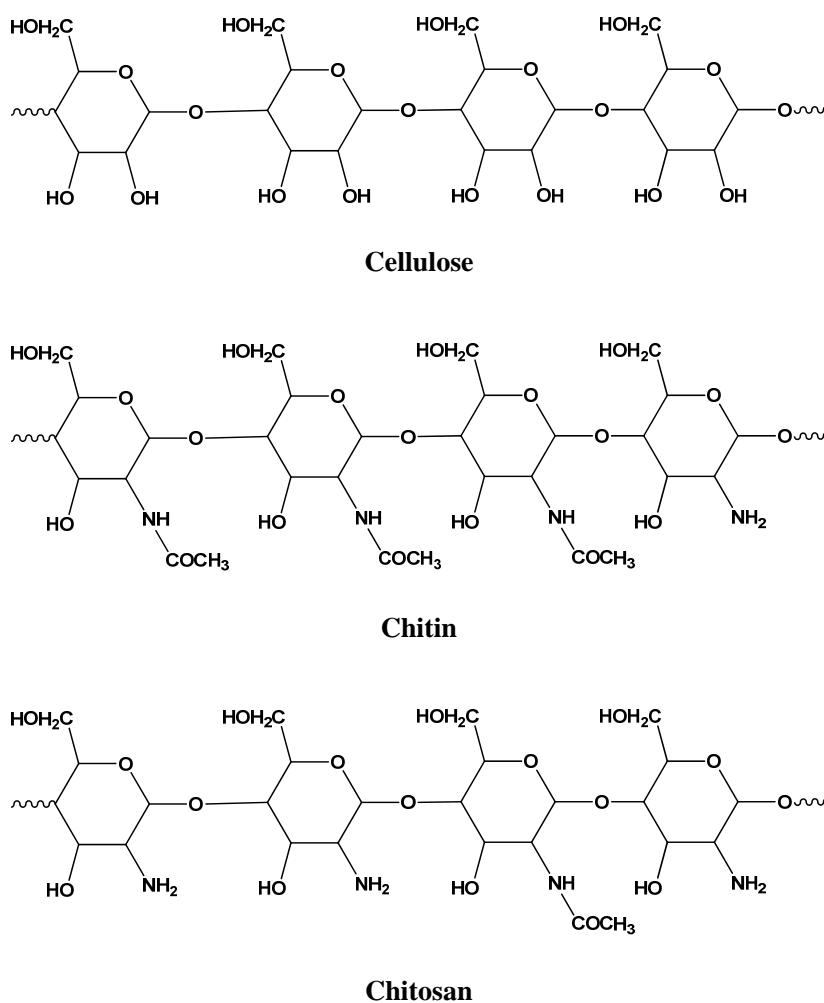


**Figure 2.1** Structures of cellulose, chitin and chitosan

### **2.1.1 Solubility of chitosan**

The solution properties of chitosan depend not only on its average DD, but also on the distribution of the acetyl groups along the main chain in addition of the molecular weight [51-53]. The deacetylation, usually done in the solid state, gives an irregular structure due the semicrystalline character of the initial polymer. Examination of the role of the protonation of chitosan in the presence of acetic acid [54] and hydrochloric acid on solubility [55] showed that the degree of ionization depends on the pH and the pK of the acid. The solubility of chitosan is usually tested in acetic acid by dissolving it in 1% or 0.1M acetic acid. It is demonstrated that the amount of acid needed depends on the quantity of chitosan to be dissolved [54]. The concentration of protons needed is at least equal to the concentration of -NH<sub>2</sub> units involved. In fact, the solubility is a very difficult parameter to control: it is related to the DD, the ionic concentration, the pH, the nature of the acid used for protonation, and the distribution of acetyl groups along the chain, as well as the conditions of isolation and drying of the polysaccharide.

Aqueous solubility of chitosan only exists in acidic solution because of its rigid crystalline structure and the deacetylation which limits its application to bioactive agents such as gene delivery carriers, peptide carriers, and drug carriers. Recently, the water-soluble form of chitosan at neutral pH was obtained by different researchers [56-60]. Stable solutions were obtained at pH 7 – 7.1 and room temperature, but a gel formed on heating to 40°C. The sol-gel transition was partially reversible and the gelation temperature depended on the experimental conditions. Water-soluble chitosan is easily soluble in neutral aqueous solutions. Its advantage is ease of modification and it is useful as gene or peptide drug carriers. Therefore, water-soluble chitosan and functional property has been developing for pharmaceutical uses. Tao et al. prepared water-soluble

chitosan nanoparticles varying from 500 nm to 800 nm by an ionic gelation method and a spray-drying technique. Their results showed that the nanoparticles reduced the blood lipids and plasma viscosity significantly and increased the serum superoxide dismutase (SOD) activities greatly. They suggested that the water-soluble chitosan nanoparticles could be used for the treatment of hypercholesterolemia [61]. They also prepared crosslinking nanoparticles composed of water-soluble chitosan and sodium tripolyphosphate (TPP) loaded with bovine serum albumin (BSA) by the same method. The size distribution was in the range of 200-400 nm and the nanoparticles were spherical [62].

### 2.1.2 Degree of deacetylation

Chitosan is the fully or partially N-deacetylated derivative of chitin with a typical DD of more than 80%. To define this DD, many techniques including  $^1\text{H}$  NMR [63-66],  $^{13}\text{C}$  or  $^{15}\text{N}$  solid-state NMR spectroscopy [67-72], IR [68, 73-79], NIR [80], UV [81-82], ninhydrin assay [83-84], colloidal titration [85], potentiometric titration [86-87], conductometric titration [88], enzymatic hydrolysis-colorimetry [89], and elemental analysis were used [90-92].

NMR spectroscopy is generally considered to be the most reliable technique for the DD determination. Figure 2.2 shows the  $^1\text{H}$  NMR spectrum of chitosan at 70°C [66]. The DD of the sample was calculated using integrals of the peak of the protons in the deacetylated monomer (H1D) and the peak of the three protons of acetyl group (HAc):

$$\text{DD}(\%) = \frac{\text{H1D}}{\text{H1D} + \text{HAc}/3} \times 100 \quad (\text{E 2.1})$$

But  $^1\text{H}$  NMR technique is applicable for a limited range of the DD, where the polymer



samples are soluble in a solvent.  $^{13}\text{C}$  NMR and  $^{15}\text{N}$  NMR can be used for both soluble and non-soluble samples in entire range of the DD. The use of solid-state ( $^{13}\text{C}$  or  $^{15}\text{N}$ ) NMR technique provides a number of advantages such as easy sample preparation and no solvent required.

The distribution of the acetyl groups along the chain (random or clockwise) may influence the inter-chain interactions due to H-bonds and the hydrophobic character of the acetyl group and also the solubility of the polymer. NMR spectroscopy also yields information on sequential distribution of the glucosamine and N-acetyl glucosamine residues [64, 93].

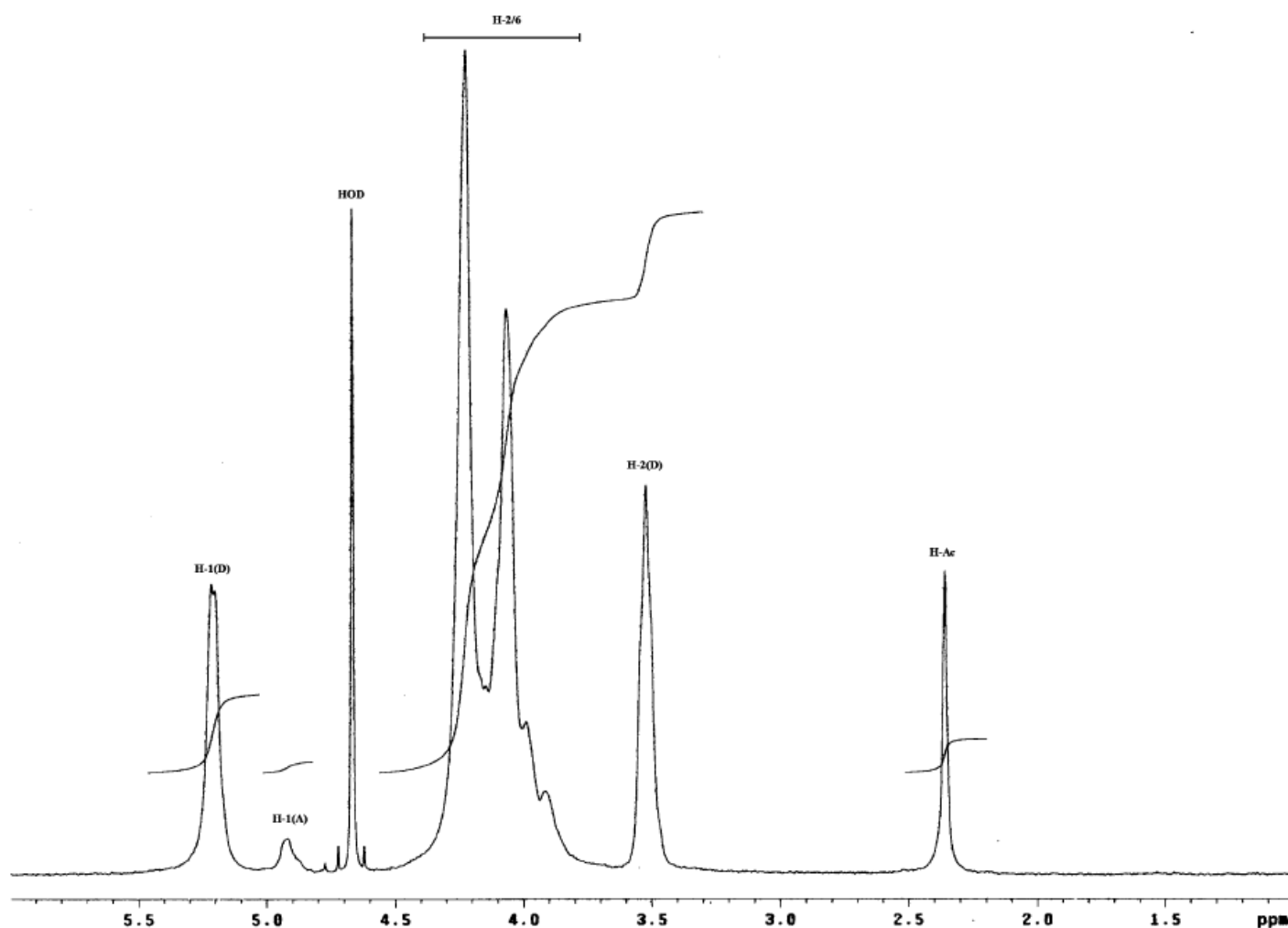


**Figure 2.2**  $^1\text{H}$  NMR spectrum of chitosan at  $70^\circ\text{C}$  [66]

IR spectroscopy is a relatively quick technique for the qualitative evaluation of the DD through the determination of absorption ratios. Several methods using different absorption ratios have already been proposed for the determination of DD. DD was typically determined by: (1) determination of the ratio of  $A_M/A_R$ : where  $A_M$  is the intensity of a probe band, which is a measure of N-acetyl or amine content; and  $A_R$  is the intensity of a reference band, having an intensity that does not change with DD. DD of unknown samples can be estimated by comparing the values of  $A_M/A_R$  with similar ratio of a few reference samples having a known  $D_A$ ; (2) creating a calibration curve by plotting the absorption ratio of chitosan samples of known DD versus their DD, where DD of the samples was determined by IR or a reference method such as  $^1\text{H}$  NMR spectroscopy. DD of unknown samples were then estimated from the calibration curve.

IR spectra are generally recorded in the range of  $1200\text{--}4000\text{ cm}^{-1}$ . Several absorption band ratios have been proposed to determine DD. Figure 2.3 and Table 2.1 show the baselines and adsorption bands adopted by different researchers.

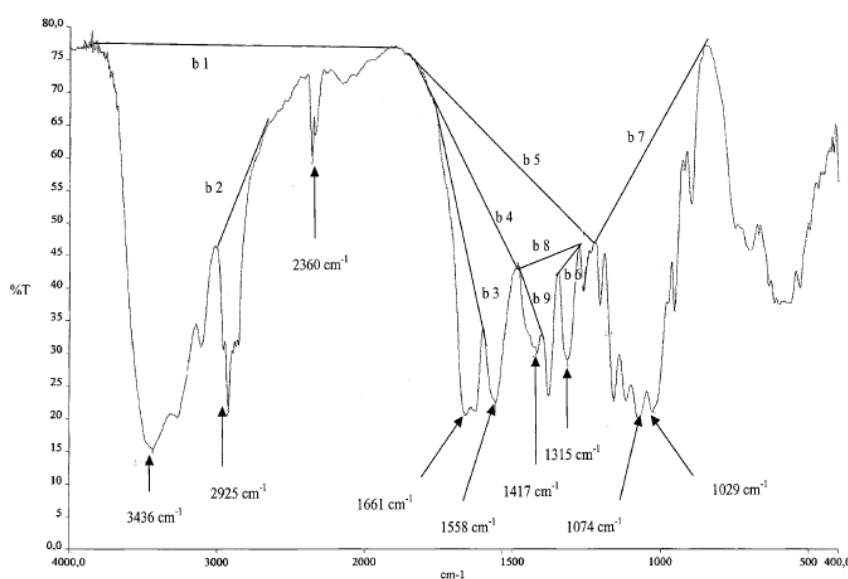


**Figure 2.3** IR spectrum of chitosan and representation of different baselines [78]

**Table 2.1** Characteristics of methods to analyze infrared spectra of chitin or chitosan

Baselines		RB <sup>a</sup>	PB <sup>b</sup> (cm-1)	Range of	Method of calibration	Natural	Ref.
For RB <sup>a</sup>	For PB <sup>b</sup>	(cm-1)		DD(%)		Source	
b1	b3	3450	1655	59-100	Potentiometry and <sup>13</sup> C CP/MAS solid state NMR	Shrimp and krill	[94]
b7	b4	1070	1560	Mixture of 0-100	<sup>1</sup> H NMR		[95-96]
b7	b4	1030	1560				
b7	b4	1070	1655+1630				
b7	b4	1030	1655+1630				
b7	b4	3450	1655+1630				
b2	b5	2878	1560	92-95	Elek and Harte method	Shrimp	[73]
b2	b4	2877	1626	32-94	<sup>13</sup> C CP/MAS solid state NMR	Crab	[68]
b2	b4	2877	1663+1626				
b7	b4	1074	1561				
b7	b4	1025	1561				
b2	b3	2865	1655	75-100	Colloidal titration	Crab	[75]
b1	b5	3450	1655	17-76	Periodate oxidation	<sup>c</sup> NR	[20]
b1	b5	3450	1655	28-86	Hydrobromide salt titration, residual salicylaldehyde determination	Prawn	[76]
b1	b3	3450	1655	45-100	Potentionmetry and dye absorption	Scampi	[77]
b1	b5	3450	1655	70-90	Titrimetric method	<sup>c</sup> NR	[97]
b8	b4	1430	1550	17-75	Chemical hydrolysis of acetyl groups	Lobster	[98]

<sup>a</sup> RB corresponds to reference band.<sup>b</sup> PB corresponds to probe band of the N-acetylation.<sup>c</sup>NR: Not reported

### 2.1.3 Molecular weight of chitosan and distribution of acetyl groups

Another important characteristic to consider for polymers is the molecular weight and the corresponding distribution. Molecular weights can be determined by many different methods including dilute solution viscometry, light scattering, gel permeation chromatography (GPC).

Dilute solution viscometry is a simple method for the determination of molecular weights. By measuring the intrinsic viscosity ( $[\eta]$ ) of dilute polymer solutions, the molecular weights can be derived. The Mark-Houwink equation, can be presented as

$$[\eta] = K[M_v]^\alpha \quad (\text{E 2.2})$$

where  $K$  and  $\alpha$  are the Mark-Houwink constants. Some values of the Mark-Houwink constants for chitosan solutions are given in Table 2.2.

**Table 2.2** Mark–Houwink constants for chitosan in various solvents

Solvent	$K / (\text{mL/g})$	$\alpha$	T/°C	Ref.
0.1M HAc/0.2M NaCl	$1.81 \times 10^{-3}$	0.93	25	[99]
0.1M HAc /0.02M NaCl	$3.04 \times 10^{-3}$	1.26	25	[99]
0.2M HAc /0.1M NaAc/4M urea	$8.93 \times 10^{-2}$	0.71	25	[100]
0.3M HAc /0.2M NaAc (DD=98%)	$8.2 \times 10^{-2}$	0.76	25	[101]
0.3M HAc /0.2M NaAc (DD>97%)	$7.9 \times 10^{-2}$	0.796	25	[102]
0.02M acetate buffer/0.1M NaCl	$8.43 \times 10^{-2}$	0.92	25	[103]

By using high-performance size exclusion chromatography (HPSEC), the molecular weight and distribution of chitosan can be precisely measured. Optimal conditions for using high-performance liquid chromatography in the size exclusion mode have been determined by many researchers [104-106]. The high-performance size exclusion chromatography is believed to be the most precise and effective method for the

measurement of molecular weight and distribution of chitosan.

## **2.2 Preparation of chitosan-based nanoparticles**

Chitosan is widely explored as functional materials, because it has good properties such as biocompatibility, 100% biodegradability, and non-toxicity [5]. Chitosan has been used in many kinds of fields such as medicine, wastewater treatments, textiles, and agriculture. Being soluble in aqueous solutions, it is largely used in different applications as particles [107-109], solutions [110-111], gels [112], membranes [113-116], or films [117-119] and fibers [120]. Meanwhile, nanotechnology provides a versatile tool to modify the properties of chitosan materials.

### **2.2.1 Methods for the preparation of chitosan nanoparticles**

Chitosan nanoparticles can be prepared using different methods. The first and mostly adopted method is the ionotropic gelation method, based on the reaction between the cationic amino groups of chitosan and additional anionic chemicals or cross-linking agents such as tripolyphosphate (TPP) or calcium salts [121-122]. The second is the water-oil-reversed-phase micro-emulsion method, in which organic solvents, emulsifiers, and cross-linking agents are used [123]. Using the reversed-phase micro-emulsion, a chitosan solution was mixed into an organic solvent to form a water-in-oil micro-emulsion. Then an aqueous solution of polyanions was added into the micro-emulsion under a high speed stirring. Nanoparticles were formed in the micro-droplet in the emulsion through the ionotropic gelation. In some cases, cross-linking agents were used instead of polyanions.

The most popular method is the ionotropic gelation method which involves the mixture of two aqueous phases at room temperature. Calvo et al. [121] prepared chitosan

nanoparticles by inducing the gelation of chitosan solution with TPP (Figure 2.4).

The relationship of nanoparticles with the concentrations of chitosan and TPP was studied. At different concentrations, three different systems were identified: a clear solution, an opalescent suspension and an aggregate. The zone of the opalescent suspension, responding to a suspension of very small particles, is illustrated in Figure 2.5, and the TEM photo of the chitosan nanoparticles is also shown in Figure 2.5.

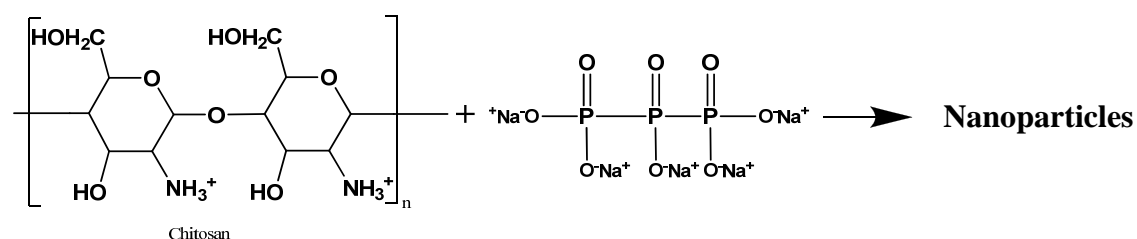


**Figure 2.4** Preparation of chitosan nanoparticles with TPP [121]

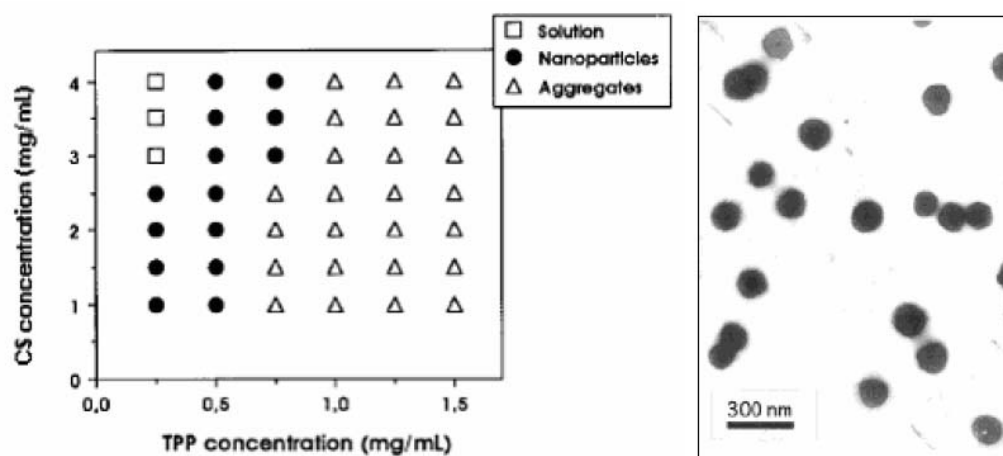


**Figure 2.5** Zones of the nanoparticles (left) and their TEM micrograph (right) [121]

Chang et al. [122] synthesized nanoscaled chitosan-poly(acrylic acid) particles by a dropping method based on the reaction between chitosan and poly(acrylic acid) (PAA). The PAA solution was used as a base material into which the chitosan solution was added. After incubation in the solution, the chitosan-PAA mixed solution was freeze-dried to

obtain the nanoparticles. In their study, extremely fine chitosan-PAA particles with a size of 30 nm were synthesized.

Banerjee et al. [123] described the preparation of cross-linked chitosan nanoparticles with a diameter size of less than 100 nm using reverse micelles as the media. The process is shown in Figure 2.6. Sodium bis(2-ethylhexyl) sulfosuccinate was used as a surfactant and glutaraldehyde was used as a cross-linking agent.

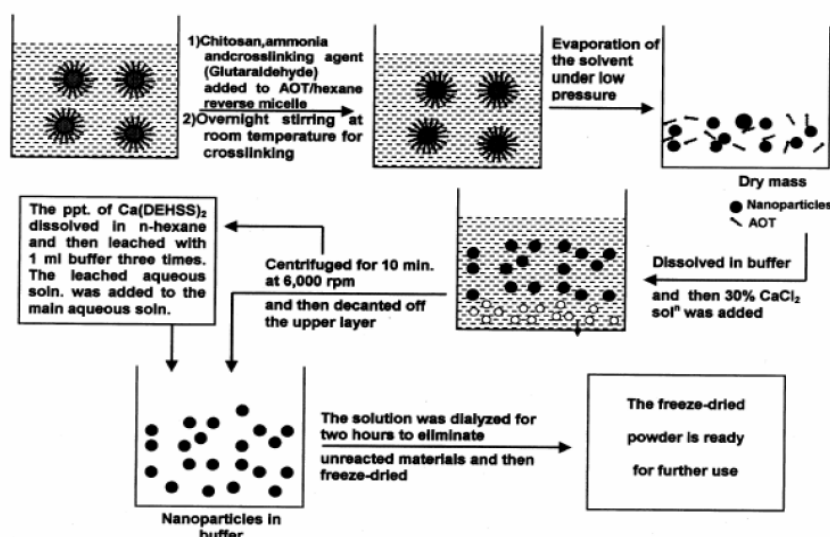


**Figure 2.6** Flow chart for the preparation of cross-linked chitosan nanoparticles [123]

### 2.2.2 Core-shell nanoparticles based on chitosan

Drug carrier systems are required to protect this drug from the gastrointestinal environment and from enzymatic degradation. Nanoparticles based on the chitosan have shown particularly promising results due to their intrinsic properties including biocompatibility, mucoadhesion and ability to transiently open the tight junctions of the intestinal barrier [124-130]. A widely-used approach for nanochitosan preparation in drug delivery is the forming of core-shell nanoparticles in which chitosan generally plays the role of shell materials.

Liu et al. prepared chitosan nanoparticles by a method in which TPP was used as a cross-linking agent [131]. TEM observation revealed a core-shell structure filled with ciprofloxacin for the chitosan nanoparticles. The influence of fabrication conditions on the physical properties and drug loading and release properties were also investigated. The study showed that the chitosan nanoparticles were rather stable and no cytotoxicity of the chitosan nanoparticles was found in an in vitro cell culture experiment. This is a typical method for preparing chitosan nanoparticles with drug loaded.

5-Fluorouracil (5-FU) is one of the most widely used antineoplastics drugs in the treatment of cancer, but it metabolizes so fast that the half-life is only 5-10 min. Xing et al. [132] prepared stable 5-FU-loaded chitosan/alginate nanoparticles with poloxamer as a surfactant. The study showed that the accumulative release of 5-FU-loaded nanoparticles was less than 50% at 12 h. Yang et al. [133] also studied the application of chitosan nanoparticles loaded with 5-FU which were prepared by using TPP as a cross-linking agent on drug delivery. The investigation of the encapsulation efficiency of 5-FU-loaded chitosan nanoparticles suggests that they could be used as effective drug delivery systems.

Chitosan nanoparticles loaded with many different drugs are extensively studied [132-139]. Bioadhesive chitosan nanoparticles loaded with drugs were usually obtained by ionic gelation between chitosan and TPP or other cross-linking agent agents. Many different properties of the nanoparticles were studied and the potential application as drug carriers was widely discussed. Ionic method is the most adopted approach for preparing chitosan nanoparticles and TPP is the very widely used cross-linking agent.

Except TPP, some other surfactants or negatively charged salts are used during the preparation of chitosan shell nanoparticles. For instance, Xing et al. [132] prepared stable 5-FU-loaded chitosan/alginate nanoparticles with poloxamer as a surfactant and Huang et



al. [136] prepared low-molecular-weight chitosan nanoparticles containing insulin by using Span 85 as surfactant. Grenha et al. [137] prepared chitosan/carrageenan (CRG) nanoparticles by ionic complexation, by means of an electrostatic interaction of chitosan with CRG anions, in which the positively charged amino groups of chitosan interact with the negatively charged sulfate groups of CRG. Avadi et al [138] prepared insulin nanoparticles by ionic gelation between positively charged chitosan and negatively charged Arabic gum. Various formulations were prepared using factorial designs to develop a system based on ionic gelation between chitosan and Arabic gum for loading of insulin.

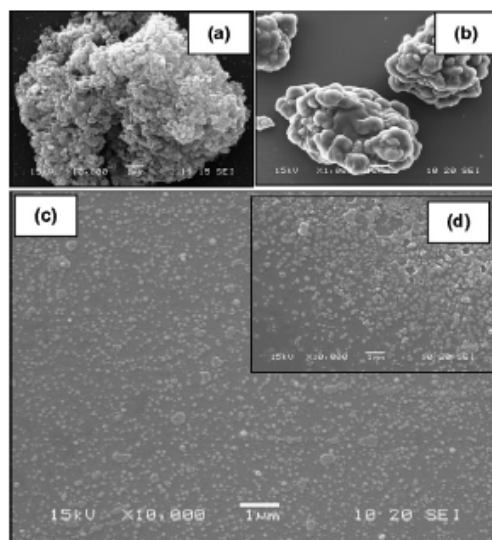


**Figure 2.7** SEM micrographs of (a) chitosan particles (10,000 $\times$ ) and (b)-(d) AP loaded chitosan particles with different chitosan to AP weight ratios: (b) 1:1.00 (1000 $\times$ ), (c) 1:1.00 (10,000 $\times$ ) and (d) 1:1.50 (10,000 $\times$ ) [139]

Some researchers also prepared chitosan nanoparticles via modified ionic gelation method. In the study of Yoksana et al. [139], the encapsulation of ascorbyl palmitate (AP) in chitosan particles was carried out by droplet formation via an oil-in-water emulsion, followed by droplet solidification via ionic gelation using TPP as a cross-linking agent. The obtained AP-loaded chitosan particles were spherical in shape with an average

diameter of 30-100 nm as observed by SEM (Figure 2.7).

Besides drug delivery, chitosan nanoparticles were also applied to many other fields, such as fabrics and textile, antibacterial property, sorption industry and many different chitosan based nanomaterials have been prepared [140-155].

## **2.3 Ultrasonic method for the preparation of nanomaterials**

Nanomaterials often exhibit properties which are distinct from their bulk counterparts, in part because the nanoparticles have electronic structures that have a high density of states, but not yet continuous bands. Nanostructured materials have been prepared by a variety of synthetic methods, including gas phase techniques, liquid phase methods, and mixed phase approaches [156]. Among a variety of approaches, the utilization of high intensity ultrasound offers a facile, versatile synthetic tool for preparation of nanomaterials.

The utilization of ultrasound for materials synthesis is now positioned as one of the most powerful tools in nanostructured materials synthesis. Nowadays, there are two most successful ultrasound-assisted synthetic methods which are the sonochemical synthesis and ultrasonic spray pyrolysis.

### **2.3.1 Sonochemical synthesis**

Chemical reactions require some form of energy (e.g., heat, light, radiation, electric potential) to proceed. Ultrasonic irradiation provides rather unusual reaction conditions (a short duration of extremely high temperatures and pressures in liquids) that cannot be realized by other methods. The chemical effects of ultrasound were explored for many years, nearly always in water [157–160]. Ultrasonic irradiation of aqueous liquids generates free radicals, and the formation of free radicals by sonolysis of water has been

particularly well-studied. Primary sonolysis products in water are hydrogen ( $\text{H}\cdot$ ) and hydroxyl ( $\text{OH}\cdot$ ) radicals [160]. These radicals can recombine to return to their original form or combine to produce  $\text{H}_2$  and  $\text{H}_2\text{O}_2$ . These strong oxidants and reductants are utilized for various sonochemical reactions in aqueous solutions.

With a simple modification in reaction conditions, various forms of nanostructured materials can be synthesized by the sonochemical method, including metals, alloys, oxides, sulfides, carbides, carbons, polymers, and biomaterials.

### 2.3.1.1 Nanostructured metals prepared by sonochemical synthesis

Sonochemical syntheses of nanostructured noble metals have been explored by a number of groups [161-166]. Sonolysis of water accounts for these sonochemical reductions; more specifically, sonochemically generated  $\text{H}\cdot$  radicals are considered to act as reductants, as shown in Figure 2.8.

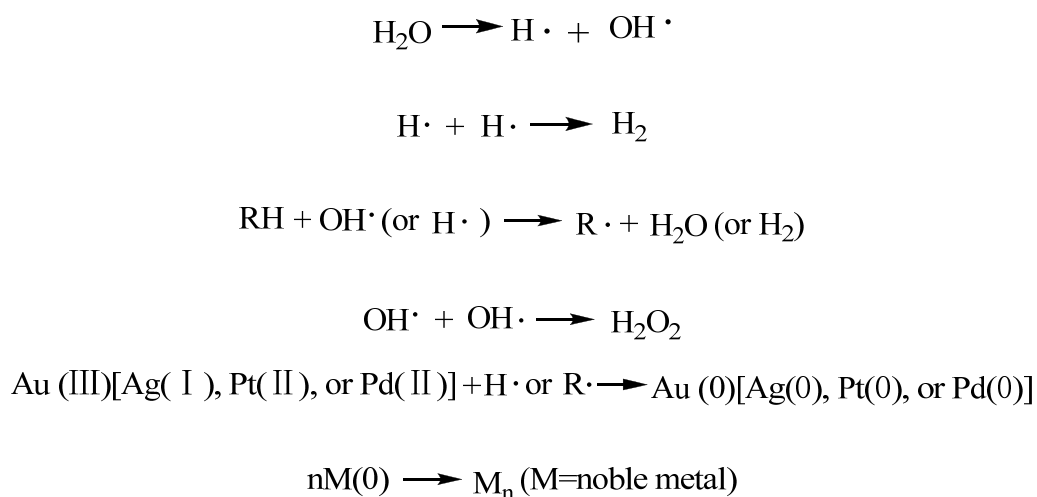


**Figure 2.8** Reaction in the sonolysis of water

Among the studies, Grieser and coworkers carried out a systematic study on sonochemical reduction to unveil the complex reduction mechanism and to understand the effect of each parameter (e.g., time, concentration, ultrasonic frequency, and different

organic additives) on particle size and shape [164, 167–170].

In general, sonochemical synthesis produces spherical metal nanoparticles. But it can also be used in preparing nanowires. Recently, Han and coworkers reported an intriguing result on shape control [161]. In their report, ultrasonic irradiation of an aqueous  $\text{HAuCl}_4$  solution containing  $\alpha$ -D-glucose produced gold nanobelts having a width of 30–50 nm and a length of several micrometers (Figure 2.9). Mechanistic study revealed that ultrasonic irradiation dramatically enhanced the Ostwald ripening process via the ultrasound induced turbulence (e.g., microstreaming and shock waves). Thus, with  $\alpha$ -D-glucose as a structure-directing agent, nanobelts could be formed by merging gold nanoparticles produced at an early stage of sonication.

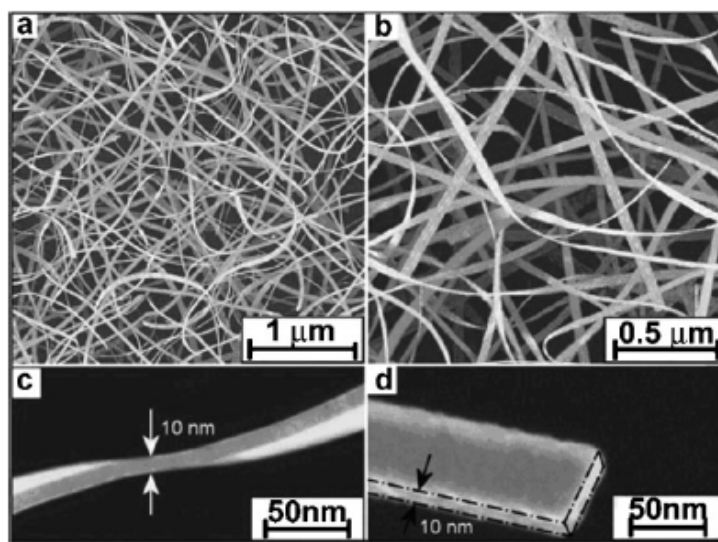


**Figure 2.9** Sonochemically prepared gold nanobelts [161]

Another shape control method using ultrasound was reported by Liz-Marzán and coworkers [171–172]. They synthesized monodispersed gold nanodecahedra with high yield and noticeably increased reproducibility via ultrasound-induced reduction of  $\text{HAuCl}_4$  on pre-synthesized gold seeds in a *N,N*-dimethylformamide (DMF) solution.

### 2.3.1.2 Nanostructured metal oxides prepared by sonochemical synthesis

The advantages of the sonochemical approach over the conventional methods in the synthesis of metal oxides, including more uniform size distribution, higher surface area, faster reaction time, and improved phase purity, have been recognized by many research groups. Examples of successful sonochemical syntheses include  $\text{TiO}_2$  [173],  $\text{ZnO}$  [174-176],  $\text{CeO}_2$  [177],  $\text{MoO}_3$  [178],  $\text{V}_2\text{O}_5$  [179],  $\text{In}_2\text{O}_3$  [180],  $\text{ZnFe}_2\text{O}_4$  [181],  $\text{PbWO}_4$  [182-183],  $\text{BiPO}_4$  [184], and  $\text{ZnAl}_2\text{O}_4$  [185]. Yu and coworkers [173] revealed that sonochemically prepared titania nanoparticles were more photocatalytically active than commercial titania nanoparticles. Such enhancement was attributed to improved crystallinity of titania caused by a faster hydrolysis rate in the presence of ultrasound.

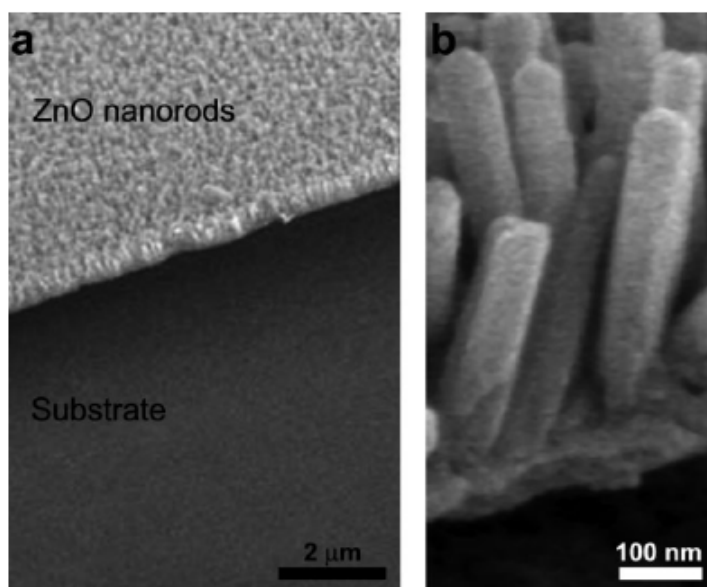


**Figure 2.10** Tilt-view SEM images of vertically aligned ZnO rods produced using sonochemical-induced anisotropic growth of ZnO along the (0001) [186]

The utilization of ultrasound has been further developed for the alignment of nanostructured metal oxides. Recent work by Jeong and coworkers [186] described a robust and rapid synthetic route to prepare vertically aligned ZnO nanorods on a substrate. In their work (Figure 2.10), ultrasonic irradiation rapidly induced anisotropic growth of

ZnO along the (0001) direction on various substrates (e.g., Zn sheet, Si-wafer, glass, and polycarbonate). Compared to conventional approaches, such as a hydrothermal method, the growth rate of ZnO was increased more than tenfold, with an average growth rate of  $500 \text{ nm h}^{-1}$ . Because of the compatibility of this novel synthetic route with various substrates, patterning ZnO nanorods could be easily achieved when this sonochemical synthesis was combined with traditional photolithography processes to localize the initial seeding.

### 2.3.1.3 Nanostructured carbons prepared by sonochemical synthesis

Sonochemistry offers an alternative synthetic route to prepare various nanostructured carbon materials including carbon nanotubes, nano-onions, nanoscrolls, etc. While traditional synthetic methods for such carbon nanostructures require high temperature, high vacuum, high-voltage arc discharge, or high-energy electron beam, the newly developed sonochemical route can be carried out under room temperature and atmospheric pressure and sometimes even without the use of a metal catalyst [187].

Teo and coworkers [187-188] synthesized hydrocarbon nanotubes and nano-onions by sonicating a suspension of HF-etched Si nanowires in common organic solvents such as  $\text{CHCl}_3$ ,  $\text{CH}_2\text{Cl}_2$ ,  $\text{CH}_3\text{I}$ , etc. Ultrasonic irradiation enhances the reactions between  $\text{SiH}_x$  species and organic molecules, resulting in exotic carbon nanostructures. Park and colleagues [189] reported the sonochemical preparation of single-walled carbon nanotubes. The extreme conditions created by ultrasound aid provided sufficient energy for the growth of high-purity carbon nanotubes from the Fe catalyst on the surface of silica powder. In addition to its ambient reaction conditions, this sonochemical process eliminated extra purification processes, opening the possibility of using this method for large-scale production of high-purity carbon nanotubes.

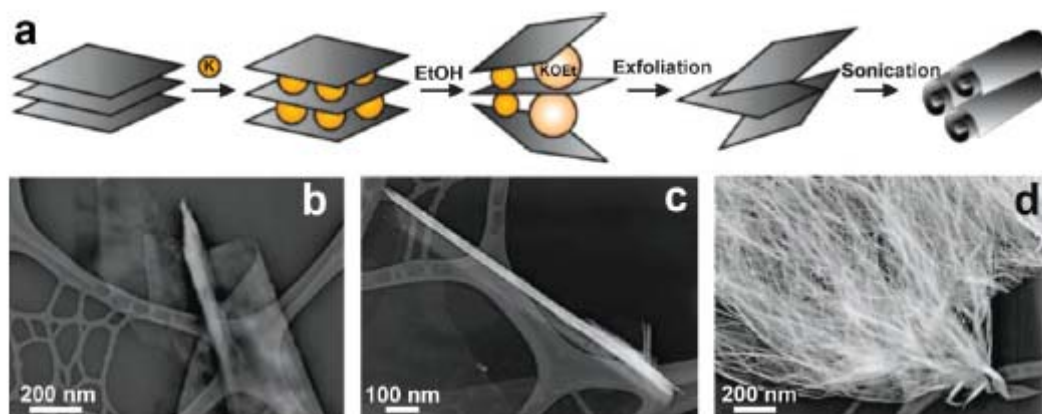


**Figure 2.11** a) Schematic of the intercalation/exfoliation process. Graphite is intercalated with potassium metal and then exfoliated with ethanol to form a dispersion of carbon sheets. Sonication produces carbon nanoscrolls. TEM images of b) a thin plate of graphitic sheets in the process of scrolling, c) an isolated carbon nanoscroll with open ends, and d) a mass of scrolled material, representative of the bulk of the sample. The lighter web pattern in the background of each image is the lacey carbon TEM grid [190]

Besides the direct synthesis of carbon nanostructures from a precursor, ultrasound can induce dramatic morphology changes in pre-synthesized carbon materials. Kaner and coworkers [190] discovered that sonicating a dispersion of exfoliated graphite in ethanol yields carbon nanoscrolls (Figure 2.11) with a high conversion efficiency of 80%.

#### 2.3.1.4 Protein and polymer nano and microstructures prepared by sonochemistry

Applications of ultrasound to materials chemistry have been further developed for biomaterial synthesis, and continually extended to polymers as well [191]. Table 2.3 summarized a few highlights for the preparation of protein and polymer nano and micromaterials.

**Table 2.3** The preparation of protein and polymer nano and micromaterials by ultrasound

Material				Particle size	Method	Ref.
Proteinaceous	microcapsule	filled	with	3 $\mu\text{m}$	Ultrasonic emulsification	192
n-dodecane						
Air-filled microbubble				5 $\mu\text{m}$	Ultrasonic emulsification	193
Proteinaceous microspheres filled with nitroxides				2.5 $\mu\text{m}$	Ultrasonic emulsification	195
Suspensions of albumin and haemoglobin microspheres				1-3 $\mu\text{m}$ (shell 30 nm)	Ultrasonic emulsification	196
Nitroxide and fatty acid mixture encapsulated proteinaceous microsphere				2 $\mu\text{m}$	Electron paramagnetic resonance	197
Arginine–glutamic acid–aspartic acid adhered proteinaceous microsphere				3 $\mu\text{m}$ (shell 100 nm)	Electrostatic adhesion approach	198
Polyglutamate/bovine serum albumin core-shell microsphere				300 nm-1 $\mu\text{m}$	Sonication	199
Polystyrene emulsion				50 nm	Ultrasonic irradiation	200
Fluorescent and phosphorescent latex particle				60 nm	Sonochemical	201
Polysilanes				/	Sonochemical synthesis	202

### 2.3.2 Ultrasonic spray pyrolysis (USP)

In contrast with sonochemistry, where ultrasound directly induces chemical reactions, in ultrasonic spray pyrolysis (USP), the ultrasound is not directly employed in chemical reactions, which are in fact thermally driven. Instead, the role of the ultrasound in USP is to provide the phase isolation of one microdroplet from another. While high intensity ultrasound with a low frequency (typically 20 kHz) is used in sonochemistry, USP generally utilizes lower intensity ultrasound with a higher frequency (e.g., 2 MHz). In USP, ultrasound nebulizes precursor solutions to produce micron-sized droplets that act as isolated, individual micron-sized chemical reactors. In USP, liquid droplets generated



by ultrasonic nebulization are heated in a gas flow, and subsequently solid-phase or sometimes liquid-phase (when precursors melt prior to decomposition or when high boiling point liquids are used) chemical reactions occur.

### **2.3.2.1 Metal salt-based nanocomposites prepared by USP**

A wide variety of nanoparticles have been prepared by ultrasonic spray pyrolysis, including Ni, Ag–Pd, NiO, CeO<sub>2</sub>, ZnO, LiCoO<sub>2</sub>, Y<sub>2</sub>O<sub>3</sub>–ZrO<sub>2</sub>, (Ba<sub>1-x</sub>Sr<sub>x</sub>)TiO<sub>3</sub>, CdS, and ZnS [203-208]. In addition to the versatility of this novel route, the molten salts served as an effective liquid flux to improve mass transport [204].

Zachariah and coworkers synthesized nanoporous metal oxides (e.g. Al<sub>2</sub>O<sub>3</sub> and SiO<sub>2</sub>) via salt-assisted aerosol decomposition [204, 209]. They used intermediate concentrations of salts in the precursor solution, so the structural integrity of nanocrystallites in USP nanocomposite could remain after salt-removal. This strategy to generate porous structures has some real advantages: the in situ templating with salts is inexpensive and non-toxic; the salts can be used with good thermal stability at very high temperatures, and it is even possible to recycle the metal salts.

The hollow interior formation via metal salt templating has also been reported. Brinker and Jiang synthesized mesoporous silica particles with NaCl cores via the aerosol-assisted self-assembly method [210]. In this synthesis, an aerosol process followed by calcination produces a nanocomposite with a cubic single crystal NaCl core surrounded by a mesoporous silica shell, and a subsequent washing procedure removes NaCl to create a hollow cubic cavity. Lu and coworkers employed ferric chloride (FeCl<sub>3</sub>) instead of NaCl to create hollow interiors [211]. In a similar manner, a nanocomposite with a ferric species-rich core surrounded by a silica-rich shell is produced.

### 2.3.2.2 Polymer-based nanocomposites prepared by USP

Colloidal polymer particles have also been utilized as a template material in USP synthesis. Okuyama and coworkers synthesized ordered macroporous (i.e., pores with diameters of >50 nm) silica spheres by employing polystyrene latex particles as a template [212, 213]. In this approach, a dilute colloidal suspension of silica and polystyrene latex was ultrasonically nebulized, and the resulting droplets were carried through heating zones with a temperature gradient. The droplets first passed through a low-temperature zone where a silica/polystyrene nanocomposite was created after solvent evaporation, and in the subsequent high-temperature zone the polystyrene particles of the intermediate nanocomposite were pyrolyzed out as gases, leaving ordered macroporous silica spheres behind.

Combining the macroporosity resulting from a polymer template and the mesoporosity achieved by a surfactant self-assembly was exploited for polymer-based nanocomposites preparation. Brinker and coworkers [214] exploited colloidal polystyrene particles and a surfactant as a structure-directing agent for macroporosity and mesoporosity, respectively. The combination of two different templates turned out to be very effective for creating multiple-sized pores in silica spheres, which were interconnected to each other, and even controlling the pore structures.

The polymer templating strategy has been further developed by Suslick and Suh who utilized an in situ generated polymer template for the preparation of macroporous silica spheres [215]. While the polymer templating method originally developed by the Okuyama research group was robust and simple, it relied on the use of expensive polymer beads for the creation of macroporosity. In Suh's method, however, the polymerization of an organic monomer styrene in the nebulized droplets having silica nanoparticles took

place at the first heating zone held at a low temperature, creating a silica/polystyrene nanocomposite in situ. The nanocomposite was then carried into a second, hotter temperature zone where the in situ generated polymer was pyrolyzed out, producing macroporous silica spheres. The morphology and surface area of the porous silica spheres were also easily controllable by manipulating the ratios of styrene and silica. Furthermore, upon  $\text{Co}_2(\text{CO})_8$  addition to the precursor solutions, the resulting porous silica spheres could possess ferromagnetism, which originated from the  $\text{Co}_2(\text{CO})_8$  decomposition product encapsulated in the silica matrix (Co nanoparticles). Magnetic studies revealed that the porous silica matrix effectively shields the Co nanoparticles from oxidation, allowing the cobalt/silica composite to retain their initial magnetism more than 6 months.

USP has now been successfully revived as a generalized synthetic route for the preparation of nanostructured materials. The synthesis of nanostructured materials via USP-produced nanocomposites is robust and efficient.

### **2.3.3 Ultrasonic method for the preparation of nanochitosans**

Nanochitosan is mainly prepared using chemical reaction approaches, such as gelation and polymerization, assisted by other chemical additives. It is difficult to determine the particle content in the emulsion and avoid the effect of dissolved chitosan as only part of chitosan in the solution. In the water-in-oil method, emulsion-droplet method and core-shell system, these additional chemicals are difficult to remove from the system, and can cause negative effects to the applications. The damage of organic solvents to protein causes limited applications in the biochemical field. A number of spray drying processes were developed [216-219]. However, these preparation procedures were usually complex and the particle size was usually in the micron scale.

Some researchers have studied the ultrasonic method for preparation of nanochitosans. For example, Popa-Nita et al. [220] studied the mechanisms involved during the ultrasonically induced depolymerization of chitosan. Two mechanisms involved in the ultrasonically induced depolymerization of chitosan were proposed: The first induced a rapid and specific scission of polymer chains and a lowering of their polydispersity, the second independent process was responsible for obtaining short polymer chains and oligomers of high polydispersity. A mathematical equation predicting the effect of these mechanisms on the chitosan molecular weight was proposed.

Tang et al. [221] also evaluated the effects of ultrasonication on chitosan molecules and nanoparticles. Molecular weight ( $M_v$ ) of chitosan ( $M_v$  146 kDa and 96% DD) decreased linearly with increasing duration and amplitude of ultrasonication. DD and FTIR absorption were unaffected. The X-ray diffraction (XRD) analysis suggested a greater disarray of chain alignment in the nanoparticle matrix. The chitosan nanoparticles had a mean diameter of 382 nm, polydispersity of 0.53 and zeta potential of 47 mV.

Liu et al. [222] suggested that ultrasonic degradation changed the DD of chitosan with a lower DD (<90%), but not the DD of chitosan with a higher DD (>90%). Baxter et al. [223] suggested that acetylated glucosamine residues was stable under acidic conditions in the presence and absence of ultrasound, but the influence of high-intensity ultrasound on the DD of chitosan in alkaline solutions may be profoundly different.

## **2.4 Applications of chitosan on dye sorption**

### **2.4.1 Dye wastewaters**

Since 1856, when the first synthetic dye was reported, to this day, the use of dyes in industries and households has increased remarkably. There are more than 10,000 dyes

available commercially, and more than  $7 \times 10^5$  tons of dyestuffs are produced annually [224]. The main consumers of dyes are the textile, tannery, paper and pulp, and electroplating industries. It is estimated that 5–10% of the dyes is lost in the effluent during the dyeing process [225], while in the case of reactive dyes, as much as 50% of the initial dye load is present in the dye bath effluent [226-227].

Wastewaters containing dyes are very difficult to treat, since the dyes are recalcitrant molecules, resistant to aerobic digestion, and are stable to oxidizing agents [228]. The treatment of wastewaters is much more difficult when the wastewaters containing low concentrations of dye molecules. In this case, common methods for removing dyes are either economically unfavorable and/or technically complicated. In practice, there is no single process capable of adequate treatment and a combination of different processes is often used to achieve the desired water quality in the most economical way. Thus, there is a need for developing new decolorization methods that are effective and acceptable in industrial use.

Textile effluents are usually treated by physical or chemical treatment processes. They include flocculation combined with flotation, electroflocculation, membrane filtration, electrokinetic coagulation, electrochemical destruction, ion-exchange, irradiation, precipitation, ozonation, and katox treatment methods [229]. However, these technologies are generally ineffective in color removal, expensive and less adaptable to a wide range of dye wastewaters [229].

Adsorption has been considered to be an effective process for color removal from wastewater. The use of activated carbon has been found to be effective, but it is too expensive. Many studies have been undertaken to investigate the use of low-cost adsorbents such as peat, bentonite, steel-plant slag, fly ash, china clay, maize cob, wood

shavings, and silica for color removal [230-232]. However, these low-cost adsorbents have generally low adsorption capacities and require large amounts of adsorbents. Therefore, there is a need to find new, economical, easily available and highly effective adsorbents.

Recently, a number of studies have focused on biomaterials that are capable of adsorbing dyes from wastewaters. Biological materials such as peat, chitosan, yeast, fungi and bacterial biomass, were used as biosorbents to concentrate and remove dyes. The variations in dye structure and their chemistries result in diverse interactions between dye and biosorbent [230, 233]. Adsorption of dyes was dependent on dye properties such as molecular structures and types, numbers and positions of substituents in the dye molecules [234]. There was limited information available on the interactions between biomaterials and dyes which can be explained by the fact that decolorization by biomaterials involved several complex mechanisms such as surface adsorption, ion-exchange, complexation (coordination), complexation chelation and micro-precipitation [230]. Biomaterials usually consisting mainly of polysaccharides, proteins and lipids offered many functional groups. The dyes could interact with these active groups on the material surface in a different manner. Adsorption was increased by the presence of hydroxyl, nitro and azo groups in the dye molecule but decreased by sulfonic acid groups [235]. It is now recognized that adsorption using low-cost biomaterial adsorbents is an effective and economical method for water decontamination. A large variety of non-conventional adsorbents materials have been proposed and studied for their ability to remove dyes [236].

Most textile effluents are produced at relatively high temperatures and hence the temperature will be an important factor in the real applications of biosorption. Arica and

Bayramoglu found that biosorption of dye increased with increasing temperature from 5°C to 35°C [237]. Aksu and Cagatay [238] also observed an increase in uptake of dye with increasing temperature up to 45°C for dried *R. arrhizus* cells showing endothermic character of sorption. Dyeing processes consume large amounts of salt and hence the dye wastewater contains a high salt concentration. For this reason, ionic strength is an important factor. Zhou and Banks [239-240] reported that a high ionic strength led to high biosorption of humic acid by *R. arrhizus*. However, adsorption capacities of *Lentinus sajor-caju* biomass showed no significant effect with increasing NaCl from 0 to 0.5 mol/L [237].

## **2.4.2 Overview of various adsorbents**

Adsorbents such as activated carbon, peat, pith, fuller's earth wood hardwood pith, waste red mud, agricultural byproducts have been used to study their effectiveness in the dye sorption [232]. A desirable adsorbent for the adsorption processes should fulfill a few of criteria: applicable to wide range of colorants, achieving high adsorption capacity and having low toxicity, and being cost effective.

### **2.4.2.1 Activated carbon and other low cost alternatives in dyes sorption**

Activated carbon is one of the most commonly studied adsorbents for adsorption. The principle involved in adsorption using activated carbon is physical adsorption. Moderate to high removal rates of cationic mordant, acid, basic, sulphur, dispersed, direct and reactive dyes by activated carbon have been reported [241]. Despite the high removal rates, activated carbon as an adsorbent has its drawbacks that a large capital is involved, the regeneration cost is high and undesirable odor would be generated during the process [242].

Other low cost alternatives include bagasse pith and wood chips. The use of bagasse pith, a by-product from the sugarcane mills, is favorable to the environment as this enable the idea of utilizing waste to remove waste. The coulombic interaction in the adsorption process promoted good removal abilities of basic and direct dyes. A limitation for choosing bagasse was the problem of the post adsorption disposal. Wood chips were found to be very suitable for the pre-discharge treatment and it was able to adsorb mixed dyes. However, the hard nature of wood chips implies that longer time is required for adsorption. Widely available and cost effective materials such as Maize cob, china clay, refuse derived fuel, chromium waste sludges, coirpith, alum sludges, hyposludge, activated petroleum coke, neem leaf powder, bentonite and modified bentonite, and spent brewery grains have also been reported for commercial potential on color removal [246].

#### **2.4.2.2 Chitosan in dye sorption**

The use of chitosan for dye removal has been studied extensively [244-260]. The adsorption capacity of chitosan depended on its physical structural parameters such as the crystallinity, surface area, porosity, particle type, particle size and water content [243]. Crystallinity is high for both chitin and fully deacetylated chitosan. Compared with conventional commercial adsorbents such as commercial activated carbons, adsorption using chitosan-based materials offered several advantages. In particular, three factors have specifically contributed to the growing recognition of chitosan as a suitable biomaterial for dye removal:

First, chitosan-based polymers are low-cost materials obtained from natural resources and their uses as biosorbents are extremely cost-effective. In many countries, fishery wastes were used as excellent sources to produce chitosan. Since such wastes are abundantly available, chitosan may be produced at relatively low costs. The volume of the sorbent



used is also reduced when compared to conventional adsorbents since the former are more efficient.

Second, chitosan possess an outstanding capacity and a high rate of adsorption, and also high selectivity in detoxifying both very dilute and concentrated dye solutions. They also have an extremely high affinity for many varieties of dyes.

Third, chitosan can be manufactured into films, membranes, fibers, sponges, gels, beads and nanoparticles, or supported on inert materials. The utilization of these materials presents many advantages in terms of applicability to a wide variety of process configurations.

Acid dyes are commonly used in the dyeing of protein fibers like wool and silk and synthetic fibers such as nylon and modified acrylic fibers. The affinity is due to the anionic nature of the dyes. Therefore, chitosan would have high adsorption capacities for acid dyes because the polymers have a high number of amino groups.

The effectiveness of chitin and chitosan to adsorb acid dye molecules has been extensively reported. Recent work on the topic is summarized in Table 2. 4.

### **2.4.3 Sorption mechanisms of dyes onto chitosan**

There are various types of interactions between dyes and chitosan. They are the ion-exchange, van der Waals forces, physical adsorption, aggregation mechanisms, dye-dye interactions, etc. The following four steps are generally involved in the adsorption process:

1. bulk diffusion: migration of dye from the bulk of the solution to the surface of the adsorbent;
2. film diffusion: diffusion of dye through the boundary layer to the surface of the adsorbent;

**Table 2.4** Recent batch studies on sorption of various dyes onto chitosan

Characteristic of chitosan	Particle size	Dye	pH	T/°C	Kinetic model	Adsorption mechanism	Equilibrium model	<sup>a</sup> q <sub>max</sub> /(mmol/g)	Ref.
Crab shell, DD 53%	355-500 µm	Acid Green 25	4	25	N/A	Ionic bonding and hydrogen bonding	Langmuir	1.036	[232]
Crab shell, DD 53%	355-500 µm	Acid Orange 10	4	25	N/A		Langmuir	1.505	[232]
Crab shell, DD 53%	355-500 µm	Acid Orange 12	4	25	N/A		Langmuir	2.778	[232]
Crab shell, DD 53%	355-500 µm	Acid Red 18	4	25	N/A		Langmuir	1.147	[232]
Crab shell, DD 53%	355-500 µm	Acid Red 73	4	25	N/A		Langmuir	1.285	[232]
Cross-linked beads, DD 85%&95%	2.3-2.5 mm	Reactive Red 189	3	30	First-order and	Diffusion	Langmuir	2.089-2.133	[244]
Cross-linked beads, DD 95.5%	2.3-2.5 mm	Reactive Blue 15	4	30	second-order kinetic	Diffusion	Langmuir	0.56	[245]
Cross-linked beads, DD 95.5%	2.3-2.5 mm	Metanil Yellow	4	30		Diffusion	Langmuir	3.56	[245]
Powder, DD 85%	0.177-1.651 mm	Remazol Black B	6.7-9.0	30-60	Pseudo-second-order	Diffusion	Langmuir	0.131	[246]
Shell of prawns, beads	<sup>b</sup> SA: 0.3622	Acid Blue 25	2-12	25	Second-order kinetic	Diffusion	Langmuir	0.429	[247]
Shell of prawns, beads	<sup>b</sup> SA: 0.3622	Acid Red 37	2-12	25	Second-order kinetic	Diffusion	Langmuir	0.729	[247]
Chitosan-glutaraldehyde beads	<sup>b</sup> SA: 1.6413	Acid Blue 25	2-12	25	Second-order kinetic	Diffusion	Langmuir	0.305	[247]
Chitosan-glutaraldehyde beads	<sup>b</sup> SA: 1.6413	Acid Red 37	2-12	25	Second-order kinetic	Diffusion	Langmuir	0.32	[247]
Chitosan-sulphuric acid beads	<sup>b</sup> SA: 1.9847	Acid Blue 25	2-12	25	Second-order kinetic	Diffusion	Langmuir	0.246	[247]
Chitosan-sulphuric acid beads	<sup>b</sup> SA: 1.9847	Acid Red 37	2-12	25	Second-order kinetic	Diffusion	Langmuir	0.271	[247]
Nanoparticles, DD 74%	180 nm	Acid Green 27	4	25	N/A	Electrostatic	Langmuir	2.976	[248]
Powder, protonation	2.3-2.5 mm	Acid Green 25	3	N/A	N/A	N/A	Langmuir	0.843	[249]
Crab shell, cross-linked beads	2.3-2.5 mm	Acid Orange 12	3	30	Second-order kinetic	N/A	Langmuir	5.57	[240]
Crab shell, cross-linked beads	2.3-2.5 mm	Acid Red 14	3	30	Second-order kinetic	N/A	Langmuir	5.86	[250]
Crab shell, cross-linked beads	2.3-2.5 mm	Acid Orange 7	4	30	Second-order kinetic	N/A	Langmuir	5.54	[250]
Crab shell, cross-linked beads	2.3-2.5 mm	Direct Red 81	3	30	Second-order kinetic	N/A	Langmuir	3.527	[250]
Crab shell, cross-linked beads	2.3-2.5 mm	Reactive Blue 2	3	30	Second-order kinetic	N/A	Langmuir	3.226	[250]
Crab shell, cross-linked beads	2.3-2.5 mm	Reactive Red 2	3	30	Second-order kinetic	N/A	Langmuir	3.936	[250]
Crab shell, cross-linked beads	2.3-2.5 mm	Reactive Yellow 2	4	30	Second-order kinetic	N/A	Langmuir	2.790	[250]
Crab shell, cross-linked beads	2.3-2.5 mm	Acid Yellow 86	3	30	Second-order kinetic	N/A	Langmuir	3.206	[250]
Cross-linked beads	2.3-3.8 mm	Reactive 189	3	30	Second-order kinetic	N/A	Langmuir	2.04-2.41	[251]
Chitosan beads	2.3-3.8 mm	Reactive 189	3	30	Second-order kinetic	N/A	Langmuir	1.48	[251]
Wet bead	N/A	Acid Orange 51	N/A	30	Elocich	Chemisorption	Langmuir	0.762	[252]

**Table 2.4** Continued

Characteristic of chitosan	Particle size	Dye	pH	T/°C	Kinetic model	Adsorption mechanism	Equilibrium model	<sup>a</sup> $q_{\max}$ / (mmol/g)	Ref.
Dried bead	N/A	Acid Orange 51	N/A	30	Elocich	Chemisorption	Langmuir	0.574	[252]
Crab Sell, powder, grafting	N/A	Basic Blue 3	3	25	Second-order kinetic	Chemisorption	Langmuir	0.463	[253]
Powder	N/A	Direct Blue	6	26	First-order	N/A	Langmuir	/	[254]
Powder	0.206 mm	Direct Scarlet B	8.47	47.5	N/A	N/A	N/A	0.055	[255]
Flake	6.15±0.13 µm	Reactive Red 4	4	25	Second-order kinetic	N/A	Langmuir	0.173	[256]
Beads, cross-linked	2.0 mm	Reactive Black 5	6	25	N/A	N/A	Freundlich	1.28	[257]
Beads	2.0 mm	Reactive Black 5	6	25	N/A	N/A	Freundlich	0.8	[257]
Beads	2.0 mm	Reactive Black 5	4	25	N/A	N/A	Freundlich	2.4	[257]
Flake	1-1.41 mm	Reactive Blue 222	N/A	30	Second-order kinetic	Chemisorption	Langmuir	0.69	[258]
Swollen beads	2.8 mm	Reactive Blue 222	N/A	30	Second-order kinetic	Chemisorption	Langmuir	0.136	[258]
Flake	1-1.41 mm	Reac. Yellow 145	N/A	30	Second-order kinetic	Chemisorption	Langmuir	0.183	[258]
Swollen beads	2.8 mm	Reac. Yellow 145	N/A	30	Second-order kinetic	Chemisorption	Langmuir	0.862	[258]
Nanoparticles	0.663-1.763 µm	Acid Orange 10	4	25	N/A	Electrostatic	Langmuir	1.77	[259]
Nanoparticles	0.663-1.763 µm	Acid Orange 12	4	25	N/A	Electrostatic	Langmuir	4.33	[259]
Nanoparticles	0.663-1.763 µm	Acid Red 18	4	25	N/A	Electrostatic	Langmuir	1.37	[259]
Nanoparticles	0.663-1.763 µm	Acid Red 73	4	25	N/A	Electrostatic	Langmuir	2.13	[259]
<sup>c</sup> CMCH-Conjugated Fe <sub>3</sub> O <sub>4</sub>	13.5 nm	Acid Orange 12	3	25	Second-order kinetic	N/A	Langmuir	5.36	[260]
<sup>c</sup> CMCH-Conjugated Fe <sub>3</sub> O <sub>4</sub>	13.5 nm	Acid Green 25	3	25	Second-order kinetic	N/A	Langmuir	2.36	[260]

<sup>a</sup> Adsorption capacities in mmol/g<sup>b</sup> Surface area in m<sup>2</sup>/g<sup>c</sup> Carboxymethylated Chitosan-Conjugated Fe<sub>3</sub>O<sub>4</sub>

3. pore diffusion or intraparticle diffusion: transport of the dye from the surface to within the pores of the particle;
4. strong attraction: adsorption of dye at an active site on the surface of material via ion-exchange, complexation and/or chelation [262].

#### 2.4.3.1 Electrostatic interactions

It is recognized that when pH is the main factor influencing the adsorption of acid dye by chitosan, the mechanism is likely to be the ionic interactions of the colored dye ions with the amino groups on the chitosan as shown in Figure 2.12 [259-260].

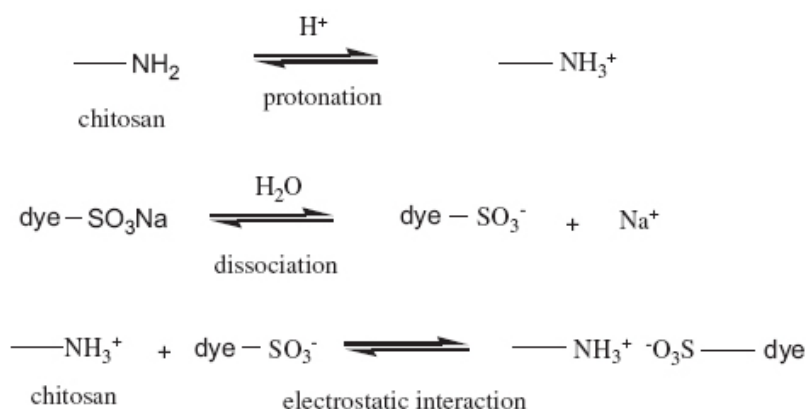


**Figure 2.12** Mechanism of anionic dye adsorption by chitosan in acidic condition [260]

In an acidic medium, the amino groups in chitosan are protonated. The acid dye is dissolved and the sulfonate groups of the acid dye dissociate and are converted to anionic dye ions. Electrostatic attractions between the two oppositely charged ions proceeds.

However, both chitin and chitosan were also effective at higher pH, in which the unprotonated form of the polysaccharide also had affinity for anionic dyes, suggesting that additional attraction forces of interaction were in operation

### **2.4.3.2 Physical surface adsorption**

Surface adsorption is another mechanism of dye molecules being bound to chitosan in which there is a surface reaction between chitosan and the dye molecules. In surface adsorption, the dye molecules are attracted by the charged chitosan surface without any exchange of ions or electrons. The surface adsorption of dye molecules by chitosan was reported to happen under alkaline conditions by physical interactions and chemisorption with Reactive Red 141 [263]. The adsorption of the dye molecule under acidic conditions, however, was only chemisorption. Uzun and Guzel reported that both physical surface adsorption happened on Acid Orange II and chitosan [264]. Gibbs et al. [249] reported the adsorption of Acid Green 25 had two main steps which were the rapid surface adsorption followed by the diffusion and chemisorptions of dye molecules on raw and pre-prontonated chitosan.

### **2.4.3.3 Aggregation**

The aggregation mechanism is a strong type of interaction involved in the chitosan-dye binding. It depends on the pH and affects the diffusion ability of dye molecules to internal porous network by increasing their sizes. Also, the aggregation phenomenon is enhanced by the ionic strength as well as the presence of electrolyte. The quick aggregation of chitosan nanoparticles after interacting with dye molecules was suggested with the replacement of hydrogen bondings between polymer chains by electrostatic interactions between dye molecules and chitosan chains [248]. Gibb et al. [265] showed that there was a relationship between the dye concentration and aggregation. Increasing the dye concentration caused the aggregation of dye molecules, which varied the size of dye aggregates, thus affected the diffusivity to chitosan.

#### 2.4.3.4 Hydrogen bonding

The existence of hydrogen bonding between chitosan and dye was suggested by Wong et al. [232, 266-267] based on the fact that dyes having various chemical structures contributed to different degree of adsorption. They demonstrated the adsorption of dye molecules onto chitosan were attached to chitosan chains in a flat or layered manner, however, the dye molecules were expected to be more spatially oriented in electrostatic interactions between the amino groups in chitosan and the sulphonated groups in the dyes and thus proved that hydrogen bonding contributed to the adsorption.

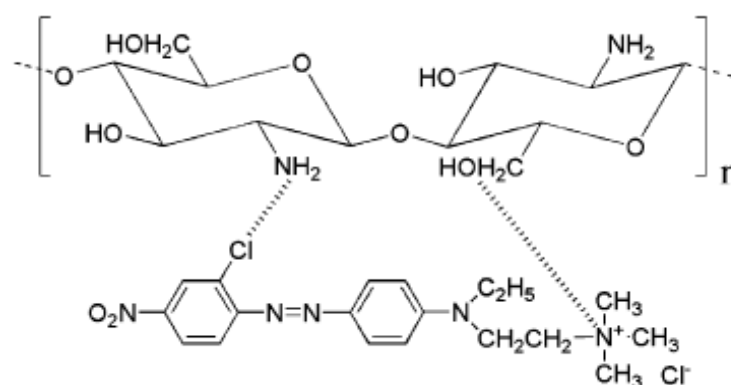


**Figure 2.13** Main interactions between dyes and chitosan in an alkaline solution [268]

Lzaridis et al. [268] studied both chitosan and its derivatives as sorbents for basic dyes. The interactions of dyes with chitosan at pH 10 and 12 were studied. The FTIR results showed that adsorption of the dye on chitosan incurred a clear shift of the broad hydroxyl band around  $3400\text{ cm}^{-1}$  to a lower wavenumber, whereas the amide I band was shifted from  $1665$  to  $1659\text{ cm}^{-1}$ . This was a substantial evidence of hydrogen bond formations between the hydroxyl and amino groups of chitosan with the dye molecules (Figure 2.13).

#### 2.4.3.5 Hydrophilic and hydrophobic interactions

Shimizu et al. showed the involvement of hydrophobic interactions between hydrophobic alkyl groups in dyes and hydrophobic functions in polymer network of crosslinked

chitosan through adsorption of Acid Red 138 [269]. Crini et al. [31, 253, 270] showed that dye adsorption on grafted chitosan was not only due to the ion exchange process but also the dye-dye hydrophobic interactions causing rejection of dye molecules from the dye solution.

Other researchers have observed the adsorption of anionic dyes onto chitosan fitted both the Langmuir (adsorption at specific sites) and the Freundlich (no specific sites, possibility of formation of multi-molecular layers) isotherms [271-272]. It was suggested that adsorption of anionic dyes onto chitin and chitosan occurred through a combination of electrostatic forces, van der Waals interactions, and hydrogen bonding, with the electrostatic forces only having a significant effect at low pH [273].

#### **2.4.4 Parameters affecting sorption**

Many studies showed that the adsorption performances of a chitosan-based material in liquid-phase were affected by the following parameters.

##### **2.4.4.1 Particle sizes**

The adsorption capacity was influenced by the particle size of chitosan. With decreasing particle sizes, the surface area of chitosan increases and the sorption capacity of adsorbent should increase. Piccin et al. [274] reported finer chitosan particles had a higher sorption capacity than larger sized particles. Annadurai et al. [246] observed that when the particle size decreased, the adsorption of acid dyes increased by 10-40%.

##### **2.4.4.2 Initial dye concentrations**

Chen et al. [275] reported that the adsorption of dyes increased with the increase in the initial dye concentration while the amount of adsorbents remained unchanged. They

explained that the higher initial dye concentration provided a higher driving force of dye diffusion due to the higher concentration gradient. However, Singh et al. [276] showed that the adsorption percentage of Reactive Blue H5G with an initial concentration of 400 mg/L on chitosan-graft-poly(methylmethacrylate) was above 90% but decreased to about 60% when the initial concentration was increased to 800 mg/L. They explained the phenomenon by using increasing dye aggregation at a higher dye concentration which led to poor diffusion.

#### **2.4.4.3 pH values**

Lower pH favored adsorption as more protons were available to the amine groups of chitosan to form  $\text{-NH}_3^+$ , thus the electrostatic attractions between negatively charged dye anions were increased [246]. The optimum pH reported was 3-6. For pH lower than this range, the adsorption capacity was lower probably due to the presence of excess  $\text{H}^+$  ions competing with the cation groups on the dye for adsorption sites. For pH above this range, physical adsorption took the lead that the hydroxyl groups were more effective than the amino groups [277].

#### **2.4.4.4 Temperature**

Yoshida et al. and Venkat et al. [278-279] reported that for large dye molecules, high temperatures were favorable for the adsorption as the mobility of the large dye ions was higher. Moreover, the swelling of the chitosan internal structure was more.

However, there were reports showing that the adsorption of dye is exothermic, the physical bonding between the dye and the adsorbent would be weakened at higher temperatures. The phenomenon was very prominent in the sorption of activated carbon [280], activated clay and activated date pits [281]. Dye adsorption using chitosan is



usually exothermic, high temperatures could reduce the sorption capacity although a shorter time was required to require the equilibrium [282].

Most adsorption studies were carried out at 25-70°C. This may be due to high temperature sorption requires high operation costs which are unfavorable in huge scale industrial applications.

#### **2.4.4.5 Molecular mechanisms**

The adsorption capacities were affected by molecular structures of dyes. Some reviews have shown that for anionic dyes, the attraction between the negatively charged sulphonate groups of dyes with positively charged protonated amino groups of chitosan was the dominating adsorption mechanism. However, Filipkowska et al. [283] reported that the adsorption affinity of a dye decreased when the degree of sulphonation increased. If a dye containing a sulphonate group was attached, the binding capacity of the next dye molecule would decrease. They also found that a dye with 10 sulphonate groups had a very low affinity with chitin.

Also, it was not only the number of sulphonate groups in the dye mattered in the adsorption capacity, but also the position of the sulphonate groups in the dye molecule. Cheng et al. reported that anionic dyes with sulphonate groups on benzene were better adsorbed than those with sulphonate groups on naphthalene [284].

#### **2.4.5 Equilibrium isotherm models**

Adsorption properties and equilibrium data, commonly known as adsorption isotherms, describe how sorbents interact with adsorbent materials. They are critical in optimizing the use of adsorbents. In order to optimize the design of an adsorption system to remove dyes from aqueous solutions, it is important to establish the most appropriate correlation

for the equilibrium curve. An accurate mathematical description of equilibrium adsorption capacity is indispensable for reliable prediction of adsorption parameters and quantitative comparison of adsorption behavior for different adsorbent systems (or for varied experimental conditions) within any given system.

**Table 2.5** The Langmuir model and the Freundlich model equations

Isotherm	Equation	Assumptions	Linear form
Langmuir	$q_e = \frac{K_L C_e}{1 + a_L C_e}$	<ul style="list-style-type: none"> <li>➤ Monolayer adsorption</li> <li>➤ The sorption takes place at specific sites within the sorbent</li> <li>➤ Once a dye molecule occupies a site</li> <li>➤ The adsorbent has a finite capacity for the adsorbate (at equilibrium, a saturation point is reached where No further adsorption can occur)</li> <li>➤ All sites are identical and energetically equivalent</li> <li>➤ The adsorbent is structurally homogeneous</li> </ul>	$\frac{C_e}{q_e} = \frac{1}{K_L} + \frac{a_L C_e}{K_L}$
Freundlich	$q_e = K_F C_e^{1/n_F}$	<ul style="list-style-type: none"> <li>➤ Multilayer adsorption</li> <li>➤ The model applies to adsorption on heterogeneous surfaces with interaction between adsorbed molecules</li> <li>➤ The adsorption energy exponentially decreases on completion of the sorptional centres of an adsorbent</li> <li>➤ This is an empirical equation employed to describe heterogeneous systems</li> </ul>	$\ln q_e = \ln K_F + \frac{\ln C_e}{n_F}$

In the equations,  $q_e$  is the solid phase adsorbate concentration at equilibrium (mmol/g),  $C_e$  is the aqueous phase adsorbate concentration at equilibrium (mmol/L),  $K_L$  and  $a_L$  are the Langmuir isotherm constants and  $K_F$  and  $n_F$  are the Freundlich isotherm constants.

The adsorption equilibrium is established when the rate of dye being adsorbed onto the adsorbent is equal to the rate being desorbed. It is possible to depict the equilibrium adsorption isotherms by plotting the concentration of the dye in the solid phase versus

that in the liquid phase. The isotherm shape can also provide qualitative information on the nature of the solute-surface interaction. In addition, adsorption isotherms have been developed to evaluate the capacity of chitosan materials for the adsorption.

There are various kinds of isotherm models including the Langmuir, Freundlich, BET, Toth, Temkin, Redlich-Peterson, Sips, Frumkin, Harkins-Jura, Halsey, Henderson and Dubinin-Radushkevich isotherms [31]. The Langmuir model and the Freundlich model are commonly used in the sorption of dyes onto chitosan. Table 2.5 shows the two most popular equilibrium isotherm equations and their linear forms and equation parameters. Most of the researcher indicated that the Langmuir model fit the sorption of dyes onto chitosan [243-254, 256, 258-260].

#### **2.4.6 Kinetic models**

An ideal adsorbent for wastewater pollution control not only should have a large adsorbate capacity but also a fast adsorption rate. Therefore, the adsorption rate is another important factor for the selection of the material and adsorption kinetics must be taken into account since they explain how fast the chemical reaction occurs and also provides information on the factors affecting the reaction rate.

Two kinds of kinetic models (Table 2.6) have been widely used in the literature for adsorption processes: (i) pseudo-first-order kinetic model; (ii) pseudo-second-order kinetic model [285-286]. The kinetic models are used to examine the controlling mechanism of adsorption process such as adsorption surface, chemical reaction and/or diffusion mechanisms. The parameters of the kinetic models can be obtained by suitable linearization procedures followed by both linear and/or non-linear regression analysis. Recent work by many researchers has shown that non-linear regression gave a more

accurate determination of parameters than linear methods [246-248, 250-251, 253, 258, 256, 260].

**Tale 2.6** The kinetic models and their linear forms

Model	Equation	Linear form
pseudo-first-order kinetic model	$\frac{dq_t}{dt} = k_1(q_e - q_t)$ $\lg\left(\frac{q_e}{q_e - q_t}\right) = \frac{k_1}{2.303}t$	$\lg(q_e - q_t) = \lg q_e - \frac{k_1}{2.303}t$
pseudo-second-order kinetic model	$\frac{dq_t}{dt} = k_2(q_e - q_t)^2$ $\frac{1}{q_e - q_t} = \frac{1}{q_e} + k_2t$	$\frac{t}{q_t} = \frac{1}{k_2 q_e^2} + \frac{1}{q_e}t$

In the equations,  $q_e$  is the sorption capacity (mmol/g) at equilibrium and  $q_t$  is the sorption capacity (mmol/g) at time  $t$  and  $k$  is the rate constant of pseudo-second.

## 2.5 Applications of chitosan on dyeing

Much research has been performed on textiles to improve their dye uptake and fastness properties. One of the approaches was to introduce cationic sites onto the substrates for better affinity with anionic dyes [287-295].

Chitosan, containing two main functional groups, namely hydroxyl and amino groups, can easily absorb anionic dyes, such as direct, acid, and reactive dyes by electrostatic attraction. It was found that chitosan could enhance the uptake of dyes and increase dye sorption on fabrics [33, 296-304]. Table 2.7 summarizes the previous work on using chitosan to improve dyeing properties of textiles.

**Table 2.7** The applications of chitosan on fabrics dyeing

Fabric	Finish agent	Dye	Effect and results	Ref.
Cotton	Chitosan solution	Lac dyes	Significant enhancement of dye uptake onto cotton was achieved.	302
Cotton	Lattices based on acrylate, chitosan and polyethylene glycol emulsion	Direct dyes	Appropriate antibacterial activity for <i>E. coli</i> , good ultraviolet-protection and excellent dyeing performance were obtained.	305
Cotton	Chitosan solution	Reactive Blue 19, Reactive Blue 5, Reactive Blue 4, and Sumifix Supra Navy Blue 2GF	Highest take-up was achieved by pad-dry method.	306
Cotton	Chitosan solution	Yellow gold 2 KX, Active Red 6c	Color intensity was improved. Fastness did not change.	307
Cotton	Chitosan solution	Evercion Blue H-ERD, Remazol Red RB133	Dye uptake of fabric was improved.	308
Cotton	Chitosan solution	Green Tea Extraction	Better dyeing and higher UV protection property was obtained	309
Polyester/ cotton blends	Corona and chitosan solution	Ostazin Red H3B (Reactive dye), Sirius Red F3B (Direct dye)	Color intensity was enhanced, especially with polyester fiber.	310
Wool	Chitosan solution	Lanasol Red 2G	The higher of the viscosity, the greater of the shrink resistance.	311
Wool	Chitosan solution	Acid dyes and reactive dyes	Color strength increased.	312
Wool	Corona and chitosan solution	Supramin Red GG (Acid Orange 19)	Wettability and dyeability of wool were improved.	313
Wool	Chitosan solution	Reactive Red 184	The higher the concentration of chitosan/surfactant added, the greater was the color strength of the dyed wool fabrics.	297
Silk	Graft the chitosan on to silk	Acid Black NBB	Higher dye ability was achieved.	314
<sup>a</sup> PET fabric	Chitosan solution	/	The dye uptake increased and the dyeing time reduced.	315
PP	Chitosan solution	Direct Red 80	Wettability, dyeing behavior and reactivity were improved.	316
Polyester polyamide	Chitosan solutions	/	The color intensity increased and the color resistance increased.	33

<sup>a</sup>PET: Poly(ethyleneterephthalate)<sup>b</sup>PP: Polypropylene.

### 2.5.1 Applications of chitosan on cotton dyeing

Anionic dyes have a low affinity to the cotton fiber because cotton fibers develop anionic surface charge (zeta potential) in water. The charge repulsion between dyes and cotton can be overcome by adding an electrolyte, such as sodium chloride or sodium sulfate, which screens the surface charge of cotton. However, the large amount of salts required in dyeing can cause serious pollution. As an attempt to reduce the use of salts, a number of researchers have cationized cotton fibers through chemical modifications with compounds containing cationic groups. Most of the chemicals used for the cationization of cotton are not environmentally safe. Therefore, the use of chitosan, a polycationic biopolymer, could be more environmentally safe and eco-friendly. A number of studies on cotton dyeing using chitosan as a finishing agent have been carried out to improve the dye uptake and fastness properties [302-306].

Rattanaphani et al. [302] studied the adsorption and thermodynamic of lac dyeing on cotton pretreated with chitosan under dyeing conditions of pH 3.0. Their batch equilibrium studies showed that the adsorption could be described by the Langmuir isotherm. The pretreatment of cotton with chitosan provided a significant enhancement of dye uptake onto the cotton and also a decrease of dye concentration in the dye solution. Saxena et al. [303] found that chitosan enhanced the uptake of lac dye and increased lac dye sorption on cotton.

Direct and reactive dyes are widely used for the dyeing of cotton. Lim et al [304] applied a chitosan derivative to cotton fabric and found that the color yield was higher than that on the untreated cotton.

It was suggested that the application of chitosan to cotton could reduce the uses of dyes

and dyes in wastewaters due to the increased dye exhaustion. The washing and wet rubbing fastness of chitosan-treated fabric was reduced by about one grey-scale step, and the dry rubbing fastness was not affected. The amount of salt required in the dyeing was also decreased by about 50% to that of untreated fabric [306].

### **2.5.2 Applications of chitosan on wool dyeing**

In wool finishing, chitosan has been used as a shrink resist agent [299, 317-320] and as an agent for improving the dyeability of wool [296-298, 311-312].

The most difficult task to control in dyeing wool fabric was its color strength and dyeing fastness. The dyeing quality of dyed wool fabrics was increased by pretreating the wool fabrics with chitosan in a nonionic surfactant, which fortified its bonding with the wool fabric surface [296]. Jocit et al. [298] applied chitosan to wool and observed an improvement in color strength on the chitosan treated wool. The study offered the possibility of producing deeper and more vivid colors without increasing the concentration of dye used. In addition to better exhaustion, the fixation of reactive dye measured by stripping in ammonia is also improved, which could assist in solving the problem of lowering wet fastness in dyeing of wool.

Yen et al. [297] also applied chitosan in reactive dyeing of wool fabrics. The results showed that the presence of the polymer enhanced the color strength when dyed at 50°C but little change was observed when dyed at 80°C. The higher the concentration of chitosan added, the greater was the color strength of the dyed wool fabrics. The optimum amounts for dyeing were found to be 0.5% chitosan. The washing fastness of the dyed wool fabrics was in the range of grey-scale scale 4-5, the dry rubbing fastness was in the range of 4-5, and the wet rubbing fastness was in the range of 3-4. Pascual et al. [311]

found that in some cases the chitosan application could obviate the need for auxiliaries in the dyeing bath, which could be economically advantageous.

### 2.5.3 Applications of chitosan on silk dyeing

In recent years, attempts have been made to make use of natural polymers such as chitin, alginate and silk by surface modification to improve their properties [321-323]. Chitosan finishing on silk is an effective method to improve the properties of silk including antibacterial property, dyeability, wrinkle-resistance property, biocompatibility and so on [324-325].

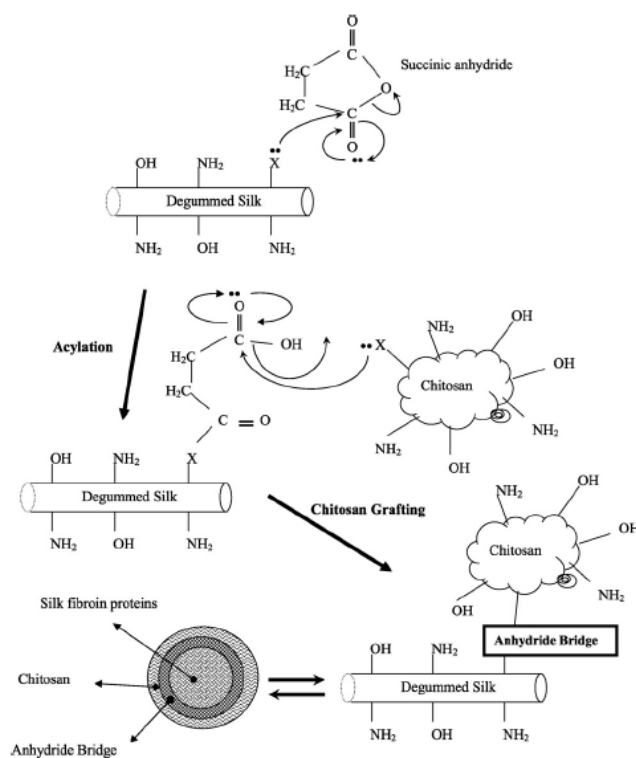


**Figure 2.14** The grafting mechanism between degummed silk and chitosan using succinic anhydride as a bridge (X = OH and NH<sub>2</sub>) [314]

Davarpanah et al. [314] prepared chitosan-grated silk fabric and studied the FT-IR spectra of samples. The researcher confirmed the formation of amide functional groups. The SEM images were in good agreement with the FT-IR spectra. Also the results of dyeing the raw, acylated and chitosan grafted-acylated samples supported the FT-IR and SEM



findings. Figure 2.19 shows the grafting mechanism between degummed silk and chitosan using succinic anhydride as a bridge. The chitosan-grafted chitosan material successfully combined the advantages of the two materials.

Lu et al. [326] prepared nanochitosan emulsions by an ionization gelation method and the chitosan nanoparticles with an average size of 20.8 nm were obtained. The silk samples were immersed in the aqueous treatment solution at 40°C for 30 min at a liquor ratio of 50:1 padded at a 90% wet pick-up. After these processes, the samples were dried at 80°C for 5 min and then cured in a laboratory oven at 160°C for 3 min. The treated samples were then washed with tap water and washed further in deionized water in an ultrasonic cleaner for 5 min to remove the unfixed materials. The antibacterial efficacy of the silk fabric treated with the chitosan nanoparticle dispersion solution was better than that of the fabric treated with chitosan solution and significantly better than that of the untreated fabric. The bacterial reductions of the silk fabric treated with nanochitosan against *S. aureus* were more than 90%, even after 20 launderings. Meanwhile, the chitosan nanoparticle treatment also improved the breaking strength and the wrinkle-resistance properties of the finished fabrics. However, the disadvantage for the finished fabrics treated with the nanochitosan dispersion solution was that the treatment resulted in yellowness in the fabrics. Lu et al. also applied chitosan/TiO<sub>2</sub> composite to the silk fabric. It was found that the dye uptake of acid dyes and reactive dyes, dye fixation of reactive dyes, the dye depth of acid dyes and reactive dyes on the finished silk fabric all increased after treatment [327].

#### **2.5.4 Applications of chitosan on nylon dyeing**

nylon is usually dyed with anionic acid dyes under weak acidic condition [328, 329]. The dyeing process is a simple anion exchange process in which the amino group in nylon is

protonated by the counter ion such as acetate and the counter ion is exchanged for a dye anion. Therefore, the dyeability of the nylon with acid dye is greatly relying on the amino groups content of nylon which acted as the dyesites. The amino group content of nylon is around 45 mmol/kg, but might vary from 15-90 mmol/kg. Comparing to the amino group content of wool which is around 820 mmol/kg, the limited amino group content in nylon makes it easily to be saturated and poses the problem in dyeing deep shade as the amount of dye that saturated all the amino group dyesites is insufficient to give the high depth of color.

### 2.5.4.1 Interactions between acid dyes and nylon

#### 2.5.4.1.1 Electrostatic forces between nylon and acid dyes

nylon is normally dyed with anionic acid dyes in a weak acidic solution. The process is a simple anion exchange process as shown below in Figure 2.15.

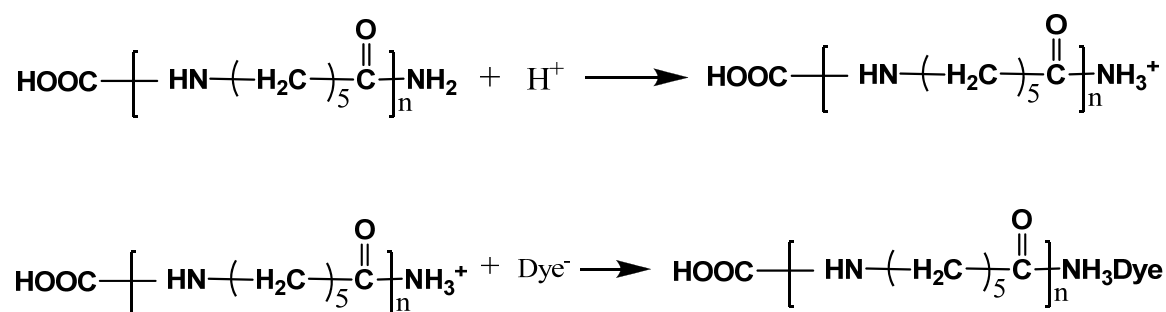


**Figure 2.15** Electrostatic forces between nylon and an acid dye

The dye anions react with charged cationic groups in the nylon polymer chain and are bound by electrostatic forces. The presence of acid in the dye-bath enables the severing of salt linkages between the molecular chains and thereby increases the available number of positively charged sites [330]. At the isoelectric point of nylon, there should be equal amount of negatively-charged acid and positively-charged amine end groups [331]. When the nylon fabrics are placed into acidic solution, the ionization of the carboxylic acid

groups decreases, leaving the nylon fiber having net positive charges. The positively charges on the nylon fiber is firstly neutralized by the acid anions which are rapidly moving and then displaced by the high affinity dye anions which were slowly moving.

The amino group content of nylon is around 45 mmol/kg which is far lower than 820 mmol/kg in wool. Therefore, when dyeing with acid dye, nylon is easily saturated due to its limited amino group content and it poses the problem on dyeing deep shade. The degree of sulphonation of acid dyes determined the saturation point of nylon. It is easier of the nylon fabric to be saturated when there are more sulphonate groups in each dye molecule. Theoretically, one mono-sulphonated dye could interact with one amine end group. One di-sulphonated dye could interact with two amine end group while one tri-sulphonated dye could interact with three amine end group. As a result, the dye uptake to reach saturation of a mono-sulphonated dye would be twice of di-sulphonated dye and triple of tri-sulphonated dye.

#### 2.5.4.1.2 Hydrophobic interaction

Hydrophobic interaction was caused by the effect of the non-polar part of water-soluble solute on the structure of water. When dye molecules are dissolved in aqueous solution through a relevant solubilizing group (i.e. sulphonate groups), the structure of water needs to be changed for accommodating the non-polar or hydrophilic residues (i.e. hydrocarbon). The change in structure of water results to gain entropy for the whole system. As a result, the dye molecules that have been absorbed by the fiber would be prevented from migration back to the dye solution because of the hydrophobic interaction. Since most of the dyeing processes are restricted to aqueous system, therefore, hydrophobic interactions is important in determining the dye uptake of fiber and the wet fastness.

#### **2.5.4.2 Application of chitosan on nylon for dyeing enhancement**

Pretreatment of nylon fabrics with chitosan could improve its dyeing properties. The depth of dyeing would be higher. The capillary and sorption properties of the fabrics were also improved due to swelling of the chitosan film on the fiber [39].

Manyukova et al. [33] found that chitosan formed a film on the surface of nylon and changed the properties of the material. Additional bonds of dye with fiber and chitosan were formed, and the affinity of the dye for the fiber also increased. The treatment with chitosan increased the resistance of the colors to do into water especially in laundering.

## **Chapter 3 Preparation and Characterization of Nanochitosan Emulsions**

### **3.1 Research background**

As described in Section 2.2, a lot of research work has been performed on the preparation of chitosan nanoparticles. However, there are some limitations in those methods, such as the difficulty in determining the particle content in the emulsion, and in removing additive chemicals from the system.

Meanwhile, ultrasound has become a widely used tool in the preparation of nanomaterials [157-215], with its particular ability in breaking up aggregates and reducing the size and polydispersity of particles, and even breaking the chemical bonds through the ultrasound cavitation [332]. Breakdown of polymers into smaller particles using ultrasound has been reported [333-334]. A similar attempt was also performed on chitosan. Tang et al. [221] evaluated and correlated the effects of ultrasonication on the properties of chitosan nanoparticles prepared by the ionotropic gelation method. However, most applications of ultrasound on chitosan focused on the degradation of chitosan [222-223, 235-336], no method directly using ultrasound for nanochitosan preparation has been reported.

We have developed a simple way to breakdown chitosan solid into size-controlled nanoparticles in deionized water without adding other assistant agents. By this method, a pure and stable emulsion, containing only chitosan and water, was achieved with a uniform particle size from 150 nm to 800 nm. The morphological character of the particle was studied by scanning electron microscope (SEM), transmission electron microscopy (TEM) and atomic force microscopy (AFM). The changes in molecule weights, particle

sizes, degree of deacetylation and crystallinity of nanochitosan prepared at different ultrasound duration will be discussed.

## **3.2 Materials**

Chitosan with 95% DD was purchased from Haidebei Co. Ltd. Other chemicals were purchased from Aldrich Co. Ltd. and used as received. The deionized water (DI water) used in experiment was obtained using a TKA GmbH water purification system.

## **3.3 Preparation of nanochitosan emulsions**

Typically, 1.5 g of chitosan was dissolved in a dilute acetic acid solution of 1% (w/v) under magnetic stirring. A NaOH solution (3 mol/L) was then added dropwise into the chitosan solution to precipitate the chitosan. The obtained gel-like swollen chitosan was then washed to neutral with DI water. All the collected chitosan was dispersed into 500 mL of DI water and then transferred into 25-mL flasks. A Sonics VC120 ultrasonic processor with a probe of 6 mm in diameter was used. The ultrasonic probe was put into the flask with a depth of 20 mm under the surface and the power was set at 40 W. Ultrasonic treatments were conducted at different duration in ice-water bath; finally, a milky stable emulsion was obtained.

In order to prepare the nanochitosan emulsions with homogenous nanoparticles, we used the factorial design to study the experiment conditions and suitable parameters for the experiment.

### 3.3.1 Using factorial design to study experiment conditions for nanochitosan

Factorial experiments are experiments that investigate the effects of two or more factors or input parameters on the output response of a process. The factorial experiment design, or simply factorial design, is a systematic method for formulating the steps needed to successfully implement a factorial experiment. Estimating the effects of various factors on the output of a process with a minimal number of observations is crucial to being able to optimize the output of the process.

In a factorial design, the effects of varying the levels of the various factors affecting the process output are investigated. Each complete trial or replication of the experiment is taken into account all the possible combinations of the varying levels of these factors. An effective factorial design ensures that the least number of experiment runs are conducted to generate the maximum amount of information about how input variables affect the output of a process.

**Table 3.1** Factors for the factorial design experiment

Factors	Low	High
Time*	10 min	60 min
Concentration*	0.3% (w/v)	0.5% (w/v)
Power*	25 watts	57 watts
Pulser*	on	off

Time\* represents the ultrasonic duration

Concentration\* represents the concentration of the original chitosan suspension

Power\* represents the intensity of the ultrasound

Pulser\* represents the interval every 20 seconds

In this study, the particle size was studied by a Zetasizer 3000HSA equipped with a 125 mW laser operating at  $\lambda = 633$  nm. Each measurement was run 3 times. The particle size

was characterized by the Z-average size. The uniformity was characterized by the polydispersity index (PDI) of particle size data. The uniformity was considered acceptable when it was below 0.3.

In order to find the conditions which affect the particle size mostly, a factorial design, with four factors and 4 replicates, was created (shown in Table 3.1).

The objectives of the experimental design were:

- Determining which variables were most influential on the output y (the size of nanochitosan)
- Determining the nature of the relationships between the input variables (different conditions) and the output variable y
- Determining where to set the influential x so that y was near the nominal requirement (uniform particles with particle size equal to or less than 500 nm)

The factorial design for the experiment is listed in Table 3.2.

The analysis (software edition: Minitab 14) of the results showed that:

all of the four factors including ultrasonic duration, the concentration of the original chitosan suspension, the intensity of the ultrasound, the pulser (the interval every 20 seconds) were significant. Figure 3.1 and Figure 3.2 show the main effects plot for size and interaction plot for size respectively.

The main effects plot indicated that all the three of the four factors had similar effects on size. For time, power, and pulser, size decreased as the three factors moved from the low level to the high level. For the concentration (con.), the size increased as the factor moved from the low level to the high level.



**Table 3.2** Factorial design, with four factors, and four replicates

StdOrder	RunOrder	CenterPt	Blocks	Time/min	Con./%	Power/w	Pulser	Size/nm
30	1	1	2	60	0.5	57	on	277.6
19	2	1	2	10	0.3	25	off	758.8
20	3	1	2	60	0.3	25	on	423.5
29	4	1	2	10	0.5	57	off	404.3
28	5	1	2	60	0.3	25	on	419.1
23	6	1	2	10	0.3	57	on	558.3
32	7	1	2	60	0.3	57	off	153.5
26	8	1	2	60	0.5	25	off	277.6
21	9	1	2	10	0.5	57	off	412.4
27	10	1	2	10	0.3	25	off	681.0
25	11	1	2	10	0.5	25	on	956.2
22	12	1	2	60	0.5	57	on	293.8
18	13	1	2	60	0.5	25	off	337.0
31	14	1	2	10	0.3	57	on	602.9
17	15	1	2	10	0.5	25	on	929.4
24	16	1	2	60	0.3	57	off	146.7
14	17	1	1	60	0.5	57	on	330.3
3	18	1	1	10	0.3	25	off	640.5
4	19	1	1	60	0.3	25	on	417.8
12	20	1	1	60	0.3	25	on	426.7
15	21	1	1	10	0.3	57	on	518.3
11	22	1	1	10	0.3	25	off	704.2
7	23	1	1	10	0.3	57	on	496.0
1	24	1	1	10	0.5	25	on	1105.2
2	25	1	1	60	0.5	25	off	275.6
8	26	1	1	60	0.3	57	off	123.5
16	27	1	1	60	0.3	57	off	130.8
5	28	1	1	10	0.5	57	off	412.4
6	29	1	1	60	0.5	57	on	293.8
9	30	1	1	10	0.5	25	on	1238.4
13	31	1	1	10	0.5	57	off	473.0
10	32	1	1	60	0.5	25	off	265.3

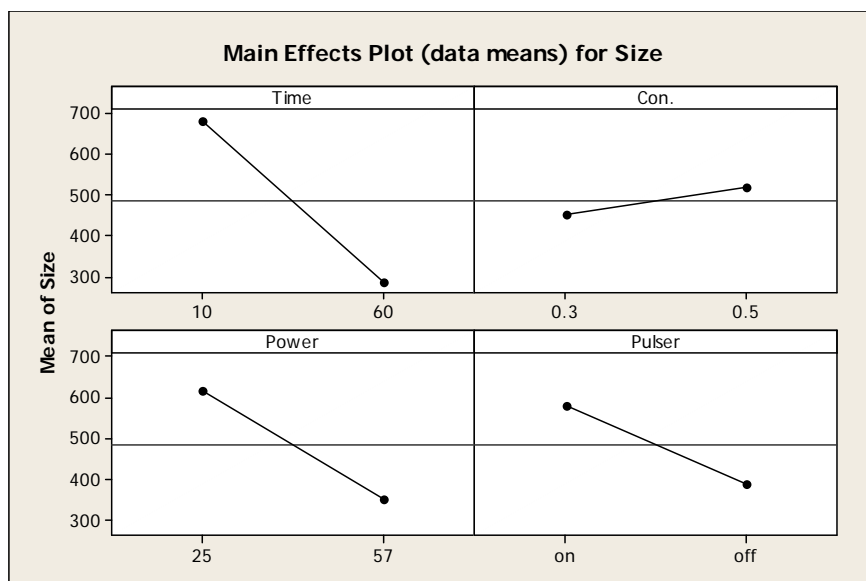


**Figure 3.1** Main effects plot for size

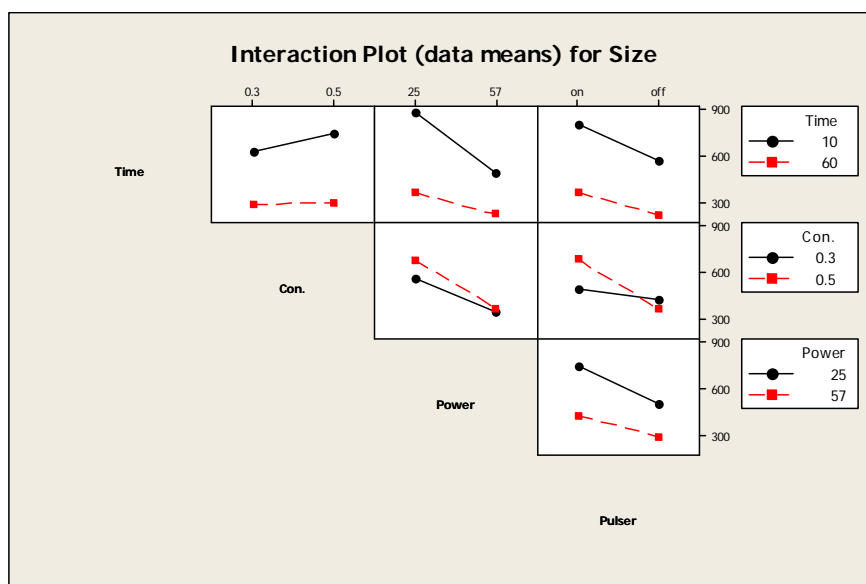


**Figure 3.2** Interaction plot for size

The surface plots and contour plots of size versus concentration, time (software edition: Minitab 14) are shown in Figures 3.3-3.4. From the surface/contour plots, we could get the approximate particle size when we chose different experiment conditions. In order to prepare nanochitosan with a certainty of particle size and concentration, we could choose a different experiment condition from the surface plot or the contour plot.

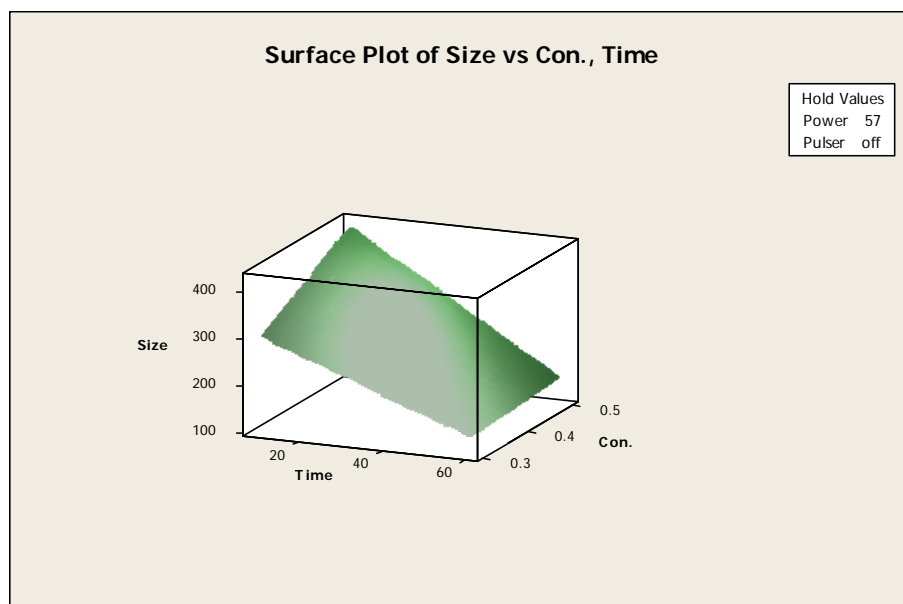


**Figure 3.3a** Surface plot of size versus concentration, time

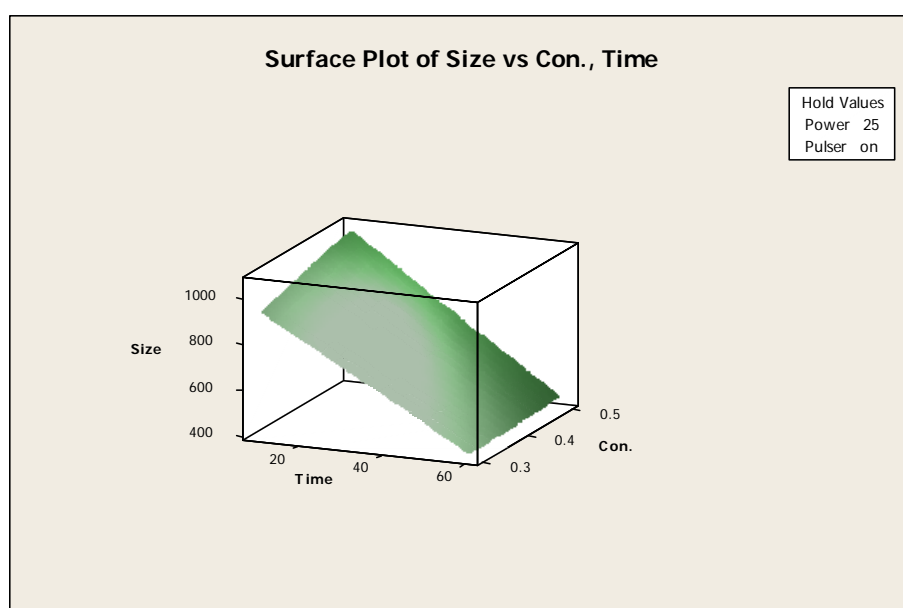


**Figure 3.3b** Surface plot of size versus concentration, time

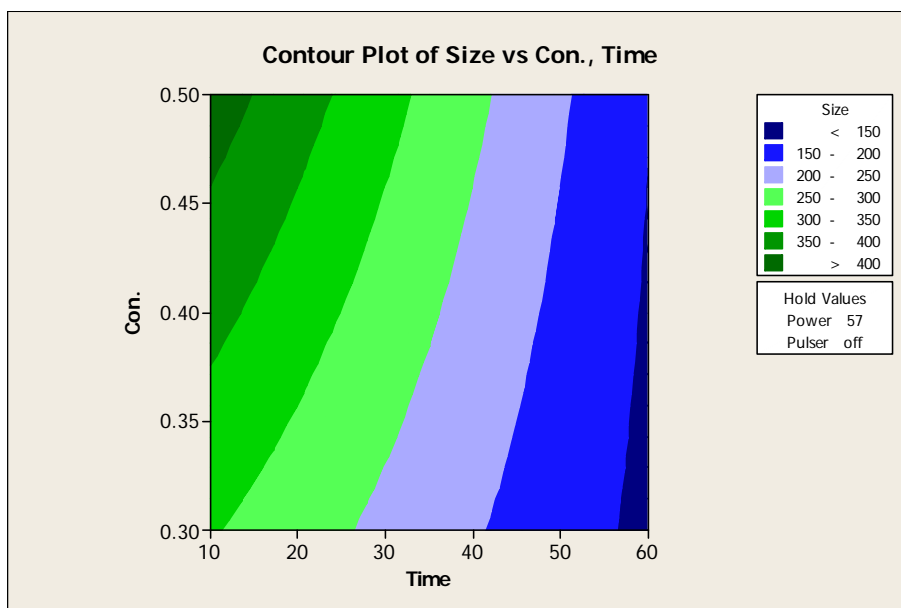


**Figure 3.4a** Contour plot of size versus concentration, time

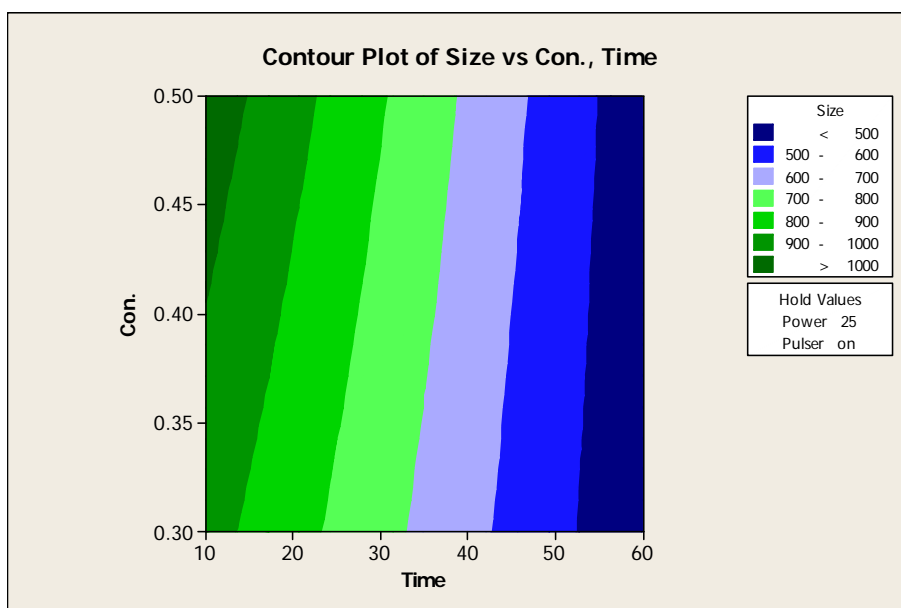


**Figure 3.4b** Contour plot of size versus concentration, time

### 3.3.2 Uniformity optimization with central composite design

The particle size of the emulsion was characterized by the Z-average size. The uniformity was characterized by the polydispersity index (PDI) of particle size data. The uniformity was considered acceptable when it was below 0.3.

Popa-Nita et al. [220] studied the mechanisms involved during the ultrasonically induced depolymerization of chitosan. Two mechanisms involved in the ultrasonically induced depolymerization of chitosan were proposed: The first induced a rapid and specific scission of polymer chains and a lowering of their polydispersity, the second independent process was responsible for obtaining short polymer chains and oligomers of high polydispersity. The two step mechanisms indicated that the uniformity should be optimized by using central composite design.

During the experiment, it was found that the uniformity was often above 0.3 when the concentration was above 0.5%. But in order to use the emulsion in the following applications, it was necessary to produce nanochitosan emulsion with the concentration above 0.3% which is the higher the better. It was also found that when the time (ultrasonic duration) was shorter than 15mins or longer than 60mins or the power was too high or too low, the uniformity was often not acceptable. A central composite design was used to get the uniformity optimization. The factors are listed in Table 3.3 and the central composite design is listed in Table 3.4.

The surface and contour plot of uniformity versus concentration and time are shown in Figures 3.5-3.6. And the surface and contour plots of uniformity versus power, concentration are shown in Figures 3.7-3.8.

From the contour plots and surface plots, the optimal condition for preparing nanochitosan

emulsions with uniform particle sizes could be obtained. For example, to prepare a nanochitosan emulsion with a uniform particle size of 200 nm at a concentration of 0.4%, we could choose a power at the high level of 57 W and the ultrasonic duration of 40 minutes. Although the condition was limited by the special apparatus used, the factorial design and uniformity optimization provided a method to obtain experimental conditions to control the particle size of the nanochitosan in emulsion.

**Table 3.3** Factors for uniformity optimization

Factors	Low	High
Time	10 min	60 min
Concentration	0.3% (w/w)	0.5% (w/w)
Power	25 Watts	57 Watts

**Table 3.4** Central composite design for nanochitosan preparation

StdOrder	RunOrder	PtType	Blocks	Time/min	Con./%	Power/W	Size/nm	Uniformity
13	1	-1	1	35	0.40	14.09	626.3	0.411
6	2	1	1	60	0.30	57.00	255.3	0.335
5	3	1	1	10	0.30	57.00	307.9	0.563
1	4	1	1	10	0.30	25.00	710.5	0.428
15	5	0	1	35	0.40	41.00	382.6	0.174
16	6	0	1	35	0.40	41.00	402.7	0.119
14	7	0	1	35	0.40	41.00	399.1	0.205
3	8	1	1	10	0.50	25.00	836.0	0.568
4	9	1	1	60	0.50	25.00	313.3	0.326
9	10	0	1	35	0.40	41.00	384.8	0.226
12	11	0	1	35	0.40	41.00	399.2	0.138
11	12	-1	1	35	0.23	41.00	340.2	0.198
10	13	0	1	35	0.40	41.00	406.7	0.105
7	14	1	1	10	0.50	57.00	438.4	0.369
2	15	1	1	60	0.30	25.00	293.5	0.365
8	16	1	1	60	0.50	57.00	178.4	0.302

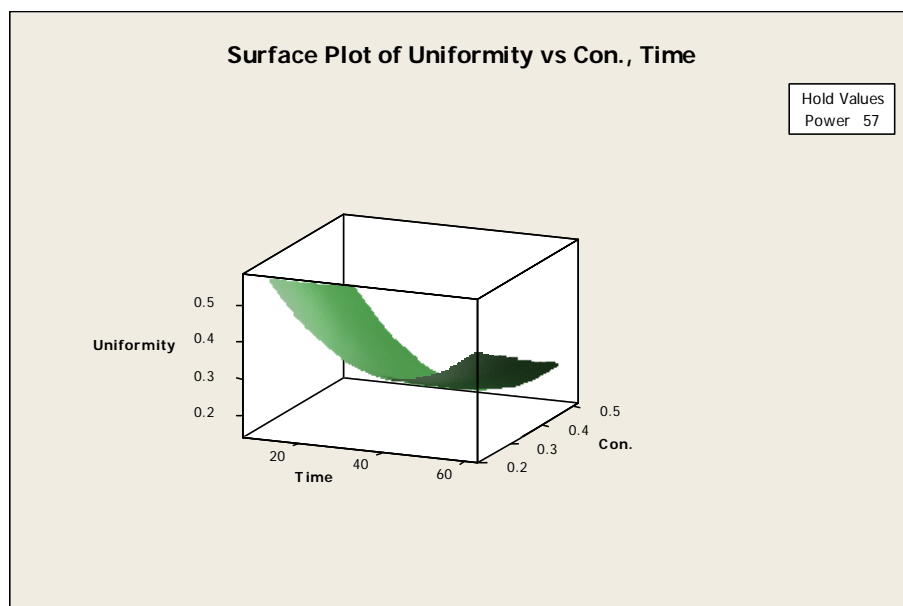


**Figure 3.5a** Surface plot of uniformity versus concentration, time

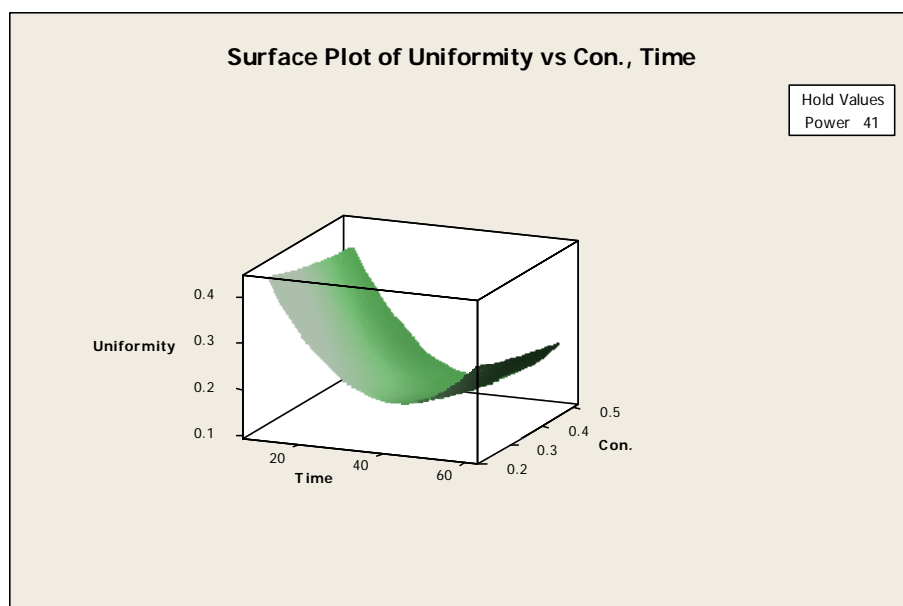


**Figure 3.5b** Surface plot of uniformity versus concentration, time

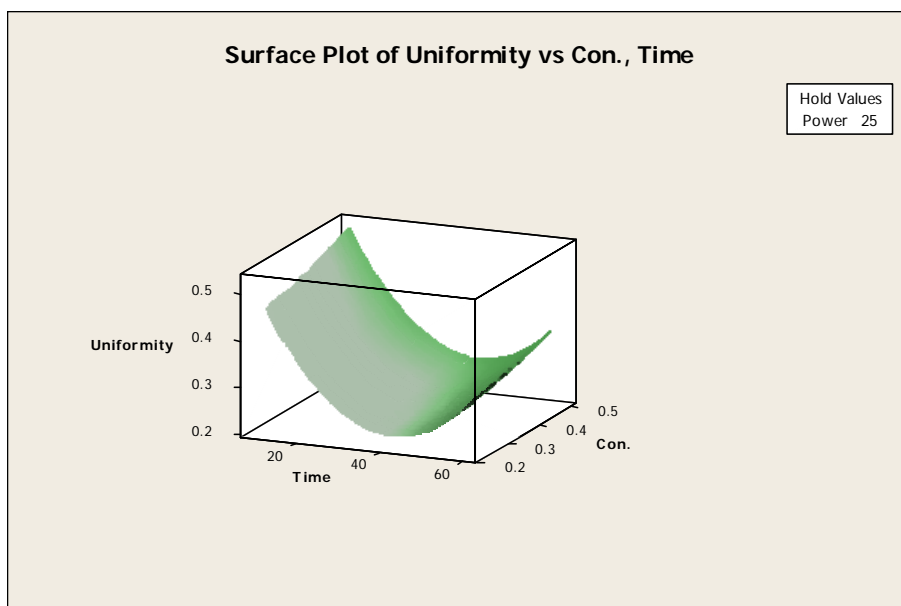


**Figure 3.5c** Surface plot of uniformity versus concentration, time

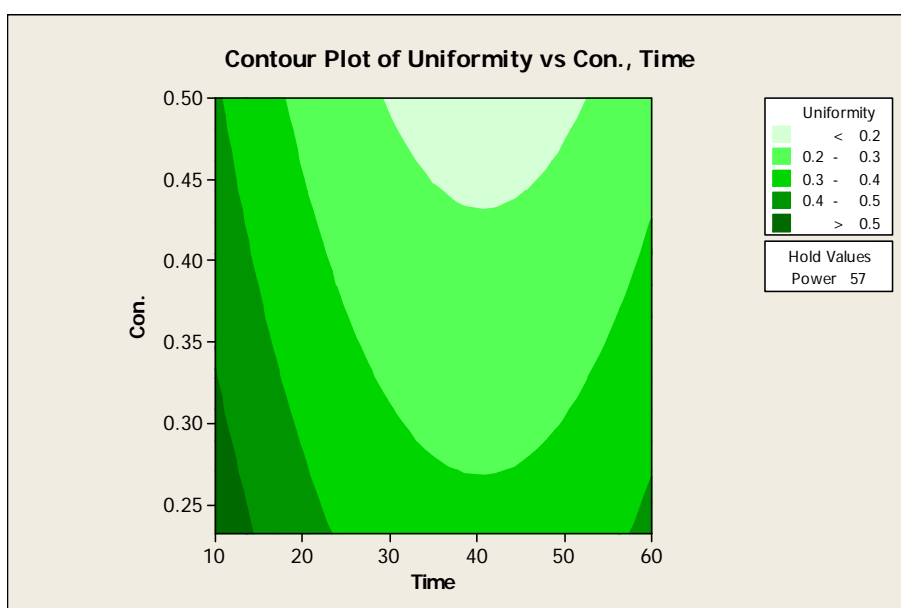


**Figure 3.6a** Contour plot of uniformity versus concentration, time



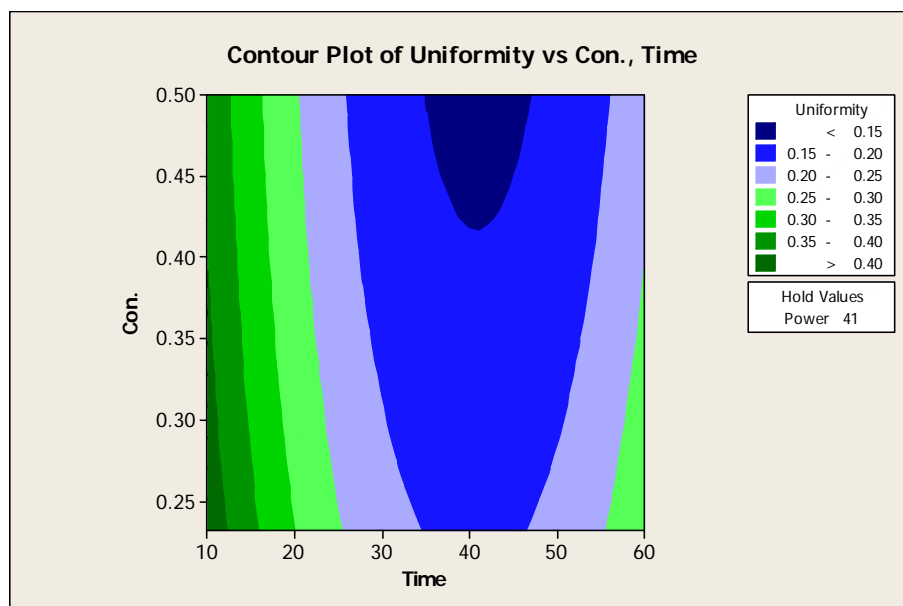


**Figure 3.6b** Contour plot of uniformity versus concentration, time

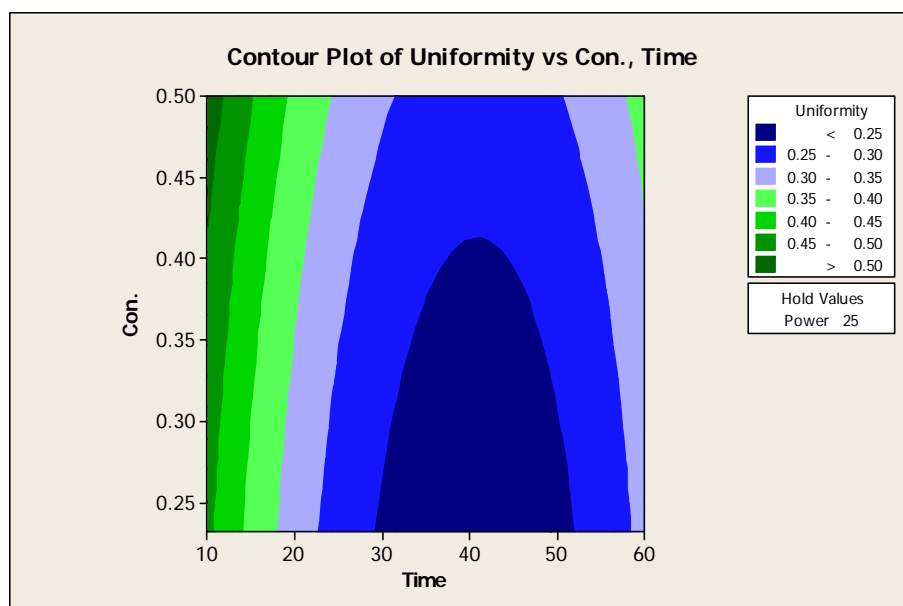


**Figure 3.6c** Contour plot of uniformity versus concentration, time

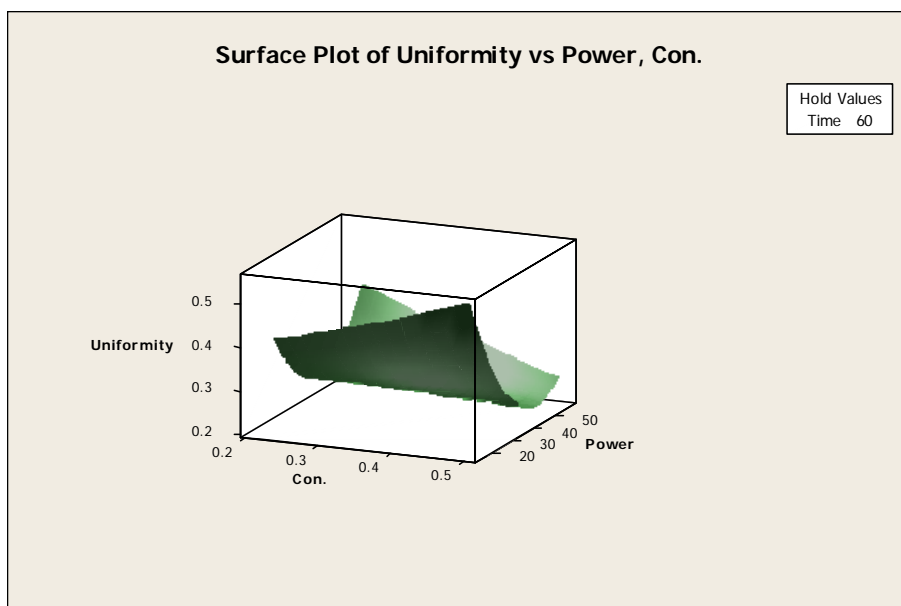


**Figure 3.7a** Surface plot of uniformity versus power, concentration

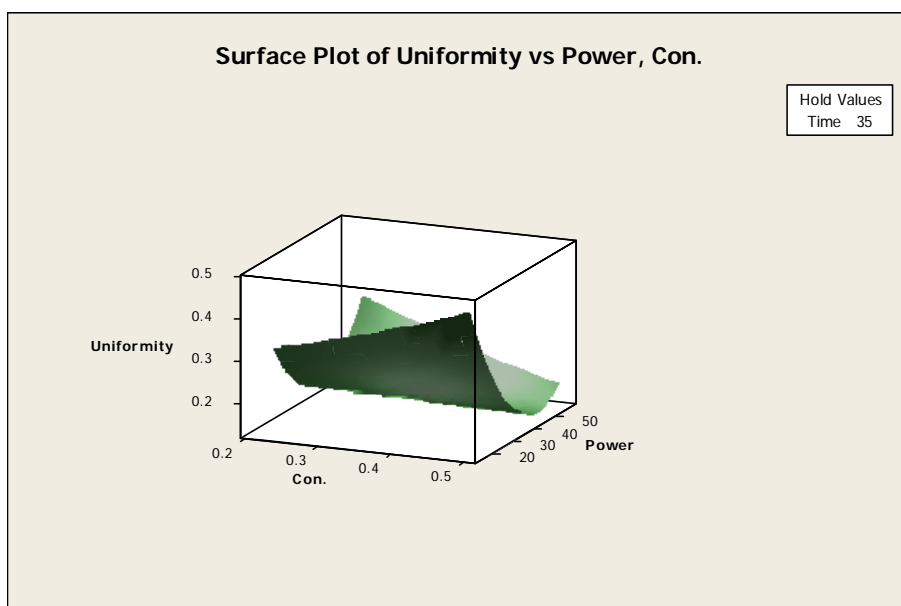


**Figure 3.7b** Surface plot of uniformity versus power, concentration

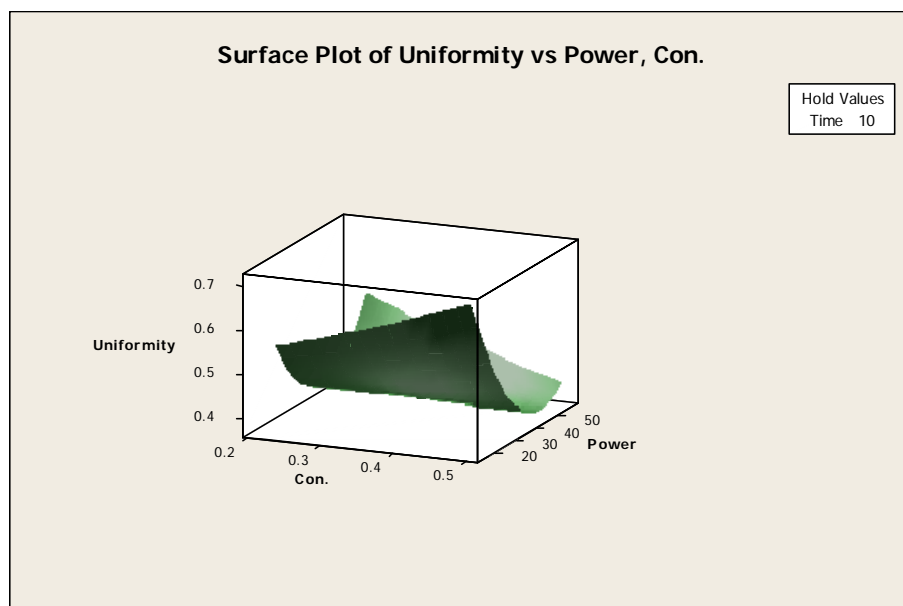


**Figure 3.7c** Surface plot of uniformity versus power, concentration

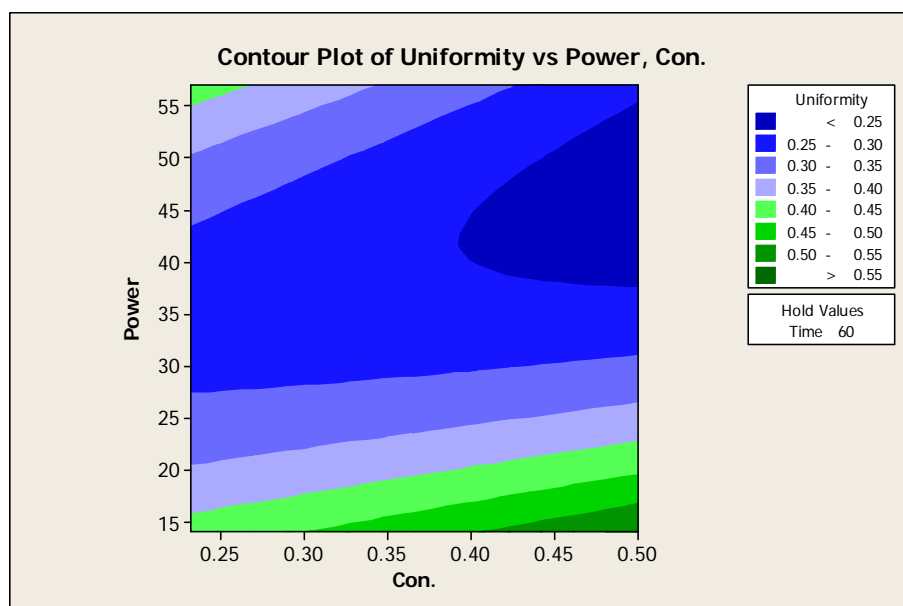


**Figure 3.8a** Contour plot of uniformity versus power, concentration

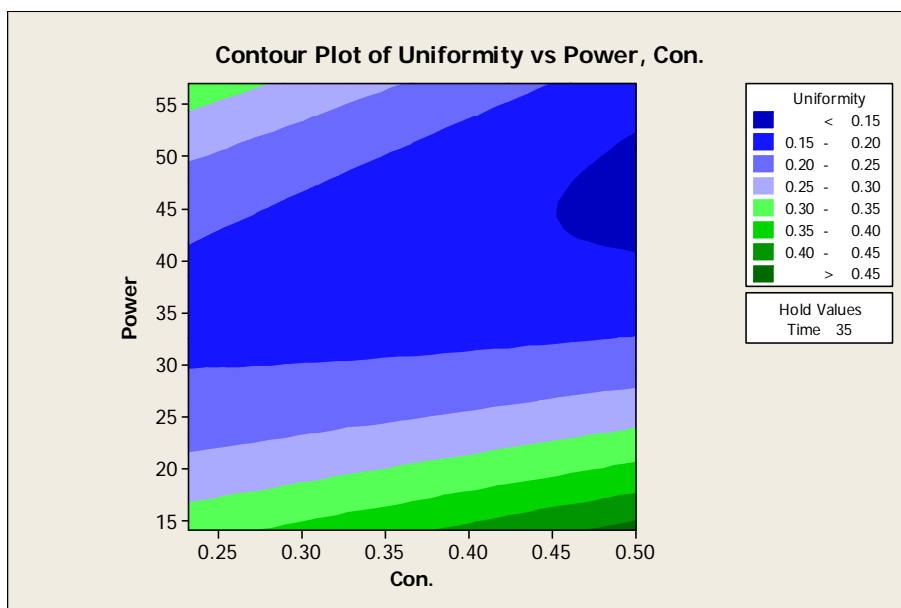


**Figure 3.8b** Contour plot of uniformity versus power, concentration

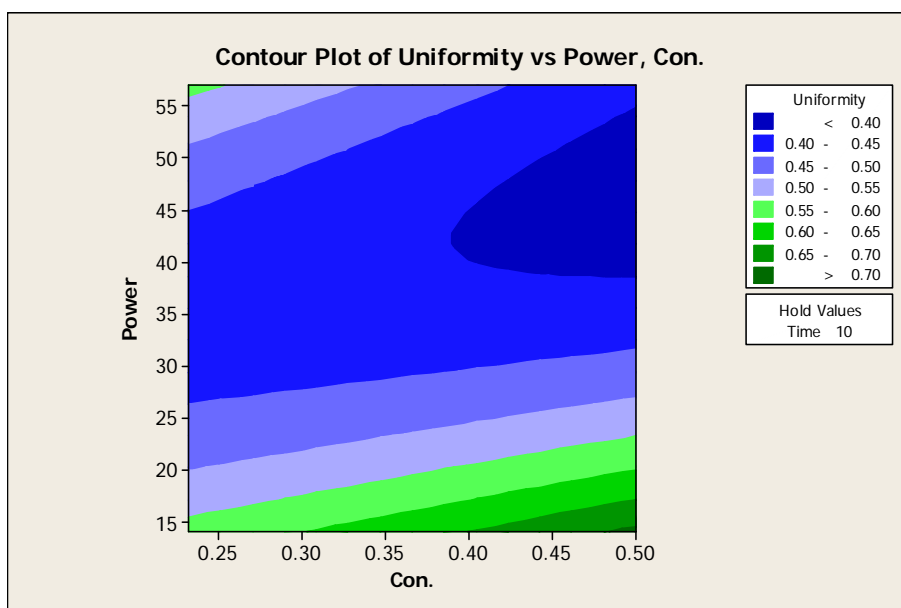


**Figure 3.8c** Contour plot of uniformity versus power, concentration

### 3.4 Characterization of nanochitosan emulsions

Some of the prepared emulsions were centrifuged at 27200G for 60 min at 4°C; the obtained solid was freeze-dried for the further  $M_v$  measurement and DD measurement.

Some of the nanochitosan emulsions were frozen very quickly using liquid nitrogen, and then the powder samples were obtained using freeze-dry machine for the X-ray diffraction analysis. The samples with different ultrasonic duration are listed in Table 3.5.

**Table 3.5** Samples with different ultrasonic duration

Sample	CS0	CS5	CS10	CS20	CS40	CS60	CS80	CS100	CS120	CS150	CS180
Ultrasonic duration/min	0	5	10	20	40	60	80	100	120	150	180

### 3.4.1 The pH value, zeta potential of nanochitosan emulsions

The pH value was recorded by a pH meter HM-21P of TOA Instruments. The zeta potential was measured by a Malvern Zetasizer 3000HSA. Each sample was measured five times. The results were then calculated automatically by the instrument.

### 3.4.2 Particle size and molecular weight ( $M_v$ ) of chitosan nanoparticles

The particle size was studied by a Malvern Zetasizer 3000HSA equipped with a 125 mW laser operating at  $\lambda = 633$  nm. Each sample was measured ten times at an interval of 30 seconds and the average results were calculated automatically by the instrument.

The viscosity properties of the chitosan samples were determined by an Ubbelohde viscometer at 25°C. A dilute 0.1 M acetic acid solution containing 0.2 M sodium chloride (NaCl) was used as a solvent. Each sample was filtrated by filter paper beforehand.

The  $M_v$  was calculated from the Mark-Houwink equation using the limiting viscosity,

$$[\eta] = K[M_v]^\alpha \quad (\text{E 2.2})$$

And the constants for the equation were determined by Robert and Domszy [99] as  $K=1.81 \times 10^{-3} \text{ cm}^3 \cdot \text{g}^{-1}$  and  $\alpha=0.93$ . Each measurement was repeated 3 times and the results were then averaged.

### 3.4.3 Degree of deacetylation (DD) measurement

#### 3.4.3.1 FT-IR method for DD measurement

The infrared spectrometry method was used to determine the DD of chitosan. The samples were vacuum-dried at 50°C for 48 hours. About 10 mg of dried sample was mixed with 120 mg of potassium bromide (KBr) and was pressed into a pellet under 10 ton pressures. The pellet was vacuum-dried at 50°C for 24 hours again and placed into desiccator before the IR measurement (Perkin Elmer Spectrum 100 FT-IR Analyzer).

The absorbance values of amide I (1655cm<sup>-1</sup>) and of the hydroxyl bond (3450cm<sup>-1</sup>) were measured. The DD of samples were given by

$$DD(\%)=[1-A_{1655}/(A_{3450}\times 1.33)]\times 100 \quad (E\ 3.1)$$

whereas  $A_{1655}$  and  $A_{3450}$  were the absorbance values at 1655 cm<sup>-1</sup> of the amide-I band as a measure of the *N*-acetyl group content, and 3450 cm<sup>-1</sup> of the hydroxyl band as an internal standard of chitosan [77]. The factor ‘1.33’ denoted the value of the ratio of  $A_{1655}/A_{3450}$  for fully *N*-acetylated chitosan. It was assumed that the value of this ratio was zero for fully deacetylated chitosan, and there was a rectilinear relationship between the *N*-acetyl group content and the absorbance of the amide-I band.

Figure 3.9 shows the baselines for calculating the amide-I band absorbance and hydroxyl band absorbance in this study. The DD of the sample was calculated by using the baseline and equation E 3.1.

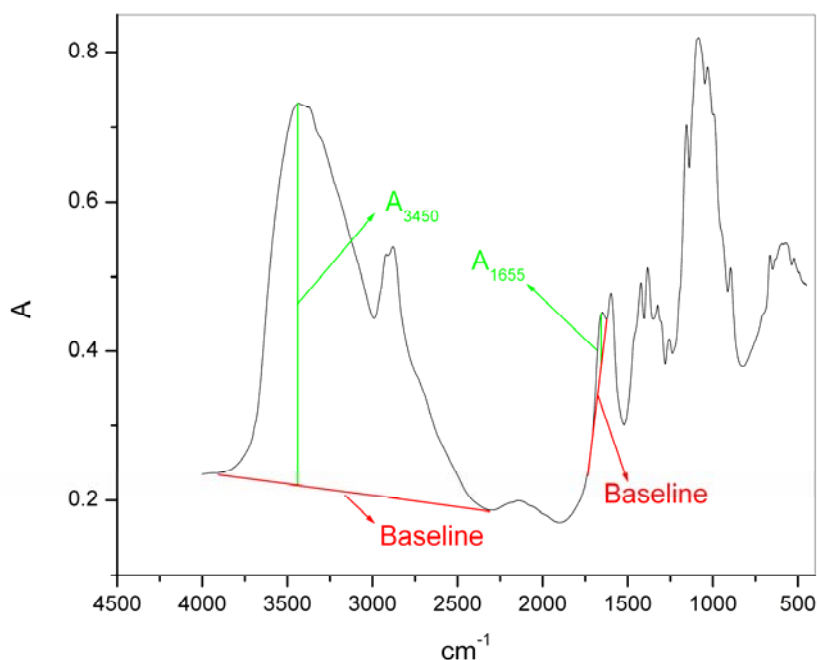


**Figure 3.9** FT-IR spectrum of chitosan showing the baselines for calculating the amide-I band absorbance and hydroxyl band absorbance

### 3.4.3.2 $^1\text{H}$ NMR method for DD measurement

The proton nuclear magnetic resonance ( $^1\text{H}$  NMR) spectral was carried out on a Bruker Advance DPX-400 FT-NMR spectrometer operating at the Larmor frequency of 400 MHz per proton. The spectral width was 5592.8 Hz, the Fourier number was 32768. The number of acquired transients was 64 corresponding to approximately 15 min of signal acquisition. A  $30^\circ$  pulse of 10  $\mu\text{s}$  and an acquisition delay of 2 s were used for  $^1\text{H}$  spectral accumulation. The Fourier Transform (FT) data were fitted using a MestRe-C software.

The chitosan sample was vacuum dried at  $50^\circ\text{C}$  for one day and 10 mg of sample was introduced into a 5 mm  $\Phi$  NMR test tube. 0.5 mL of  $\text{DCl}/\text{D}_2\text{O}$  solution (1 mol/L) was then added and the test tube was kept to dissolve the chitosan in the solution. 100  $\mu\text{L}$  of

newly prepared  $\text{NaNO}_2$  solution (10 g/L in  $\text{D}_2\text{O}$ ) was added. The tube was kept in dark for more than 3 hours. And then the test was performed at room temperature.

As the solubility of chitosan in  $\text{DCl}/\text{D}_2\text{O}$  solution at room temperature was low, newly prepared  $\text{NaNO}_2$  solution was then added. In the chitosan/ $\text{NaNO}_2$ / $\text{DCl}$  solution, the following reaction (Figure 3.10) occurred and there were three different units in the prepared sample (Figures 3.11).

The DD was calculated using integrals of the peak of H-1 of deacetylated units, peak of H-1 of dehydrate units, and peak of the three protons of acetylated units (Figure 3.12) as following equation (E 3.2) [63].

$$\text{DD}(\%) = 100 - \left( \frac{\text{H-Ac}/3}{\text{H-1(Deh)} + \text{H-1(D)} + \text{H-Ac}/3} \right) \times 100 \quad (\text{E } 3.2)$$

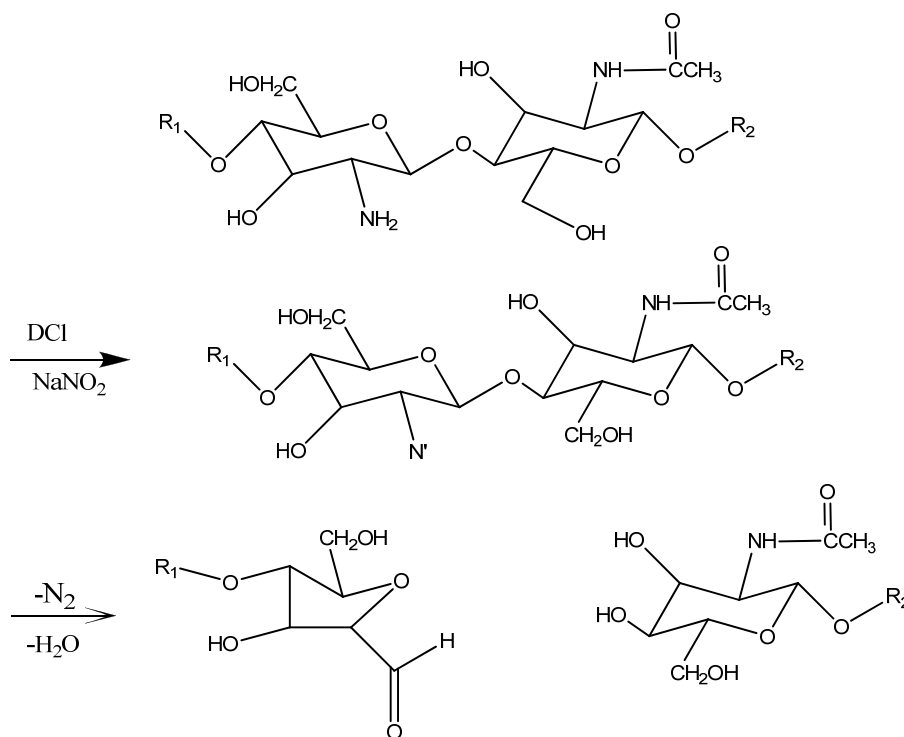


**Figure 3.10** Reaction scheme



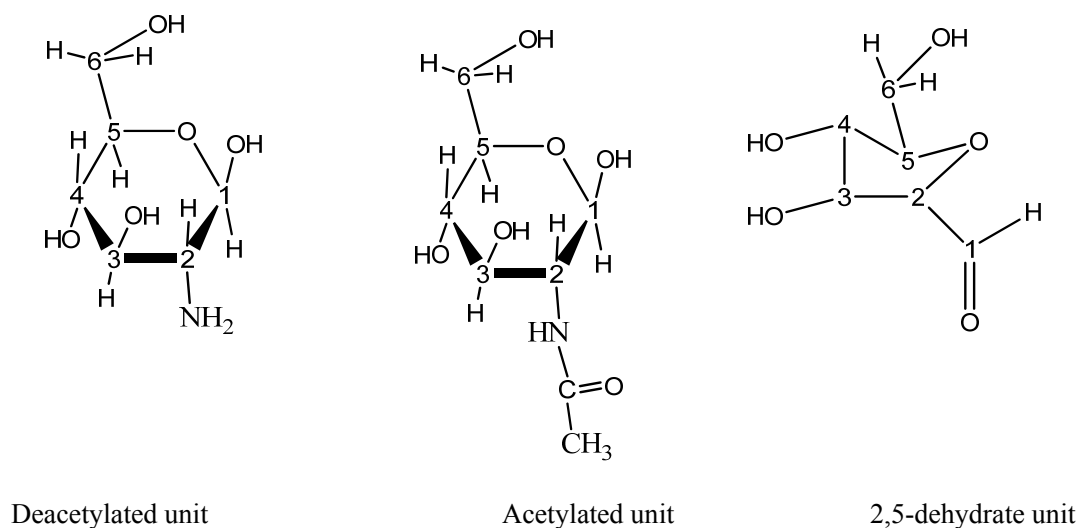


**Figure 3.11** Three kinds of units in the  $^1\text{H}$  NMR sample solution

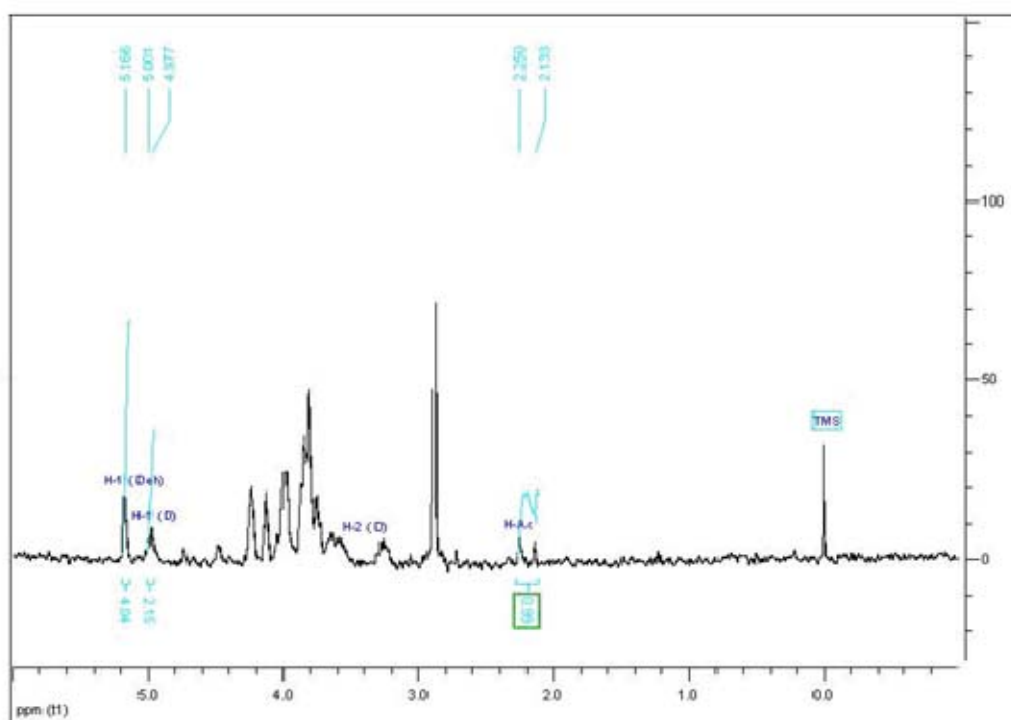


**Figure 3.12**  $^1\text{H}$ -NMR spectrum of chitosan with signal assignments

### 3.4.3.3 Elemental analysis for DD measurement

The samples were vacuum-dried at  $50^\circ\text{C}$  for 48 hours. The elemental analyzer (Vario EL III, Varian) was used to determine the carbon, hydrogen, nitrogen and sulphur contents of the sample. By using cystine (ultra-high purity, 99.999%) as a standard, the element content of the sample was evaluated.

The DD of chitosan was calculated by using the following equation [91]:

$$DD(\%)=100\times\left(4-0.583093\times\frac{W_C}{W_N}\right) \quad (E\ 3.3)$$

#### 3.4.4 Powder X-ray diffraction (XRD)

The nanochitosan emulsion was frozen very quickly using liquid nitrogen, and then the powder samples were obtained using a freeze-dry machine.

X-ray diffraction measurements were conducted using a Philips Analytical X-Ray B V 1830 at  $K_\alpha$  ray  $\lambda=1.54\text{ \AA}$  in the  $2\theta$  range  $5^\circ$ - $30^\circ$ . The spectra were recorded at 40 kV and 35 mA with a scan rate of  $0.05^\circ$  per second.

The crystallinity was characterized by the crystalline index. The crystalline index (CrI; %) [337-339] was determined by using the equation:

$$CrI(\%)=(I_{110}-I_{am})\times 100/I_{110} \quad (E\ 3.4)$$

where  $I_{110}$  is the maximum intensity at  $20^\circ$ , and  $I_{am}$  is the intensity of amorphous diffraction at  $16^\circ$ .

#### 3.4.5 Morphological characterization

Typically, one drop of the diluted emulsion was dropped on the surface of a piece of washed silicon wafer, and then dried in vacuum-oven or freeze-dry machine before the SEM measurements. The SEM measurement was performed by a JOEL JSM 6300F.

The diluted emulsion was dropped on to the sample grid directly, and then dried in ambient atmosphere, followed by vacuum-drying for 24 hours before the TEM

measurements. The TEM studies were carried out on a JEOL JEM-2010 microscope at 200 kV.

One drop of the emulsion was placed on the surface of a piece of washed silicon wafer, and then dried in ambient atmosphere, followed by vacuum-drying for 24 hours before the AFM measurements. The AFM was performed by a SPI 4000 in the dynamic force mode.

### 3.5 Results and discussion

#### 3.5.1 Nanochitosan emulsion images and stability

The nanochitosan emulsions with different ultrasonic duration were shown in Figure 3.13. It can be seen that the emulsions were more transparent when the ultrasonic duration increased. It was because the particle sizes of chitosan became smaller at a longer ultrasonic duration. After 10 days, almost all the treated emulsions remained the same while the untreated chitosan settled (Figure 3.14). It can be concluded that the nanochitosan emulsions had a good stability at the ambient conditions.

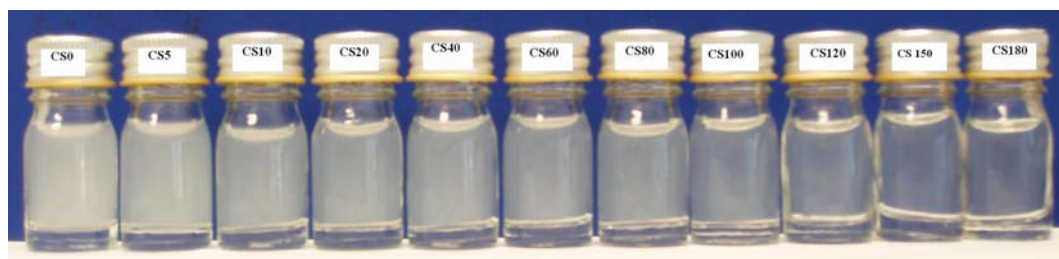


**Figure 3.13** Newly prepared chitosan emulsions with different ultrasonic duration

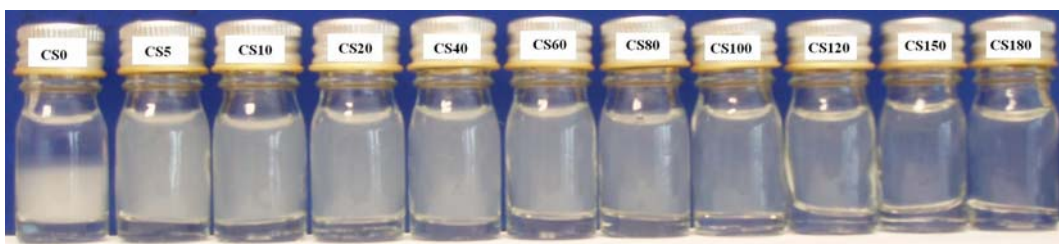


**Figure 3.14** Chitosan emulsions with different ultrasonic duration after 10 days of preparation

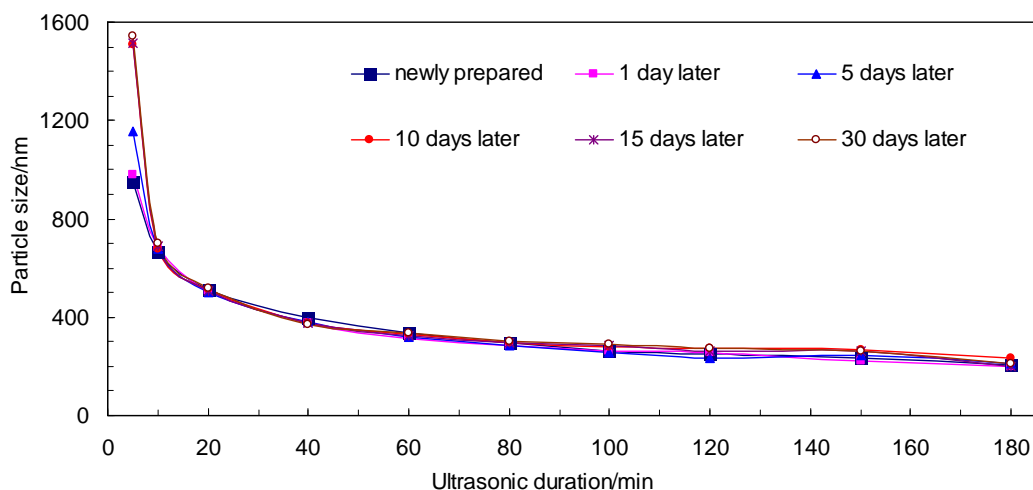


**Figure 3.15** Particle size of nanochitosan with different ultrasonic duration in 30 days

Figure 3.15 shows the particle size variety of nanochitosan in 30 days. After a month of storage, the results of the laser scanning showed that the particles size of nanochitosans with more than 10-minute ultrasonic treatment had no obvious change and the nanoparticles were stable.

Figure 3.16 shows a laser through sample CS0 and CS60. The CS60 showed a clearer light line which is the result of Tyndall effect. The particle sizes in the emulsion are smaller than the light wave (400-700 nm). The chitosan particles in CS0 were much bigger than CS60 and the light line is shorter.

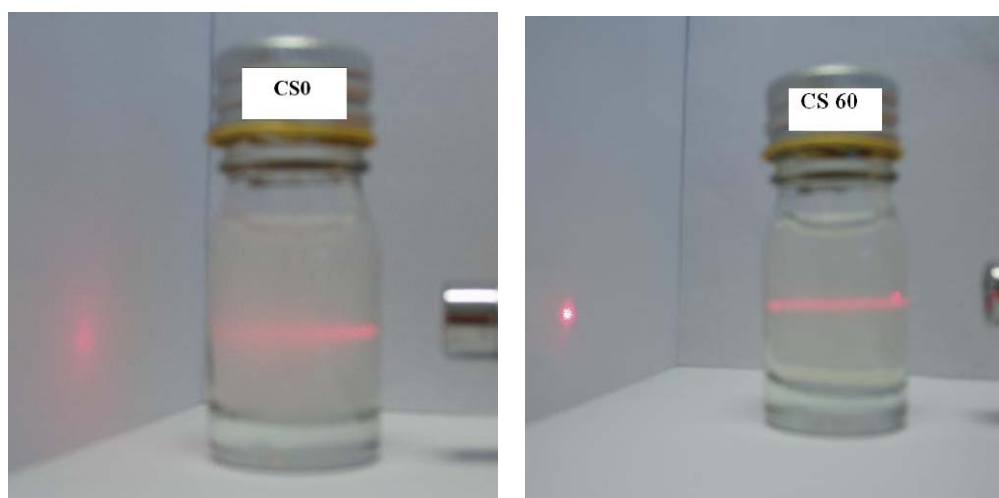


**Figure 3.16** A laser through samples CS0 and CS60

After dry of the nanochitosan emulsion, a thin film was obtained as shown in Figure 3.17.

Chitosan could easily form a film when the emulsion was dried.

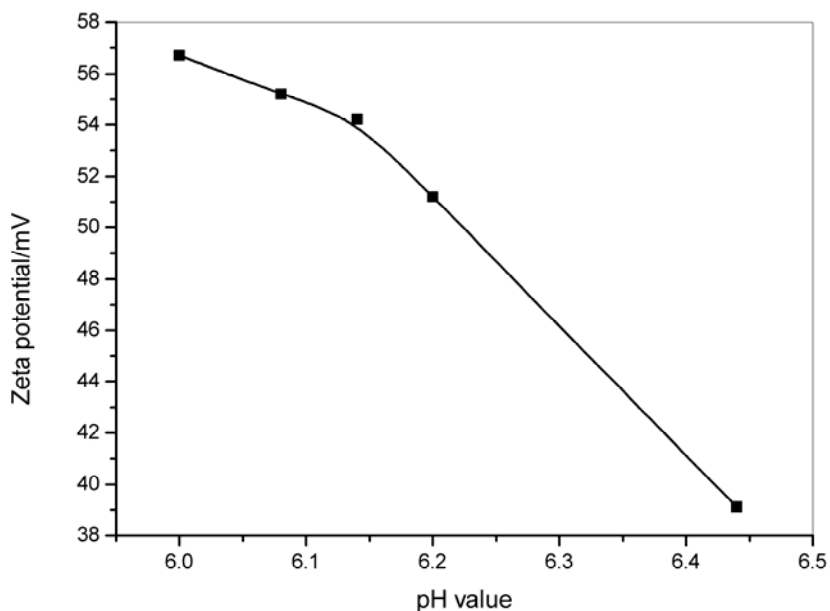


**Figure 3.17** Chitosan film

### 3.5.2 The pH value and zeta potential of nanochitosan emulsions

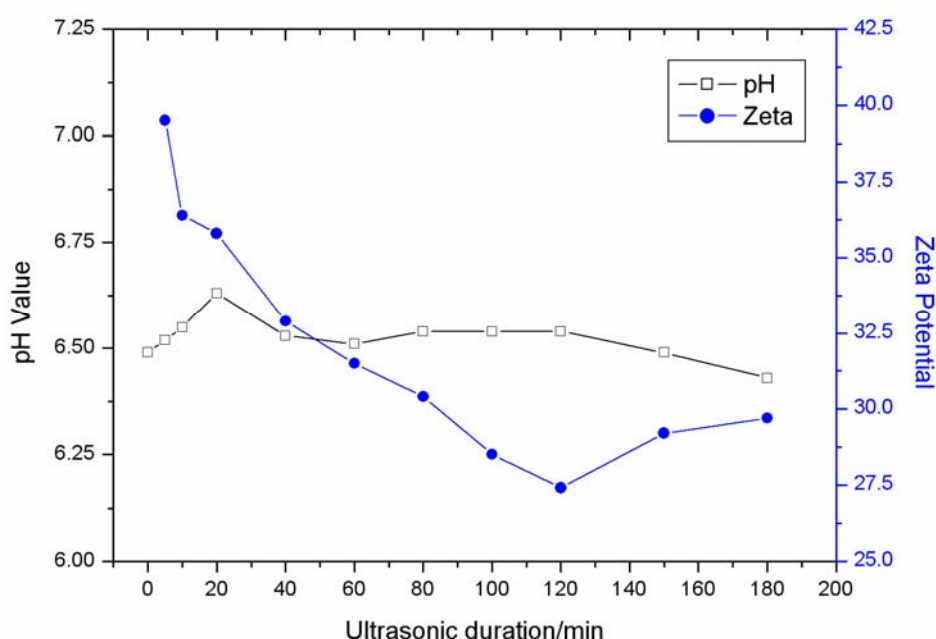
The pH value of sample CS60 was adjusted by using acetic acid solution (0.1% w/w).

The different pH value and corresponding zeta potential value of sample CS60 is shown in Figure 3.18. The zeta potential of the emulsion depended greatly on the pH value.



**Figure 3.18** Effect of pH on zeta potential of nanochitosan emulsion (CS60)

The pH value of the chitosan water mixture before sonolysis was 6.19. After the sonolysis, the pH value increased. And the pH values of the nanochitosan emulsions after the ultrasound treatment had an obviously trend—the longer of the ultrasonic duration, the bigger of the pH value. But the difference of the pH value dropped as the emulsions were put a few days after the ultrasound. After 10 days, the pH value of the emulsions tended to be similar ranging from 6.48-6.60 (Figure 3.19).



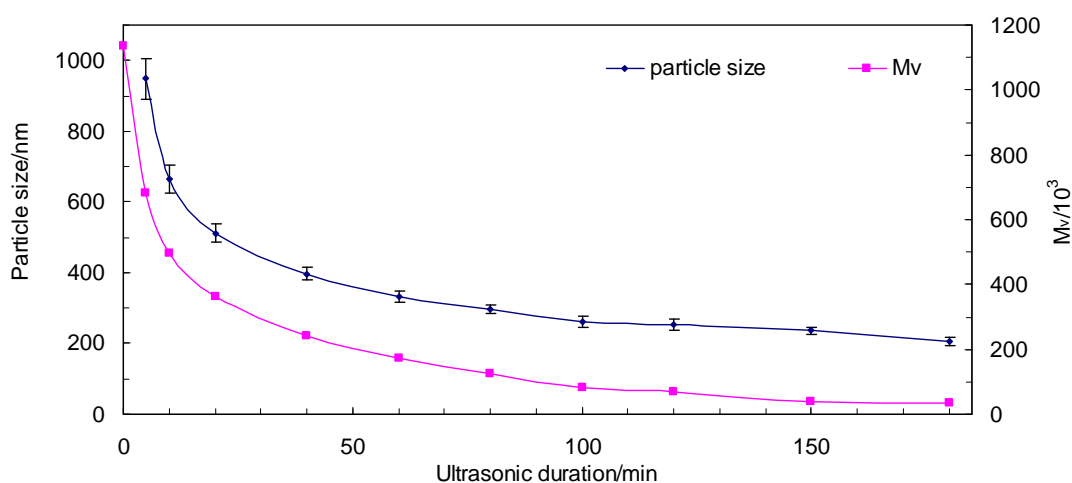
**Figure 3.19** The relationships among pH, zeta potential and ultrasonic duration

Figure 3.19 also shows the relationship between zeta potential and ultrasonic duration after 10 days of the preparation. The emulsions with different ultrasonic duration has a zeta potential between 25mV-40mV. It showed that the emulsions prepared are stable. Many researchers have demonstrated the stable structure of the hydrogen bond between water molecules and the amino groups [340-344]. In the structure water molecules acted as the provider of hydrogen when amino groups are the receiver. The positive charge of the chitosan nanoparticles suggested that the emulsions were stabilized by the hydrogen

bond between the amino groups and hydroxyl groups of chitosan and water respectively. In the hydrogen bonds, amino groups were positively charged, which made the surface of the nanoparticles positively charged.

### 3.5.3 Particle size and molecular weight of nanochitosan

The relationships among the particle size,  $M_v$ , and ultrasonic duration are shown in Figure 3.20. A sharp decrease of both the particle size and  $M_v$  was observed at the beginning. It suggested that effect mainly happened in the early part of the ultrasound treatment when the amorphous structure of the swollen chitosan was broken quickly; after that, the remained compact structure was more difficult to break, the particle size became stable. Meanwhile, the diversity of particle size became smaller with the ultrasonic duration from 5-60 minutes which is consistent with the study of Popa-Nita et al. [220]. Two mechanisms involved in the ultrasonically induced depolymerization of chitosan were proposed: the first led to a rapid scission of polymer chains and a lowering of the polydispersity, and the second was responsible for obtaining short polymer chains and oligomers with a polydispersity increase [220].



**Figure 3.20** Relationships among particle size,  $M_v$ , and ultrasonic duration

### 3.5.4 DD of the nanochitosan

The DD results measured by FT-IR,  $^1\text{H}$  NMR and elementary analysis are listed in Table 3.6. The DD of chitosan nanoparticles did not change much after ultrasound treatment. This result agreed with the work of Liu et al. [222]. It was believed that the ultrasound wave did not destroy the bonds between carbon and amino group and carbon and acyl group in water. The degradation mainly happened in the main chain.

**Table 3.6** DD of chitosan calculated by different methods

DD of Sample	CS0	CS5	CS10	CS20	CS40	CS60	CS80	CS100	CS120	CS150	CS180
FT-IR	95.2%	94.2%	95.5%	95.3%	94.4%	94.7%	95.6%	92.6%	94.7%	94.7%	95.1%
$^1\text{H}$ NMR	97.2%	96.4%	96.2%	95.1%	94.5%	94.7%	95.1%	95.0%	95.5%	95.5%	96.1%
<sup>a</sup> E. A.	95.1%	90.4%	93.4%	92.9%	94.3%	95.8%	94.4%	90.2%	90.4%	90.4%	91.3%

<sup>a</sup>E. A. elemental analysis

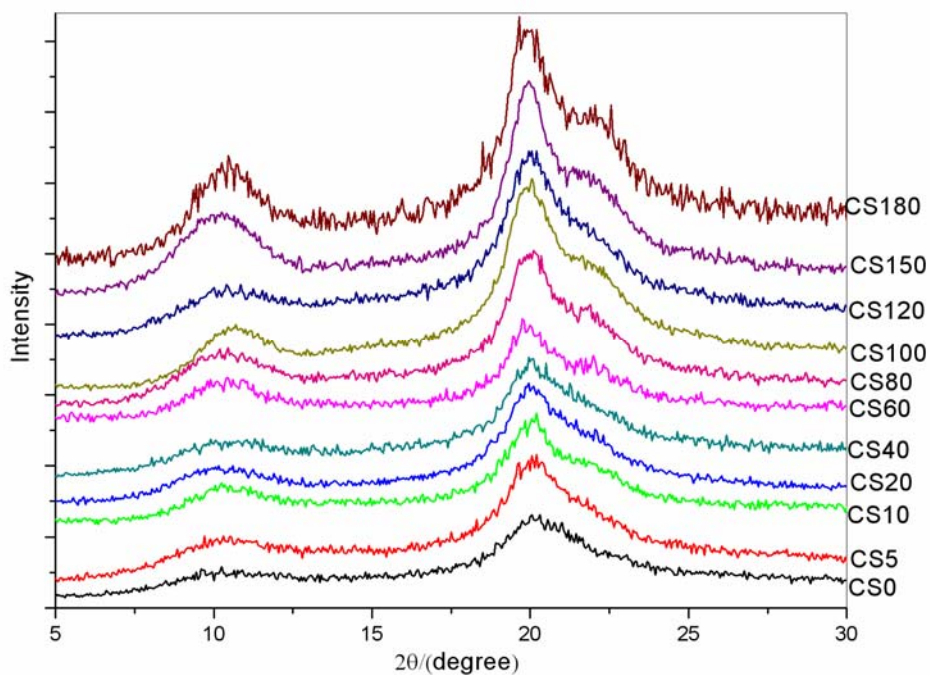
### 3.5.5 Crystallinity of nanochitosan

Figure 3.21 shows the XRD profiles of untreated and treated chitosan. Two major peaks were observed at  $2\theta=10^\circ$  and  $2\theta=20^\circ$ . The crystallinity was characterized by a crystalline index. The crystalline index (CrI; %) is determined by using the equation  $\text{CrI}(\%) = (I_{110} - I_{\text{am}}) \times 100 / I_{110}$ , where  $I_{110}$  is the maximum intensity of XRD at  $2\theta=20^\circ$  degree, and  $I_{\text{am}}$  is the intensity of amorphous diffraction at  $2\theta=16^\circ$  degree. The relationship between the crystallinity and the ultrasonic duration is summarized in Table 3.7 and Figure 3.22. The crystallinity of chitosan increased slightly. The improvement of dye absorption ability may attribute to the fact that chitosan crystallite was broken into nano crystallite to expose more amine groups by the ultrasound treatment.

In the study of Liu et al., the crystallinity increased with the ultrasonic duration [222]. In our study, the crystallinity generally increased slowly with the ultrasonic duration, but the



crystallinity did not increase much. The possible reason was that the chitosan used in this experiment had a much lower molecular weight than Liu's samples and the crystallinity was rather high. When the ultrasonic treatment was applied, although the molecular weight became smaller, the crystallinity did not increase much.



**Figure 3.21** XRD patterns of the chitosan nanoparticles with different ultrasonic duration

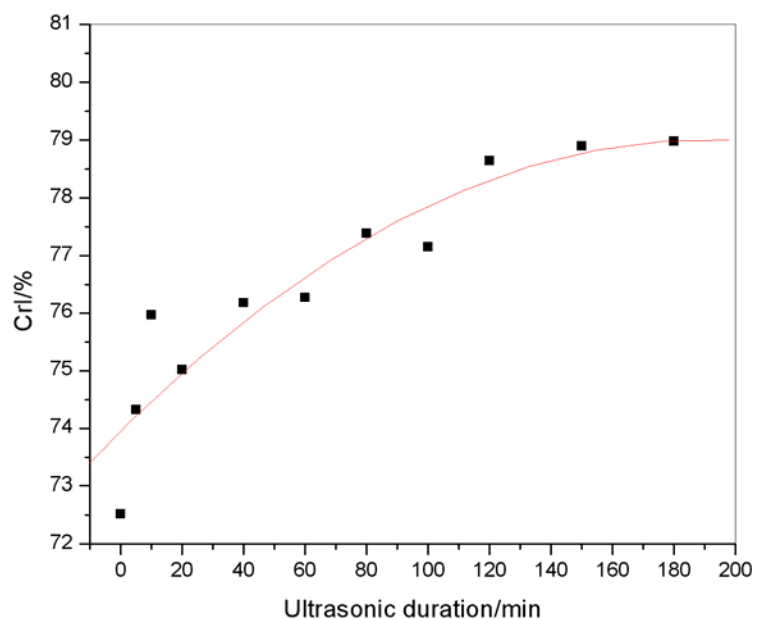


**Figure 3.22** The relationship between the crystallinity and ultrasonic duration

**Table 3.7** Crystalline index (CrI; %) of the chitosan nanoparticles

Ultras./min	0	5	10	20	40	60	80	100	120	150	180
$I_{20}$	655	976.8	868	980	917	838.1	1224.6	1630	1410	1723.2	1948.5
$I_{16}$	180	250.8	208.6	244.8	218.4	198.9	276.9	372.5	301.2	363.6	409.5
$(I_{20}-I_{16})/I_{20}$	72.52	74.32	75.97	75.02	76.18	76.27	77.39	77.15	78.64	78.90	78.98

### 3.5.6 Morphological characterization

#### 3.5.6.1 SEM images

As shown in Figure 3.17, the particles in the emulsion (sample CS60) formed a film on the wafer. It was very difficult to observe the particles after the emulsion was dried by using vacuum oven in the SEM (but could be seen in the AFM). In Figure 3.23, the particles in the emulsion formed a film on the wafer. The nanoparticles could not be clearly observed and only film can be observed.

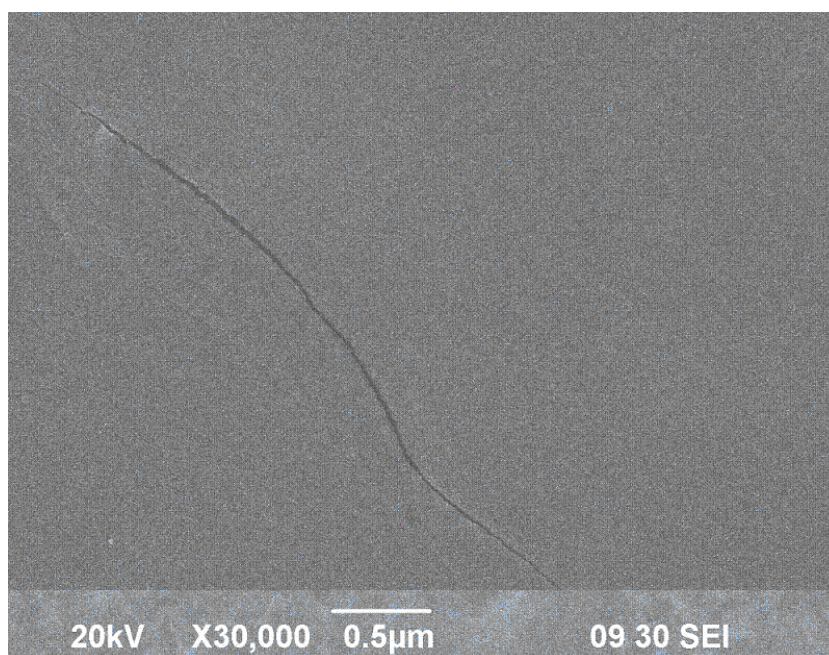
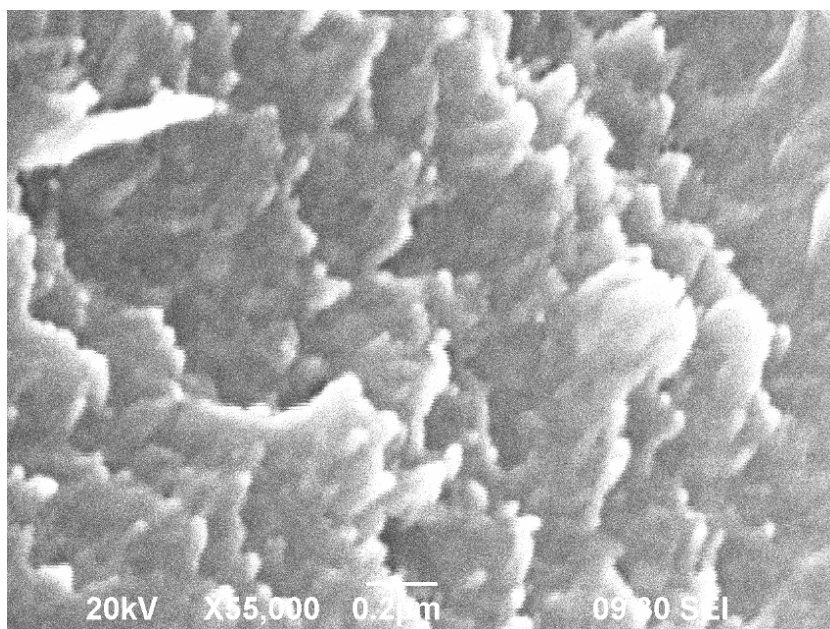
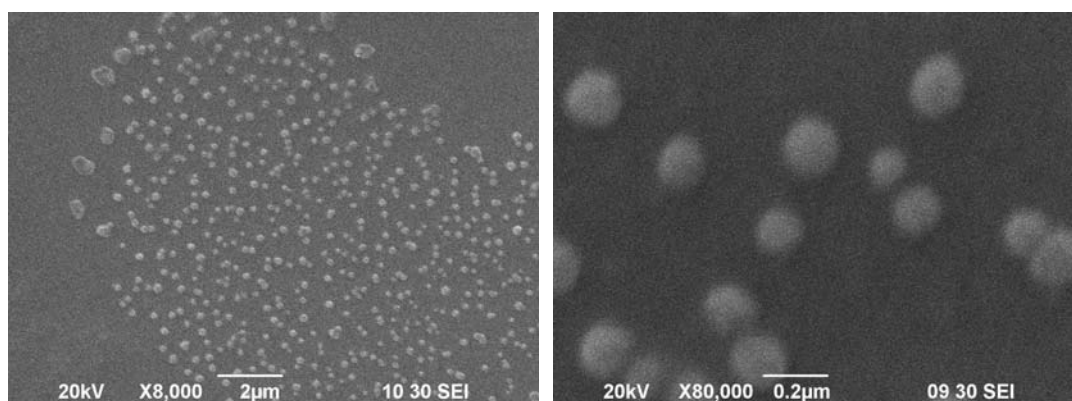
**Figure 3.23** SEM image of the nanochitosan using vacuum-dry (CS60)

Figure 3.24 shows the SEM image of the freeze-dried nanochitosan. The chitosan formed a kind of solid foam with many pores in it. The nanoparticles could not be clearly observed either.

By diluting the emulsion more than 50 times and using the freeze-dry technique, the nanoparticles could be observed (Figure 3.25). Some of the chitosan nanoparticles aggregated in the process of drying on the wafer to form bigger particles. The particle size of nanochitosan was about 100-300 nm (CS60).



**Figure 3.24** SEM image of the freeze-dried nanochitosan



**Figure 3.25** SEM image of the nanochitosan using freeze-dry process (CS60)

### 3.5.6.2 TEM images

Figure 3.26 shows the TEM images of nanochitosan from the emulsion. The diameter of the nanochitosan was about 150 nm. The chitosan nanoparticles would aggregate during the drying process and single nanoparticles is difficult to observe. Most of the dried chitosan aggregated to form a film on the surface of the grid.

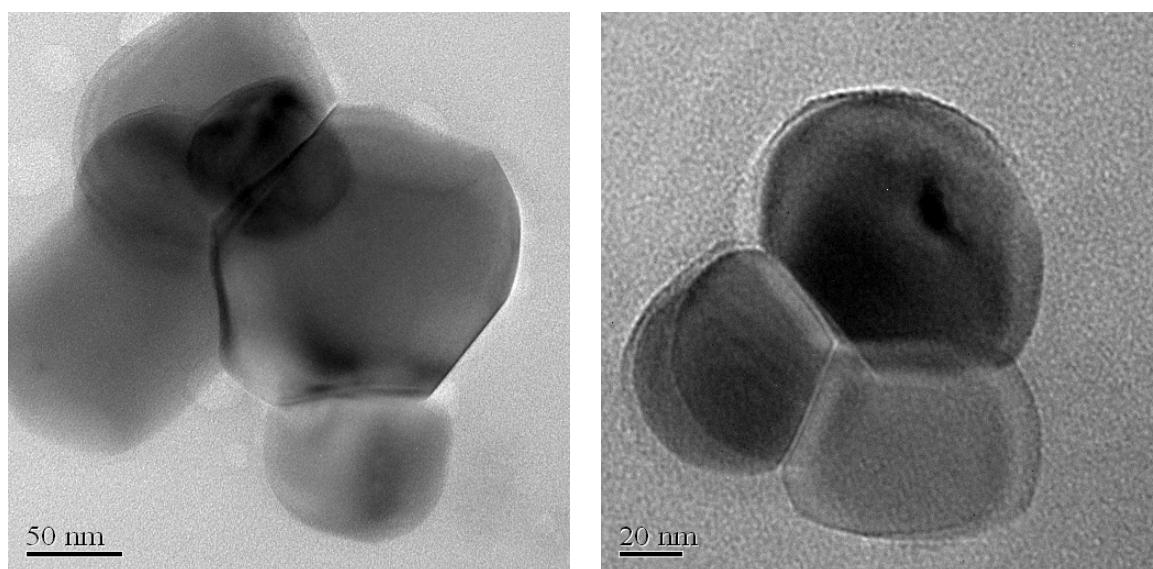


**Figure 3.26** TEM images of the nanochitosan (CS60)

### 3.5.6.3 AFM images

The nanochitosan particles were also studied by AFM (shown in Figures 3.27 and 3.29). These particles aggregated in the process of drying and formed a film with rough surfaces. As shown on the left of Figure 3.27, the nanoparticles were about 164.0 nm (average) in size and formed a rough surface. Figure 3.29 shows the nanoparticles packed together to form the film and the 3-dimension image of the film surface.

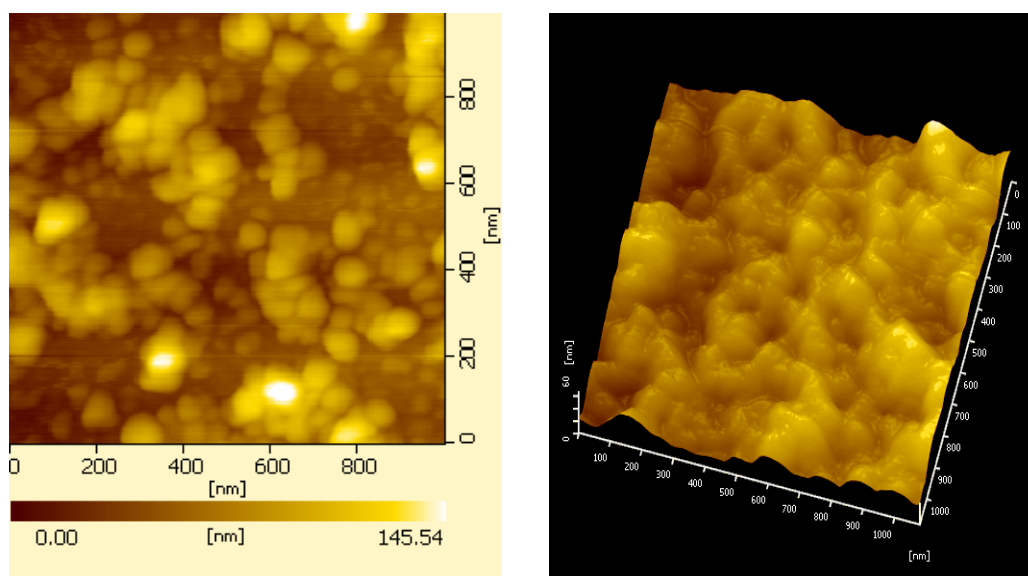


**Figure 3.27** AFM images of nanochitosan (CS60)

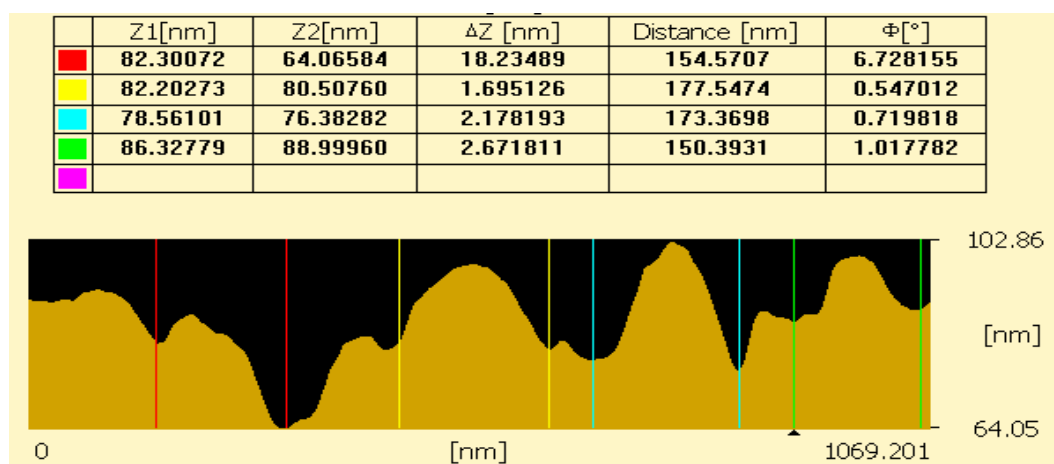


**Figure 3.28** Particle sizes of the nanochitosan

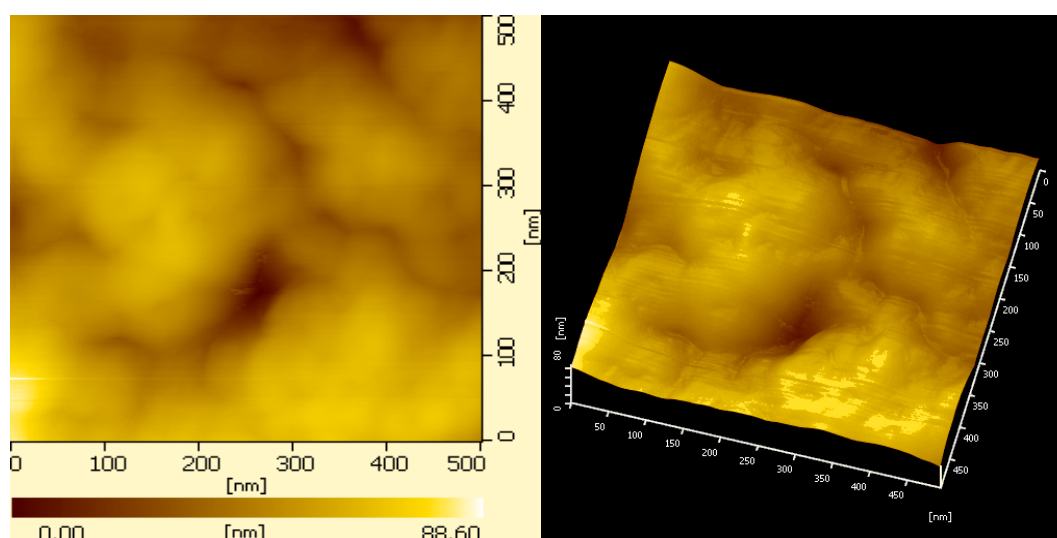


**Figure 3.29** AFM images of a nanochitosan film (CS60)

### 3.6 Conclusions

In this chapter, a new dissolving-precipitating-ultrasound method has been developed for the preparation of the nanochitosan emulsions by using the ultrasound treatment. The optimal conditions for preparing nanochitosan emulsions with uniform nanochitosan particles were investigated by using experiment design. The emulsions prepared could maintain a good stability because of the hydrogen bond between the amino groups and hydroxyl groups of water and chitosan molecules. Laser scanning, SEM, TEM and AFM were performed to obtain the particle size and image. The particle size and molecule weight decreased with the ultrasonic duration. The DD of chitosan had no significant changes in the ultrasound treatment. The crystallinity of chitosan nanoparticles were investigated by X-ray.

The method for preparing the chitosan nanoparticles by using the ultrasound treatment did not require additional chemicals in the process. It was easy to determine the particle size in the emulsions and the emulsions were stable. By using the ultrasound treatment, we could obtain nanochitosan emulsions containing water and chitosan only which is important for further uses in medicines and textiles.

## **Chapter 4 Application of Nanochitosan Emulsion on Dye Sorption**

### **4.1 Research background**

The textile industry is one of the industries that have been causing concerns on the problem of serious water pollution. During textile processing, inefficiencies in dyeing result in a large amount of dyestuffs being lost in the wastewater which ultimately finds way into the environment. It is estimated that 5%–10% of the dyes are lost in the effluent during the dyeing process [225], while in the case of reactive dyes, as much as 50% of the initial dyes are in the dye bath effluent [226-227].

It has been reported that the total dye consumption of the textile industry worldwide is in excess of  $7 \times 10^8$  kg/year and an estimated 90% of this end up on fabrics [345]. As a consequence, approximately  $7 \times 10^7$  kg/year of dyes with strong persistent color, high biochemical oxygen demand (BOD), and toxicity loading are present in wastewaters [346-347]. Wastewaters containing dyes are very difficult to treat, since the dyes are recalcitrant molecules, resistant to aerobic digestion, and are stable to oxidizing agents [228].

Current treatments for dye effluents can only get rid of about half of the dyes lost in residual liquors. Over 400 tons of wastewater with dyes dissolved or suspended in water are discharged into the environment every day. The effluent with dyes would affect the absorption and reflection of sunlight into water and hinder the growth of bacteria and plants. The dye effluents would create severe problems in the aquatic ecology due to the toxicity and low biodegradability of dyes [262].



Many researchers have devoted to study on different methods of dye removal. Nowadays there are various types of dye removal methods available such as conventional methods like biodegradation, coagulation/flocculation, established recovery processes including oxidation, membrane separation, ion-exchange and some emerging recovery technologies such as advanced oxidation and biomass [31]. However, many of the dye removal methods cannot fulfill the task of efficiently achieving high water quality economically nor handling large quantities of wastewater.

Another category of dye removal method is adsorption using different kinds of sorbents such as activated carbon, peats, wood chips. [236]. Those methods provide good removal efficiency and do not form harmful substances in the dye removal process. However, there are limitations for the methods. Activated carbon is cost intensive; peat is not as effective as using activated carbon and wood chips require long processing time and a large quantity of sorbent.

Chitosan, a kind of natural polysaccharide derived from chitin, demonstrated outstanding removal capabilities for different classes of dyes, especially for anionic dyes including acid, reactive and direct dyes due to its unique polycationic structure [278, 282, 348-351]. The main raw material for chitosan manufacture is the shell of crustaceans which is a waste in food industry [1, 3-4]. The conversion of the shell of crustaceans to useful polymer is an effective strategy to prevent pollution. The use of chitosan as a sorbent for sorption has been assessed in various studies that generally give good sorption ability for a number of dyes. Chitosan is biodegradable and it is not very expensive. The most important advantage is that chitosan does not harm the environment [1, 3-4].

The sorption ability of chitosan has drawn intensive interest in the study area. Wataru et al. [352] studied adsorption of organic acids on polyaminated highly porous chitosan. Yoshida et al. [278, 350] studied the sorption of various dyes onto chitosan fibers and



reported its high potential for dye sorption. Chiou and Li [244] reported the sorption of chemical cross-linked chitosan beads to Reactive Red 189 at pH 3.0 and 30°C. Wong et al. [232] studied the sorption of acid dye onto chitosan. Annadurai et al. [246] studied sorption of reactive dyes from an aqueous solution by chitosan. Gibbs et al. [266] studied the influence of chitosan pre-protonation on Reactive Black 5's sorption. Chang and coworkers [353] prepared chitosan-based aerogels and studied their adsorption performance.

Nowadays nanotechnology provides a versatile tool to modify the properties of materials. But chitosan in nanosize as adsorbent is rarely studied. Hu et al. [248] studied the sorption ability of acid dyes onto chitosan nanoparticles prepared by using a typical gelation reaction between the positively charged amino groups of chitosan and the negatively charged counter-ions of sodium tripolyphosphate. It is believed that nanochitosan has a larger capacity because of its large surface area to volume value comparing with microchitosan [248].

In this chapter, the abilities of nanochitosan as an adsorbent for the removal of 5 anionic dyes including Acid Orange 7, Acid Red 1, Acid Red 18, Direct Red 84 (Sirius Brown 3RL) and Direct Red 80 (Sirius Red F3B) in aqueous solutions were studied respectively at different temperatures. Similar experiments were done with microchitosan. The sorption kinetics of dyes onto nanochitosan and microchitosan was investigated. The sorption of dyes onto chitosan fits the pseudo-second-order model. The Langmuir equilibrium isotherms were used to analyze the equilibrium data. It was found that the nanochitosan had a higher sorption capacity than that of the microchitosan, and the sorption process using nanochitosan was more efficient. The results demonstrated that the sorption capacity of nanochitosan increased as much as 8 times for the dyes with large molecular sizes comparing with the sorption capacity of microchitosan. It was because

the dyes with large molecules were difficult to penetrate into micro-sized chitosan. Meanwhile, the dyes were easier to be adsorbed onto nano-sized chitosan with a much higher surface area/volume ratio. The desorption and regeneration studies were investigated and the desorption efficiency was higher at pH 10, ranging from 70%-88%. The recycled chitosan and dyes could be used many times which makes the sorption process environmentally friendly.

## **4.2 Materials**

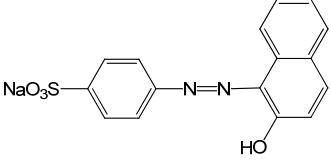
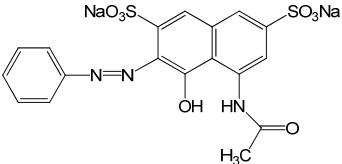
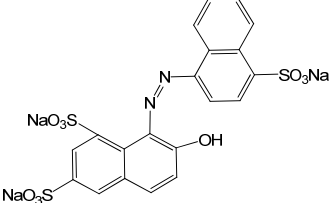
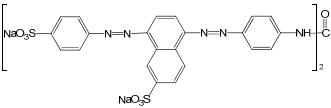
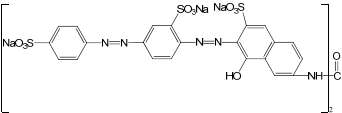
Chitosan with 95% DD was purchased from Haidebei Co. Ltd. Direct Red 84 (Sirius Brown 3RL) and Direct Red 80 (Sirius Red F3B) were gifts from DyStar Company. Other chemicals were purchased from Aldrich Co. Ltd. and used as received. The deionized water used in experiment was obtained using a TKA GmbH water purification system. The characteristics of the dyes are listed in Table 4.1. The molecular dimensions of the dyes were estimated by using ChemBioOffice (2008).

## **4.3 Experimental**

### **4.3.1 Preparation of nanochitosan emulsions (CsNano)**

Typically, 1.5 g of chitosan was dissolved in 250 mL of an acetic acid solution (0.45% w/w) under magnetic stirring. 50 mL of NaOH solution (0.3 mol/L) was then added dropwise into the chitosan solution to precipitate the chitosan. The pH value of the mixture was about 6.2. A Sonics Vibra-Cell™ Ultrasonic Processor VCX 750 was used to treat the mixture for different duration using power setting at 300 watts. The emulsion with ultrasonic duration of 60 minutes with particles of 300-400 nm was prepared for sorption study. The concentration of nanochitosan emulsion obtained was 0.5% (w/w).

**Table 4.1** Characteristics of acid dyes

Dye	C.I. No.	Molecular formula	No. of $-SO_3^-$	Dimensions/Å	M <sub>w</sub> /(g/mol)	Purity	UV $\lambda_m$ /nm
Acid Orange 7(AO 7)	15510	 $C_{16}H_{11}N_2NaO_4S$	1	7.36×12.87×4.54	350.32	85%	484
Acid Red 1(AR 1)	18050	 $C_{18}H_{13}N_3Na_2O_8S_2$	2	12.92×7.75×8.94	509.42	60%	506
Acid Red 18(AR 18)	16255	 $C_{20}H_{11}N_2Na_3O_{10}S_3$	3	14.87×13.54×2.24	604.47	75%	506
Direct Red 84 (DR 84)	35760	 $C_{45}H_{28}N_{10}Na_4O_{13}S_4$	4	24.86×23.19×6.47	1137.0	45~55 %	470
Direct Red 80 (DR 80)	35780	 $C_{45}H_{26}N_{10}Na_6O_{21}S_6$	6	11.51×20.88×17.0	1373.1	70~75 %	528

### **4.3.2 Preparation of 180 $\mu\text{m}$ chitosan (CsMicro)**

The purchased chitosan was sieved by a sieve shaking machine (USA Standard Testing Sieve, ASTM E-11 Spec). Chitosan particles between 80 mesh and 60 mesh were collected to obtain the chitosan with a dry particle size of 180-250  $\mu\text{m}$  (CsMicro).

### **4.3.3 Sorption kinetics experiments**

Typically, 1.0 mmol of pure dye was dissolved in 500 mL of buffer (pH=5.5, 2 mL of 10% HAc and 1.5 g of NaAc/1 liter buffer) to obtain an initial dye concentration of 2 mmol/L. 10 mL of the chitosan emulsion (0.05 g of nanochitosan) with a particle size range of 300-400 nm (CsNano) was pipetted into a 250 mL Duran bottle and brought into contact with 100 mL of dye solution respectively. The bottles were sealed and agitated at 100 rpm in a thermostatic shaker bath (Grant OLS200 shaking bath).

For the sorption of microchitosan, the procedures were repeated with 0.05 g of chitosan with a particle size range of 180-250  $\mu\text{m}$  (CsMicro). When the microchitosan was added into the dye solution, 10 mL of deionized water was also added.

For the sorption, the concentration of the dye was determined every 30 minutes during the first 3 hours and then the concentration was determined daily for 7 days. The sorption kinetics experiment was performed at temperatures of 30°C, 50°C, 70°C and 90°C. The initial dye concentration was 2 mmol/L for each dye.

### **4.3.4 Sorption equilibrium experiments**

Typically, 0.5 mmol of dye was dissolved in 500 mL of a buffer (pH=5.5, 2 mL of 10% HAc and 1.5 g of NaAc/1 liter buffer) to obtain an initial dye concentration of 1 mmol/L. 10 mL of the chitosan emulsion (0.05 g of nanochitosan) with a particle size range of

300-400 nm (CsNano) was pipetted into a 250 mL Duran bottle and brought into contact with 100 mL of dye solution respectively. The bottles were sealed and agitated at 100 rpm in the thermostatic shaker bath (Grant OLS200 shaking bath).

For the sorption of microchitosan, the procedures were repeated with 0.05 g of chitosan with a particle size range of 180-250  $\mu\text{m}$  (CsMicro). When the microchitosan was added into the dye solution, 10 mL of deionized water was also added.

When the equilibrium was achieved after 7 days, 0.5 mL of the solution was aliquotted and the concentration of the dye solution was determined. The sorption was performed at temperatures of 30°C, 50°C, 70°C and 90°C respectively with different initial dye concentrations ranging from 0.5 mmol/L to 7 mmol/L.

#### **4.3.5 Desorption experiments**

In order to desorb the dye, a higher pH value in the sample was maintained at pH 8 by dropping sodium hydroxide solution (4 mol/L) into the sample at room temperature. Then 1 mL of the sample was pipetted for the concentration determination. The above procedures were repeated for pH 10 and pH 12. Before the concentration determination, the diluted sample was adjusted to pH 7 or below for the UV-vis measurement.

### **4.4 Characterization**

#### **4.4.1 Particle size of chitosan nanoparticles**

The particle size was analyzed by a Brookhaven Instruments particle analyzer equipped with a 15 mW solid-state laser. Each sample was measured ten times at an interval of 1 minute. The effective diameter was recorded automatically by obtaining the average data.

#### **4.4.2 Morphology of chitosan nanoparticles**

One drop of the emulsion and one drop of the diluted emulsion was placed on the surface of a piece of washed silicon wafer respectively, and then dried in freeze-dry machine, followed by vacuum-drying for 24 hours before the SEM measurements. The SEM measurement was performed by a Field Emission Scanning Electron Microscope JSM-6335F.

#### **4.4.3 Concentration of dye solutions**

Seven different concentrations of one dye were prepared and the absorbance was measured using a UV-vis Spectrophotometer Lambda 18 at the maximum absorption wavelength ( $\lambda_{\max}$ ) of the dye. The calibration curve of the dye was drawn and recorded automatically. Calibration curve of each dye was obtained in the same way.

The extracted dye solutions were diluted by deionized water and measured with the UV-vis spectrophotometer at  $\lambda_{\max}$  of each dye. The concentration can be calculated automatically by the instrument through calling of each calibration curve. The data were used to calculate the sorption ability ( $q_t$ ) of nanochitosan and microchitosan.

#### **4.4.4 Hydrophobic/hydrophilic ratio of dyes**

Hydrophobic/hydrophilic ratios of dyes were determined using the method similar to that of Hadfield and Lemin [354, 355]. In the present study, dye solutions (0.05 g/L) were prepared using a pH 5.5 buffer solution (HAc/NaAc), and then equal volume (100 mL) of dye solution and n-butanol were thoroughly mixed for 12 h. After separation of the two phases for 24 h, the equilibrium concentration of dye in both phases was determined using UV-vis spectroscopy, and the hydrophobic/hydrophilic ratio of the dye was

calculated from Eq. (4.1):

$$\text{hydrophobic/hydrophilic ratios} = \frac{\text{dye concentration in butanol}}{\text{dye concentration in aqueous buffer}} \quad (\text{E } 4.1)$$

#### 4.4.5 Sorption ability

The sorption ability of dye adsorbed at time  $t$  was calculated from:

$$q_t = \frac{C_0 V_0 - C_t V_t}{m} \quad (\text{E } 4.2)$$

where  $q_t$  = Sorption ability of dye at time  $t$  (mmol/g)

$C_0$  = Initial concentration of dye solution (mmol/L)

$V_0$  = Initial volume of dye solution (0.1 L)

$C_t$  = Concentration of dye solution at time  $t$  (mmol/L)

$V_t$  = Total volume of dye solution at time  $t$  (0.11 L)

$m$  = Mass of nanochitoan and microchitosan (g)

When time  $t = t_e$  (time to achieve equilibrium),  $q_t = q_e$ , that is,

$$q_t = q_e = \frac{C_0 V_0 - C_e V_e}{m} \quad (\text{E } 4.3)$$

where  $q_e$  = Sorption capacity of dye at equilibrium (mmol/g)

#### 4.4.6 Desorption efficiency

Desorption efficiency is calculated by the results of dye concentration in the desorption studies ( $C_{des}$ ). The equation is described below:

$$\text{Desorption efficiency} = \frac{C_{des} V_e - C_e V_e}{C_0 V_0 - C_e V_e} \times 100\% \quad (\text{E } 4.4)$$

## 4.5 Results and discussion

### 4.5.1 Particle size of chitosan nanoparticles

The relationship between the particle size and ultrasonic duration is shown in Figure 4.1. The results have been discussed in section 3.5.3. The emulsion with ultrasonic duration of 60 minutes and particles of 300-400 nm was used for sorption study.

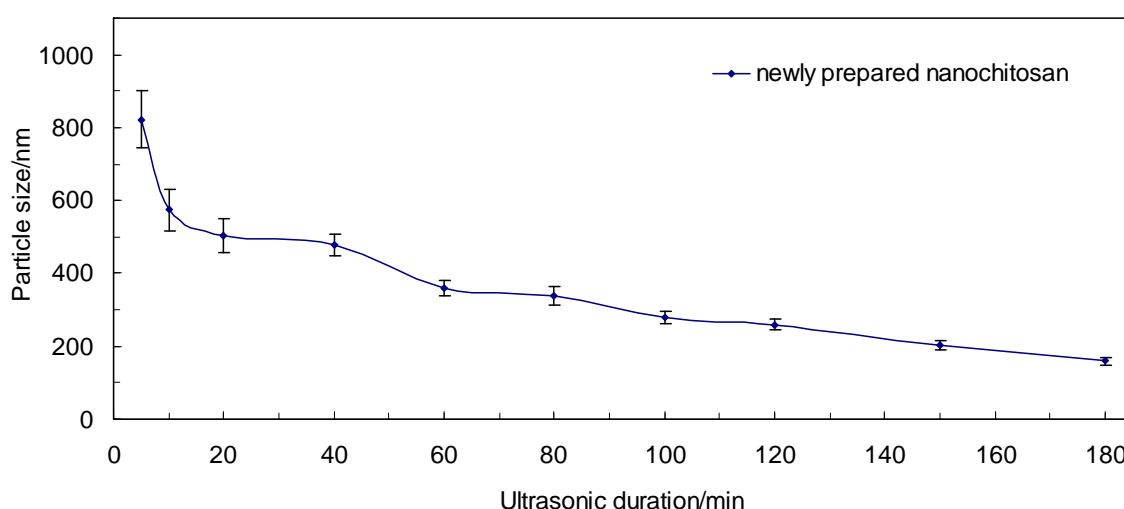


**Figure 4.1** Relationship between particle size and ultrasonic duration

### 4.5.2 Morphology of chitosan nanoparticles

Figure 4.2 shows the SEM images of the nanochitosan particles. These dried particles were only one-third of their sizes in the emulsion. The particles in the emulsion could not be separated when it was not diluted; we could observe the nanoparticles in the emulsion when it was dried by diluting the emulsion 100 times.

The surface/volume ratio of sphere is calculated as  $\frac{3}{r}$ , which  $r$  is the radius of the sphere.

If the nanochitosan in the emulsion is sphere with diameter size of 350 nm, the



surface/volume ratio is  $1.71 \times 10^7 \text{ m}^{-1}$ . As the particle size of microchitosan is about 400  $\mu\text{m}$  in water when it was swollen (observed by Nikon FX-35DX microscope), the surface/volume ratio of microchitosan is  $1.5 \times 10^4 \text{ m}^{-1}$ . The surface/volume ratio of nanoparticles is more than 1000 times bigger than that of the microchitosan. It is believed that the large surface area/volume value of nanochitosan led to the improvement of its sorption ability.

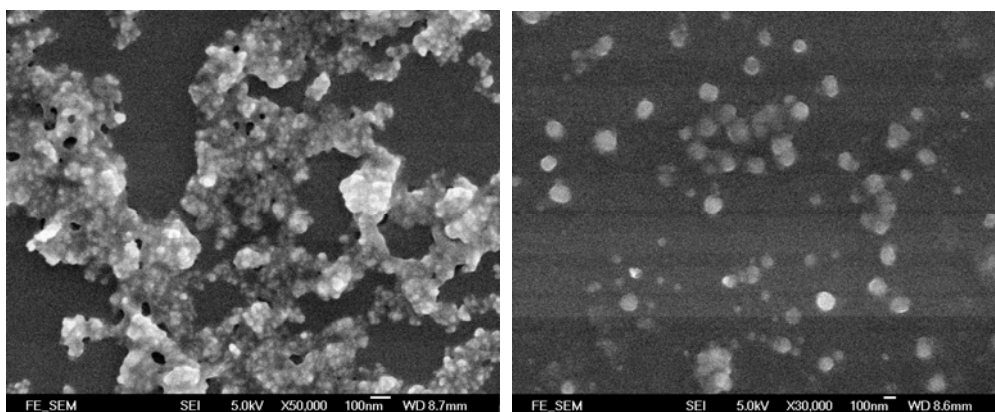


**Figure 4.2** SEM images of the nanochitosan particles with ultrasonic duration of 60 minutes (left: emulsion without dilution, right: 100 times diluted emulsion)

### 4.5.3 Sorption kinetic results

The sorption ability of nanochitosan and microchitosan at time  $t$ ,  $q_t$ , was calculated by using equation (E 4.2). The results of sorption of dyes onto nanochitosan and microchitosan at time  $t$  are shown in Figures 4.3-4.7.

The kinetic experimental results for Acid Orange 7 onto nanochitosan and microchitosan at different temperatures are shown in Figure 4.3. Nanochitosan had higher sorption capacities than microchitosan at the same temperature. The sorption ability of nanochitosan and microchitosan both increased as the temperature increased. But the improvement was not obvious from  $30^\circ\text{C}$  to  $70^\circ\text{C}$ . It is because the sorption of dyes onto chitosan is an exothermic process. Increasing the temperature can decrease the dye

aggregation and thus improve the sorption ability of chitosan, but it can also accelerate the desorption equilibrium. The opposite effect happened at the same time and the sorption ability of chitosan did not change much from 30°C to 70°C.

At 90°C, it was believed inter- and intra- molecular hydrogen bonding between chitosan polymer chain were broken down and the potentiality for additional hydrogen bondings with the dye molecules occurred [273]. That may be the reason why the sorption ability was improved greatly at 90°C.

The time to achieve the equilibrium for Acid Orange 7 onto nanochitosan was less than 30 minutes and it took about 1 day for Acid Orange 7 onto microchitosan to achieve the equilibrium. The nanochitosan was much more efficient during the sorption process comparing with microchitosan.

The experimental results for Acid Red 1 onto nanochitosan and microchitosan at different temperatures are shown in Figure 4.4. Similar to the sorption of Acid Orange 7, the nanochitosan had higher sorption capacities than those of the microchitosan at the same temperature and time to achieve the equilibrium for the nanochitosan was much shorter than that for microchitosan. The sorption ability of nanochitosan and microchitosan both increased as the temperature increased and the effect was much more obvious for microchitosan. The sorption ability of microchitosan increased as much as 48.84% at 90°C when comparing with the temperature at 30°C. The higher temperature could also reduce the time to achieve the equilibrium, especially for microchitosan.

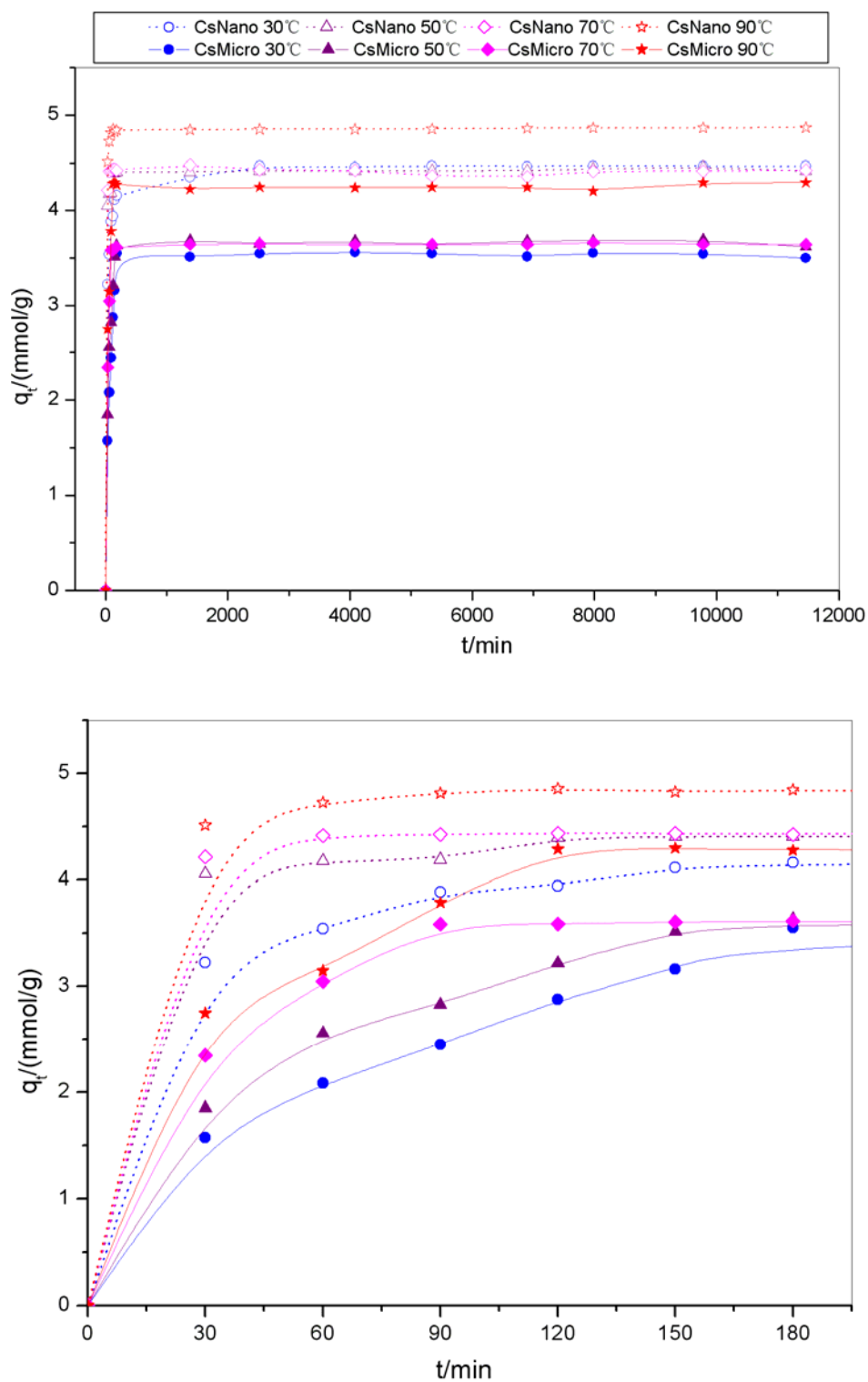


**Figure 4.3** Plots of sorption ability of nanochitosan and microchitosan for Acid Orange 7 at different temperatures

The sorption ability of nanochitosan and microchitosan for Acid Red 18 are shown in Figure 4.5. The nanochitosan had higher sorption capacities; however the difference between sorption capacities of nanochitosan and microchitosan was not as much as that for Acid Orange 7 and Acid Red 1. That is because the molecular dimensions of Acid Red 18 ( $14.87 \text{ \AA} \times 13.54 \text{ \AA} \times 2.24 \text{ \AA}$ ) are relatively small, especially there is one dimension which is only  $2.24 \text{ \AA}$ . The molecules of Acid Red 18 could penetrate into micro-sized chitosan to get adsorbed eventually. The time to achieve the equilibrium for the nanochitosan was much less than that of microchitosan.

Figures 4.6 and 4.7 show the plots of sorption ability of nanochitosan and microchitosan for Direct Red 84 and Direct Red 80 at temperatures of  $30^\circ\text{C}$ ,  $50^\circ\text{C}$ ,  $70^\circ\text{C}$  and  $90^\circ\text{C}$ . The nanochitosan demonstrated a much higher sorption capacity than that of the microchitosan at the same temperature. For Direct Red 84 and Direct Red 80 whose molecular sizes are large ( $24.86 \text{ \AA} \times 23.19 \text{ \AA} \times 6.47 \text{ \AA}$  and  $11.50 \text{ \AA} \times 20.88 \text{ \AA} \times 17.0 \text{ \AA}$ ), it was difficult to penetrate into the microchitosan to get adsorbed, while nanochitosan with much higher surface area/volume ratio could easily adsorb the dye molecules. It took less than 30 minutes for nanochitosan to achieve equilibrium while microchitosan needed more than 2 days. Nanochitosan could greatly increase the sorption capacity of chitosan and reduce the equilibrium time especially when the chitosan was used to adsorb dyes with large molecular sizes.

For large dye molecules, as diffusion is an endothermic process, increasing the temperature can also reduce dye aggregation and thus improve the sorption capacity. The sorption capacity of microchitosan was improved up to 83% when the sorption of Direct Red 84 was done at  $90^\circ\text{C}$  comparing with that at  $30^\circ\text{C}$ .

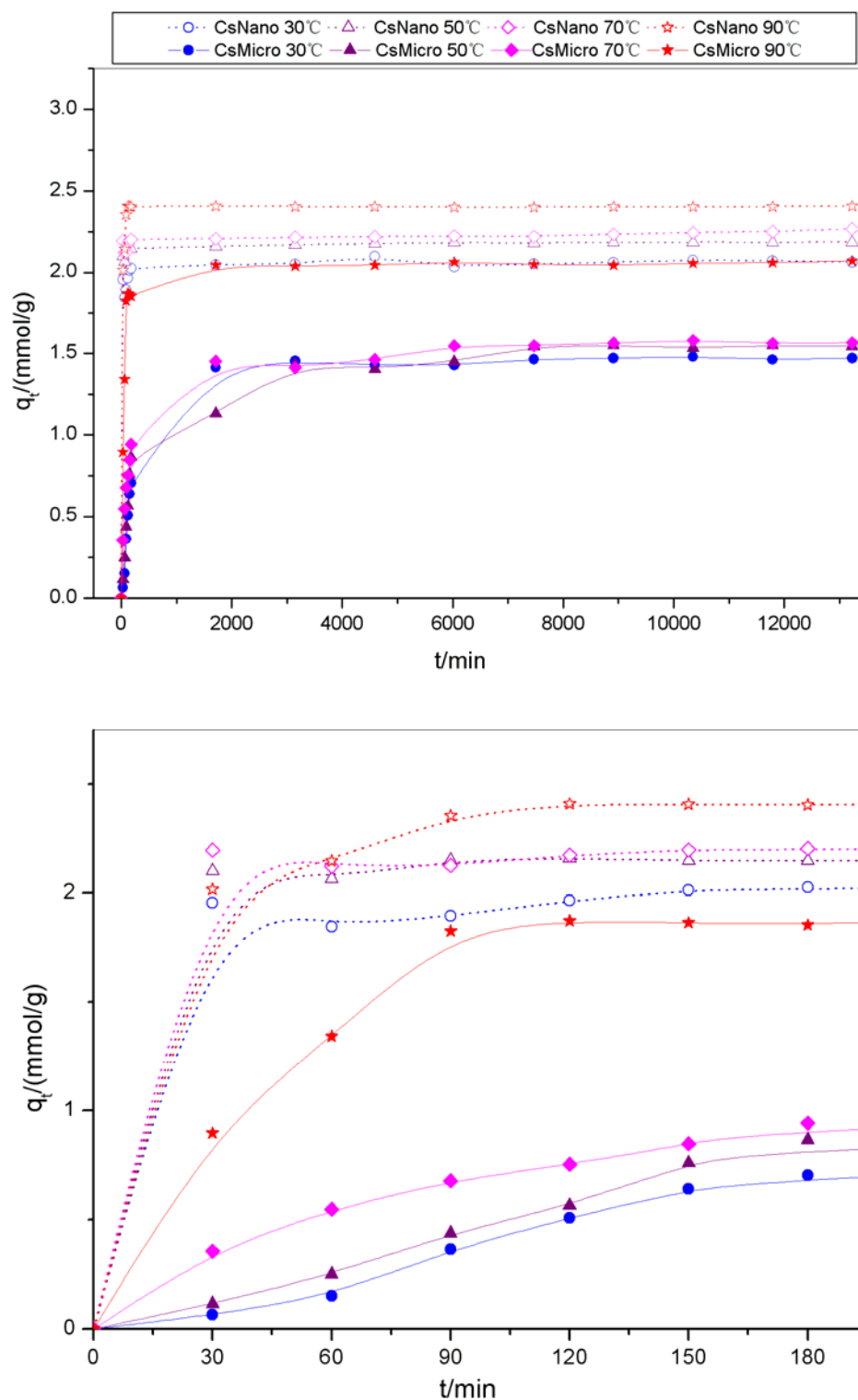


**Figure 4.4** Plots of sorption ability of nanochitosan and microchitosan for Acid Red 1 at different temperatures

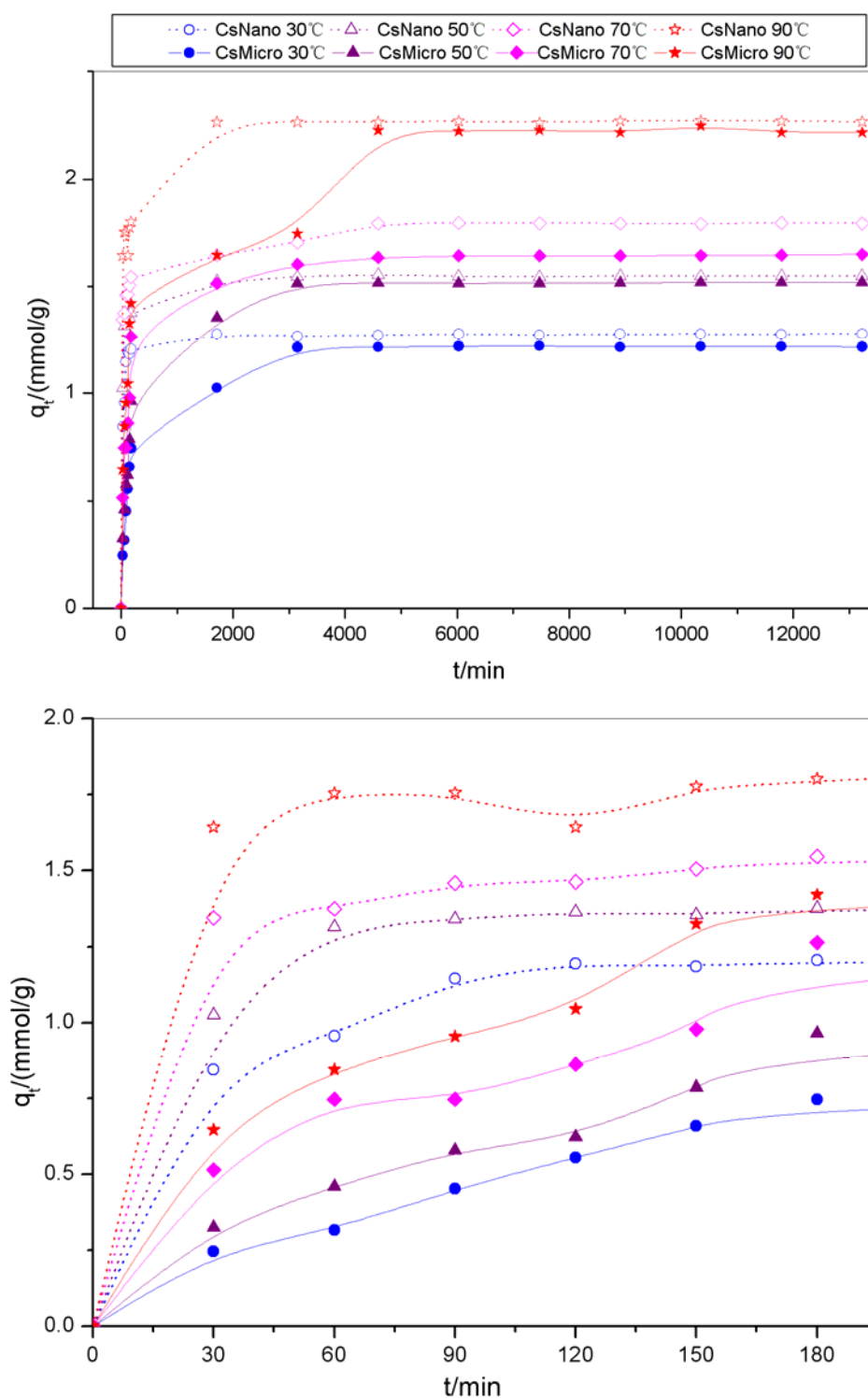


**Figure 4.5** Plots of sorption ability of nanochitosan and microchitosan for Acid Red 18 at different temperatures

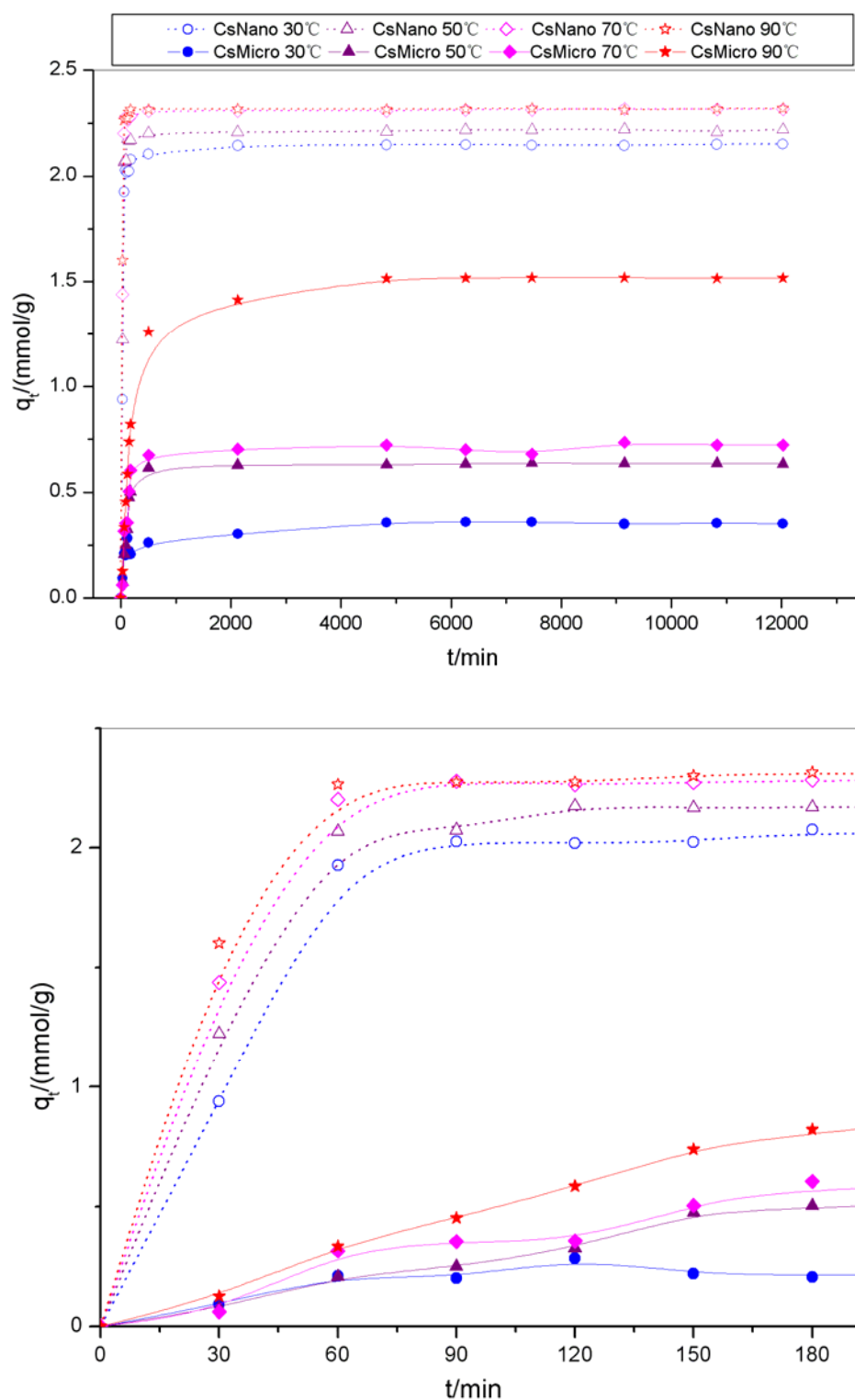


**Figure 4.6** Plots of sorption ability of nanochitosan and microchitosan for Direct Red 84 at different temperatures

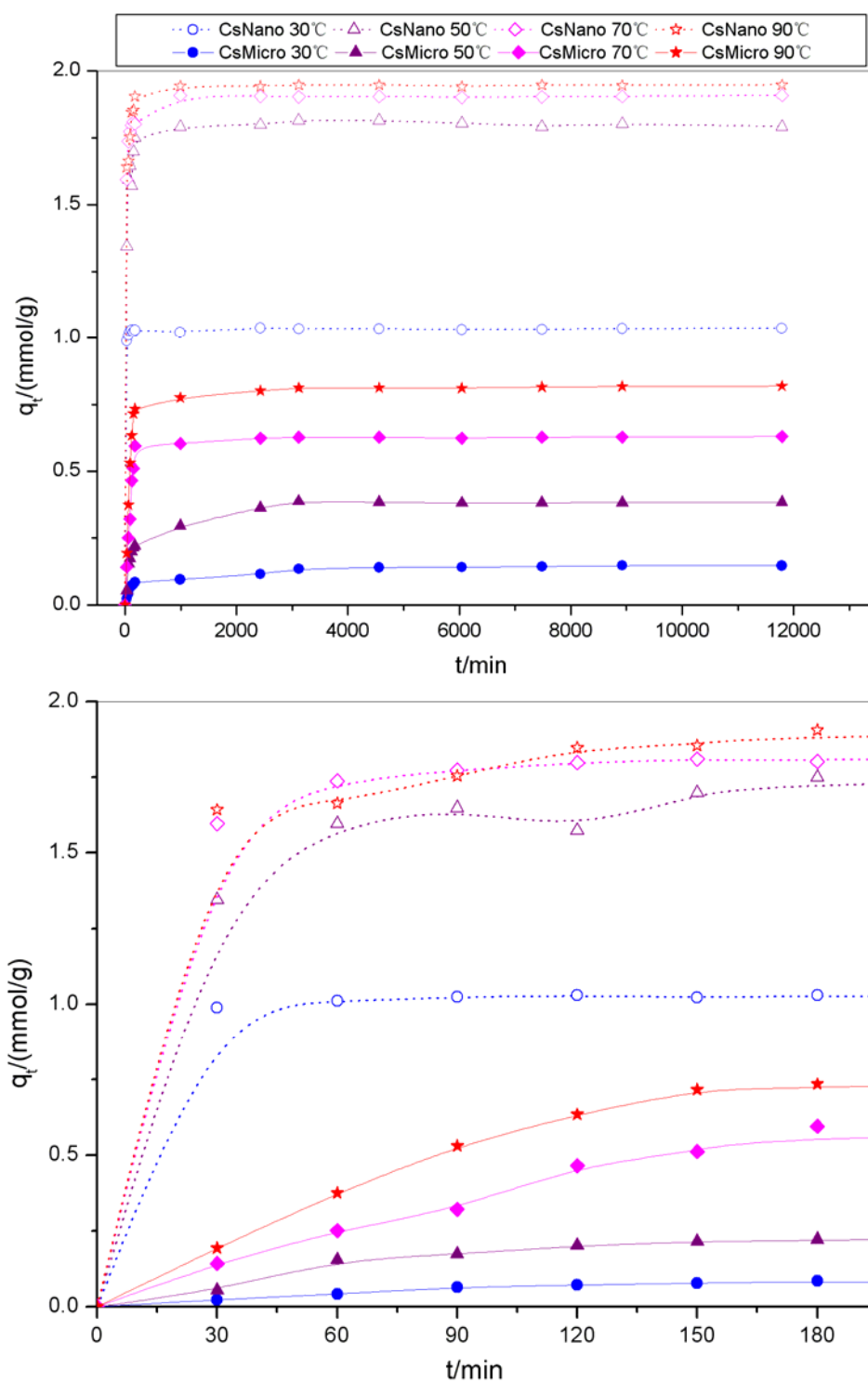


**Figure 4.7** Plots of sorption ability of nanochitosan and microchitosan for Direct Red 80 at different temperatures



#### 4.5.4 Sorption kinetics study

Many kinetic models and mechanisms have been proposed [285-286, 355]. In this part, a pseudo-first-order kinetic model and a pseudo-second-order kinetic rate equation was used to analyze the results.

##### 4.5.4.1. The pseudo-first-order kinetic model

For the first order chemical sorption,

$$\frac{dq_t}{dt} = k_1 (q_e - q_t) \quad (\text{E } 4.5)$$

where  $q_e$  is the sorption capacity (mmol/g) at equilibrium and  $q_t$  is the sorption capacity (mmol/g) at time  $t$  and  $k_1$  is the rate constant of pseudo-first-order sorption (1/min). Integrating this for the boundary conditions  $t = 0$  to  $t = t$  and  $q_t = 0$  to  $q_t = q_e$ , gives:

$$\lg(q_e - q_t) = \lg q_e - \frac{k_1}{2.303} t \quad (\text{E } 4.6)$$

The intercept of the straight line plots of  $\lg(q_e - q_t)$  against  $t$  should equal to  $\lg q_e$ . However, if the intercept does not equal to  $\lg q_e$ , then the reaction is not suitable to use a first order fitting even the plots has high correlation coefficient with the experiment data. In order to check the model, the data obtained from kinetic sorption experiment for each dye was calculated. The data of  $\lg(q_e - q_t)$  against  $t$  was plotted. The pseudo-first-order kinetics for the sorption of Acid Orange 7 at 30°C are shown in Figure 4.8 and the parameters for sorption of different dyes at different temperature onto nanochitosan and microchitosan are list in Table 4.2.

**Table 4.2** Pseudo-first-order rate constants for the anionic dyes

Dye	Nanochitosan (CsNano)			Microchitosan (CsMicro)		
	$q_e$ /(mmol/g)	$K_1$ /[g/(mmol·min)]	$R^2$	$q_e$ /(mmol/g)	$K_1$ /[g/(mmol·min)]	$R^2$
Acid Orange 7						
30 °C	4.465	$1.326 \times 10^{-2}$	0.8781	3.551	$1.389 \times 10^{-2}$	0.9859
50 °C	4.415	$2.464 \times 10^{-3}$	0.2596	3.650	$2.644 \times 10^{-2}$	0.8981
70 °C	4.462	$2.294 \times 10^{-2}$	0.6325	3.645	$2.805 \times 10^{-2}$	0.8987
90 °C	4.867	$2.733 \times 10^{-2}$	0.7515	4.259	$2.296 \times 10^{-2}$	0.9637
Acid Red 1						
30 °C	2.068	$1.644 \times 10^{-2}$	0.6940	1.471	$3.961 \times 10^{-3}$	0.9750
50 °C	2.185	$1.819 \times 10^{-2}$	0.5916	1.544	$4.698 \times 10^{-3}$	0.9804
70 °C	2.250	$1.453 \times 10^{-2}$	0.4856	1.567	$4.790 \times 10^{-3}$	0.9740
90 °C	2.405	$4.083 \times 10^{-2}$	0.9887	2.058	$1.409 \times 10^{-2}$	0.9407
Acid Red 18						
30 °C	1.276	$1.573 \times 10^{-2}$	0.8943	1.217	$5.067 \times 10^{-3}$	0.9931
50 °C	1.549	$1.048 \times 10^{-2}$	0.7042	1.518	$4.974 \times 10^{-3}$	0.9614
70 °C	1.794	$8.383 \times 10^{-3}$	0.6729	1.645	$6.633 \times 10^{-3}$	0.9029
90 °C	2.269	$5.988 \times 10^{-3}$	0.4845	2.223	$5.182 \times 10^{-3}$	0.9563
Direct Red 84						
30 °C	2.146	$6.264 \times 10^{-3}$	0.5337	0.3539	$1.948 \times 10^{-3}$	0.9575
50 °C	2.216	$8.268 \times 10^{-3}$	0.5953	0.6363	$6.886 \times 10^{-3}$	0.9706
70 °C	2.315	$8.751 \times 10^{-3}$	0.5721	0.7158	$5.758 \times 10^{-3}$	0.9011
90 °C	2.317	$1.170 \times 10^{-2}$	0.5631	1.517	$3.523 \times 10^{-3}$	0.9875
Direct Red 80						
30 °C	1.034	$2.400 \times 10^{-2}$	0.7043	0.1449	$4.974 \times 10^{-3}$	0.9742
50 °C	1.797	$1.639 \times 10^{-2}$	0.8451	0.3830	$4.951 \times 10^{-3}$	0.9205
70 °C	1.905	$1.372 \times 10^{-2}$	0.6952	0.6274	$1.499 \times 10^{-2}$	0.9003
90 °C	1.946	$1.796 \times 10^{-2}$	0.8893	0.8158	$1.361 \times 10^{-2}$	0.9885

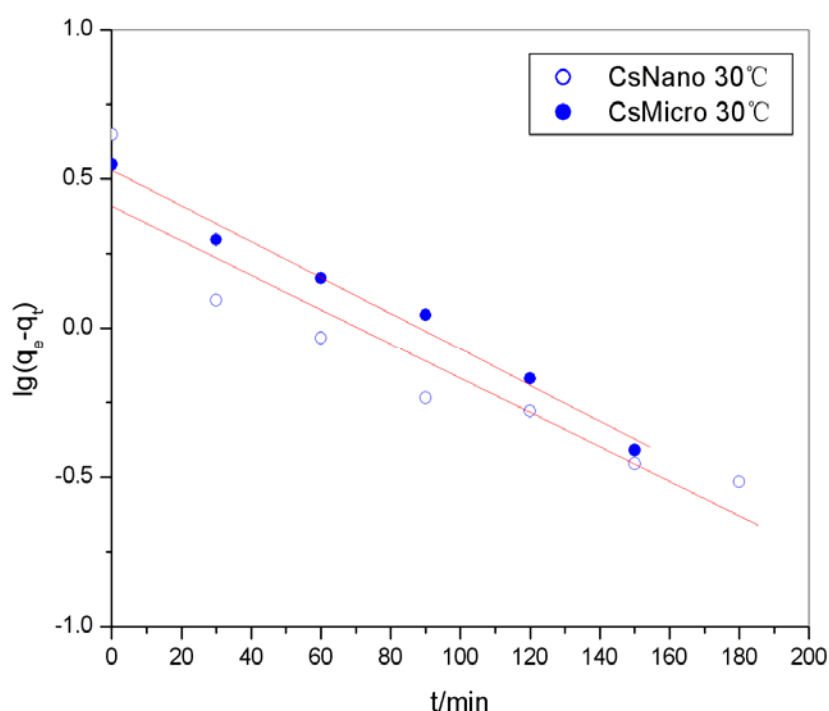


**Figure 4.8** Pseudo-first-order kinetics for the sorption of Acid Orange 7 at 30°C

Although some of the sorption of dyes onto the microchitosan could fit the first order, all of the sorption of dyes onto nanochitosan could not fit the first order equally at all. It was not suitable to use first order kinetic model to fit the sorption here.

#### 4.5.4.2. The pseudo-second-order kinetic model

When the rate of sorption is a second order mechanism, the pseudo-second-order chemisorption kinetic rate equation can be written as,

$$\frac{dq_t}{dt} = k_2 (q_e - q_t)^2 \quad (\text{E } 4.7)$$

where  $q_e$  is the sorption capacity (mmol/g) at equilibrium and  $q_t$  is the sorption capacity (mmol/g) at time  $t$  and  $k_2$  is the rate constant of pseudo-second-order sorption [g/(mmol·min)]. For the boundary conditions  $t=0$  to  $t=t$  and  $q=q_t$ , the integrated form of

equation (E 4.7) becomes:

$$\frac{1}{q_e - q_t} = \frac{1}{q_e} + k_2 t \quad (\text{E 4.8})$$

Equation (E 4.8) can be rearranged to obtain equation (E 4.9) as following,

$$q_t = \frac{t}{\frac{1}{k_2 q_e^2} + \frac{t}{q_e}} \quad (\text{E 4.9})$$

From equation (4.9), the linear form of  $t/q_t$  versus  $t$  can be obtained. That is

$$\frac{t}{q_t} = \frac{1}{k_2 q_e^2} + \frac{1}{q_e} t \quad (\text{E 4.10})$$

If the pseudo second-order kinetics is applicable, the plot of  $t/q_t$  versus  $t$  should give a linear relationship as shown in the equation (E 4.10).  $q_e$  and  $k$  can be determined from the slope and intercept of the plot respectively. The sorption kinetic study has an important guiding function in both theoretical research and industrial applications.

The relationship of  $\frac{t}{q_t}$  versus  $t$  for the sorption of Acid Orange 7 at 30°C is shown in

Figure 4.9. And the relationship of  $\frac{t}{q_t}$  versus  $t$  for other dyes was also analyzed. The

correlation coefficient  $R^2$  shows that pseudo-second-order model which is indicative of a chemisorption mechanism, fit the experimental data well. This model could be successfully applied to describe the kinetics of sorption of nanochitosan and microchitosan for the anionic dyes. The calculated  $k_2$  [g/(mmol·min)] and  $q_e$  (mmol/g) values for each dye are listed in Table 4.3.

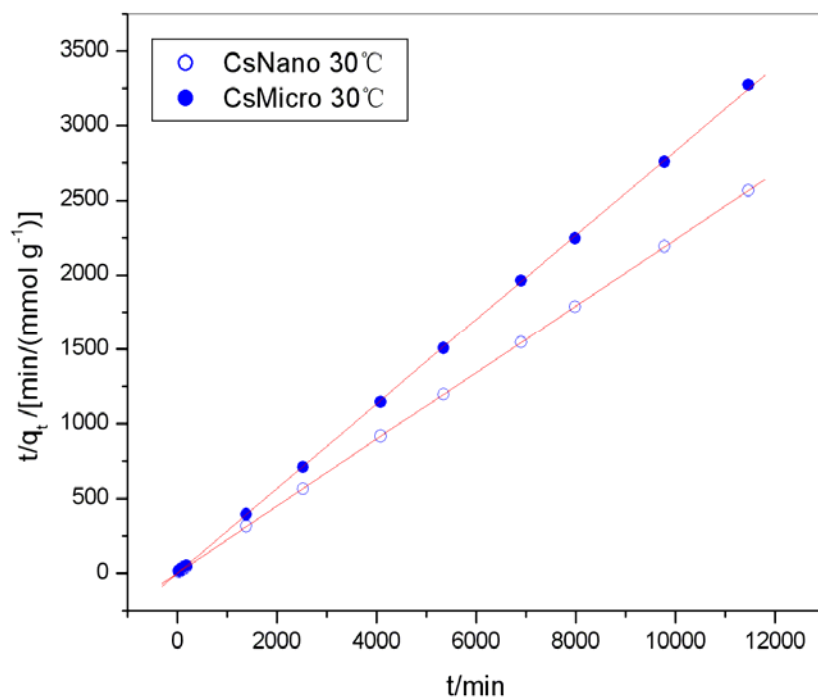


**Figure 4.9** Pseudo-second-order kinetics for the sorption of Acid Orange 7 at 30°C

The experimental data and the pseudo-second-order model of each dye are shown in Figures 4.10-4.14. This pseudo-second-order model could be successfully applied to describe the kinetics of sorption of anionic dyes onto nanochitosan and microchitosan. The sorption kinetic study has an important guiding function in both theoretical research and industrial applications.

**Table 4.3** Pseudo-second-order rate constants for the anionic dyes

Dye	Nanochitosan (CsNano)			Microchitosan (CsMicro)		
	$q_e$ /(mmol/g)	$K_2$ /[g/(mmol·min)]	$R^2$	$q_e$ /(mmol/g)	$K_2$ /[g/(mmol·min)]	$R^2$
Acid Orange 7						
30 °C	4.474	0.0149	0.9999	3.535	0.0206	0.9999
50 °C	4.431	0.0488	0.9999	3.662	0.0345	0.9998
70 °C	4.408	0.1053	0.9999	3.650	0.0582	0.9997
90 °C	4.868	0.049	0.9999	4.277	0.0127	0.9998
Acid Red 1						
30 °C	2.067	0.0508	0.9999	1.513	0.0022	0.9990
50 °C	2.186	0.0601	0.9999	1.582	0.0019	0.9988
70 °C	2.253	0.0168	0.9999	1.584	0.0038	0.9996
90 °C	2.406	0.1207	0.9999	2.065	0.017	0.9999
Acid Red 18						
30 °C	1.277	0.0522	0.9999	1.235	0.0057	0.9997
50 °C	1.551	0.0389	0.9999	1.538	0.0049	0.9999
70 °C	1.801	0.0115	0.9998	1.661	0.0064	0.9999
90 °C	2.274	0.0172	0.9999	2.262	0.0190	0.9974
Direct Red 84						
30 °C	2.150	0.0384	0.9999	0.357	0.0280	0.9994
50 °C	2.217	0.0648	0.9999	0.642	0.0164	0.9999
70 °C	2.316	0.0667	0.9999	0.728	0.0115	0.9988
90 °C	2.318	0.124	0.9999	1.548	0.0034	0.9998
Direct Red 80						
30 °C	1.035	0.2454	0.9999	0.149	0.0259	0.9978
50 °C	1.797	0.4928	0.9999	0.390	0.0188	0.9997
70 °C	1.908	0.0703	0.9999	0.633	0.0283	0.9999
90 °C	1.949	0.0754	0.9999	0.822	0.0231	0.9999

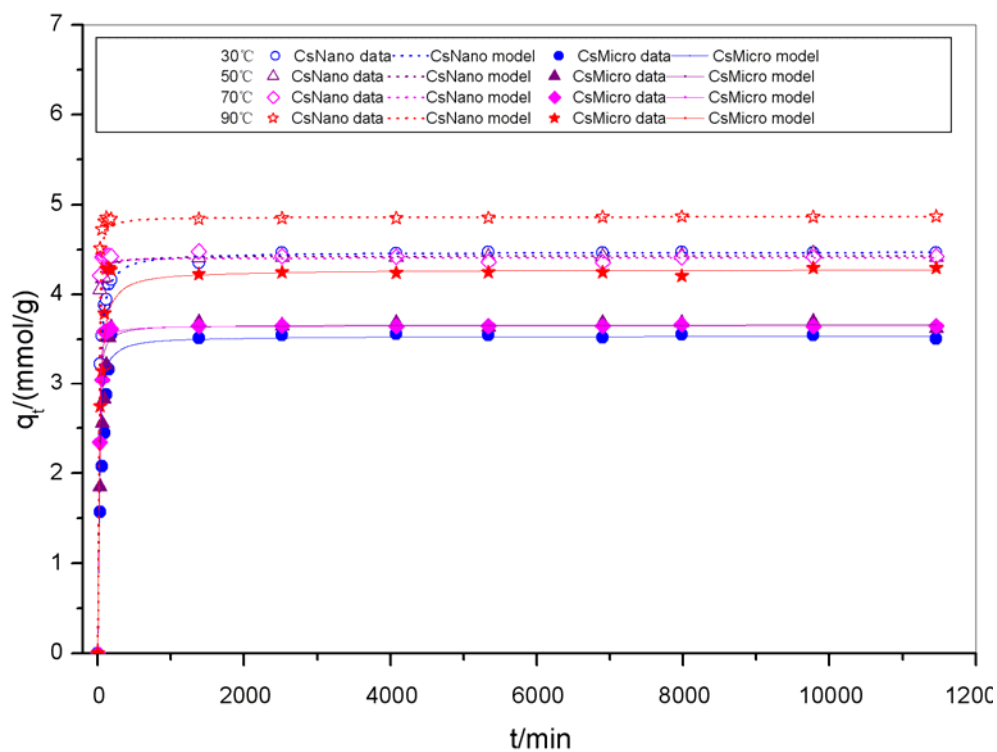


**Figure 4.10** Pseudo-second-order model for sorption kinetics of Acid Orange 7 onto nanochitosan and microchitosan at different temperatures

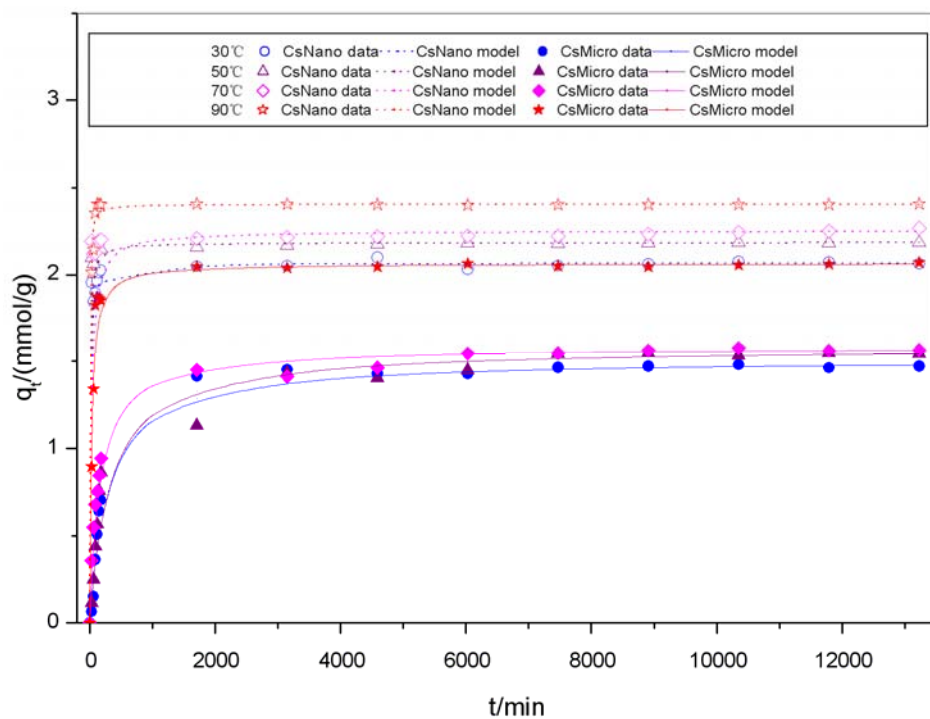


**Figure 4.11** Pseudo-second-order model for sorption kinetics of Acid Red 1 onto nanochitosan and microchitosan at different temperatures

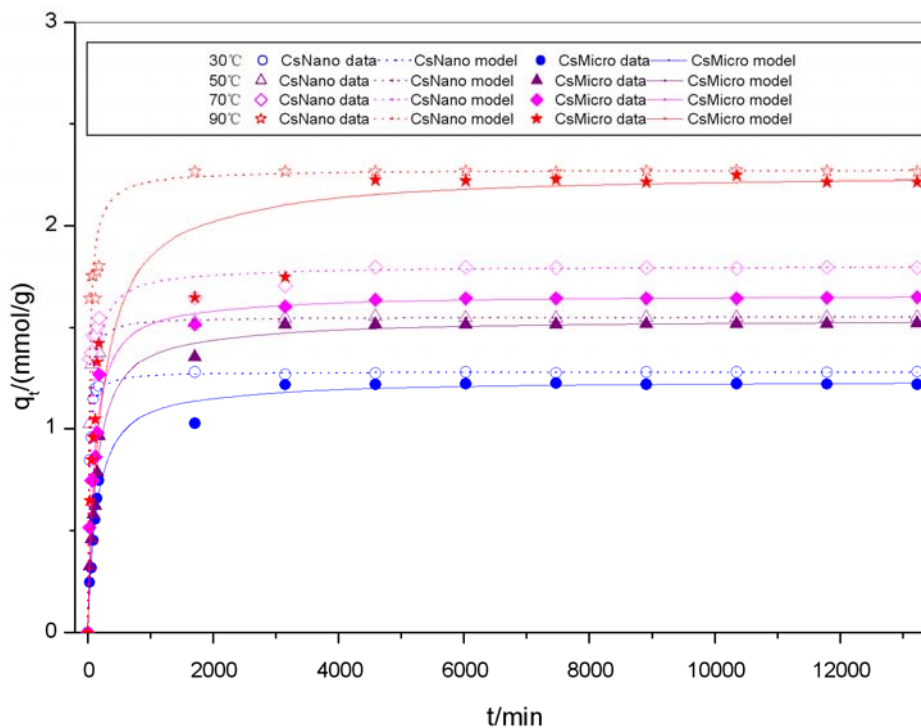


**Figure 4.12** Pseudo-second-order model for sorption kinetics of Acid Red 18 onto nanochitosan and microchitosan at different temperatures

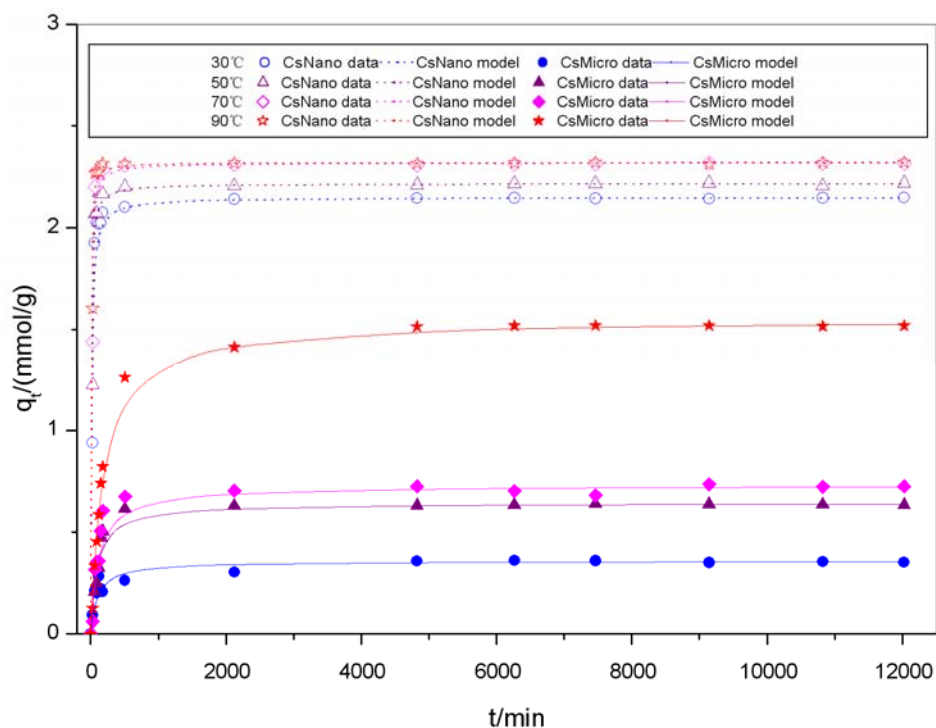


**Figure 4.13** Pseudo-second-order model for sorption kinetics of Direct Red 84 onto nanochitosan and microchitosan at different temperatures



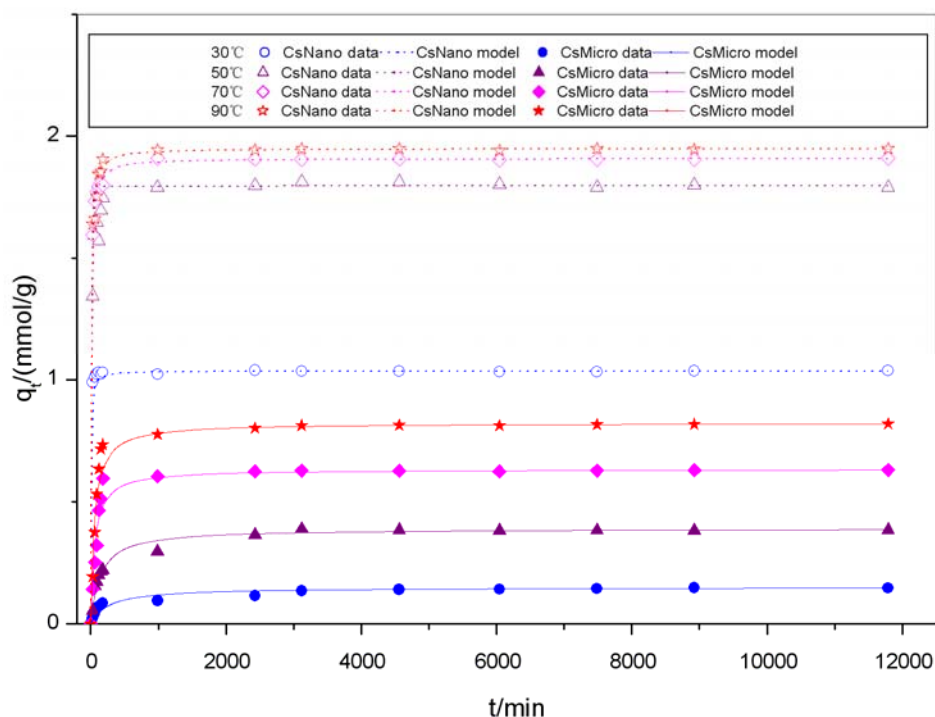


**Figure 4.14** Pseudo-second-order model for sorption kinetics of Direct Red 80 onto nanochitosan and microchitosan at different temperatures

#### 4.5.5 Sorption isotherms results

Adsorption isotherms describe how adsorbates interact with adsorbents and so are critical in optimizing the use of adsorbents. The equilibrium sorption capacity curves can be obtained by measuring the sorption isotherm of the acid dyes onto chitosan. The results of sorption of dyes onto nanochitosan and microchitosan at different equilibrium concentration and temperature are plotted in Figures 4.15-4.19.

The Langmuir equilibrium isotherms model and Freundlich equilibrium isotherms model were used to analyze the sorption isotherm data. And the correlation coefficient  $R^2$  were used to compare the applicability of the models.

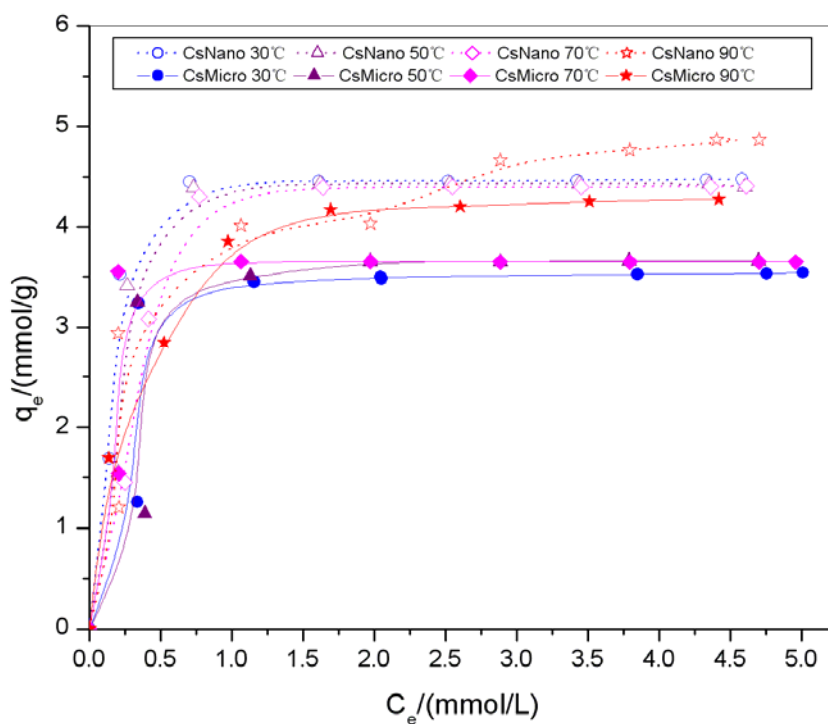


**Figure 4.15** Sorption capacities of nanochitosan and microchitosan for Acid Orange 7 at different temperatures, pH=5.5

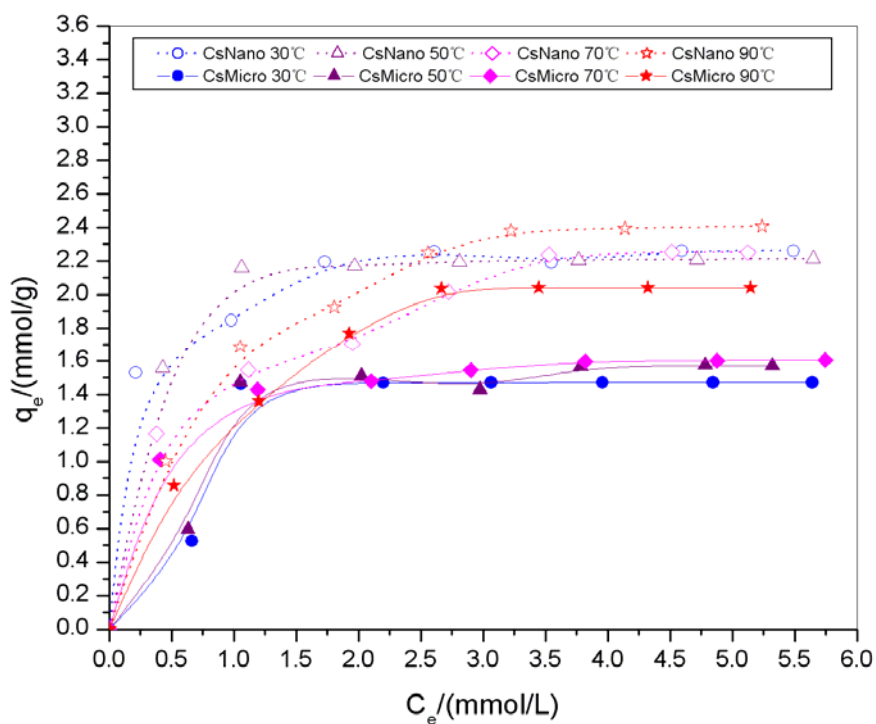


**Figure 4.16** Sorption capacities of nanochitosan and microchitosan for Acid Red 1 at different temperatures, pH=5.5

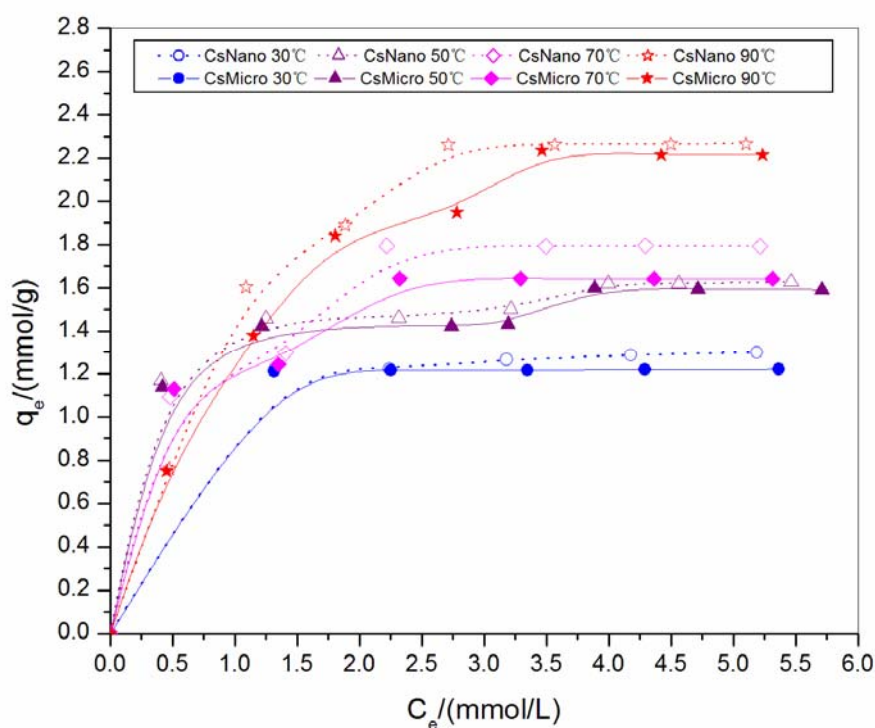


**Figure 4.17** Sorption capacities of nanochitosan and microchitosan for Acid Red 18 at different temperatures, pH=5.5

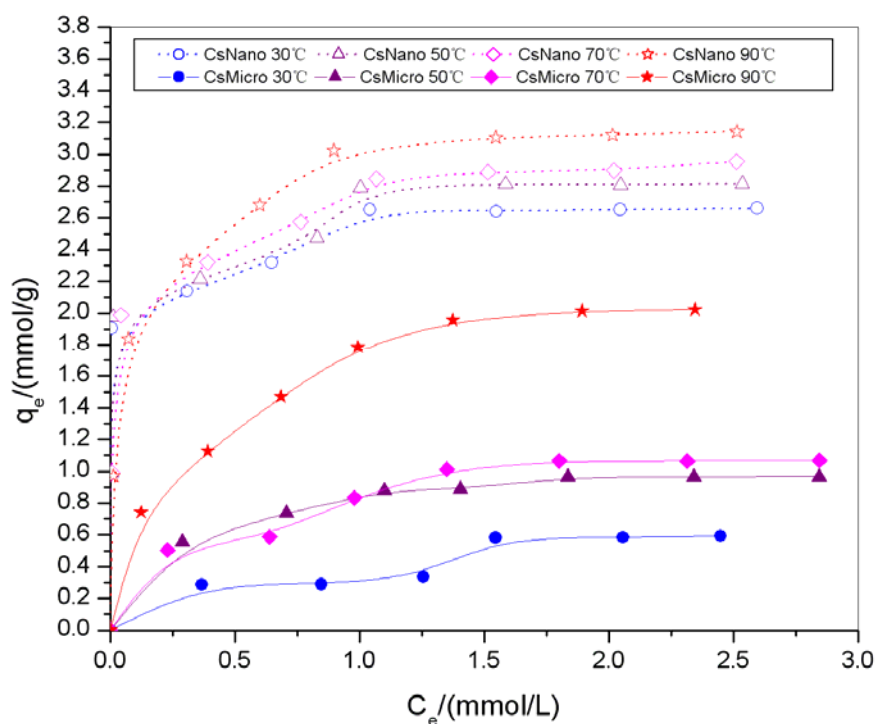


**Figure 4.18** Sorption capacities of nanochitosan and microchitosan for Direct Red 84 onto at different temperatures, pH=5.5

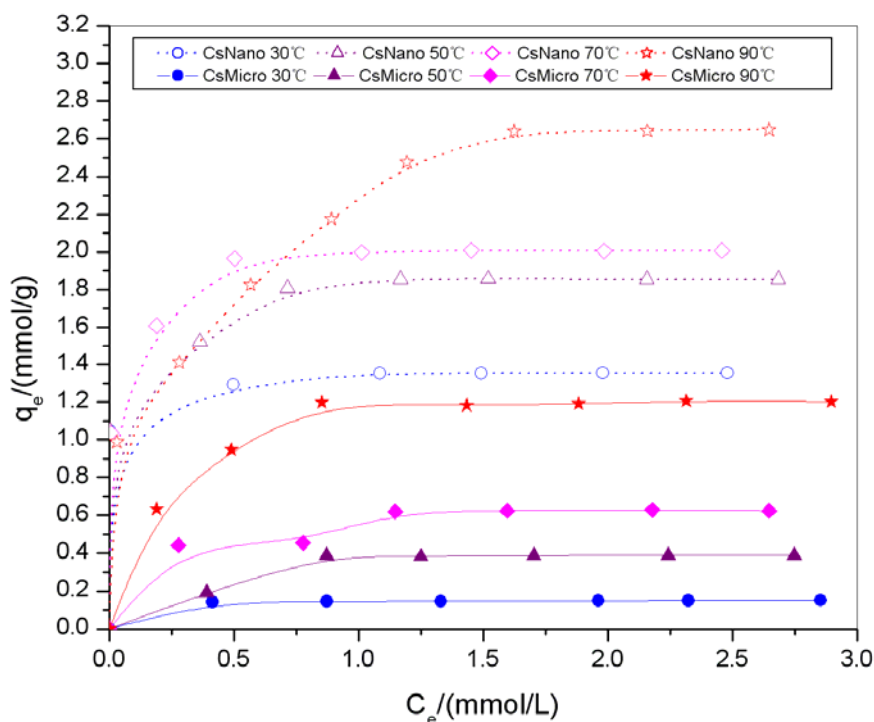


**Figure 4.19** Sorption capacities of nanochitosan and microchitosan for Direct Red 80 at different temperatures, pH=5.5

## 4.5.6 Equilibrium isotherms

### 4.5.6.1 Langmuir equilibrium isotherms

The Langmuir theory is based on the assumption of a structurally homogeneous adsorbent where all sorption sites are identical and energetically equivalent. The Langmuir isotherm has been successfully applied to explain the sorption of dyes onto chitosan by many researchers. [232, 244-254, 256, 258-260]. In the previous study, the Langmuir equation has been found to provide the best prediction for the adsorption of many dyes in the entire concentration range [232, 266].

The analogous form of the Langmuir isotherm equation for liquid state sorption can be presented as:

$$q_e = \frac{K_L C_e}{1 + a_L C_e} \quad (\text{E 4.11})$$

where  $q_e$  is the solid phase adsorbate concentration at equilibrium (mmol/g),  $C_e$  is the aqueous phase adsorbate concentration at equilibrium (mmol/L),  $K_L$  and  $a_L$  are the Langmuir isotherm constants. From equation (E 4.11), the linear form of  $C_e/q_e$  versus  $C_e$  can be obtained:

$$\frac{C_e}{q_e} = \frac{1}{K_L} + \frac{a_L C_e}{K_L} \quad (\text{E 4.12})$$

where  $K_L/a_L$  gives the theoretical monolayer saturation capacity,  $Q_0$ .

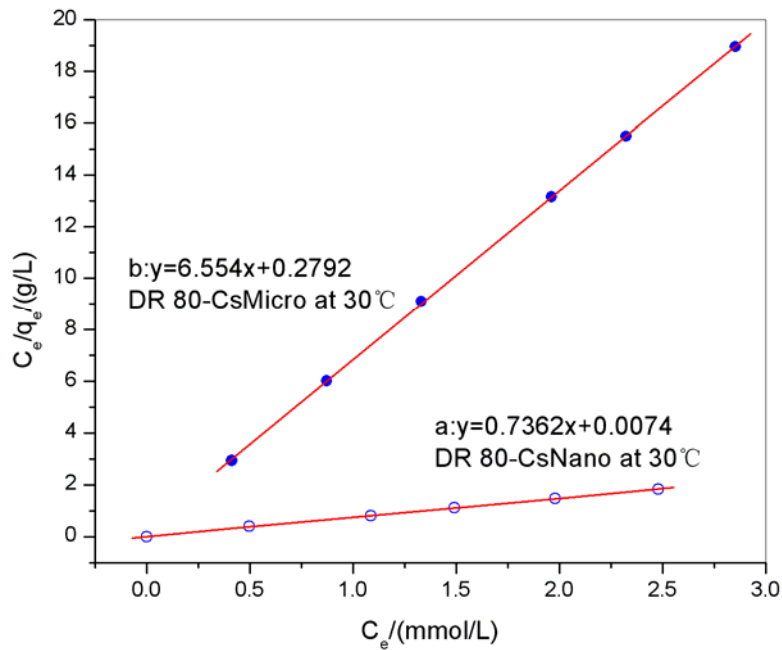


**Figure 4.20** Langmuir isotherm linear plots (a: Direct Red 80 onto nanochitosan at 30°C  
b: Direct Red 80 onto microchitosan at 30°C)

The relationship between  $C_e/q_e$  and  $C_e$  for the sorption of Direct Red 80 at 30°C is shown in Figure 4.20. The experimental data and the Langmuir isotherm model of Direct

Red 80 onto the nanochitosan and microchitosan at 30°C are shown in Figure 4.21. The model fit the data well and gave the result of sorption capacity.

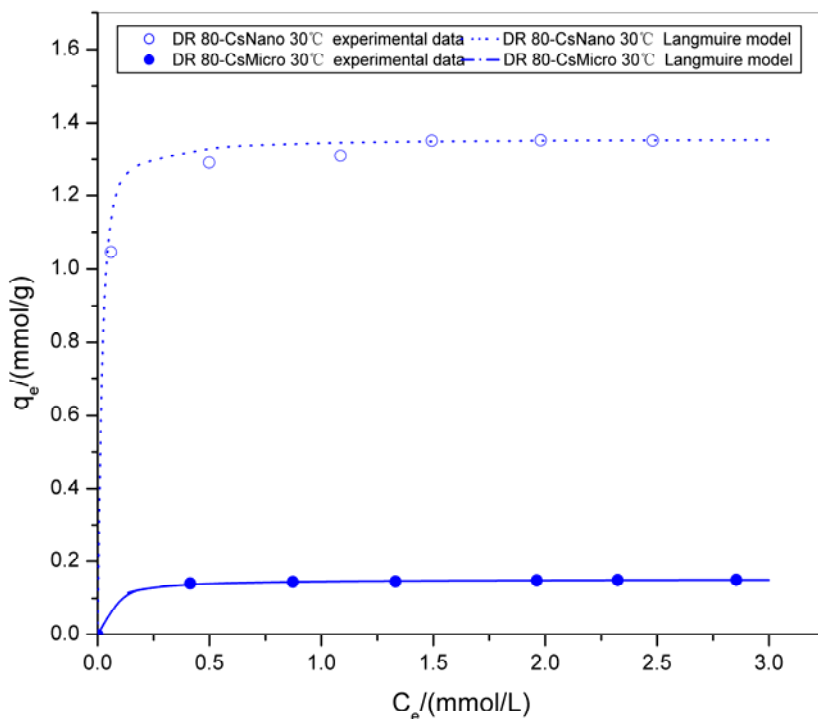


**Figure 4.21** Langmuir isotherm model for Direct Red 80 onto nanochitosan and microchitosan at 30°C

The relationship of  $C_e/q_e$  versus  $C_e$  for the other dyes at different temperatures were also analyzed. The isotherm constants,  $a_L$ ,  $K_L$  and equilibrium monolayer capacities,  $Q_0$  are presented in Table 4.4. The correlation coefficient  $R^2$  shows the applicability of the Langmuir isotherm.

**Table 4.4** Langmuir sorption isotherm constants for the anionic dyes

Dye	Nanochitosan (CsNano)				Microchitosan (CsMicro)			
	$K_L$ /(L/g)	$a_L$ /(L/mmol)	$Q_0$ /(mmol/g)	$R^2$	$K_L$ /(L/g)	$a_L$ /(L/mmol)	$Q_0$ /(mmol/g)	$R^2$
Acid Orange 7								
30°C	45.93	10.00	4.591	0.9986	33.24	8.987	3.699	0.9631
50°C	29.61	6.500	4.556	0.9956	10.64	2.600	4.054	0.9687
70°C	18.06	4.012	4.502	0.9927	36.79	9.819	3.747	0.9977
90°C	11.92	2.239	5.325	0.9915	20.72	4.584	4.521	0.9988
Acid Red 1								
30°C	15.59	6.706	2.325	0.9989	2.507	1.566	1.601	0.9492
50°C	7.848	4.159	1.887	0.9973	2.249	1.369	1.643	0.9606
70°C	3.808	1.570	2.426	0.9936	2.110	1.273	1.657	0.9984
90°C	3.579	1.376	2.601	0.9959	2.731	1.216	2.246	0.9999
Acid Red 18								
30°C	7.994	5.976	1.338	0.9995	7.698	6.292	1.224	0.9999
50°C	6.727	3.973	1.693	0.9974	5.992	3.611	1.659	0.9942
70°C	3.725	1.846	2.018	0.9661	5.034	3.025	1.664	0.9926
90°C	2.806	1.096	2.560	0.9841	2.386	0.937	2.546	0.9905
Direct Red 84								
30°C	705.3	243.2	2.900	0.9988	4.993	8.146	0.613	0.9992
50°C	64.98	22.73	2.859	0.9978	3.934	3.665	0.973	0.9979
70°C	51.81	19.12	2.710	0.9979	2.635	2.055	1.082	0.9759
90°C	43.14	13.34	3.233	0.9989	2.284	0.912	2.054	0.9938
Direct Red 80								
30°C	135.1	99.47	1.358	0.9998	3.581	23.47	0.153	0.9999
50°C	58.14	30.90	1.882	0.9993	3.470	8.876	0.391	0.9846
70°C	92.76	45.72	2.029	0.9998	3.281	4.796	0.684	0.9874
90°C	13.21	4.584	2.883	0.9908	2.818	2.212	1.274	0.9978

#### 4.5.6.2 Freundlich equilibrium isotherms

The Freundlich isotherm describes reversible adsorption and is not restricted to the formation of the monolayer. The Freundlich equation is an empirical equation employed to describe heterogeneous systems, in which it is characterized by the heterogeneity factor  $\frac{1}{n_F}$ . The equation can be written as,

$$q_e = K_F C_e^{1/n_F} \quad (\text{E 4.13})$$

The linear form of the equation is:

$$\ln q_e = \ln K_F + \frac{\ln C_e}{n_F} \quad (\text{E 4.14})$$

In the equation,  $K_F$  and  $n_F$  are the isotherm constants for Freundlich isotherm, which can be calculated from the equation (E 4.13). The Freundlich equilibrium isotherms were also analyzed in this study and Figure 4.22 shows the Freundlich isotherm model for Direct Red 80 onto the nanochitosan and microchitosan at 30°C.

For some dyes, the Freundlich isotherm could fit the whole concentration fairly (Figure 4.22). But for some dyes, as shown in Figure 4.23, it was clear that the Freundlich isotherm could not be used to fit the whole concentration. It was reported that the Freundlich equilibrium isotherms fit the sorption data when concentration was low [232, 266].

The Freundlich isotherm was not suitable in the sorption of dyes onto the nanochitosan and microchitosan while the Langmuir isotherm provided the best prediction for the sorption of the five dyes including acid dyes and direct dyes in the entire concentration range.



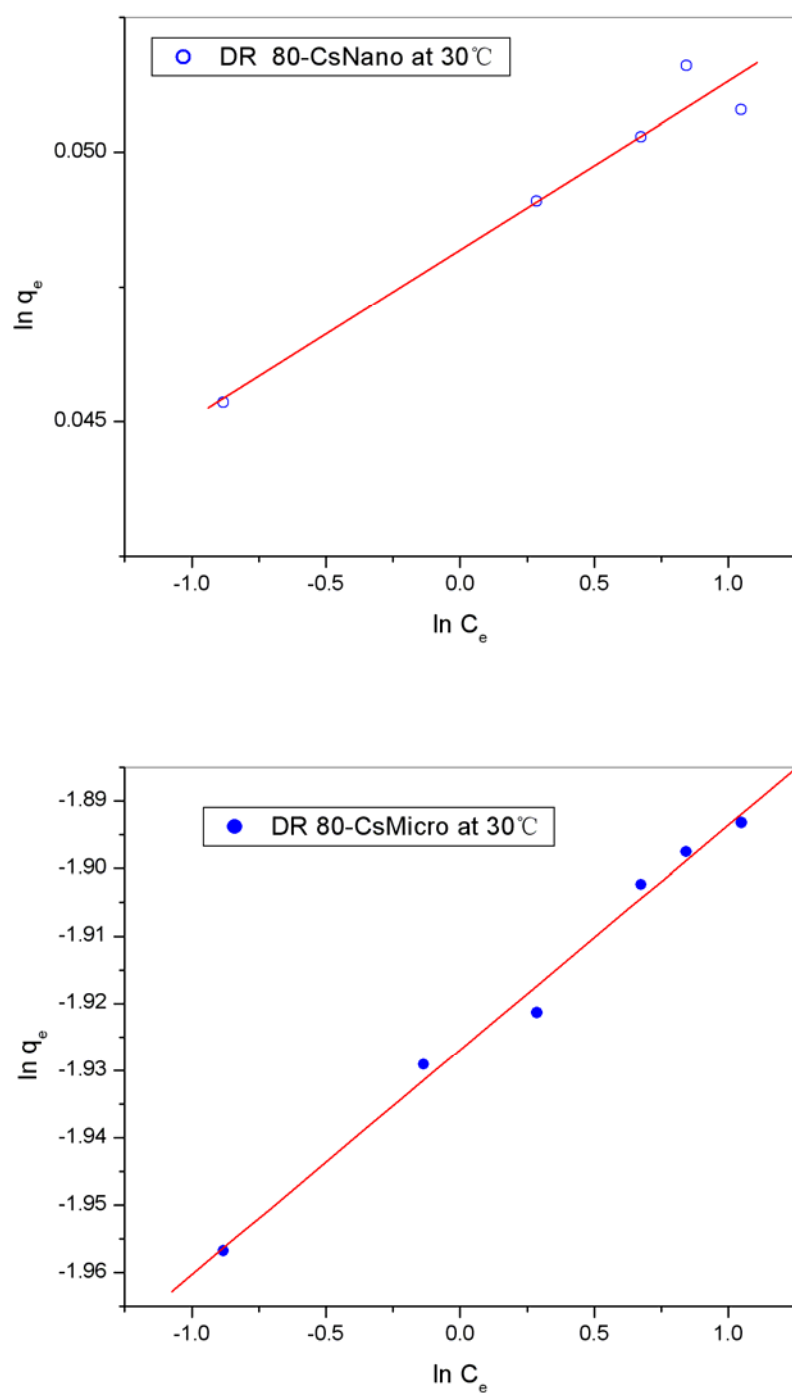


**Figure 4.22** Freundlich isotherm model for Direct Red 80 onto nanochitosan and microchitosan at 30°C

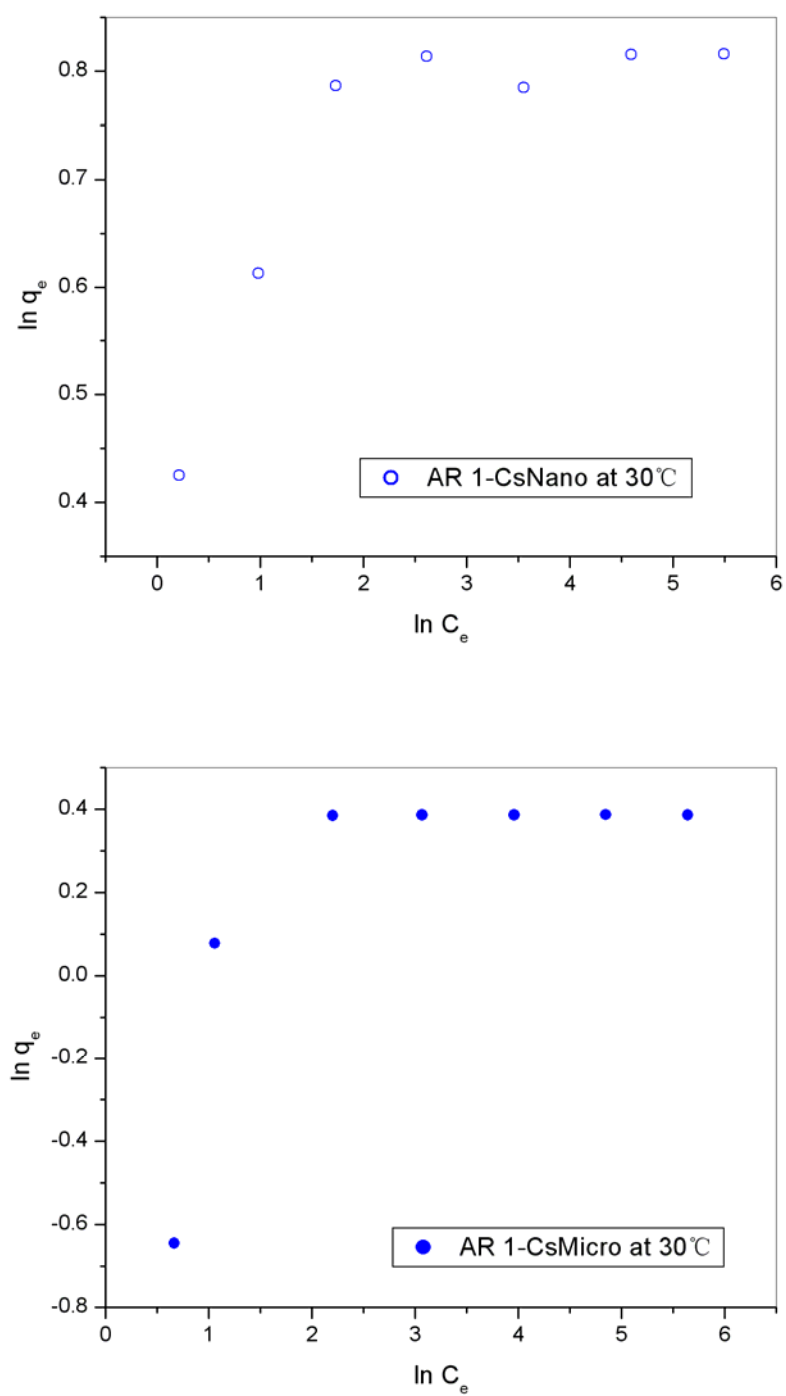


**Figure 4.23** Freundlich isotherm data for Acid Red 1 onto nanochitosan and microchitosan at 30°C

### 4.5.7 Sorption mechanisms

The mechanisms of sorption of dyes onto chitosan are mainly based on ionic attraction between anionic sulphonate group(s) of dissolved dye molecules and the cationic amino groups of protonated chitosan, hydrogen bonding between polysaccharide hydroxyl groups and electronegative residues in the dye molecule, Yoshida H-bonding between the polysaccharide hydroxyl groups and aromatic residues in the dyes as shown in Figure 4.24 [273].

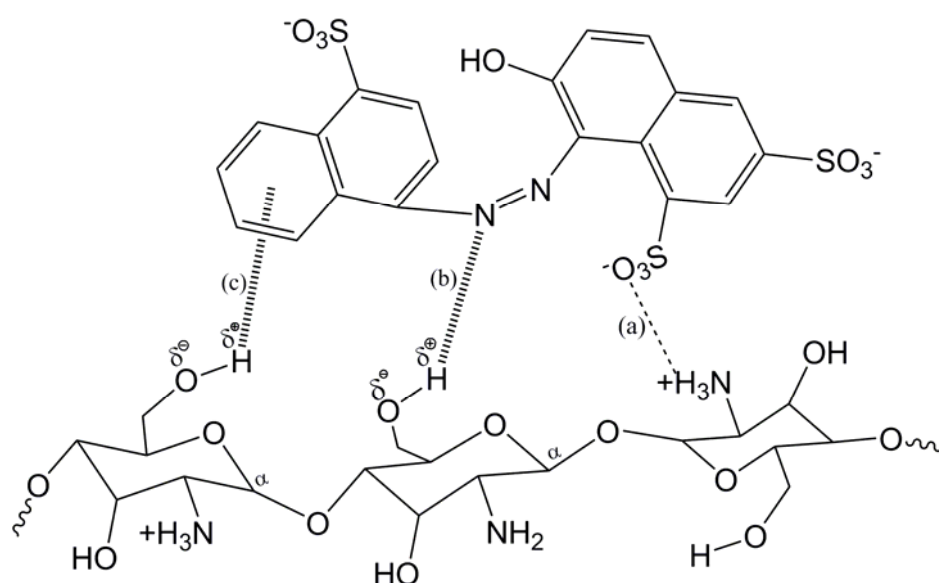


**Figure 4.24** Dye-chitosan interactions (a) ionic attraction between anionic sulphonate group(s) of dissolved dye molecules and the cationic amino groups of protonated chitosan, (b) dipole-dipole hydrogen bonding interactions between chitosan hydroxyl groups and electronegative residues in the dye molecule; (c) Yoshida H-bonding between chitosan hydroxyl groups and aromatic residues in dye

Many researchers have suggested that the mechanism of adsorption of anionic dye molecules by chitin and chitosan was mainly based on electrostatic attraction between  $-NH_3^+$  of chitosan and  $-SO_3^-$  of dyes. The electrostatic forces had a significant effect at low pH value. The sorption mainly happened at the specific sites of chitosan and dye molecules, so the Langmuir isotherms fit the sorption result. Theoretically, 1 g of chitosan with 95% degree of deacetylation contains 5.9 mmol of

$-NH_2$  groups. If all the  $-NH_2$  groups are protonated, 1 g of chitosan can adsorb 5.9 mmol of  $-SO_3^-$ . That means a maximum of 5.9 mmol of mono-sulphonated dye can be adsorbed by 1 g of chitosan at low pH value.

Chemisorption, (electrostatic attraction between  $-NH_3^+$  of chitosan and  $-SO_3^-$  of dyes) is commonly cited as the main mechanism for the adsorption of anionic dyes in acidic conditions [252, 258]. The dipole-dipole hydrogen bonding interactions between the hydroxyl groups of chitosan and electronegative residues in the dye molecule and Yoshida H-bonding between the hydroxyl groups of chitosan and the aromatic residues in the dye mainly took effect at high pH values. In order to allow hydrogen bondings with the dye molecules (Figure 4.24b), high temperatures were required to break down inter- and intra- molecular hydrogen bonding between chitosan polymer chains [357]. Therefore, there was potential for additional hydrogen bonding with the dye molecules to remove them from solutions when the temperature increased. That might contribute to the fact that the sorption ability was improved along with the increase of temperature. Other researchers [271] have observed that the Freundlich (no specific sites, possibility of formation of multi-molecular layers) isotherm would fit at high pH values for the sorption of dyes onto chitosan.

Hence, it was likely that adsorption of anionic dyes onto chitosan occurred through a combination of electrostatic forces, van der Waals interactions, and hydrogen bonding, with the electrostatic forces having a significant effect at low pH.

In our study, the sorption ability of the acid dyes with small molecules generally related to the sulphonate groups which solubilize the dye in water and provide the hydrophilic

property of the dye. But for the direct dyes whose molecular sizes were big, the other groups including the conjugated aromatic core also contributed a lot to the sorption.

## **4.5.8 Factors affecting sorption**

### **4.5.8.1 Effect of sorbent particle size**

The experimental results for Orange 7 onto the nanochitosan and microchitosan are shown in Figure 4.15. The nanochitosan had higher sorption capacities than those of the microchitosan and the difference was the largest 0.9 mmol/g at 30°C. Comparing with micro-sized adsorbent, the solid-liquid interfacial area of nanosized adsorbent is much larger. If the nanochitosan was spherical with a diameter size of 350 nm, the surface/volume ratio is  $1.71 \times 10^7 \text{ m}^{-1}$ . As the particle size of microchitosan is 400  $\mu\text{m}$ , the surface/volume ratio of microchitosan is  $1.5 \times 10^4 \text{ m}^{-1}$ . It was believed that the large surface area/volume value of the nanochitosan was the main reason that explains why adsorption capacity of nanochitosan is bigger than that of microchitosan. The sorption of Acid Red 1 and Acid Red 18 also showed similar results; however the difference between sorption capacities of Acid Red 18 onto the nanochitosan and the microchitosan was not as much as that of Acid Orange 7 and Acid Red 1 (Figure 4.17). At each temperature, the adsorption capacity of Acid Red 18 onto the nanochitosan and microchitosan was very closed. This may attribute to the smaller Acid Red 18 molecules. The molecules of Acid Red 18 could penetrate into micro-sized chitosan to get adsorbed eventually.

Figure 4.18 shows the plots of the sorption capacity of the nanochitosan and the microchitosan for Direct Red 84 at different temperatures. The nanochitosan demonstrated a much higher sorption capacity than that of the microchitosan at the same temperature. Dyes with a larger molecule size were more difficult to penetrate into the

microchitosan to get adsorbed, while the nanochitosan with much higher surface area/volume ratio could easily adsorb the dye molecules. The sorption of Direct Red 80 onto the nanochitosan and the microchitosan showed similar results (Figure 4.19).

The results demonstrated that comparing with the sorption capacity of the microchitosan, the sorption capacity of nanochitosan increased as much as 5 times for the dyes with large molecular sizes at the same temperature. The nanochitosan is more effective for the sorption of commercial dyes with large molecular sizes comparing with the micro-sized chitosan.

#### **4.5.8.2 Effect of sorbate molecules**

##### **4.5.8.2.1 Dimensions of dye molecules**

The dimensions of the dye molecules were estimated by using ChemBioOffice (2008) and shown in Figure 4.25. As the direct dyes with big molecular size could not penetrate into the compact structure of the chitosan molecules, the sorption capacities of microchitosan for Direct Red 84 and Direct Red 80 were very low at lower temperatures.

##### **4.5.8.2.2 Hydrophobic/hydrophilic ratio of dyes**

The hydrophobic/hydrophilic ratios of each dye were calculated according to equation (E 4.1) and listed in Table 4.5 below.

The hydrophobic/hydrophilic ratios of the dyes are presented with the bigger value first as following: AO7>DR 84>AR 1>DR 80>AR 18. The comparison of sorption capacities of nanochitosan for different dyes was also in the same order (Figure 4.26). Generally, the sorption capacity of nanochitosan increased as the hydrophobic/hydrophilic ratio increased.

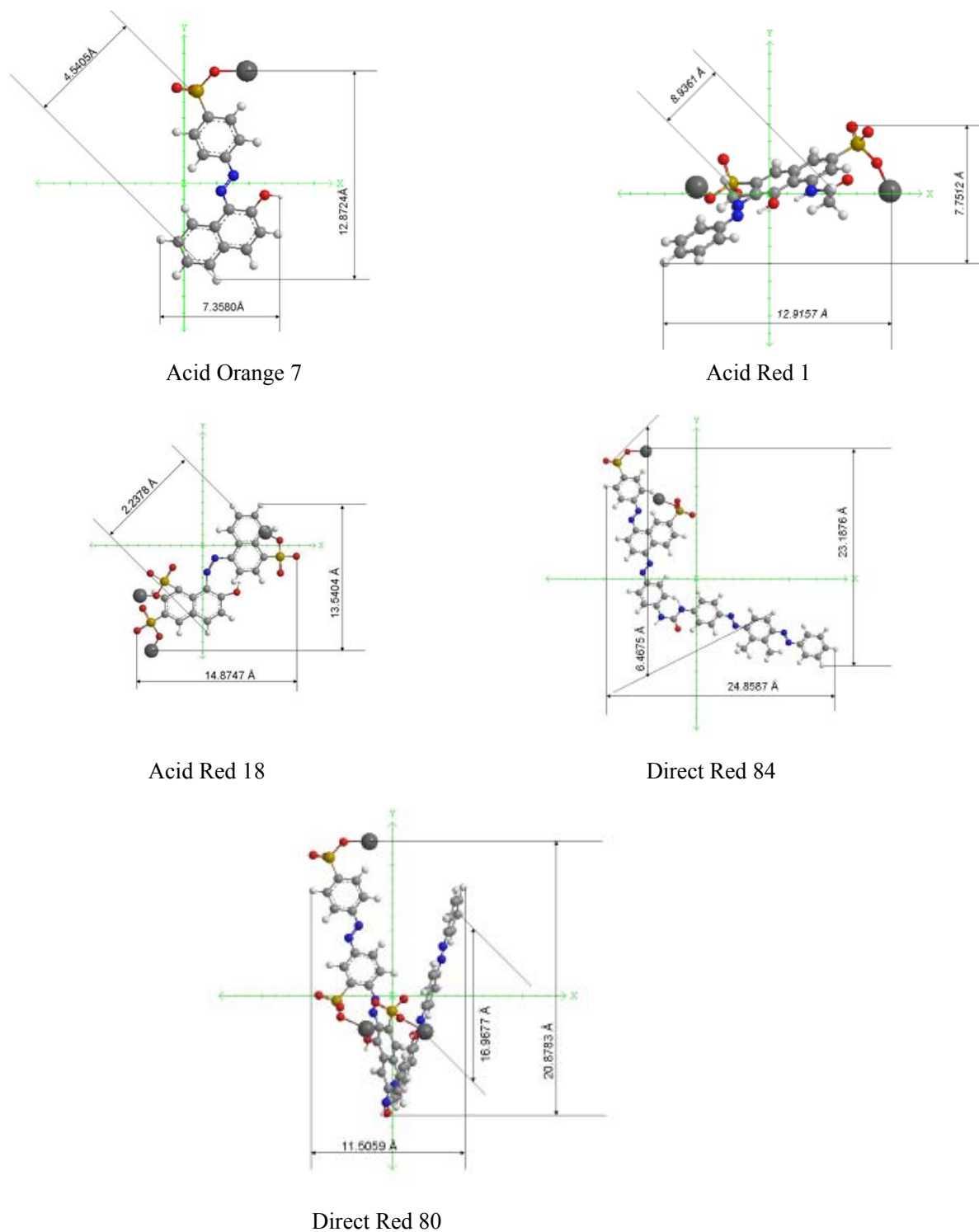


**Figure 4.25** The dimensions of Acid Orange 7, Acid Red 1, Acid Red 18, Direct Red 84, Direct Red 80

**Table 4.5** Hydrophobic/hydrophilic ratio of AO 7, AR1, AR 18, DR 84, and DR 80

Dye	AO 7	AR 1	AR 18	DR 84	DR 80
Hpho./Hphi.	12.69	$3.745 \times 10^{-2}$	$3.184 \times 10^{-3}$	$7.260 \times 10^{-2}$	$7.204 \times 10^{-3}$

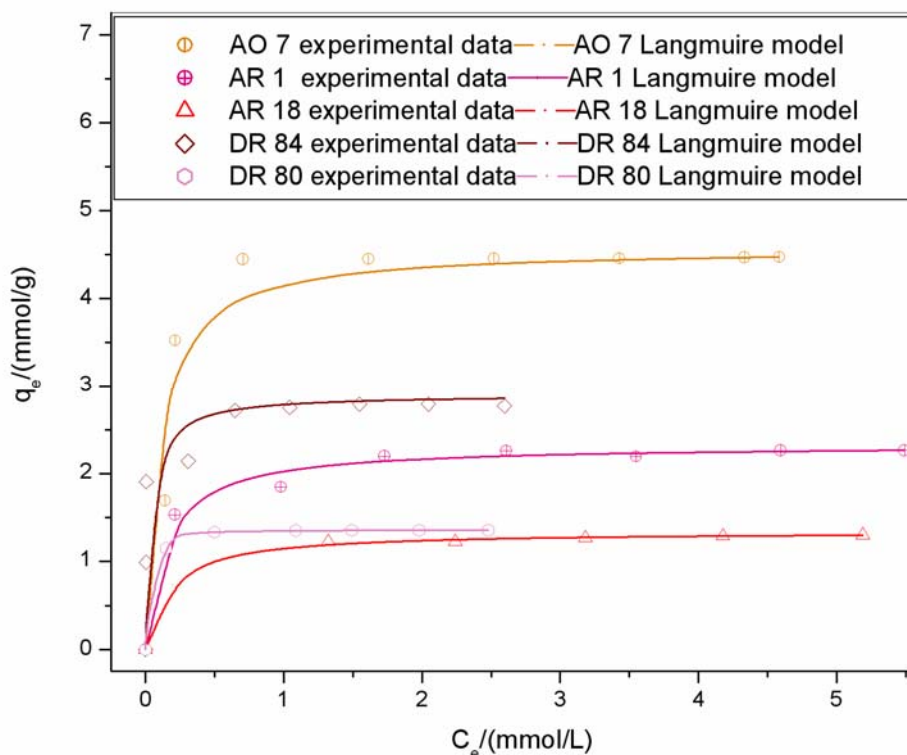


**Figure 4.26** Sorption capacities of nanochitosan for Acid Orange 7 (AO 7), Acid Red 1 (AR 1), Acid Red 18 (AR 18), Direct Red 84 (DR 84) and Direct Red 80 (DR 80) at 30°C, pH=5.5

#### 4.5.8.3 Effect of temperature

The effect of temperature on the adsorption of Acid Orange 7, Acid Red 1, Acid Red 18, Direct Red 84 and Direct Red 80, are shown in Figures 4.15 to 4.19 respectively. The effect of temperature on different dyes was not quite the same.

For Acid Orange 7, the sorption capacity of the nanochitosan slightly decreased when the temperature increased from 30°C to 70°C. On the other hand, the sorption capacity of microchitosan increased when the temperature increased from 30°C to 50°C, but the sorption capacity of microchitosan decreased after 50°C before 90°C. Both the sorption



capacities of nanochitosan and microchitosan reached the peak at 90°C.

For Acid Red 1, the sorption capacity of the nanochitosan decreased when the temperature increased from 30°C to 50°C, but increased from 70°C and reached the highest at 90°C. The sorption capacity of the microchitosan for Acid Red 1 increased slightly from 30°C to 50°C, and reached the highest at 90°C.

For Acid Red 18, the sorption capacities of nanochitosan and microchitosan both increased from 30°C to 70°C, and reached the highest at 90°C.

For Direct Red 84, the sorption capacity of the nanochitosan decreased when the temperature increased from 30°C to 50°C, but the sorption capacity increased at 70°C and reached the highest at 90°C while the sorption capacity of microchitosan for Direct Red 84 increased slightly from 30°C to 70°C, and greatly increased at 90°C.

For Direct Red 80, the sorption capacities of the nanochitosan and the microchitosan increased when the temperature was increased from 30°C to 90°C.

In summary, the sorption capacities of the nanochitosan and the microchitosan for the acid dyes did not change much from 30°C to 70°C, but greatly increased at 90°C. The sorption capacity of the nanochitosan for the direct dyes increased or slightly decreased from 30°C to 70°C, and greatly increased at temperature 90°C. The sorption capacities of the microchitosan for the direct dyes increased from 30°C to 70°C, and greatly increased at temperature 90°C.

The sorption process is affected by the following factors: aggregation and diffusion of the dye molecules, the swelling of chitosan and sorption reaction. All the three factors are

affected by temperatures. By increasing the temperature, the aggregation of the dye molecules decreases and the swelling of chitosan increases. The two factors will increase the sorption capacity. Meanwhile, as the sorption equilibrium is an exothermic process, the sorption capacity will be lowered by increasing the temperature due to the increase of desorption [359].

For dyes which sorption and desorption are the leading effect in sorption process, the desorption process is accelerated and sorption capacity will be lower, when the temperature increases. Meanwhile, for some dyes which aggregation needs much energy and the aggregation is a leading problem, the sorption capacity will increase when the temperature increases.

Comparing the sorption capacities of the nanochitosan for Direct Red 80 at different temperatures (Figure 4.19), the increase in the temperature could reduce the dye aggregation and improve the sorption capacity, as diffusion is an endothermic process. The sorption capacity of nanochitosan for Direct Red 80 was improved up to 38.6% when the sorption was done at 50°C comparing with 30°C. For the sorption of Direct Red 84, the sorption capacity of the nanochitosan was not improved by increasing the temperature, but lowered from 30°C to 70°C. It was because the aggregation of Direct Red 84 was not as strong as that of Direct Red 80. By increasing the temperature, the desorption equilibrium increased which led to the decrease of sorption capacity of the nanochitosan for Direct Red 84.

It was observed in the results, the sorption capacities increased at 90°C. This may attribute to the breaking down of inter- and intra- molecular hydrogen bondings between the chitosan polymer chains to allow hydrogen bondings with dye molecules for affinity, adsorption, and diffusion at high temperature. Therefore the sorption capacities increased

greatly at 90°C [273].

For the sorption of the dyes onto nanochitosan and microchitosan which desorption is prominent in the sorption process including most of the acid dyes with smaller molecules, we could use a low temperature to increase the sorption capacity and save energy. For the sorption of dyes onto microchitosan which diffusion is prominent in the sorption process including many commercial dyes with bigger molecules, a higher temperature should be chosen to increase the sorption capacities and reduce pollution.

#### 4.5.9 Thermodynamic parameters

The plots of the specific adsorption ( $1/q_e$ ) against the equilibrium concentration ( $1/C_e$ ) for the dye adsorption onto chitosan at different temperatures were found to be linear over the studied concentration range and the linear correlation coefficient ( $R^2$ ) had a high value as shown in Table 4.4. The correlation coefficient values indicated that the dye and chitosan sorption data satisfactorily followed the Langmuir sorption model. The changes in the enthalpy ( $\Delta H$ ) and entropy ( $\Delta S$ ) of the sorption processes were determined from the data obtained at different temperatures using the following equations [246, 360];

$$\ln K = -\frac{\Delta H}{RT} + \frac{\Delta S}{R} \quad (\text{E 4.15})$$

where  $K$  is the adsorption equilibrium constant obtained from the Langmuir isotherms,  $\Delta H$  is the change of enthalpy in the sorption and  $\Delta S$  is the change of entropy in the sorption processes.  $R$  is the universal gas constant 8.314 J/mol, and  $T$  is the absolute temperature.

$\Delta H$  and  $\Delta S$  were calculated from the slope and intercept of the van't Hoff plots of  $\ln k$  versus  $1/T$ . The values of the enthalpy and entropy changes of each dye onto the

nanochitosan and the microchitosan are listed in Table 4.6.  $\Delta G$  can be calculated then by using equation (E 4.16) as following:

$$\Delta G = -RT \ln K \quad (\text{E 4.16})$$

**Table 4.6** Thermodynamic parameters of sorption onto microchitosan and nanochitosan

Dye	Dye onto microchitosan			Dye onto nanochitosan		
	$\Delta H$ / (kJ/mol)	$\Delta S$ / [J/(mol·K)]	$R^2$	$\Delta H$ / (kJ/mol)	$\Delta S$ / [J/(mol·K)]	$R^2$
Acid Orange 7	-1.160	22.49	0.8885	-20.55	-35.72	0.9951
Acid Red 1	-1.811	12.88	0.8944	-22.598	-52.51	0.9988
Acid Red 18	-15.574	-33.69	0.8797	-15.98	-34.92	0.9426
Direct Red 84	-12.581	-28.03	0.9760	-40.51	-83.86	0.9992
Direct Red 80	-34.69	-0.6062	0.8501	-41.37	-88.55	0.9779

The negative values of  $\Delta G$  and  $\Delta H$  indicate that the adsorption of dye onto chitosan is a spontaneous and an exothermic process. All the dyes have an essentially flat thin conjugated aromatic core, with sulphonate groups on the periphery. The sulphonates are necessary to solubilize the dye in water and the aromatic core provides the color. When the dye molecules approach the chitosan molecules, these sulphonate groups have strong electrostatic interactions with the amino groups in chitosan and also the aromatic core binds with chitosan main chain through van der Waals forces. So the sorption of dyes onto chitosan is very strong.

For the nanochitosan, the sorption of all five dyes are driven by enthalpy which can be concluded from the big value of  $\Delta H$ . But for the microchitosan, chitosan is not soluble until a very low pH value is reached and it took a long time for microchitosan to swell to extend its surface area. Therefore, the dye molecules could not approach the chitosan molecules very soon especially for the chitosan molecules inside the microsized particles. For the sorption of dyes with less sulphonate groups including Acid Orange 7 and Acid

Red 1 onto microchitosan, the binding enthalpy was small and the sorption process was driven by entropy.

#### 4.5.10 Desorption and regeneration studies

Higher desorption efficiency is more favorable for the regeneration as more dyes can be taken out from the adsorbent indicating a higher possibility for the reuse of both the adsorbate and the adsorbent, reducing the overall costs of the dye removal system. It has been shown that the alkaline medium was effective in the desorption process [31]. Originally, the electrostatic interactions between chitosan and dye molecules was favorable by the protonation of amino groups under acidic conditions. However, the positively charged amino groups were deprotonated under alkaline conditions by the addition of sodium hydroxide, thus the electrostatic interactions between chitosan and dye molecules became much weaker.

**Table 4.7** Desorption efficiency of microchitosan and nanochitosan

Dye	Dye desorption from microchitosan			Dye desorption from nanochitosan		
	pH=8	pH=10	pH=12	pH=8	pH=10	pH=12
Acid Orange 7	10.24%	70.52%	6.19%	15.34%	75.19%	20.68%
Acid Red 1	30.45%	82.48%	47.52%	25.61%	85.53%	19.88%
Acid Red 18	23.84%	85.16%	28.75%	12.64%	83.16%	35.48%
Direct Red 84	14.24%	80.43%	7.64%	17.58%	86.47%	8.92%
Direct Red 80	16.45%	81.06%	8.96%	18.46%	87.51%	6.84%

To evaluate the desorption efficiency, dye solutions with an initial concentration of 2 mmol/L were used. The dye concentration of the solution at equilibrium after the desorption studies could be used to calculate the desorption efficiency. The results were summarized in Table 4.7. The desorption efficiency was higher at pH 10, ranging from 70%-88%. The recycling chitosan and dyes could be used repeatedly which makes the

sorption process environmentally friendly.

Similar findings has been reported, the desorption efficiency was higher at pH 10 than at pH 8 and pH 12. Chen et al. [275] showed that the desorption efficiency was 78.2% for Remazol Black 5 under the condition of 30°C and pH 10 and the desorption efficiency for Remazol Black 5 under the condition of 30°C and pH 12 was about 58%. These findings were consistent with the results found in the desorption efficiency of our experiments.

## **4.6 Conclusions**

The nanochitosan emulsions with particle sizes of 300 nm~400 nm were prepared by using a novel sonolysis method. The capacities of nanochitosans as an adsorbent for the removal of 5 anionic dyes including Acid Orange 7, Acid Red 1, Acid Red 18, Direct Red 80 and Direct Red 84 from aqueous solutions were studied. Similar experiments were done with microchitosan (180  $\mu\text{m}$ ~250  $\mu\text{m}$ ). It was found that the nanochitosan had higher capacities than those of the microchitosan, especially for the dyes with large molecular size. The results demonstrated that comparing with the sorption capacity of microchitosan, the sorption capacity of nanochitosan increased as much as 8 times for the dyes with large molecular sizes.

Sorption capacities of dyes onto nanochitosan and microchitosan at different temperatures were investigated. It was found that the adsorption capacities of microchitosan increased with increasing temperature for direct dyes with big molecular sizes. The sorption kinetics of dyes onto nanochitosan and microchitosan fits the pseudo-second-order model. The Langmuir equilibrium isotherms were suitable to analyze the equilibrium data. The sorption capacities of nanochitosan were 4.591 mmol/g for Acid Orange 7, 2.325 mmol/g

for Acid Red 1, 1.338 mmol/g for Acid Red 18, 2.900 mmol/g for Direct Red 84, and 1.358 mmol/g for Direct Red 80 at 30°C.

$\Delta H$  of the sorption process was obtained from the van' t Hoff equation. The negative value of  $\Delta H$  suggested that the adsorption phenomenon was an exothermic reaction. The sorption studies provide both theoretical and practical values to the research area and also support the dyeing studies in the next chapter.

## **Chapter 5 Application of Nanochitosan Emulsion on Dyeing:**

### **Dyeability Enhancement of nylon Using Nanochitosan Emulsion**

#### **5.1 Research background**

High color depths are difficult to be achieved in the dyeing of nylon with acid dyes due to the limited terminal amino groups on nylon, which act as the dyesites. Nowadays, surface modification of textile fibers is regarded as the best route to achieve desired surface properties. It modifies the fiber surface only for the beneficial effects. This minimizes the whole fiber attack and deterioration in fiber qualities. Hence a surface modification on nylon is a viable method to improve the dyeability of nylon.

Chitosan is a good candidate for textile finishing due to its low toxicity and good biodegradability. It exhibits basic rather than acidic characteristics, which differs from the other polysaccharides. The positive charge of chitosan makes it attractive for many applications in the textile industry. Many studies reported that chitosan could improve the dyeability of textiles [39, 296-327]. This may attribute to the enhanced electrostatic interactions between the protonated amino groups in chitosan and the anionic dyes. Compared with the commercial synthetic polymers and resins derived from petroleum-based raw materials, which are used for surface modifications of fibers, chitosan is relatively inexpensive, nontoxic and more environmentally friendly because it is a modified natural polymer which has good biocompatibility and biodegradability.

Many studies have investigated the enhancement of dyeability of wool and silk by



chitosan [307-308, 318-319], but the interrelation between nylon and chitosan was rarely explored. Due to the low saturation point in nylon fabrics, the increase in the number of amino group dyesites is of great importance in dyeing darker shades.

We aimed to study the enhancement in dyeability of nylon 6 fabrics after the treatment with the nanochitosan emulsion. First, the nanochitosan emulsion was prepared following the procedure in Section 3.3. And then, it was applied on the nylon fabrics through a pad-dry-cure method.

The surface of nylon after nanochitosan treatment was studied by SEM. The nanochitosan-treated and control fabrics were then dyed with eight anionic dyes to study the enhancement of dyeability after the treatment with nanochitosan emulsion. Three commercial dyes without knowing of chemical structures were Telon Red M-BL, Telon Yellow M-4GL and Telon Blue M-RLW. The other five dyes were Acid Orange 7, Acid Red 1, Acid Red 18, Sirius Brown 3RL (Direct Red 84) and Sirius Red F3B (Direct Red 80), and their chemical structures were known. The exhaustive data of dyeing were measured for both chitosan-treated and control fabrics. They helped to determine the initial, equilibrium and final exhaustion of dyeing process. Also, the time of half dyeing was derived.

Color evaluations of dyed fabrics were carried out by the subjective visual assessment under  $D_{65}$  and objective measurements using a spectrophotometer. CIE  $L^*a^*b^*$  were used to evaluate the color of dyed fabrics and comparisons were done between chitosan-treated and control fabrics. K/S values are used to evaluate the color depths of the fabrics. The color fastness to water (ISO 105 E01:1996) and color fastness to washing (ISO 105 C01:1989) of the fabrics were evaluated for the durability of the treatment

## 5.2 Materials and instruments

### 5.2.1 Fabric

A nylon 6 warp knitted fabric was bought from the Tianlong fabric store in Sham Shui Po. The fabric weight was 128.44 g/m<sup>2</sup>. The nylon fabric was washed with Sandopan DTC to remove any dirt or chemicals left on the fabric. Fiber identification tests were carried out on the washed fabric to ensure that it was nylon 6 through IR spectroscopy and melting point determination.

### 5.2.2 Dyestuffs

Acid Orange 7, Acid Red 1 and Acid Red 18 were purchased from Sigma-Aldrich Co. Ltd. Sirius Brown 3RL (Direct Red 84), Sirius Red F3B (Direct Red 80), Telon Red M-BL, Telon Yellow M-4GL and Telon Blue M-RLW were gifts from DyStar company. The chemical structures and molecular weights of the five dyes, namely Acid Orange 7, Acid Red 1, Acid Red 18, Sirius Brown 3RL and Sirius Red F3B, are listed in Table 4.1. The other three dyes, Telon Red M-BL, Telon Yellow M-4GL and Telon Blue M-RLW which were commercial dyes do not have their structures published.

### 5.2.3 Chemicals

Phenol (99.5%), Thymol blue indicator (98+%), Triton X-100 (wetting agent) were purchased from Acros Company. Sera Gal N-FS (anionic levelling agent) was a gift from DyStar. Other chemicals were purchased from Aldrich Co. Ltd. and used as received. The deionized water used in experiment was obtained using a TKA GmbH water purification system.

## **5.3 Experimental and characterization**

### **5.3.1 Cleaning of nylon fabric**

Non-ionic detergent (1 g/L) was added to the winch machine and the liquor to goods ratio was 50:1. After adding the detergent and the corresponding amount of water, the weighed nylon fabric was washed at 60°C for 20 minutes with stirring. Then, it was rinsed in running cold water for 5 minutes and the process was repeated 5 times. The fabric was then hydro-extracted for 15 minutes and hanged to dry at room temperature. After drying, the fabric was then cut into 2-gram of fabric samples with a dimensions of 4.5 inches×4.5 inches.

### **5.3.2 Preparation and characterization of chitosan-treated nylon fabric samples**

#### **5.3.2.1 Preparation of nanochitosan emulsion**

Typically, 1.5 g of chitosan was dissolved in 250 mL of acetic acid solution [0.45% (w/w)] under magnetic stirring. 50 mL of NaOH solution (0.3 M) was then added dropwise into the chitosan solution to precipitate the chitosan. The pH value of the mixture was about 6.2. A Vibra-Cell™ Ultrasonic Processor VCX 750 was used to treat the mixture for 60 minutes. Finally, stable emulsions were obtained. The concentration of nanochitosan emulsion obtained was 0.5% (w/w). The pH value of the nanochitosan emulsion was 6.5.

#### **5.3.2.2 Pad-dry-cure of chitosan on fabric samples**

Before soaking the nylon fabric sample to the chitosan emulsion, 4 drops of wetting agent were added to the emulsion with stirring. The fabric was then dipped into the emulsion

for 30 seconds before padding. In this study, the wet pick-up of the nylon fabric was 62%. After padding, the fabric was put into an oven at 105°C for 5 minutes. The process was repeated for 3 times and then followed by curing at 150°C for 5 minutes.

### 5.3.2.3 FT-IR spectroscopy

Infrared spectrometry method was used to analyze the nylon fabric and chitosan-treated nylon fabric. A PerkinElmer 100 FT-IR spectrometer with a PerkinElmer flat plate (01331) was used.

### 5.3.2.4 Scanning electron microscopy (SEM)

Scanning electron microscopy was used to study the difference in structure of chitosan-treated and nylon control fabrics with the use of a JOEM JSM 6335F. The change in fabric thickness between chitosan-treated and control fabric was determined.

### 5.3.2.5 Measurement of the coefficient of friction

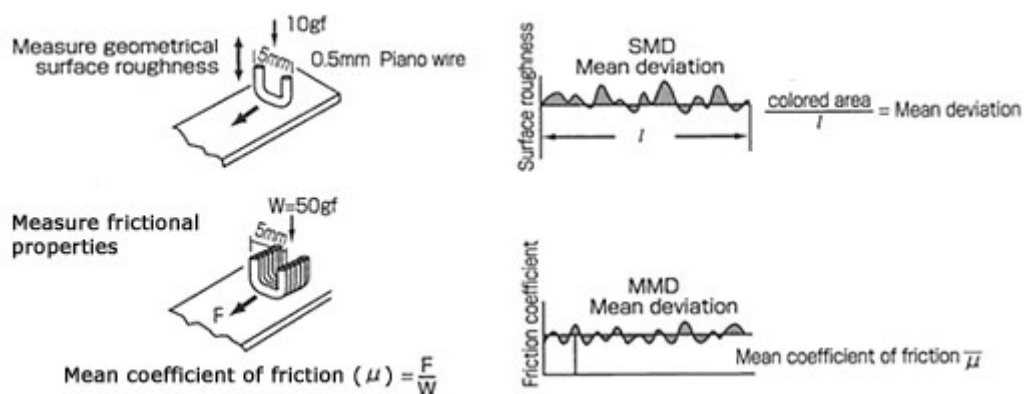


**Figure 5.1** Measuring frictional properties and geometrical surface roughness [361]

The geometrical surface roughness and frictional properties were measured by a surface tester. After mounting the specimen to the surface tester, the surface and roughness sensors were automatically set in position to start the measurement. After one

measurement was completed, the sensor moved to measure a different position of the specimen. Two different positions of the specimen were measured. Geometrical surface roughness was characterized by standard deviation of the coefficient of friction as shown in Figure 5.1.

#### **5.3.2.6 Amine group analysis of nylon fabric**

The amine end group analysis of nylon fabric [362] which helped to evaluate the dyeability of nylon fabrics was conducted. Three 1.5-2.0 grams of nylon fabric samples were cut into very fine powders with dimensions smaller than 1 mm and their dry weights were accurately weighed on a heating balance. After that, 19 mL of methanol and 35 g of phenol crystal were added to a round bottle flask and stirred with a magnetic stirrer. After dissolving all the phenol crystal into methanol, the fiber sample was added to the flask as the flask was heated under reflux with Liebig condenser to cool down the temperature. The mixture was stirred for around 6 hours to ensure that the nylon sample was dissolved in methanol and phenol and the solution in the flask turned transparent. 0.4 mL of 1% Thymol blue indicator was added to the solution and it was then titrated against standardized 0.05 mol/L HCl. The end point of the titration was reached when the solution turned pink.

### **5.3.3 Dyeing of fabric**

#### **5.3.3.1 Recipe of dyeing**

The recipes for the dyes in three depths are summarized in Tables 5.1. Typically, different volumes of the dye solution were used for different depths. An anionic levelling agent was added to facilitate levelling of dyeing by blocking some cationic dyesites in the initial stage of dyeing and the leveling agent were then gradually replaced by the anionic dyes in

the later stage of dyeing. The solution of sodium acetate and acetic acid were used as a buffer solution at pH=5.5 (1.5 g of  $\text{CH}_3\text{COONa}$  and 2 mL of 10%  $\text{CH}_3\text{COOH}$  in 1 L of distilled water). The pH values of the dye-baths were kept at pH 5.5( $\pm 0.1$ ) by adding 1% acetic acid or 0.3 mol/L sodium hydroxide solutions. The fabrics were dyed at a liquor to goods ratio of 50:1.

**Table 5.1** Dyeing recipes for Acid Orange 7 (AO 7), Acid Red 1 (AR 1), Acid Red 18 (AR 18), Sirius Brown 3RL (SB 3RL), Sirius Red F3B (SR F3B), Telon Red M-BL (TR), Telon Yellow M-4GL (TY) and Telon Blue M-RLW (TB) at different depths

Reagent	Depths		
	Depth 1	Depth 2	Depth 3
Dye solution : (AO 7: 3 mmol/L; AR 1, SB 3RL: 2 mmol/L; AR 18, SR F3B: 1 mmol/L; TR, TY and TB: 2000 ppm)	20 mL	40 mL	80 mL
Anionic levelling agent (1%)	10 mL	10 mL	10 mL
pH=5.5 buffer solution	70 mL	50 mL	10 mL
Total volume	100 mL	100 mL	100 mL

For Acid Orange 7, Acid Red 1, and Acid Red 18, Sirius Brown 3RL and Sirius Red F3B, the depths chosen were based on the amount of amino groups (i.e. saturation point) in the nylon fabrics. For other dyes which are commercial dyes, 2%, 4% and 8% depths were used because the commercial dyes are generally have lower purities.

### 5.3.3.2 Dyeing profile

The nylon fabrics which were either the nanochitosan-treated or the control fabrics were added to the dye bath. The first pH measurement was carried out before putting the nylon fabric to the dye bath to ensure that the pH is 5.5 ( $\pm 0.1$ ) while the second pH measurement was carried out right after the addition of the fabric. The pH adjustment was

made by using 1% acetic acid or 0.3 M sodium hydroxide solution. The dye bath was shaken in the water bath for 10 minutes at 30°C. A third pH measurement and adjustment were carried out to make sure the pH was still maintained at pH 5.5 ( $\pm 0.1$ ) before rising the dyeing temperature. The dye bath temperature was then rose steadily with an increment of 1.2°C per minute. And after around 45 minutes, the temperature in the dye bath was 80°C. The dye bath was then kept at 80°C for 30 minutes. At the end of the dyeing, a final pH measurement was conducted.

The dyed fabric was then rinsed in hot tap water for 5 minutes and cold tap water for 2 minutes. After being rinsed, the dyed fabric was dried in an oven at 75°C for 30 minutes.

The dyeing profile is shown in Figure 5.2.

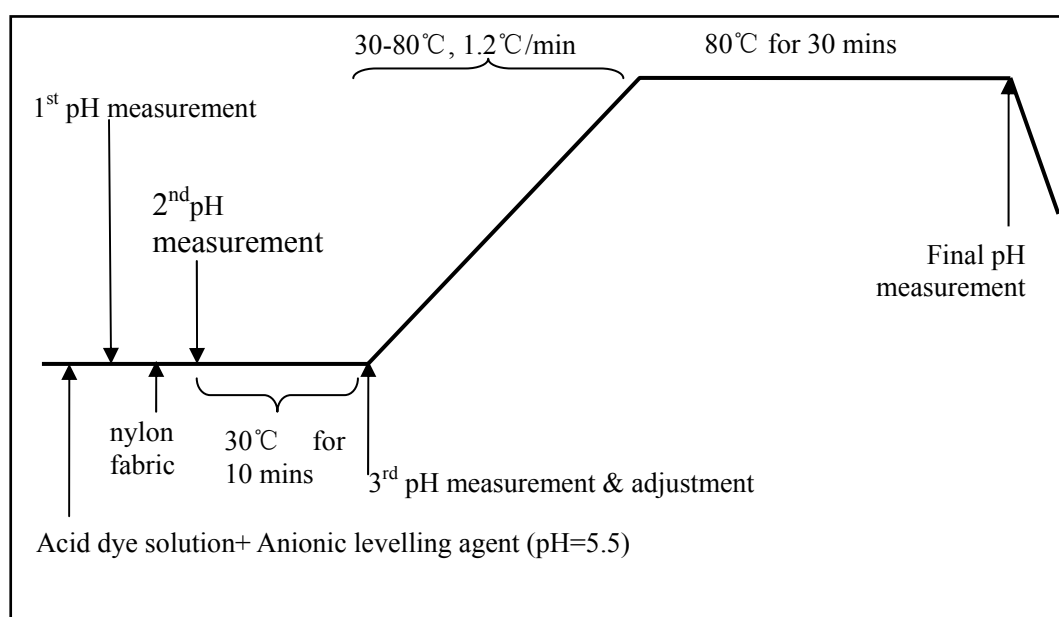


**Figure 5.2** Dyeing profile for nylon dyeing

### 5.3.4 Study of the dyeing exhaustion rate

#### 5.3.4.1 Concentration measurement and calibration

The calibration curve of each dye was prepared so that the dye concentration data could be obtained by referring to the calibration curve. For each dye, 7 different concentrations

were prepared and their absorbance values were measured by using a Perkin-Elmer UV-vis Spectrophotometer Lambda 18. The maximum absorbance ( $\lambda_{\max}$ ) of each dye was used in determining the absorbance of the dye at different concentrations as  $\lambda_{\max}$  values of the dye solutions provided the greatest sensitivity. A linear graph of absorbance versus concentration was obtained by plotting the absorbance against the corresponding concentration. The concentration of the dye bath was derived by referring to the calibration curve automatically by the spectrophotometer.

#### 5.3.4.2 Evaluation of exhaustion

The absorption rate and final exhaustions of the chitosan-treated and untreated fabric were determined by checking the concentrations of the dye liquor at specific intervals during the dyeing process as shown in Figure 5.3 and Table 5.2. Typically, 0.5 mL of dyeing liquor was aliquoted from the dye bath with the use of an auto-pipette. It was then diluted to the concentration within the analytical range of  $A=0-1$ . The absorbance of these samples was measured by a Perkin-Elmer UV-vis Spectrophotometer Lambda 18.

The dye concentrations in the dye bath at different time slots were measured. And from the dye concentration, the amount of dye that absorbed by the fabric can be calculated by the following equation:

$$E = \frac{C_0 - C_t}{C_0} \times 100\% \quad (\text{E } 5.1)$$

where  $E$  = Exhaustion percentage

$C_0$  = Initial concentration of dye solution (mmol/L)

$C_t$  = Concentration of dye solution at time  $t$  (mmol/L)



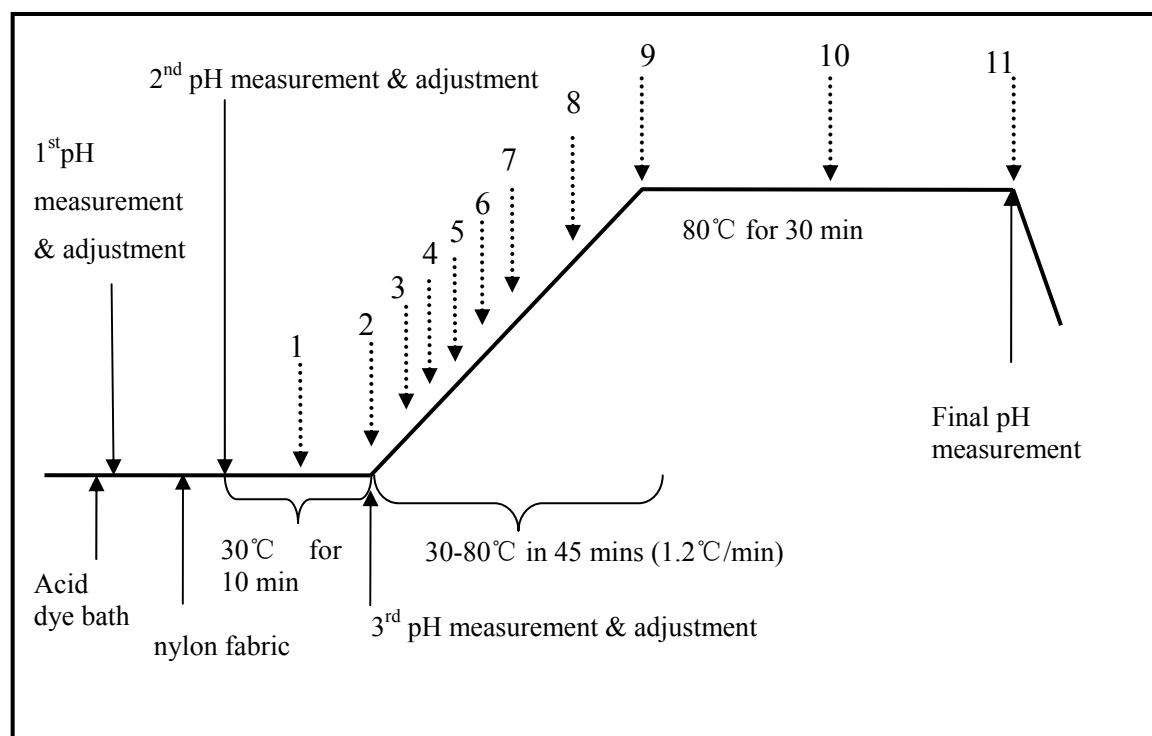


**Figure 5.3** Extraction of dye liquor from dye bath

**Table 5.2** Detailed information on extraction of dye liquor from dye-bath

Dye bath sample	1	2	3	4	5	6	7	8	9	10	11
Experiment time/min	5	10	15	20	25	30	35	45	55	70	85
Time of dyeing after raising temp./min	-	0	5	10	15	20	25	35	45	60	75
Temperature /°C	30	30	36	42	48	54	60	70	80	80	80

### 5.3.5 Evaluation of un-dyed fabrics

#### 5.3.5.1 CIE Whiteness index

The effect of curing on the whiteness of the fabric was determined using the CIE whiteness index. Whiteness index is defined by Equation (E 5.2) as following:

$$W=Y+800(x_n-x)+1700(y_n-y) \quad (\text{E } 5.2)$$

In the formula, Y is the Y tristimulus values of the sample, x and y are its chromaticity

coordinates, and  $x_n$  and  $y_n$  are the chromaticity coordinates of the standard illuminant depending on the illuminant and standard observer. Under illuminant  $D_{65}$ , standard observer  $10^\circ$ ,  $x_n=0.3138$ ,  $y_n=0.3310$ . A higher value of  $W$  means a higher degree of whiteness.

A Macbeth color-eye 7000A spectrometer was used in the measurement.

### 5.3.5.2 Yellowness index (ASTM E 313)

The yellowness index was also used to conjunct with the whiteness index in the determination of the effect of curing on the fabric. The yellowness index was defined as following:

$$YI = 100(C_x X - C_z Z)/Y \quad (E 5.3)$$

where  $X$ ,  $Y$ , and  $Z$  were the CIE Tristimulus values and the coefficients ( $C_x$  and  $C_z$ ) depending on the standard illuminants and observers. Under illuminant  $D_{65}$ , standard observer  $10^\circ$ ,  $C_x=1.3013$  and  $C_z=1.1498$ .

A Macbeth color-eye 7000A spectrometer was also used in the measurement

## 5.3.6 Evaluation of dyed fabrics

### 5.3.6.1 Visual assessment under daylight $D_{65}$

All of the dyed fabrics were cut into a size of  $4.5 \text{ cm} \times 4.5 \text{ cm}$  and mounted on the white board. The chitosan-treated samples and the control samples were observed under standard illuminant  $D_{65}$ . The viewing geometry was  $45^\circ$  as shown in Figure 5.4. The color differences were assessed with a pair of grey scales.

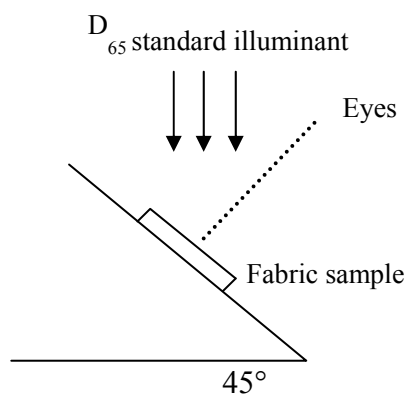


**Figure 5.4** Viewing geometry in color visual assessment

### 5.3.6.2 CIE L\*a\*b\*

The CIE LAB system was recommended by the CIE in 1976 and it is a very popular system for color and color difference specification. There are three parameters, namely,  $L^*$ ,  $a^*$  and  $b^*$ .  $L^*$  give a measure of the lightness of color and its values range from 0 to 100 with 0 representing perfect black and 100 representing perfect white.  $a^*$  give a measure of the red-green character of the color. Positive values of  $a^*$  represent red shades while negative values represent green shades. The values of  $b^*$  are responsible for giving yellow-blue character with positive values for yellow shades and negative values for blue shades. With the use of a spectrophotometer, the  $L^*$ ,  $a^*$  and  $b^*$  values of fabric samples are derived. As a result, the color difference between the chitosan-treated and control fabric samples can be represented by  $\Delta L^*$ ,  $\Delta a^*$  and  $\Delta b^*$  while the total color difference ( $\Delta E_{ab}$ ) between chitosan-treated and control samples were calculated based on  $\Delta L^*$ ,  $\Delta a^*$  and  $\Delta b^*$  as following:

$$\Delta E_{ab} = [(\Delta L^*)^2 + (\Delta a^*)^2 + (\Delta b^*)^2]^{1/2} \quad (E\ 5.4)$$

Chroma ( $C^*$ ) and hue ( $h$ ) are calculated as the following.  $\Delta C^*$  and  $\Delta h$  represent the chroma and hue difference between two samples.

$$C^* = [(a^*)^2 + (b^*)^2]^{1/2} \quad (E\ 5.5)$$

$$h = \arctan(b^*/a^*) \quad (E\ 5.6)$$

### 5.3.6.3 K/S value of the dyed fabrics

The K/S value is used to evaluate the dye uptake of the fabrics as it indicate the actual amount of dyestuffs in the fabric samples. Therefore, by comparing the K/S values of chitosan-treated and control fabrics, the difference in the amounts of dyes between the fabrics were known. The equation is shown below:

$$K/S = (1-R)^2/(2R) \quad (E\ 5.7)$$

where K is the coefficient of absorption, S is the coefficient of scatter and R is the reflectance of the sample at a given wavelength.

### 5.3.6.4 Colorfastness test

#### 5.3.6.4.1 Colorfastness to water (ISO 105-E01:1996)

The dyed fabric with a size of 40 mm×100 mm was in contact with a multi-fiber fabric by stitching one of the shorter sides together and the fabric composite was immersed in water, drained and placed between two acrylic-resin plates under a specific pressure of 12.5 kPa in a persperimeter. The persperimeter was then put into an oven at 37±2°C for 4 hours. The specimen was then dried by hanging in air at a temperature not exceeding 60°C. After drying, the color change of the specimen was assessed by the grey scales for assessing color change while the staining of the multi-fiber fabric was assessed by grey scales.

#### 5.3.6.4.2 Colorfastness to washing (ISO 105-C01:1989)

The dyed fabric with a size of 40 mm×100 mm was in contact with a multi-fiber fabric by stitching one of the shorter sides together and treated with a soap solution at 40°C±2°C for 30 minutes. The amount of soap in the soap solution was 5 g/L and the liquid to good ratio of the bath is 50:1. After washing, the specimen was then rinsed twice in cold grade

3 water and in cold running water for 10 minutes and squeezed. The specimen was then dried by hanging in air at a temperature not exceeding 60°C. After drying, the color change of the specimen was assessed by the grey scales.

## **5.4 Results and discussion**

### **5.4.1 FT-IR spectroscopy**

The FT-IR spectra of the chitosan treated and control fabrics are shown in Figures 5.5-5.6. The N-H stretching and bending vibrations in polyamide usually appear at 3100-3500 $\text{cm}^{-1}$  and 1550-1640 $\text{cm}^{-1}$  respectively, depending on the type of amide (primary and secondary), chemical environment (solid and liquid) and intra- or inter-molecular hydrogen bonds. The C=O stretching vibration band usually appears in the normal region between 1640 and 1670  $\text{cm}^{-1}$  [363].

In Figure 5.5, N-H stretching of a secondary amide at 3290.4  $\text{cm}^{-1}$  was assigned, and the peak at 1540.55  $\text{cm}^{-1}$  is also characteristic of the N-H stretching vibration. The peak at 1629.70  $\text{cm}^{-1}$  was assigned to C=O stretching of the secondary amide. In Figure 5.6, the intensity of peak at 1536.92  $\text{cm}^{-1}$ , which indicates the N-H vibration, increased. This is a result of the coating of chitosan.

Since both nylon 6 and nylon 6.6 have similar peaks at the frequencies mentioned above, it is rather difficult to distinguish whether it is nylon 6 and nylon 6.6. Therefore, the melting point of the fabric was tested to determine whether it was nylon 6.

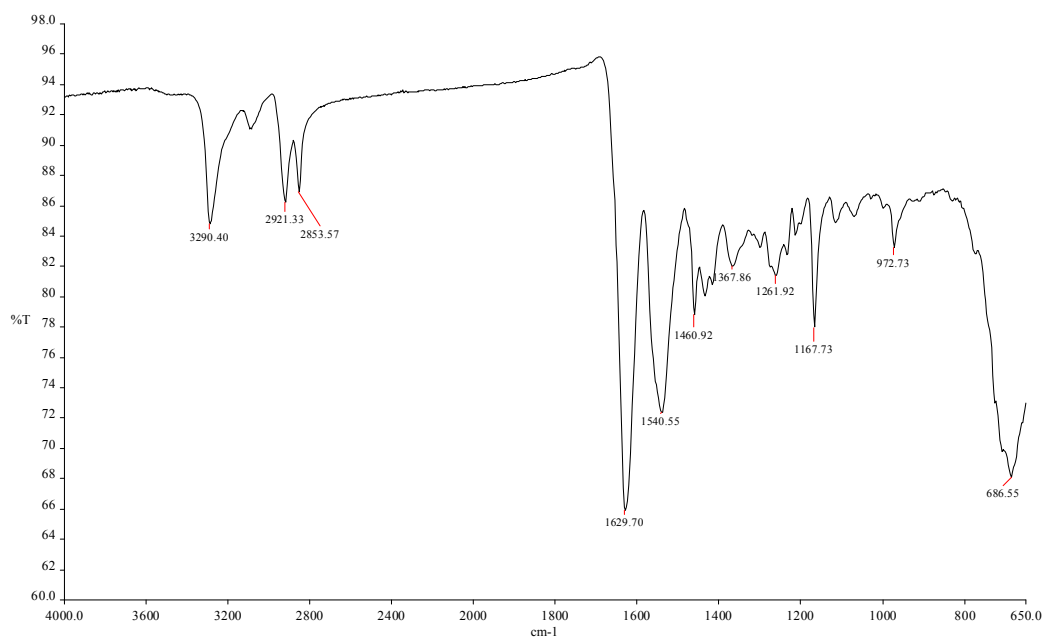


**Figure 5.5** The IR spectrum of nylon fabric

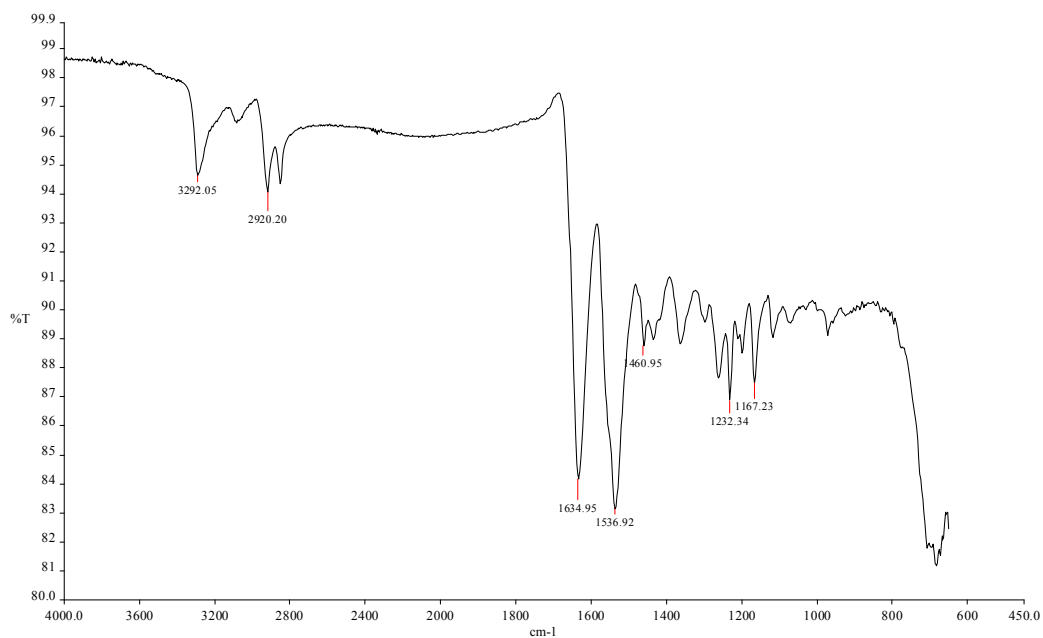


**Figure 5.6** The IR spectrum of nanochitosan-emulsion-treated nylon fabric

### 5.4.2 Melting point

The melting point of nylon 6 is 215-220°C while that of nylon 6.6 is 250°C. Because of their difference in melting point; it is an effective way to use their specific melting point to classify them. Based on the observation in melting point test, the fiber specimen melt at around 205°C which showed that the nylon fabric used in the study was nylon 6.

### 5.4.3 Scanning electron microscopy (SEM)

The SEM images of the chitosan-treated and control nylon fabrics are shown in Figure 5.7. The fiber diameter of nylon fiber in the control fabric was 11.36  $\mu\text{m}$  while that in chitosan-treated fabric was 12.30  $\mu\text{m}$ . Thus, the fiber diameter increased by around 11% after the treatment with the nanochitosan emulsion. Also, there was a white ring of chitosan as shown in the cross-sectional view of the SEM micrograph (Figure 5.7d') and the thickness of the chitosan coating was about 500 nm. The fiber surface also became rougher after the chitosan treatment when comparing Figure 5.7c' with Figure 5.7c. And Figure 5.7c also shows that there was chitosan polymer on the fabric surface.

The nanochitosan in the emulsion accumulated onto the surface of nylon, aggregated together during drying and finally formed a rough film with the thickness of around 500 nm, providing more surface areas and more  $-\text{NH}_2$  groups that would be useful in the dyeing process.

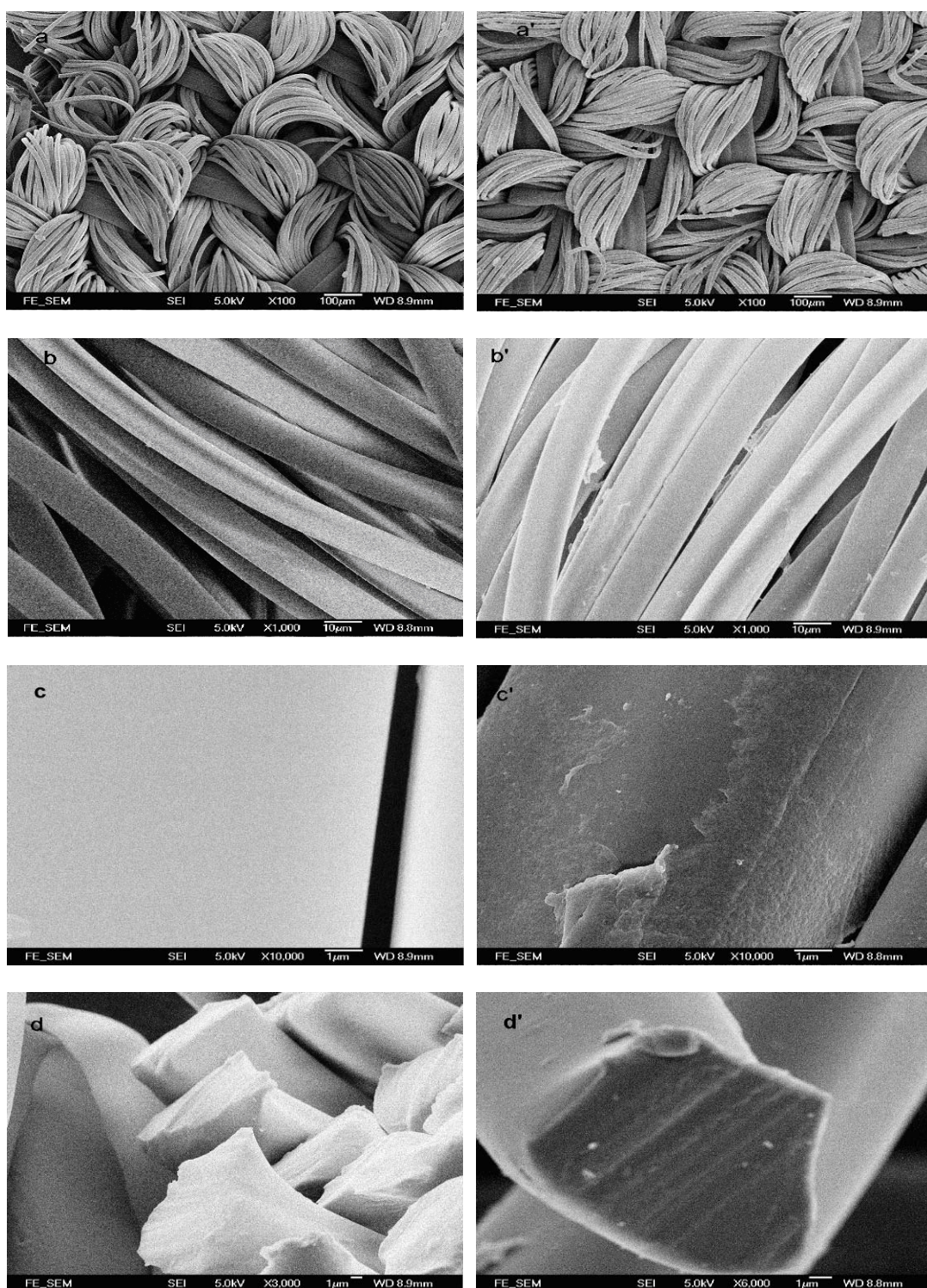


**Figure 5.7** Surface of control and chitosan-treated nylon fabrics (a: control nylon fabric ×100, a': chitosan-treated nylon fabric ×100, b: control nylon fabric ×1000, b': chitosan-treated nylon fabric ×1,000, c: control nylon fabric ×10,000, c': chitosan-treated nylon fabric ×10,000, d: control nylon fabric cross section ×3,000, d': chitosan-treated nylon fabric cross section ×6,000)



### 5.4.4 Coefficient of friction

Table 5.3 summarized the effect of the chitosan treatment on the coefficient of friction of the fabrics. The chitosan-treated fabrics had a lower coefficient of friction than that of the untreated samples. That means that the chitosan-treated sample had a better hand feel than the untreated one.

**Table 5.3** Coefficients of friction of the chitosan-treated and control fabrics

Sample		Mean coefficient of friction/ $\mu$	Mean deviation of mean coefficient of friction/ $\mu$	Standard deviation of mean coefficient of friction/ $\mu$
Untreated sample				
Warp	1	0.211	0.0078	1.135
	2	0.179	0.0064	1.450
	Mean	0.195	0.0071	1.383
Weft	1	0.240	0.0088	1.470
	2	0.233	0.0087	1.615
	Mean	0.236	0.0087	1.543
Chitosan-treated sample				
Warp	1	0.182	0.0067	1.365
	2	0.167	0.0076	1.170
	Mean	0.175	0.0071	1.268
Chitosan-treated sample				
Weft	1	0.221	0.0082	2.005
	2	0.231	0.0088	1.820
	Mean	0.226	0.0084	1.913

The standard deviation of the coefficient of friction represents the roughness of the sample. For the warp direction in the chitosan-treated sample, the standard deviation values is lower than that of the untreated samples, that means the roughness of chitosan-treated sample is lower than that of the untreated sample. But in the weft

direction, the standard deviation of mean coefficient of friction of the chitosan-treated sample is greater than the untreated sample. That means in the weft direction, the roughness of chitosan-treated sample is higher than that of the untreated sample.

#### 5.4.5 Determination of amine end group in nylon fabric

In the determining of amino end group in the nylon 6 fabric, three samples were prepared and their exactly weights were measured. A HCl solution with concentration of 0.05 mol/L was used as the titer in titration. By using the following equation (E 5.8), the molecular weight of nylon 6 could be determined and the result is shown in Table 5.4.

$$\overline{M}_n = (W \times 1000) / (V \times C) \quad (\text{E 5.8})$$

where  $\overline{M}_n$  = Molecular weight of nylon (g/mol)

$W$  = Sample weight of nylon fabric (g)

$V$  = Volume of HCl solution (mL)

$C$  = Concentration of HCl solution (mol/L)

Each nylon 6 molecule has one carboxylic acid and one amine end group in the polymer chain. As a result, the number of mole of amine group was 0.11 mmol [ $2 \text{ g} / \overline{M}_n$ ] in a 2 g nylon fabric.

**Table 5.4** Data of amine end group analysis

Sample	Weight/g	Volume of titer/mL	Concentration/M	$\overline{M}_n$ /(g/mol)
1	1.633g	2	0.05	16330
2	1.641g	3.2	0.03	19656
3	1.565g	1.5	0.03	17988
Mean	1.613g	-	-	17991

### 5.4.6 Determination of number of amino dyesites in chitosan-treated fabric

The basic structure of chitosan is glucosamine with the chemical formula of  $C_6H_{13}NO_5$  ( $M_w=161.079\text{g/mol}$ ). Chitin, on the other hand, has the chemical formula of  $C_8H_{13}O_5N$  ( $M_w=203.079\text{g/mol}$ ). For the 95% DD chitosan used in this study, 95% of chitosan polymer chain is chitosan while the remaining 5% is chitin in a repeated unit as shown in Figure 5.8.

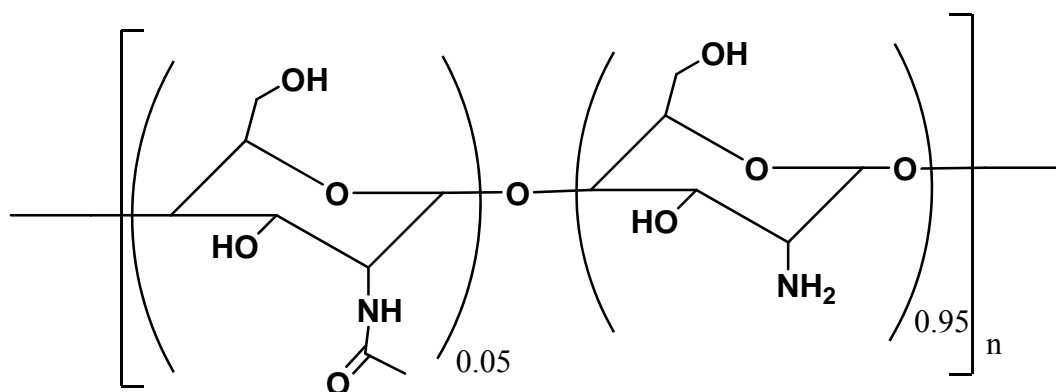


**Figure 5.8** Repeat unit of 95% DD chitosan polymer chain

The weight proportion of  $C_6H_{13}NO_5$  unit (P) in the whole polymer was calculated using the following equation (E 5.9) and the result was 0.934:

$$P = (M_w \text{ of } C_6H_{13}NO_5 \times DD) / [M_w \text{ of } C_6H_{13}NO_5 \times DD + M_w \text{ of } C_8H_{13}O_5N \times (1-DD)] \quad (\text{E } 5.9)$$

Since the chitosan-treated nylon fabric samples were 2 g each for dyeing and they were all padded with 0.5% chitosan emulsion 3 times with a wet pick-up of 62%, thus the weight of chitosan on the padded nylon could be calculated. The weight of chitosan padded on the nylon fabrics was 18.6 mg which meant the amino groups padded on nylon fabric was 0.11 mmol.

The total number of amino groups in chitosan-treated fabric could be calculated by adding the corresponding number of amino groups after whole padding process and that on the fabric itself before padding (i.e. 0.11 mmol from calculation in Section 5.4.5). So, if the pick-up was 62%, the total number of amine group after padding in 2 g chitosan-treated nylon fabric was 0.22 mmol.

#### **5.4.7 Estimation of depths of dyeing**

Based on the calculation in Section 5.4.6, the saturation point of 2 g of nylon fabric dyeing with acid dye was known. As a result, the maximum depth of dyeing could be estimated and it was important in dyeing as it helped to avoid the over dyeing. Therefore, the number of dyes required to reach the saturation point in the dyeing of control fabrics was 0.11 mmol while that of chitosan-treated fabric was 0.22 mmol.

The electrostatic interactions between the dye molecules and dyesites were varied by the number of sulphonate group(s). A mono-sulphonated dye can interact with one amino group while a di-sulphonated dye can interact with two amino groups. In this study, the chemical structures of Acid Orange 7, Acid Red 1, Acid Red 18, Sirius Brown 3RL and Sirius Red F3B were known, thus, the maximum depth of dyeing of the dyes could be estimated. The estimation of the depths for Acid Orange 7, Acid Red 1 and Acid Red 18 used the sulphonate groups as a reference assuming that the sorption of the dyes onto nylon and chitosan both followed the stoichiometry of the sulphonate groups. For Sirius Brown 3RL and Sirius Red F3B, the sorption capacities of the nanochitosan did not follow the stoichiometry of the sulphonate groups; we used the sorption capacities of nanochitosan as a reference.

**Table 5.5** No. of sulphonate groups in the dyeing solutions of Acid Orange 7, Acid Red 1, Acid Red 18, Sirius Brown 3RL and Sirius Red F3B at different depths

Dye concentration	Depth	No. of dye molecules in the dyeing solution /mmol	No. of sulphonate groups in the dyeing solution /mmol	Sulph. groups above/ below saturation point of fabric	
				Chitosan-treated fabric	Control fabric
Acid Orange 7 (1:1 electrostatic interaction)					
0.6 mmol/L	1.05%	0.06	0.06	Below	Below
1.2 mmol/L	2.10%	0.12	0.12	Below	Above
2.4 mmol/L	4.20%	0.24	0.24	Above	Above
Acid Red 1 (1:2 electrostatic interaction)					
0.4 mmol/L	1.02%	0.04	0.08	Below	Below
0.8 mmol/L	2.04%	0.08	0.16	Below	Above
1.6 mmol/L	4.08%	0.16	0.32	Above	Above
Acid Red 18 (1:3 electrostatic interaction)					
0.2 mmol/L	0.60%	0.02	0.06	Below	Below
0.4 mmol/L	1.21%	0.04	0.12	Below	Above
0.8 mmol/L	2.42%	0.08	0.24	Above	Above
Sirius Brown 3RL					
0.4 mmol/L	2.27%	0.04	0.16	Above	Below
0.8 mmol/L	4.55%	0.08	0.32	Above	Above
1.6 mmol/L	9.10%	0.16	0.64	Above	Above
Sirius Red F3B					
0.2 mmol/L	1.37%	0.02	0.12	Above	Below
0.4 mmol/L	2.75%	0.04	0.24	Above	Above
0.8 mmol/L	5.50%	0.08	0.48	Above	Above

#### **5.4.7.1 Mono-sulphonated dyes: Acid Orange 7**

Since Acid Orange 7 has one sulphonate group, therefore one dye molecule can only interact with one amino group. As shown in Table 5.5, the numbers of sulphonate groups of Acid Orange 7 at a 2.10% depth was higher than the saturation point of control fabric but still lower than the saturation point of the chitosan-treated nylon fabric.

#### **5.4.7.2 Di-sulphonated dye: Acid Red 1**

Since Acid Red 1 has two sulphonate groups, therefore, one Acid Red 1 dye molecule can form electrostatic interaction with two amino groups in theory. In other words, the numbers of dye molecules needed to saturate 2 g of both chitosan-treated and untreated control nylon fabric was half of their corresponding numbers of amino groups. As shown in Table 5.5, the number of sulphonate groups of Acid Red 1 at 2.04% depth was over the saturation point of control nylon fabric and the number of sulphonate groups of Acid Red 1 at 4.08% depth was over the saturation point of the chitosan-treated nylon fabric.

#### **5.4.7.3 Tri-sulphonated dye: Acid Red 18**

Since Acid Red 18 has three sulphonate groups, therefore, one Acid Red 18 dye molecule can interact with three amino groups. In other words, the number of dye molecules needed to saturate 2 g of both chitosan-treated and untreated control nylon fabric was one-third of their corresponding number of amino groups. As shown in Table 5.5, the number of sulphonate groups of Acid Red 18 at 1.21% depth was over the saturation point of control nylon fabrics and the number of sulphonate groups of Acid Red 18 at 2.42% depth was over the saturation point of the chitosan-treated fabric.

#### **5.4.7.4 Tetra-sulphonated dye and other multi-sulphonated dyes**

The estimation of depths of dyeing in tetra-sulphonated dye and other multi-sulphonated dyes were much less accurate than that of the mono-sulphonated dye. The sorption capacity of tetra-sulphonated dye and other multi-sulphonated dyes onto chitosan did not follow the stoichiometry of sulphonate groups. In the prior study in Chapter 4, the sorption capacity of Sirius Brown 3RL onto the nanochitosan was close to di-sulphonated dye Acid Red 1, while Sirius Red F3B was close to tri-sulphonated dye Acid Red 18. Thus, we choose the depths in which the stoichiometries of dyes were the same with Acid Red 1 and Acid Red 18.

#### **5.4.8 Exhaustion of dyeing**

The dyeing procedures have been described in Section 5.3.3.2 and the exhaustion curves of the eight anionic dyes are shown in Figures 5.9-5.16. In the dyeing of nylon, many of the higher molecular weight dyes tended to exhaust very rapidly at 65°C-75°C [364]. It was usually known as the critical bath temperature in dyeing. Since the glass transition temperature ( $T_g$ ) of water-saturated nylon is not much higher than 40°C, so there are movements of polymer chain segments when the dyeing temperature exceeds 40°C. As a result, the diffusion of dye molecules into the polymer matrix becomes easier when temperature increases. Dyeing transition temperature ( $T_D$ ) was often 20°C-30°C above the glass transition temperature ( $T_g$ ). When the dyeing temperature is above  $T_g$  (i.e. 40°C), the voids between the polymer chains in the amorphous region is still too small to accommodate the larger dye molecules. However, when the dyeing temperature is above the  $T_D$ , i.e. 60-70 °C in the case of nylon, the larger dye molecules were allowed to enter the voids due to the greater ease of chain mobility [363].

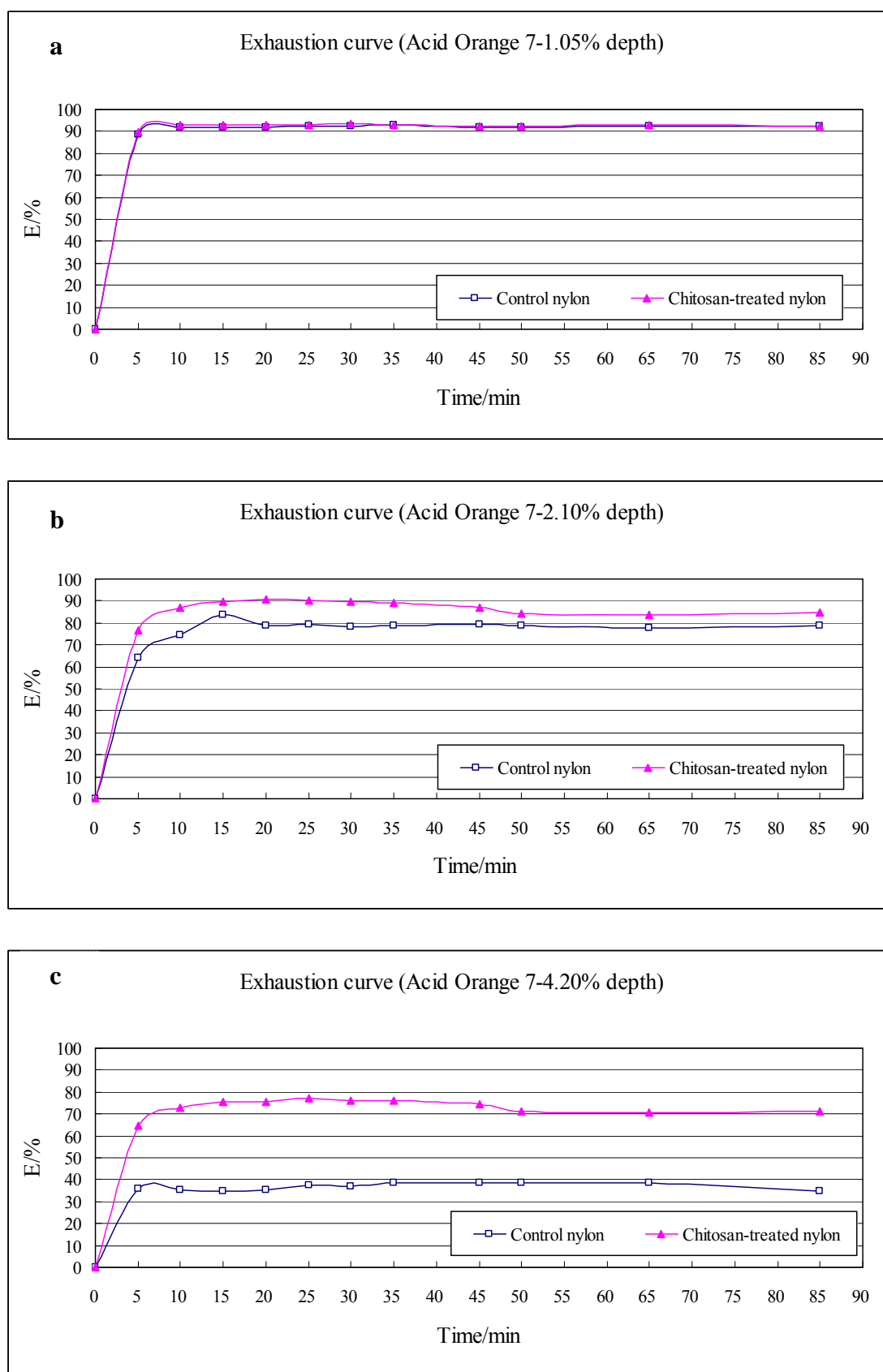


**Figure 5.9** Exhaustion curves of Acid Orange 7 at different depths: a (1.05% depth), b (2.10% depth), and c (4.20% depth)



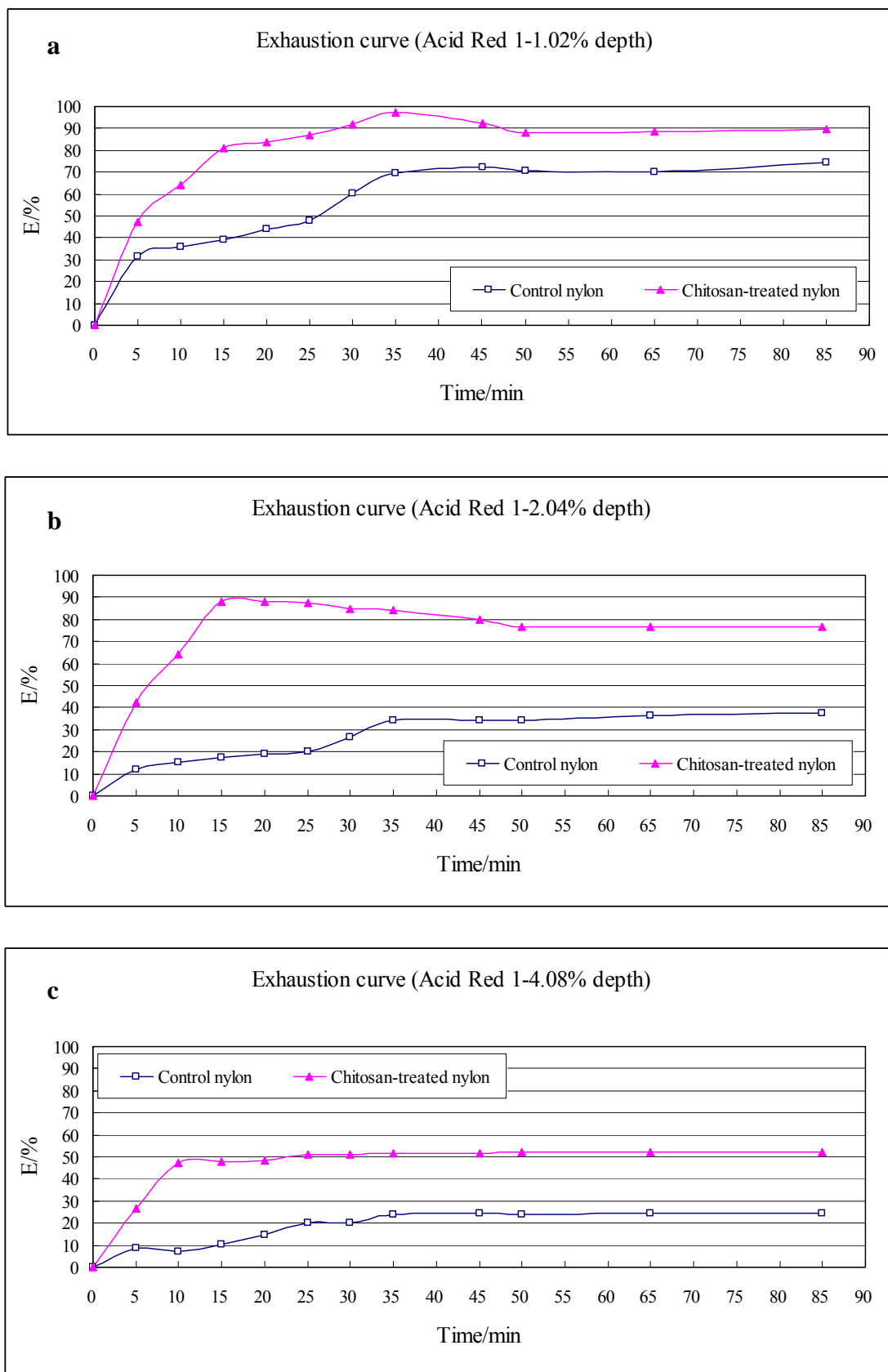


**Figure 5.10** Exhaustion curves of Acid Red 1 at different depths: a (1.02% depth), b (2.04% depth), and c (4.08% depth)

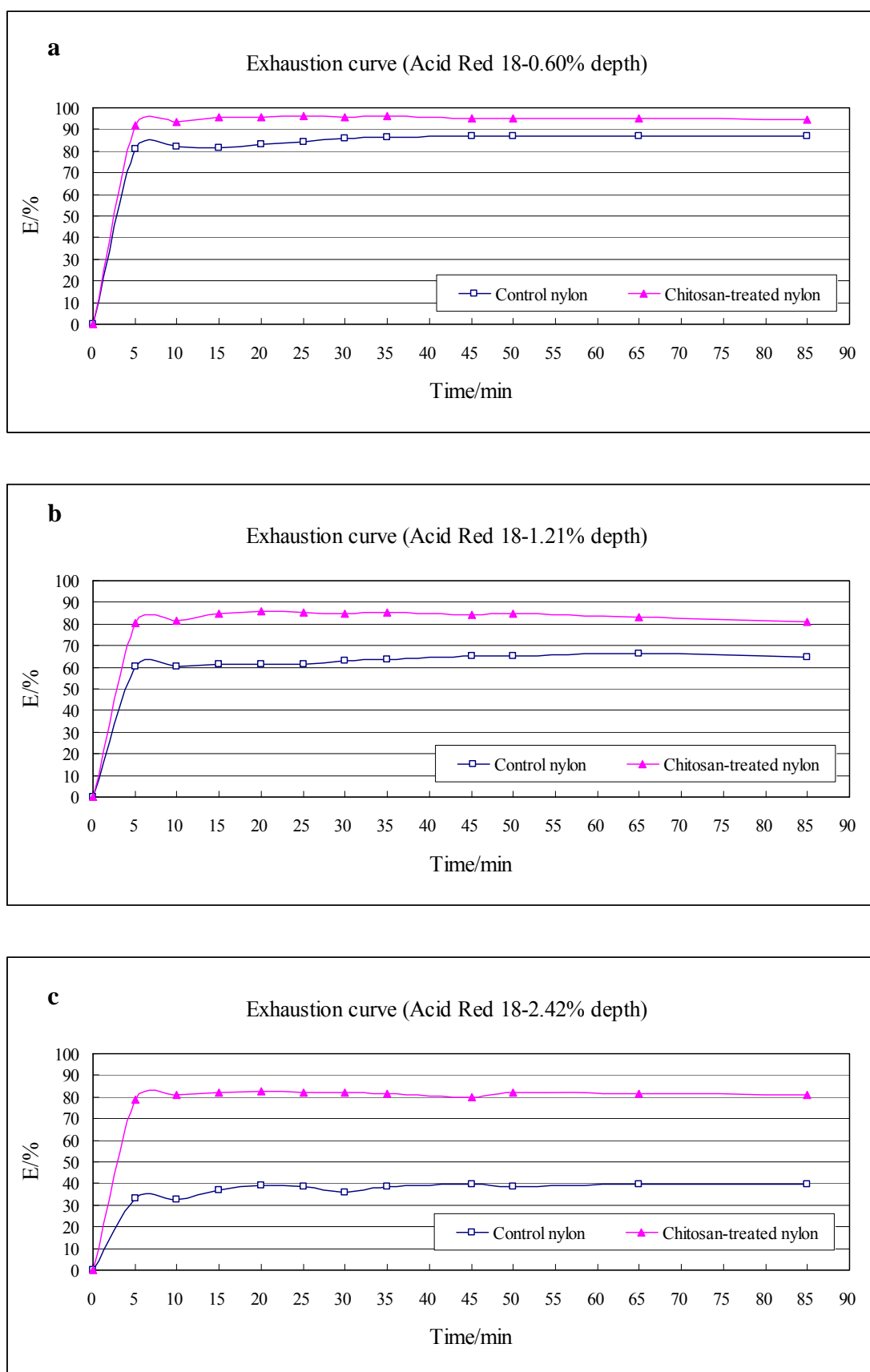


**Figure 5.11** Exhaustion curves of Acid Red 18 at different depths: a (0.60% depth), b (1.21% depth), and c (2.42% depth)

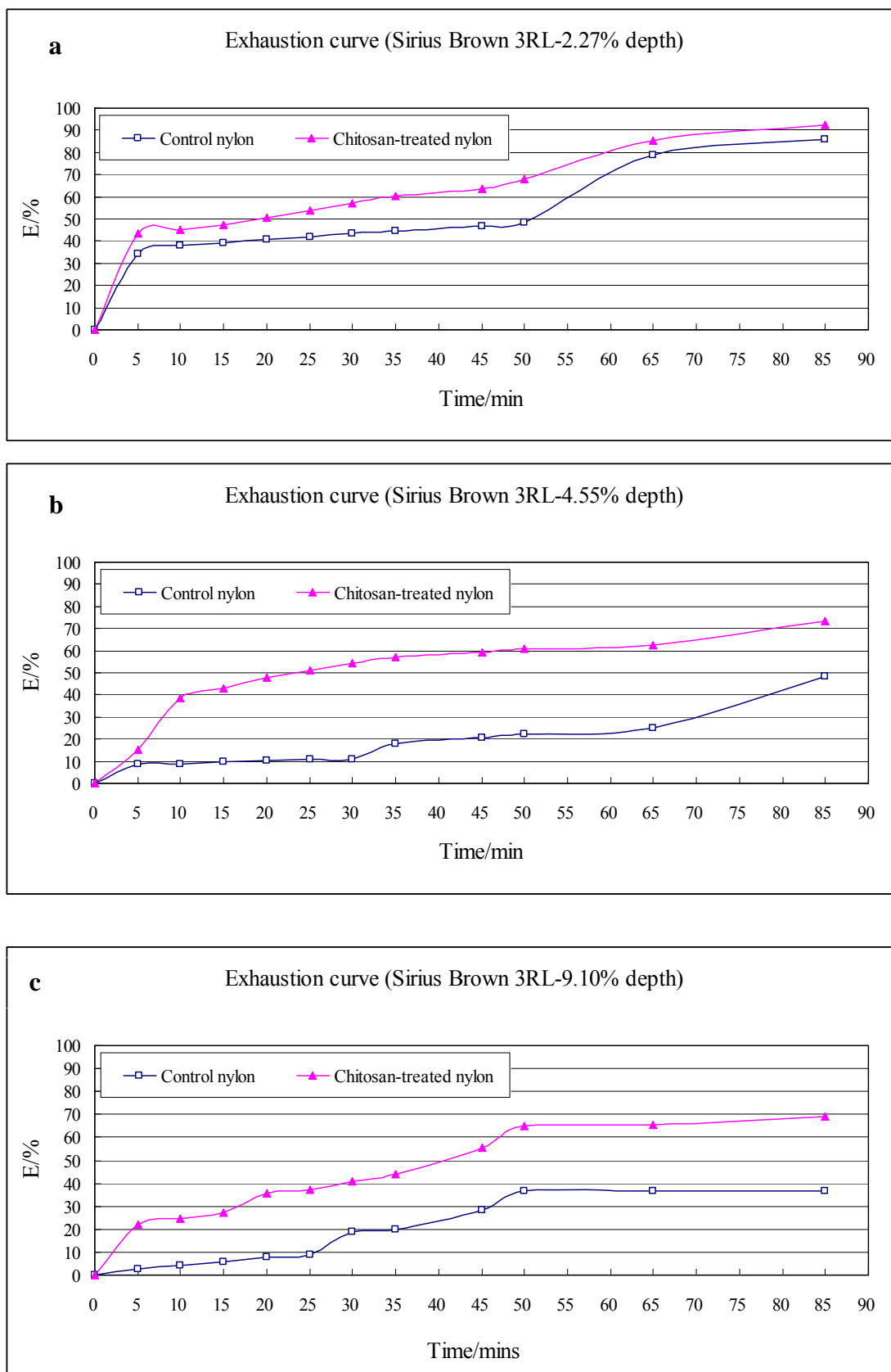


**Figure 5.12** Exhaustion curves of Sirius Brown 3RL at different depths: a (2.27% depth), b (4.55% depth), and c (9.10% depth)

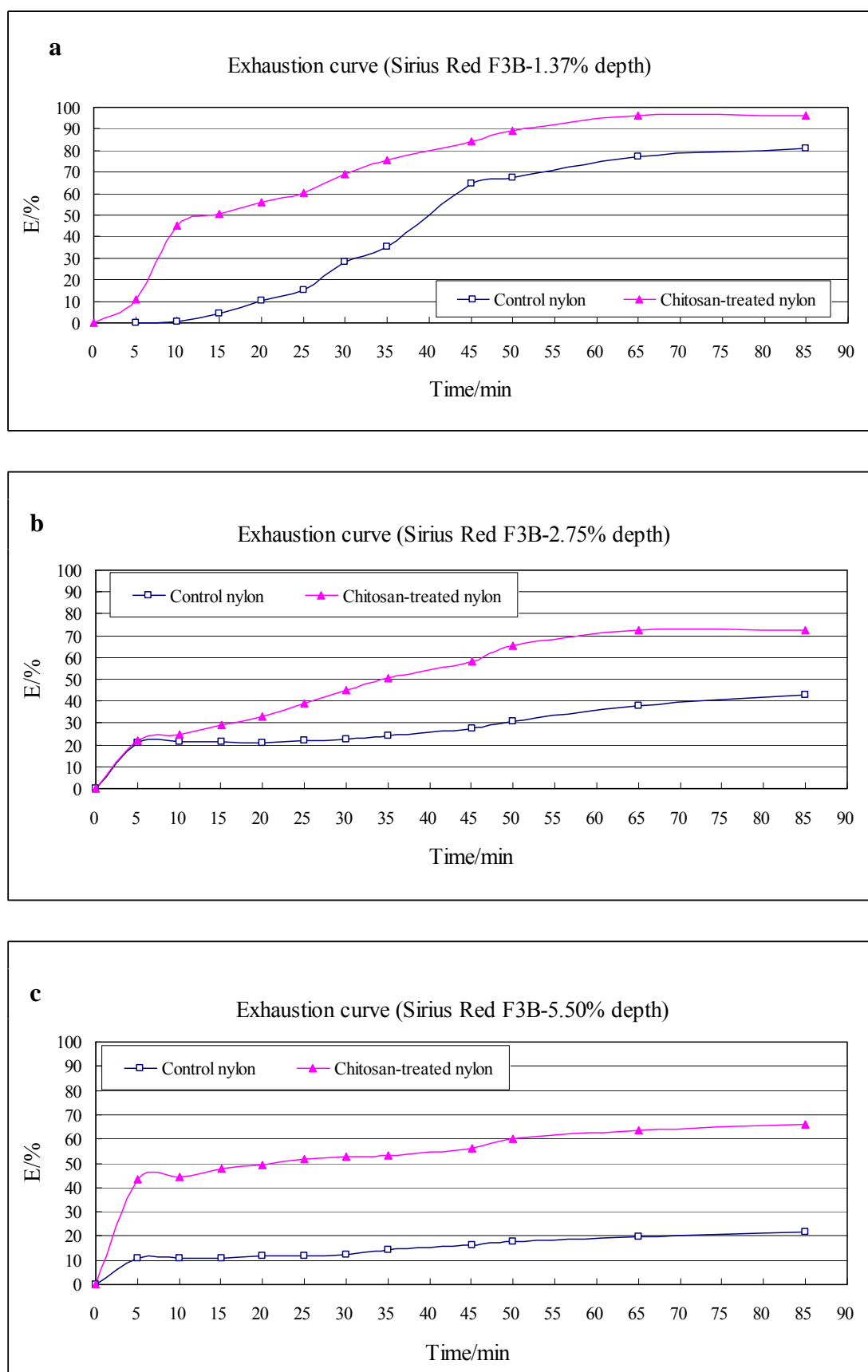


**Figure 5.13** Exhaustion curves of Sirius Red F3B at different depths: a (1.37% depth), b (2.75% depth), and c (5.50% depth)

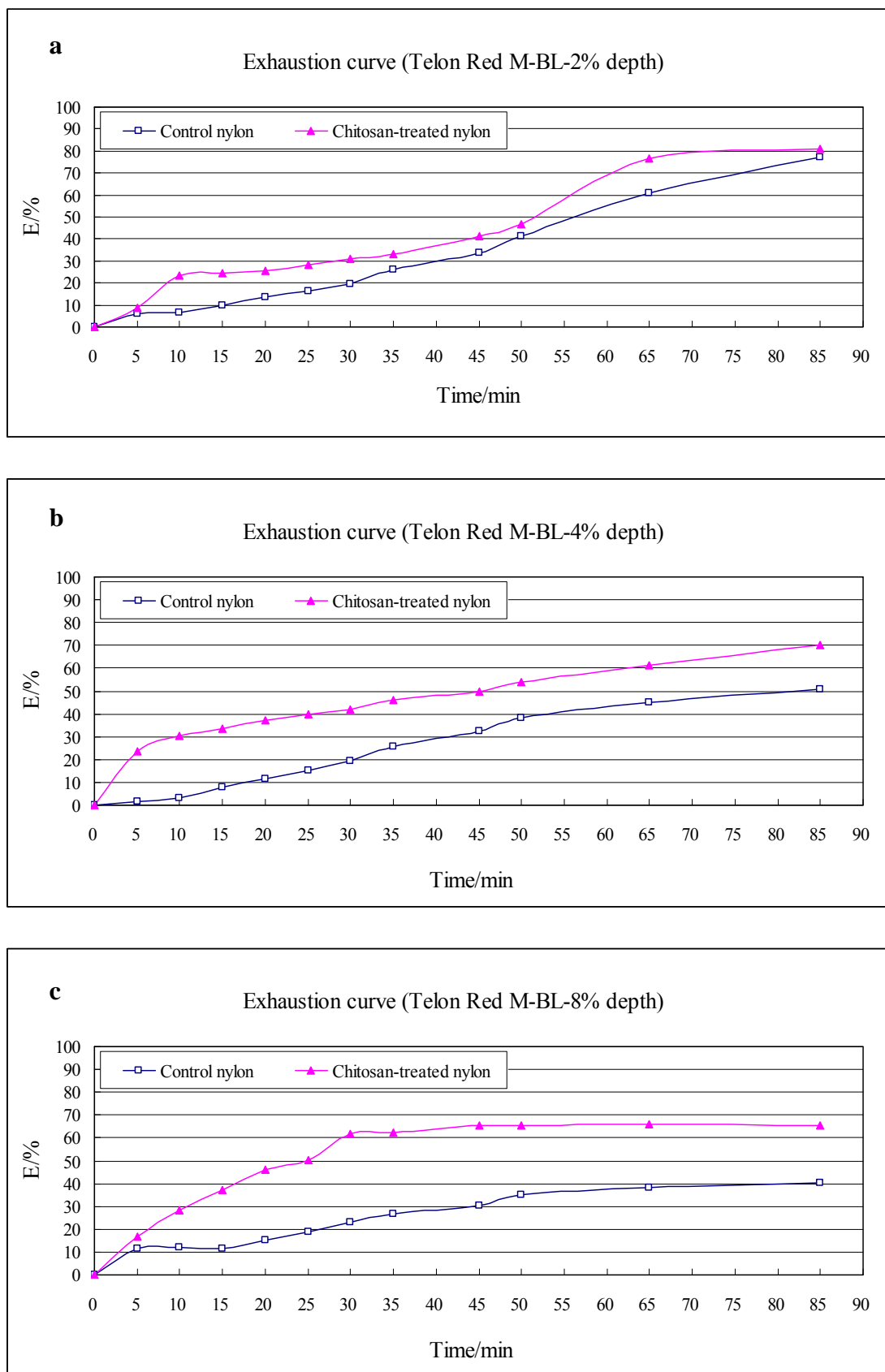


**Figure 5.14** Exhaustion curves of Telon Red M-BL at different depths: a (2% depth), b (4% depth), and c (8% depth)

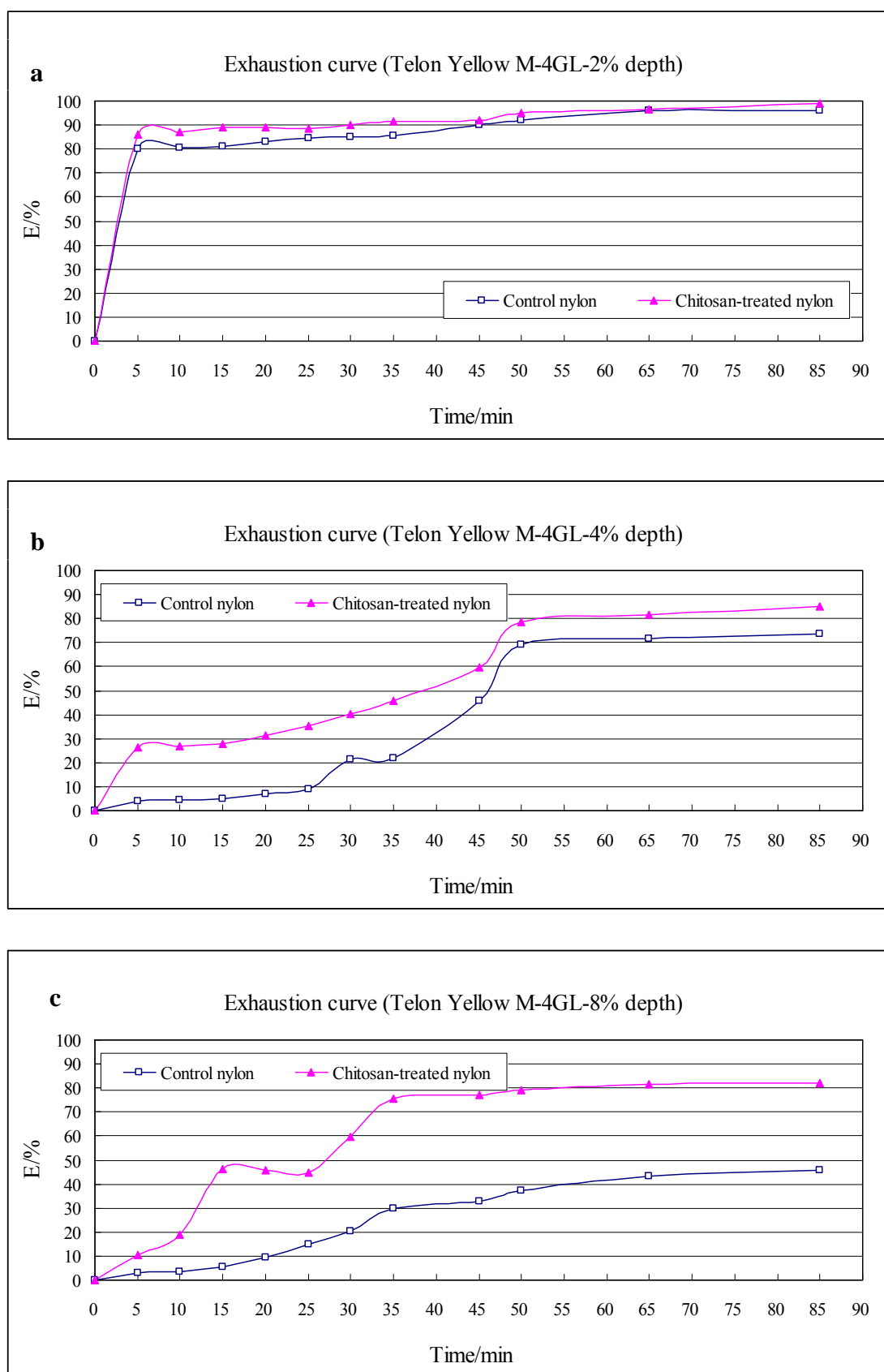


**Figure 5.15** Exhaustion curves of Telon Yellow M-4GL at different depths: a (2% depth), b (4% depth), and c (8% depth)

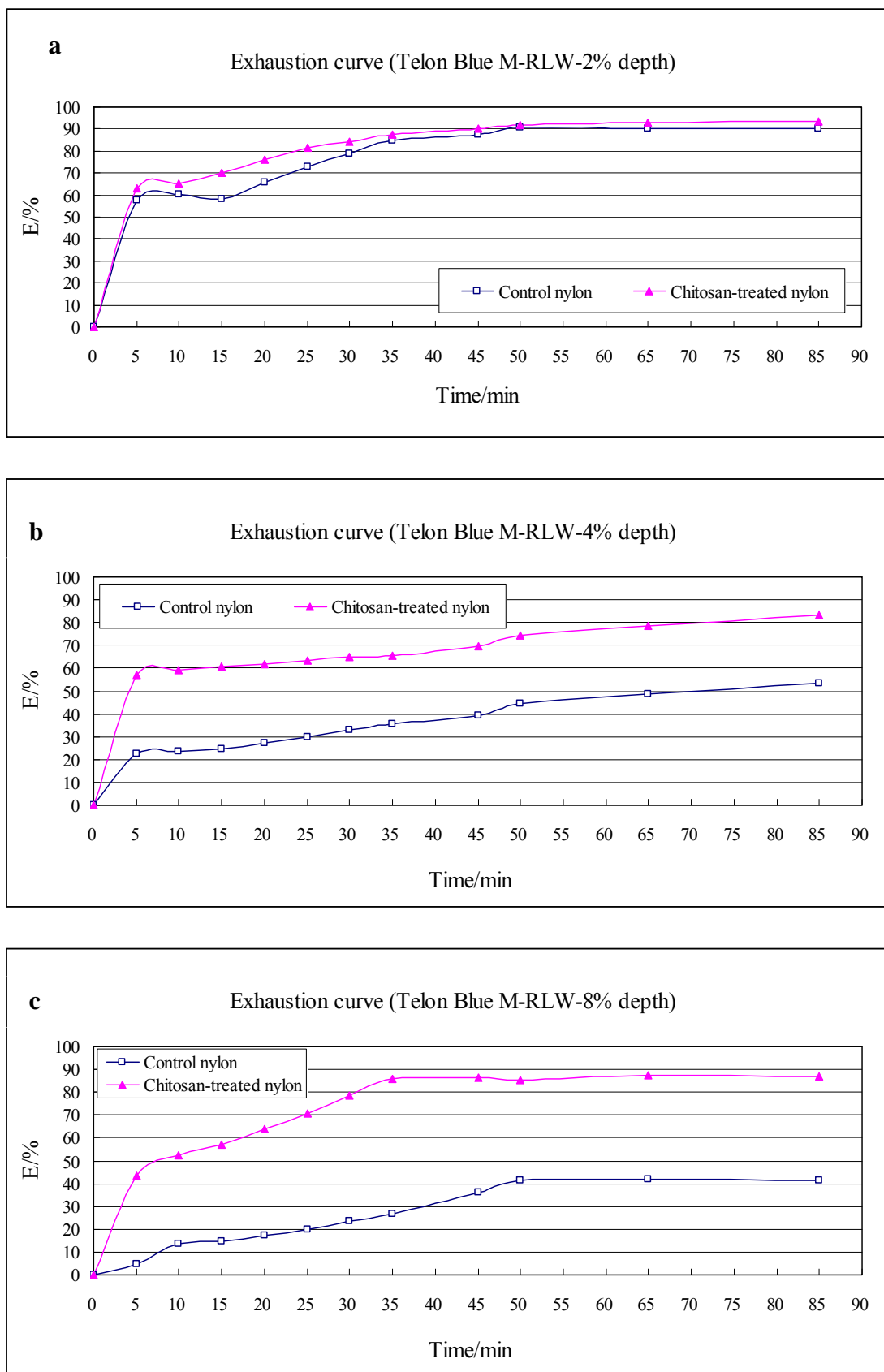


**Figure 5.16** Exhaustion curves of Telon Blue M-RLW at different depths: a (2% depth), b (4% depth), and c (8% depth)

As shown in the exhaustion curves of Acid Orange 7, Acid Red 1, and Acid Red 18, a high exhaustion which was close to the equilibrium was achieved very quickly. The exhaustion increased significantly after dyeing 10 minutes at 30°C. That was because dyes molecules of Acid Orange 7, Acid Red 1, and Acid Red 18, which have lower molecular weights, could be adsorbed and diffused into the polymer matrix when the size of voids was large enough to accommodate them.

As shown in the exhaustion curves of Sirius Brown 3RL, Sirius Red F3B, Telon Red M-BL and Telon Yellow M-4GL and Telon Blue M-RLW, the exhaustion increased significantly after 30 minutes of dyeing (Temperature at 54°C-60°C). It was because the molecular dimensions of Sirius Brown 3RL, Sirius Red F3B, Telon Red M-BL, Telon Yellow M-4GL and Telon Blue M-RLW, are relatively large and they can aggregate easily; the molecules of dyes could not penetrate into the fabric and chitosan to get adsorbed at low temperature. When the dyeing temperature increased, the dye aggregates were broken down into individual dye molecules; thus, there was a significant increase in the exhaustion. Since the molecular weights of the commercial dyes were higher than that of the other three dyes being studied, therefore, the critical bath temperature played an important role in the rate of dyeing.

Table 5.6 shows the summarized data of dyeing of the dyes. The equilibrium exhaustion revealed the dyeability of the fabrics; the chitosan-treated nylon fabric showed much higher equilibrium exhaustion which meant it had better dyeability than the control fabrics at the same depths. The time to achieve the equilibrium of exhaustion and the time half dyeing could be derived. The chitosan-treated nylon used less time to achieve the equilibrium. The chitosan-treated method can improve the dyeability of fabrics effectively and efficiently.



**Table 5.6** Exhaustion data of the anionic dyes

Dye at different depths		Equilibrium (or final) exhaustion	Time to achieve equilibrium of exhaustion /min	Time of half dyeing /min	Difference in equilibrium exhaustion /%	Difference in equilibrium exhaustion
Acid Orange 7						
1.05%	Chit-treated	92.2%	10	2.6	0.2%	1.20×10 <sup>-4</sup> mmol
1.05%	Control	92.0%	10	2.7		
2.10%	Chit-treated	87.9%	15	2.9	8.4%	1.01×10 <sup>-2</sup> mmol
2.10%	Control	79.5%	20	3.1		
4.20%	Chit-treated	78.5%	25	3.8	40.1%	9.62×10 <sup>-2</sup> mmol
4.20%	Control	38.4%	35	3.3		
Acid Red 1						
1.02%	Chit-treated	89.1%	25	5.2	19.1%	7.64×10 <sup>-3</sup> mmol
1.02%	Control	70.0%	35	17.5		
2.04%	Chit-treated	78.0%	45	6.4	43.5%	3.48×10 <sup>-2</sup> mmol
2.04%	Control	34.5%	40	27.5		
4.08%	Chit-treated	50%	25	6.5	24%	3.84×10 <sup>-2</sup> mmol
4.08%	Control	26.0%	35	22.5		
Acid Red 18						
0.60%	Chit-treated	94.5%	7	3.2	8.5%	1.7×10 <sup>-3</sup> mmol
0.60%	Control	86.0%	25	3.4		
1.21%	Chit-treated	81.5%	5	3.5	16.5%	0.66×10 <sup>-2</sup> mmol
1.21%	Control	65%	20	3.7		
2.42%	Chit-treated	81.5%	10	3.5	42.5%	3.4×10 <sup>-2</sup> mmol
2.42%	Control	39.0%	15	4.0		
Sirius Brown 3RL						
2.27%	Chit-treated	92.5%	85	35	4.2%	1.68 ×10 <sup>-3</sup> mmol
2.27%	Control	88.3%	85	55		

**Table 5.6** Continued

Dye at different depths		Equilibrium (or final) exhaustion	Time to achieve equilibrium of exhaustion /min	Time of half dyeing /min	Difference in equilibrium exhaustion /%	Difference in equilibrium exhaustion
Sirius Brown 3RL						
4.55%	Chit-treated	74.4%	85	8	24.4%	1.95×10 <sup>-2</sup> mmol
4.55%	Control	50.0%	85	50		
9.10%	Chit-treated	67.0%	65	33	27.1%	4.32×10 <sup>-2</sup> mmol
9.10%	Control	39.9%	85	37		
Sirius Red F3B						
1.37%	Chit-treated	98.5%	70	15	18.0%	3.6×10 <sup>-3</sup> mmol
1.37%	Control	80.5%	85	37.5		
2.75%	Chit-treated	72.0%	85	16	28.0%	1.12×10 <sup>-2</sup> mmol
2.75%	Control	44.0%	85	65		
5.50%	Chit-treated	67.5%	85	28	46.0%	3.68×10 <sup>-2</sup> mmol
5.50%	Control	21.5%	85	47.5		
Telon Red M-BL						
2%	Chit-treated	81.0%	85	45	3.9%	1.56×10 <sup>-3</sup> g
2%	Control	77.1%	85	49		
4%	Chit-treated	80.4%	85	26	7.7%	6.16×10 <sup>-3</sup> g
4%	Control	72.7%	85	47		
8%	Chit-treated	79.9%	65	16	41.9%	6.70×10 <sup>-2</sup> g
8%	Control	38.0%	65	24		
Telon Yellow M-4GL						
2%	Chit-treated	98.9%	85	3	2.7%	1.08×10 <sup>-3</sup> g
2%	Control	96.2%	85	3		
4%	Chit-treated	81.8%	65	30	10.4%	8.32×10 <sup>-3</sup> g
4%	Control	71.4%	65	42		
8%	Chit-treated	83.5%	65	18	13.5%	2.16×10 <sup>-2</sup> g
8%	Control	70.0%	85	47		

**Table 5.6** Continued

Dye at different depths		Equilibrium (or final) exhaustion	Time to achieve equilibrium of exhaustion /min	Time of half dyeing /min	Difference in equilibrium exhaustion /%	Difference in equilibrium exhaustion
Telon Blue M-RLW						
2%	Chit-treated	92.4%	50	3.5	1.9%	$7.6 \times 10^{-4}$ g
2%	Control	90.5%	50	3.7		
4%	Chit-treated	83.5%	85	2	30%	$2.4 \times 10^{-2}$ g
4%	Control	53.5%	85	15		
8%	Chit-treated	87.6%	65	6	46%	$7.36 \times 10^{-2}$ g
8%	Control	41.6%	65	26		

In order to verify the sorption ability of nanochitosan, we repeated the experiment of Section 4.3.4 at 80°C and obtained the sorption capacities of the nanochitosan and microchitosan at 80°C. Since the amount of chitosan on the fabric is 18.6 mg (Section 5.4.6), the capacities of nanochitosan and microchitosan for the dyes could be derived.

**Table 5.7** Sorption data obtained from sorption study and dyeing data

Acid Orange 7	Acid Red 1	Acid Red 18	Sirius Brown 3RL	Sirius Red F3B
Sorption capacity of nanochitosan in sorption at 80°C/(mmol/g)				
5.205	2.651	2.414	2.854	2.145
Sorption capacity of microchitosan in sorption at 80°C/(mmol/g)				
4.064	1.942	2.054	1.464	0.941
Sorption ability of 18.6 mg of nanochitosan in sorption at 80°C/(mmol)				
$9.68 \times 10^{-2}$	$4.93 \times 10^{-2}$	$4.49 \times 10^{-2}$	$5.31 \times 10^{-2}$	$3.99 \times 10^{-2}$
Sorption ability of 18.6 mg of microchitosan in sorption at 80°C/(mmol)				
$7.56 \times 10^{-2}$	$3.61 \times 10^{-2}$	$3.82 \times 10^{-2}$	$2.72 \times 10^{-2}$	$1.75 \times 10^{-2}$
Difference in equilibrium exhaustion in dyeing/(mmol)				
$9.62 \times 10^{-2}$	$3.84 \times 10^{-2}$	$3.4 \times 10^{-2}$	$4.32 \times 10^{-2}$	$3.68 \times 10^{-2}$

The sorption data obtained from the sorption study and the actual dyeing data are list in Table 5.7. The difference in the exhaustion was consistent with the sorption data obtained in the sorption of dyes onto nanochitosan. The sorption capabilities of nanochitosan in the dyeing were lower than that in the sorption study. It was because the concentrations of dye solution in dyeing were much lower than those in the sorption studies.

### **5.4.9 Comparisons between dyes exhaustion of chitosan-treated and control fabrics**

#### **5.4.9.1 Final exhaustion**

In Table 5.6, all the eight dyes showed higher equilibrium exhaustion in the chitosan-treated fabrics than those in control fabrics at all depths of dyeing. The high exhaustion in the chitosan-treated fabric was because of the additional protonated amino groups from chitosan. The additional amino groups in the chitosan-treated fabrics could still adsorb more dye molecules when the control fabrics reached the saturation point. Thus, the final exhaustion of chitosan-treated fabrics was higher than those of the control fabrics.

The difference in the final exhaustion became higher when the depths of dyes increased. It was because when the concentration of the dye solution was below the saturation point of the control nylon fabric, both the control fabric and chitosan-treated fabric could adsorb most of the dye onto the fabrics. The difference was not very obvious then..

#### **5.4.9.2 Time to achieve equilibrium exhaustion**

As shown in Tables 5.6, all the eight dyes showed that time required to achieve the equilibrium exhaustion in chitosan-treated fabrics was either shorter than or equal to that in control fabrics at all depths.

At a lower depth of dyeing, the number of amino groups was in excess when compared to the number of sulphonate groups in dye solution. Although there was great difference in the number of dyesites between chitosan-treated and control fabrics, the difference of equilibrium exhaustion at the lower depths of dyeing was not as significant as that at the higher depths of dyeing due to the insufficiency of dye. In chitosan-treated fabric, the additional protonated amino groups from chitosan provided more dyesites. The increase of available dyesites enabled dye molecules to be exhausted more quickly, therefore, the time needed to achieve the equilibrium exhaustion in chitosan-treated fabric was shorter than that in the control fabric at lower depths.

At higher depths of dyeing, the increase in available dyesites enabled more dye molecules to be exhausted. Although the initial rate of dyeing increased, the final or equilibrium exhaustion also increased. However, the time needed to achieve the equilibrium exhaustion in chitosan-treated fabric was usually shorter than that in the control fabric at higher depths.

#### **5.4.9.3 Time of half dyeing ( $T_{1/2}$ )**

The time of half dyeing is the time to achieve 50% of the dyeing. As summarized in Table 5.6, the  $T_{1/2}$  of chitosan-treated fabrics was shorter than that of the control fabrics in general.

The number of amino groups in the chitosan-treated fabric was 0.22 mmol which was doubled to that in the control fabric as discussed in Section 5.4.6. Because of the increase in the number of amino groups, dye molecules could be adsorbed in chitosan-treated fabric more quickly at the initial stage of dyeing.

For Acid Orange 7 at 4.20% depth, although dye molecules could be adsorbed in the chitosan-treated fabric more quickly at the initial stage of dyeing, the additional amino

groups also provided a higher saturation point for adsorbing more dye molecules than the control fabric and extended the equilibrium time. As a result, the time of half dyeing for chitosan-treated fabric was a little longer than that of the control fabric.

**Table 5.8** Initial ratios of the number of amino group dyesites to the number of sulphonate groups in the dye solution

Dye at different depth	Initial ratio of amino group dyesites (mmol) to sulphonate groups (mmol)	
	Chitosan-treated	Control
Acid Orange 7		
1.05%	3.67:1	1.83:1
2.10%	1.83:1	0.92:1
4.20%	0.92:1	0.46:1
Acid Red 1		
1.02%	5.5:2	2.75:2
2.04%	2.75:2	1.38:2
4.08%	1.38:2	0.69:2
Acid Red 18		
0.60%	11:3	5.5:3
1.21%	5.5:3	2.75:3
2.42%	2.75:3	1.38:3
Sirius Brown 3RL		
2.27%	5.5:4	2.75:4
4.55%	2.75:4	1.38:4
9.10%	1.38:4	0.69:4
Sirius Red F3B		
1.37%	11:6	5.5:6
2.75%	5.5:6	2.75:6
5.50%	2.75:6	1.38:6

Table 5.8 shows the ratio of the initial number of amino groups to the initial number of sulphonate groups in the dye solution. The higher of the value was, the faster of the initial rate of adsorption would be. As shown in Table 5.8, the ratio of the number of amino

groups in chitosan-treated nylon fabric to the initial number of sulphonate groups in dye solution was higher than that in the control nylon fabric. The adsorption rate in the chitosan-treated nylon fabric was higher than that in the control nylon fabric and the time of half dyeing was shorter than that in the control fabric.

As shown in Table 5.8, the ratios of number of amino groups to the initial number of sulphonate groups in dye solution at lower depths were bigger than those at higher depths. Thus, the adsorption rates at lower depths were higher and the data of  $T_{1/2}$  were smaller.

#### **5.4.10 Evaluation of un-dyed fabrics**

The original color of the nylon fabric used in this study was white, therefore, the whiteness index were used to evaluate whether the whiteness of the fabrics was affected by the curing process. During the padding process, the wet pick-up was important and needed to be controlled carefully so as to yield consistent pick-up in each fabric. The pick-up was directly proportional to the addition of amino groups of the fabric.

The curing conditions were needed to be controlled so as to yield the best result but did not affect the whiteness of the fabrics. Higher curing temperatures and longer curing time could yield better fixation result. However, yellowing became more significant when the temperature was high and curing time was long. The whiteness index and yellowness index of the fabrics are shown in Table 5.9.

The results showed that the whiteness of the un-dyed chitosan-treated fabric and the control fabric were reduced when the curing temperature increased. When the curing temperature increased from 130°C to 160°C, the reduction in whiteness was doubled to that from 130°C to 150°C in both the chitosan-treated fabric and control fabric. The curing at 150°C for 5 minutes was chosen to minimize the yellowness problem in this study. In this condition, the difference of the whiteness index of chitosan-treated fabric

and control fabric was less than 10%

**Table 5.9** Whiteness and yellowness of chitosan-treated and control fabrics in various curing conditions

Fabrics at different curing Condition	C.I.E. Whiteness Index	Reduction in whiteness (%)	Yellowness Index (ASTM E 313)
Chitosan-treated fabric			
No curing	159.65	-	-29.20
Cure at 130°C for 5 mins	155.67	-2.5%	-27.23
Cure at 150°C for 5 mins	147.02	-7.9%	-23.68
Cure at 160°C for 5 mins	140.37	-12.1%	-20.71
Control fabric			
No curing	164.33	-	-31.01
Cure at 130°C for 5 mins	163.41	-0.6%	-30.50
Cure at 150°C for 5 mins	161.39	-1.8%	-29.52
Cure at 160°C for 5 mins	158.33	-3.7%	-28.29

#### 5.4.11 Visual assessment under $D_{65}$ of dyed fabrics

Figures 5.17 to 5.24 show the photos of the chitosan-treated and control fabric dyed by different dyes under  $D_{65}$ . The chitosan-treated fabric s at same depths of dyeing showed darker shade than the control fabrics. The color difference of the chitosan-treated and the control fabrics were assessed and summarized in Table 5.10. In general, the results agree with the exhaustion discussion in Section 5.4.8. The difference was more significant at higher depths of dyeing.



## Acid Orange 7



**1.05% depth**  
**Chitosan-treated fabric**



**1.05% depth**  
**Control fabric**



**2.10% depth**  
**Chitosan-treated fabric**



**2.10% depth**  
**Control fabric**



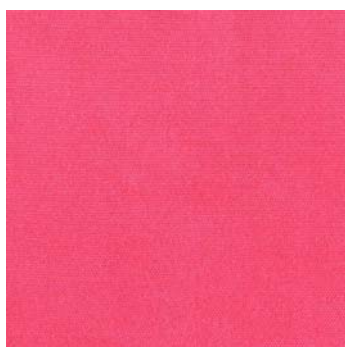
**4.20% depth**  
**Chitosan-treated fabric**



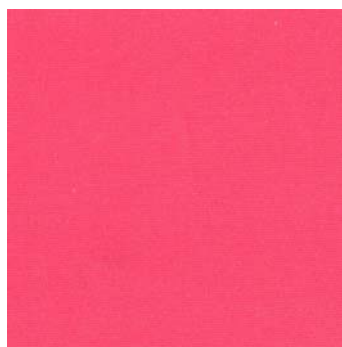
**4.20% depth**  
**Control fabric**

**Figure 5.17** Fabric samples dyed by Acid Orange 7

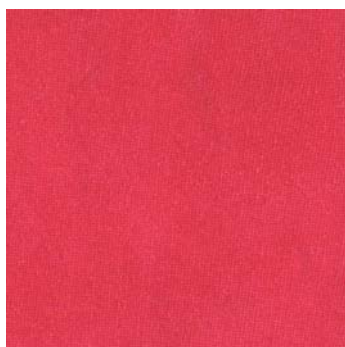
## Acid Red 1



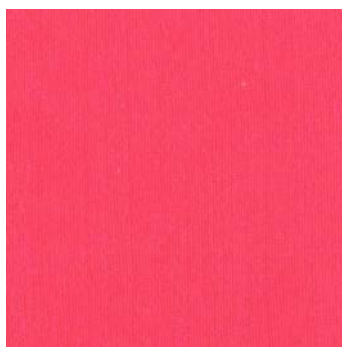
**1.02% depth  
Chitosan-treated fabric**



**1.02% depth  
Control fabric**



**2.04% depth  
Chitosan-treated fabric**



**2.04% depth  
Control fabric**



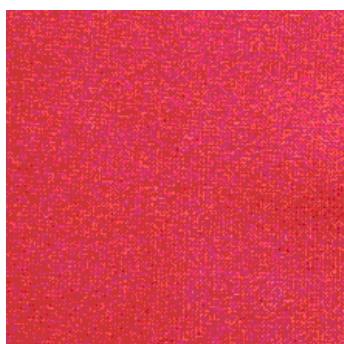
**4.08% depth  
Chitosan-treated fabric**



**4.08% depth  
Control fabric**

**Figure 5.18** Fabric samples dyed by Acid Red 1

## Acid Red 18



**0.60% depth**  
**Chitosan-treated fabric**



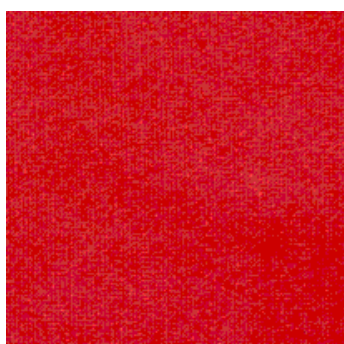
**0.60% depth**  
**Control fabric**



**1.21% depth**  
**Chitosan-treated fabric**



**1.21% depth**  
**Control fabric**



**2.42% depth**  
**Chitosan-treated fabric**



**2.42% depth**  
**Control fabric**

**Figure 5.19** Fabric samples dyed by Acid Red 18

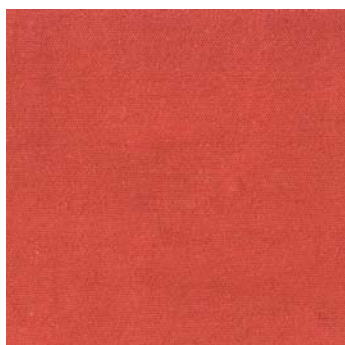
### **Sirius Brown 3RL**



**2.27% depth**  
**Chitosan-treated fabric**



**2.27% depth**  
**Control fabric**



**4.55% depth**  
**Chitosan-treated fabric**



**4.55% depth**  
**Control fabric**



**9.10% depth**  
**Chitosan-treated fabric**



**9.10% depth**  
**Control fabric**

**Figure 5.20** Fabric samples dyed by Sirius Brown 3RL



## Sirius Red F3B



**1.37% depth**  
**Chitosan-treated fabric**



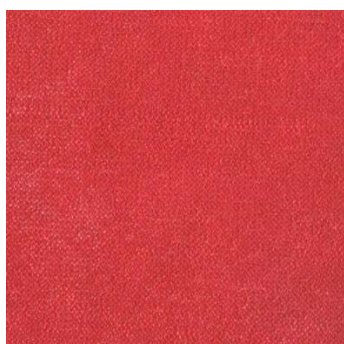
**1.37% depth**  
**Control fabric**



**2.75% depth**  
**Chitosan-treated fabric**



**2.75% depth**  
**Control fabric**



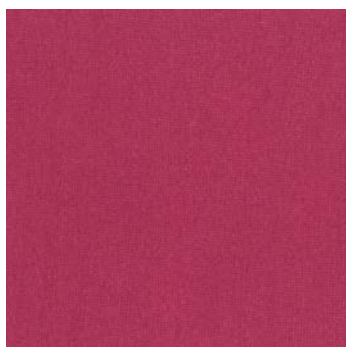
**5.50% depth**  
**Chitosan-treated fabric**



**5.50% depth**  
**Control fabric**

**Figure 5.21** Fabric samples dyed by Sirius Red F3B

### **Telon Red M-BL**



**2% depth  
Chitosan-treated fabric**



**2% depth  
Control fabric**



**4% depth  
Chitosan-treated fabric**



**4% depth  
Control fabric**



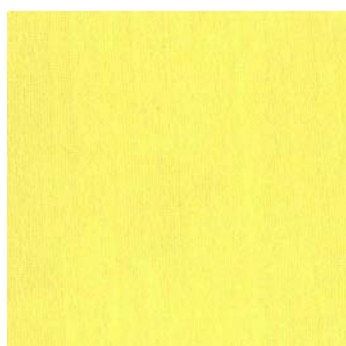
**8% depth  
Chitosan-treated fabric**



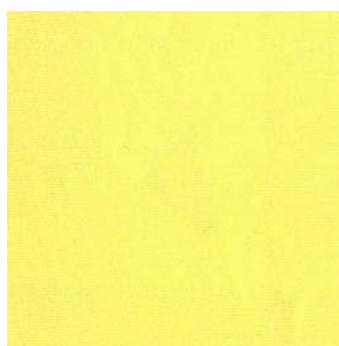
**8% depth  
Control fabric**

**Figure 5.22** Fabric samples dyed by Telon Red M-BL

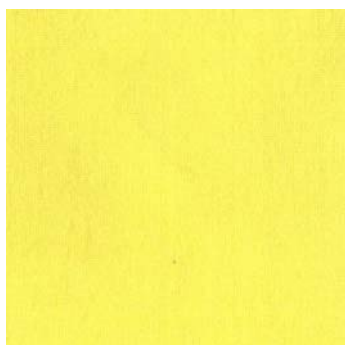
### **Telon Yellow M-4G**



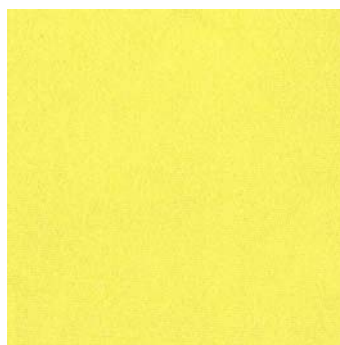
**2% depth  
Chitosan-treated fabric**



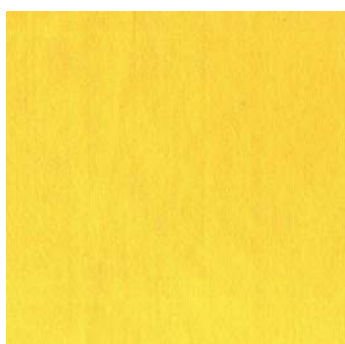
**2% depth  
Control fabric**



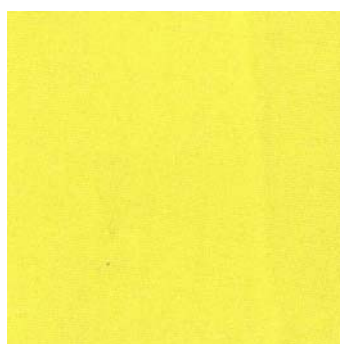
**4% depth  
Chitosan-treated fabric**



**4% depth  
Control fabric**



**8% depth  
Chitosan-treated fabric**



**8% depth  
Control fabric**

**Figure 5.23** Fabric samples dyed by Telon Yellow M-4GL

## **Telon Blue M-RLW**



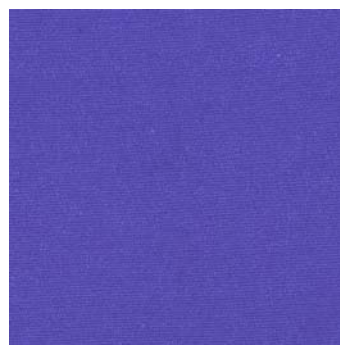
**2% depth  
Chitosan-treated fabric**



**2% depth  
Control fabric**



**4% depth  
Chitosan-treated fabric**



**4% depth  
Control fabric**



**8% depth  
Chitosan-treated fabric**



**8% depth  
Control fabric**

**Figure 5.24** Fabric samples dyed by Telon Blue M-RLW



**Table 5.10** The color difference of the chitosan-treated and the control fabrics (grey scales)

Dyes	AO7	AR 1	AR 18	SB	SR	TR	TY	TB
Diff. at low depth	5	5	5	5	3-4	5	5	5
Diff. at middle depth	3-4	3	3	4	3	4-5	4-5	4
Diff. at high depth	3	2	2	2-3	1-2	3	3-4	2-3

### 5.4.12 CIE L\*a\*b\* of dyed fabrics

CIE L\*a\*b\* data of the chitosan-treated and control fabrics dyed by the eight dyes are listed in Tables 5.11-5.26. The data provided detailed color assessments of the chitosan-treated and control fabrics dyed by the eight dyes.

$\Delta E$  is used in comparing the color difference between two samples, which were the chitosan-treated and control fabrics in this case.  $\Delta L^*$  is the difference in lightness,  $\Delta a^*$  is the difference in red-green character,  $\Delta b^*$  is the difference in yellow-blue character between chitosan-treated and control fabrics.  $\Delta C^*$  is the difference in saturation between chitosan-treated and control fabrics and  $\Delta h$  is the difference in hue angle between the chitosan-treated and control fabrics.

#### 5.4.12.1 Acid Orange 7

Tables 5.11-5.12 show the CIE L\*a\*b\* and color difference of the chitosan-treated and control fabrics dyed by Acid orange 7. At all depths of dyeing, the chitosan-treated fabrics had smaller values of  $L^*$  which meant the chitosan-treated fabrics were darker than the control fabrics.  $L^*$  values of the chitosan-treated and control fabrics were getting smaller when the depth of dyeing increased due to more dyes were adsorbed by the fabrics. The absolute values of  $\Delta L^*$  were getting larger as the depth of dyeing increased. Because the difference in exhaustion became larger as we had shown in Figure 5.9 and Table 5.6.  $\Delta E$

values which are the total color differences increased when the depth of dyeing increased.

**Table 5.11** CIE L\*a\*b\* of the chitosan-treated and control fabrics dyed by Acid Orange 7

Sample	L*	a*	b*	C*	h
Acid Orange 7 at 1.05%					
Chitosan-treated	66.02	48.18	64.32	80.37	53.17
Control	68.82	45.38	61.15	76.15	53.42
Acid Orange 7 at 2.10%					
Chitosan-treated	62.24	51.58	68.78	85.97	53.14
Control	66.46	48.43	67.23	82.86	54.23
Acid Orange 7 at 4.20%					
Chitosan-treated	54.59	56.24	62.71	84.24	48.11
Control	64.72	49.67	69.19	85.17	54.33

**Table 5.12** Color difference between the chitosan-treated and control fabrics dyed by Acid orange 7

Sample	$\Delta E$	$\Delta L^*$	$\Delta a^*$	$\Delta b^*$	$\Delta C^*$	$\Delta h$
Acid Orange 7 at 1.05%	5.07	-2.8	2.8	3.17	4.22	-0.25
Acid Orange 7 at 2.10%	5.49	-4.22	3.15	1.55	3.11	-1.09
Acid Orange 7 at 4.20%	13.70	-10.13	6.57	-6.48	-0.93	-6.22

At all depths of dyeing, the chitosan-treated fabrics had greater values of  $a^*$  which meant the chitosan-treated fabrics were redder than the control fabrics at all depths of dyeing.  $\Delta a^*$  values between the chitosan-treated and control fabrics were getting larger when the depths of dyeing increased. At 1.05% and 2.10% depths,  $b^*$  of the chitosan-treated fabric was greater than that of the control fabric which meant the chitosan-treated fabric was yellower than the control fabric but it became more blue than the control fabric at 4.20% depth of dyeing.

The  $C^*$  values of the chitosan-treated fabrics were all smaller than that of control fabrics and the  $\Delta C^*$  values decreased as the depth of dyeing increased. Those meant that the

chitosan-treated fabrics were less saturated than the control fabrics. The absolute values of  $\Delta h$  increased from 0.25 to 6.22 which meant that the change in hue was getting larger when depth increased.

#### 5.4.12.2 Acid Red 1

**Table 5.13** CIE L\*a\*b\* of the chitosan-treated and control fabrics dyed by Acid Red 1

Sample	L*	a*	b*	C*	h
Acid Red 1 at 1.02%					
Chitosan-treated	50.708	61.411	2.939	56.151	2.608
Control	53.280	62.316	3.409	62.410	3.131
Acid Red 1 at 2.04%					
Chitosan-treated	42.721	58.347	11.561	59.482	11.207
Control	51.506	63.137	5.996	63.421	5.425
Acid Red 1 at 4.08%					
Chitosan-treated	41.321	57.665	11.546	58.810	11.322
Control	50.144	63.484	8.036	63.991	7.215

**Table 5.14** Color difference between the chitosan-treated and control fabrics dyed by Acid Red 1

Sample	$\Delta E$	$\Delta L^*$	$\Delta a^*$	$\Delta b^*$	$\Delta C^*$	$\Delta h$
Acid Red 1 at 1.02%	2.767	-2.572	-0.905	-0.470	-0.875	-0.523
Acid Red 1 at 2.04%	11.449	-8.785	-4.79	5.565	-3.939	5.782
Acid Red 1 at 4.08%	11.137	-8.823	-5.819	3.51	-5.181	4.107

Similar to the dyeing of Acid Orange 7, the chitosan-treated fabrics dyed by Acid Red 1 had smaller values of  $L^*$  which meant the chitosan-treated fabrics were darker than the control fabrics at all depths.  $L^*$  values of the chitosan-treated and control fabrics were getting smaller when the depth of dyeing increased due to more dyes were adsorbed onto the fabrics. The absolute values of  $\Delta L^*$  were getting larger as the depth of dyeing increased.  $\Delta E$  value which is the total color difference increased greatly comparing the

depth of 2.04% with 1.02%. But at the depth of 4.08% when the dye concentration are much above the saturation point of the chitosan-treated and control fabrics, the total color difference became stable.

At all depths of dyeing, the chitosan-treated fabrics had smaller  $a^*$  values at all depths than the untreated fabrics. That meant the chitosan-treated fabrics were greener than the control fabrics. It was because the chitosan-treated fabrics were much darker than the control fabrics. The absolute values of  $\Delta a^*$  between the chitosan-treated and control fabrics were getting larger as the depth of dyeing increased. At the depth of 1.02%, the chitosan-treated fabric had lower  $b^*$  value than the untreated sample, that meant the chitosan-treated fabric was a little less yellow than the untreated sample. At the depth of 2.04% and 4.08%, the chitosan-treated samples had higher  $b^*$  values than the untreated samples, that meant the chitosan-treated fabrics became more yellow than the untreated fabrics.

$C^*$  values of chitosan-treated fabrics were all smaller than those of control fabrics and the absolute values of  $\Delta C^*$  increased as the depth of dyeing increased. The chitosan-treated fabrics were less saturated than the control fabrics and the difference became larger as the depth of dyeing increased.

#### **5.4.12.3 Acid Red 18**

As shown in Tables 5.15-5.16, the chitosan-treated fabrics were darker than the control fabrics at all depths of dyeing of Acid Red 18. And the difference was getting larger as the depths of dyeing increased which was shown by the increase of the absolute values of  $\Delta L^*$ . The results of  $\Delta E$  values were similar to the results of Acid Red 1.

**Table 5.15** CIE L\*a\*b\* of the chitosan-treated and control fabrics dyed by Acid Red 18

Sample	L*	a*	b*	C*	h
Acid Red 18 at 0.60%					
Chitosan-treated	51.61	57.12	16.69	59.51	16.29
Control	62.36	50.98	6.17	51.35	6.91
Acid Red 18 at 1.21%					
Chitosan-treated	47.22	57.24	20.77	60.37	22.31
Control	60.60	52.72	8.02	53.33	8.65
Acid Red 1 at 2.42%					
Chitosan-treated	43.79	55.85	22.92	60.37	22.31
Control	58.38	55.50	10.77	56.54	10.98

**Table 5.16** Color difference between the chitosan-treated and control fabrics dyed by Acid Red 18

Sample	$\Delta E$	$\Delta L^*$	$\Delta a^*$	$\Delta b^*$	$\Delta C^*$	$\Delta h$
Acid Red 18 at 0.60%	16.25	-10.75	6.14	10.52	8.16	9.38
Acid Red 18 at 1.21%	19.03	-13.38	4.52	12.75	7.04	13.66
Acid Red 1 at 2.42%	18.99	-14.59	0.35	12.15	3.83	11.33

At all depths of dyeing of Acid Red 18, the chitosan-treated fabrics had greater values of  $a^*$  which meant that the chitosan-treated fabrics were redder than the control fabrics at all depths.  $\Delta a^*$  values between chitosan-treated and control fabric were getting smaller when the depth of dyeing increased.  $b^*$  values of chitosan-treated fabrics were higher than that of the control samples. Those meant the chitosan-treated fabrics were yellower than the control ones.  $\Delta b^*$  values between chitosan-treated and control fabrics ranged from 10.52 to 12.75 at all depths of dyeing.

$C^*$  values of chitosan-treated fabrics were all larger than those of the control fabrics and the  $\Delta C^*$  values decreased as the depth of dyeing increased. It meant that the chitosan-treated fabrics were more saturated than the control fabrics.  $\Delta h$  ranged from

9.38-13.66 at all depths of dyeing.

#### 5.4.12.4 Sirius Brown 3RL

**Table 5.17** CIE L\*a\*b\* of the chitosan-treated and control fabrics dyed by Sirius Brown 3RL

Sample	L*	a*	b*	C*	h
Sirius Brown 3RL at 2.27%					
Chitosan-treated	47.096	46.436	33.100	57.026	35.482
Control	46.019	43.486	28.293	51.880	33.049
Sirius Brown 3RL at 4.55%					
Chitosan-treated	36.716	40.652	27.844	49.274	34.409
Control	41.351	47.887	36.007	59.914	36.940
Sirius Brown 3RL at 9.10%					
Chitosan-treated	33.589	38.987	26.677	47.240	34.382
Control	40.390	48.775	38.270	61.996	38.119

**Table 5.18** Color difference between the chitosan-treated and control fabrics dyed by Sirius Brown 3RL

Sample	$\Delta E$	$\Delta L^*$	$\Delta a^*$	$\Delta b^*$	$\Delta C^*$	$\Delta h$
Sirius Brown 3RL at 2.27%	5.74	1.077	2.95	4.807	5.146	2.433
Sirius Brown 3RL at 4.55%	11.85	-4.635	-7.235	-8.163	-10.64	-2.531
Sirius Brown 3RL at 9.10%	16.63	-6.801	-9.788	-11.593	-14.756	-3.737

As data shown in Tables 5.17-5.18, the chitosan-treated fabric had larger values of L\* at the depth of 2.27% which meant the chitosan-treated fabrics were a little brighter than the control fabrics at the depth of 2.27%. And the chitosan-treated fabrics had smaller values of L\* at the depths of 4.55% and 9.10% which meant the chitosan-treated fabrics were darker than the control fabrics. L\* values of chitosan-treated and control fabrics were getting smaller when the depths of dyeing increased due to more dyes were adsorbed onto the fabrics. The absolute values of  $\Delta L^*$  were getting bigger as the depth of dyeing increased.  $\Delta E$  values increased as the depths of dyeing increased.

The chitosan-treated fabric had a bigger  $a^*$  value than the untreated fabric at the depth of 2.27%, while the chitosan-treated fabrics had smaller  $a^*$  values than the untreated fabrics at the depths of 4.55% and 9.10%. That meant the chitosan-treated fabric was redder than the control sample at depth of 2.27%, but greener than the control fabrics at the depths of 4.55% and 9.10%. That was because the chitosan-treated fabrics became much darker as the depth increased, but the control fabrics did not increase much. The absolute values of  $\Delta a^*$  between chitosan-treated and control fabrics were getting larger when the depths of dyeing increased. At the depth of 2.27%, the chitosan-treated fabric had a higher  $b^*$  value than the untreated fabric. That meant the chitosan-treated fabric was yellower than the untreated fabric at the depth of 2.27%. At the depths of 4.55% and 9.10%, the chitosan-treated fabrics had lower  $b^*$  values than the untreated fabrics; the chitosan-treated fabrics were yellower than the untreated fabrics.  $C^*$  value of chitosan-treated fabric was larger than that of control fabric at the depth of 2.27% while  $C^*$  values of chitosan-treated fabric were smaller than those of the control fabrics at the depths of 4.55% and 9.10%.

#### **5.4.12.5 Sirius Red F3B**

CIE  $L^*a^*b^*$  data of the chitosan-treated and control fabrics dyed by Sirius Red F3B are shown in Table 5.19 and 5.20. The chitosan-treated fabric had smaller values of  $L^*$  at all three depths which meant the chitosan-treated fabrics were darker than the control fabrics.  $L^*$  values of chitosan-treated and control fabrics were getting smaller when the depths of dyeing increased due to more dyes were adsorbed onto the fabrics. The absolute values of  $\Delta L^*$  were getting larger as the depths of dyeing changed from 1.37% to 2.75% and then become stable as both of the chitosan-treated fabric and control fabric could not adsorb more dyes even the depth increase.

**Table 5.19** CIE L\*a\*b\* of the chitosan-treated and control fabrics dyed by Sirius Red F3B

Sample	L*	a*	b*	C*	h
Sirius Red F3B at 1.37%					
Chitosan-treated	39.822	48.836	21.096	53.198	23.364
Control	48.092	61.285	31.470	68.893	27.181
Sirius Brown 3RL at 2.75%					
Chitosan-treated	38.366	51.801	24.018	57.098	24.875
Control	47.410	60.715	32.654	68.939	28.273
Sirius Brown 3RL at 5.50%					
Chitosan-treated	40.697	53.152	25.230	58.836	25.393
Control	49.138	58.123	28.124	64.570	25.821

**Table 5.20** Color difference between the chitosan-treated and control fabrics dyed by Sirius Red F3B

Sample	$\Delta E$	$\Delta L^*$	$\Delta a^*$	$\Delta b^*$	$\Delta C^*$	$\Delta h$
Sirius Red F3B at 1.37%	18.193	-8.270	-12.449	-10.374	-15.695	-4.033
Sirius Red F3B at 2.75%	15.357	-9.045	-8.914	-8.636	-11.841	-3.720
Sirius Red F3B at 5.50%	10.215	-8.441	-4.972	-2.894	-5.734	-0.461

The chitosan-treated fabrics had smaller  $a^*$  values than the untreated fabrics at all the three depths. That meant the chitosan-treated fabrics were greener than the control fabrics. It was because the chitosan-treated fabrics were much darker. The chitosan-treated fabrics had lower  $b^*$  values than the untreated fabrics, that meant the chitosan-treated fabrics were more blue than the untreated fabrics.

#### 5.4.12.6 Telon Red M-BL

Tables 5.21-5.22 show the CIE L\*a\*b\* data of the chitosan-treated and control fabrics dyed by Telon Red M-BL. The values of  $\Delta L^*$  between chitosan-treated and control fabric were negative and the differences became larger as the depths increased. The  $a^*$  of chitosan-treated fabrics were smaller than that of the control fabrics which meant that



they were less red than the control fabrics at all depths of dyeing in Telon Red M-BL. Value of  $\Delta b^*$  between chitosan-treated and control fabrics was getting greater from 2% depth to 4% depth. However, it reduced from 4% depth to 8% depth. The  $b^*$  values of chitosan-treated fabric were larger than that of control fabrics which resulted to a positive  $\Delta b^*$  value. The chitosan-treated fabrics were yellower than the control fabrics at all three depths of dyeing.

**Table 5.21** CIE  $L^*a^*b^*$  of the chitosan-treated and control fabrics dyed by Telon Red M-BL

Sample	$L^*$	$a^*$	$b^*$	$C^*$	$h$
Telon Red M-BL at 2%					
Chitosan-treated	39.56	49.37	0.03	49.37	0.04
Control	42.50	52.23	-3.26	52.33	356.43
Telon Red M-BL at 4%					
Chitosan-treated	31.62	43.28	7.18	43.87	9.42
Control	36.86	53.43	2.80	53.50	3.00
Telon Red M-BL at 8%					
Chitosan-treated	28.14	38.47	9.61	39.65	14.02
Control	33.96	52.73	7.12	53.21	7.69

**Table 5.22** Color difference between the chitosan-treated and control fabrics dyed by Telon Red M-BL

Sample	$\Delta E$	$\Delta L^*$	$\Delta a^*$	$\Delta b^*$	$\Delta C^*$	$\Delta h$
Telon Red M-BL at 2%	5.26	-2.94	-2.86	3.29	-2.96	3.61
Telon Red M-BL at 4%	12.23	-5.24	-10.15	4.38	-9.63	6.42
Telon Red M-BL at 8%	15.60	-5.82	-14.26	2.49	-13.56	6.33

$C^*$  values of chitosan-treated fabrics were lower than the control fabrics at all three depths of dyeing by Telon Red M-BL. It meant that the chitosan-treated fabrics were less saturated than the control fabrics.  $\Delta h$  values, however, ranging from 3.61 to 6.33 which showed a comparatively small and uncritical difference in all depths of dyeing.

### 5.4.12.7 Telon Yellow M-4GL

**Table 5.23** CIE L\*a\*b\* of the chitosan-treated and control fabrics dyed by Telon Yellow M-4GL

Sample	L*	a*	b*	C*	h
Telon Yellow M-4GL at 2%					
Chitosan-treated	85.18	0.27	78.67	78.68	89.80
Control	86.19	-0.55	76.80	76.80	90.41
Telon Yellow M-4GL at 4%					
Chitosan-treated	81.97	5.96	89.94	90.14	86.21
Control	84.71	3.32	91.73	91.79	87.93
Telon Yellow M-4GL at 8%					
Chitosan-treated	78.40	13.83	92.14	93.17	81.46
Control	83.82	5.29	95.18	95.33	86.82

**Table 5.24** Color difference between the chitosan-treated and control fabrics dyed by Telon Yellow M-4GL

Sample	$\Delta E$	$\Delta L^*$	$\Delta a^*$	$\Delta b^*$	$\Delta C^*$	$\Delta h$
Telon Yellow M-4GL at 2%	2.28	-1.01	0.82	1.87	1.88	-0.61
Telon Yellow M-4GL at 4%	4.20	-2.74	2.64	-1.79	-1.65	-1.72
Telon Yellow M-4GL at 8%	10.56	-5.42	8.54	-3.04	-2.16	-5.36

Tables 5.23-5.24 show the CIE L\*a\*b\* of the chitosan-treated and control fabrics dyed by Telon Yellow M-4GL. The values of  $\Delta L^*$  between chitosan-treated and control fabrics were getting larger when the depths of dyeing increased at all three depths of dyeing, the chitosan-treated fabrics had greater values of  $a^*$  which meant the chitosan-treated fabrics were redder than the control fabrics at the three depths of dyeing.  $b^*$  of chitosan-treated fabric was larger than that of control fabric at 2% depth which meant that it was yellower than the control fabric. At 4% and 8% depths of dyeing, however,  $b^*$  of chitosan-treated fabrics were smaller than the control fabrics which meant that they were less yellow than the control fabrics.  $\Delta b^*$  value between chitosan-treated and control fabric

was positive at 2% depth while were negative at 4% and 8% depths. When the depth of dyeing increased from 4% to 8%, the absolute values of  $\Delta b^*$  increased.

$C^*$  values of chitosan-treated fabrics were lower than those of control fabric at 2% and 4% depths of dyeing which meant that the chitosan-treated fabrics were less saturated than the control fabrics. At 1% depth of dyeing,  $C^*$  value of chitosan-treated fabric was higher than that of control fabric which meant that it was more saturated than the control fabric.  $\Delta h$  value, however, ranging from -0.61 to -5.36 which showed a comparatively small and uncritical differences at all depths of dyeing

#### 5.4.12.8 Telon Blue M-RLW

**Table 5.25** CIE  $L^*a^*b^*$  of the chitosan-treated and control fabrics dyed by Telon Blue M-RLW

Sample	$L^*$	$a^*$	$b^*$	$C^*$	$h$
Telon Blue M-RLW at 2%					
Chitosan-treated	52.17	1.15	-43.29	43.30	271.53
Control	53.38	1.83	-44.98	45.02	272.33
Telon Blue M-RLW at 4%					
Chitosan-treated	43.76	3.05	-44.50	44.61	273.92
Control	46.47	3.39	-46.01	46.14	274.22
Telon Blue M-RLW at 8%					
Chitosan-treated	37.88	6.44	-44.62	45.08	278.22
Control	44.52	3.60	-46.07	46.21	274.47

**Table 5.26** Color difference between the chitosan-treated and control fabrics dyed by Telon Blue M-RLW

Sample	$\Delta E$	$\Delta L^*$	$\Delta a^*$	$\Delta b^*$	$\Delta C^*$	$\Delta h$
Telon Blue M-RLW at 2%	2.19	-1.21	-0.68	1.69	-1.72	-0.80
Telon Blue M-RLW at 4%	3.12	-2.71	-0.34	1.51	-1.53	-0.30
Telon Blue M-RLW at 8%	7.37	-6.64	2.84	1.45	-1.13	3.75

For the fabrics dyed by Telon Bule M-RLW, values of  $\Delta L^*$  between the chitosan-treated and control fabrics increased at all three depths which were shown in Table 5.26. Values of  $a^*$  of chitosan-treated fabrics at dyeing 2% and 4% depths were smaller than those of control fabrics which meant that they were less red than the control fabrics. However, at 8% depth,  $a^*$  of chitosan-treated fabric was larger than that of control fabric which meant that chitosan-treated fabric was redder than the control one.  $b^*$  values of chitosan-treated fabrics were negative and were greater than those of control fabrics which meant the chitosan-treated fabrics were less blue than the control fabrics.  $\Delta b^*$  values of chitosan-treated fabrics decreased as the depths increased.

$C^*$  values of chitosan-treated fabrics were smaller than those of control fabrics at all three depths of dyeing which meant that the chitosan-treated fabrics were less saturated than the control fabrics.  $\Delta C^*$  values between chitosan-treated and control fabrics were negative and they decreased as the depth of dyeing increased.  $\Delta h$  values showed a comparatively small and uncritical differences at all three depths of dyeing.

In all, all the chitosan-treated fabrics dyed by the dyes had smaller  $L^*$  value than the control fabrics at all three depths. The chitosan-treated fabrics could adsorb more dyes at the same condition. Chitosan treatment provided a good method to improve the dyeability of nylon fabrics.

#### 5.4.13 K/S measurement of dyed fabrics

The K/S values and K/S change at  $\lambda_{\max}$  of chitosan-treated and the control fabrics are shown in Figures 5.25-5.32 and Table 5.27 respectively. The K/S values indicate the actual amount of dyestuffs in the fabric samples. Clearly, all the chitosan-treated fabrics had higher uptake of dyes comparing with the control fabrics at all depths.

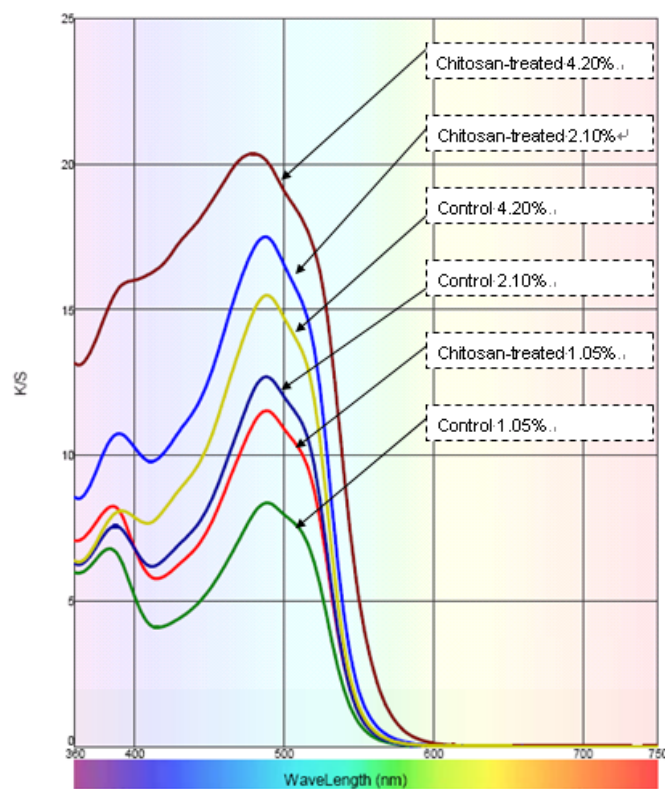


**Figure 5.25** K/S curves of fabrics dyed by Acid Orange 7

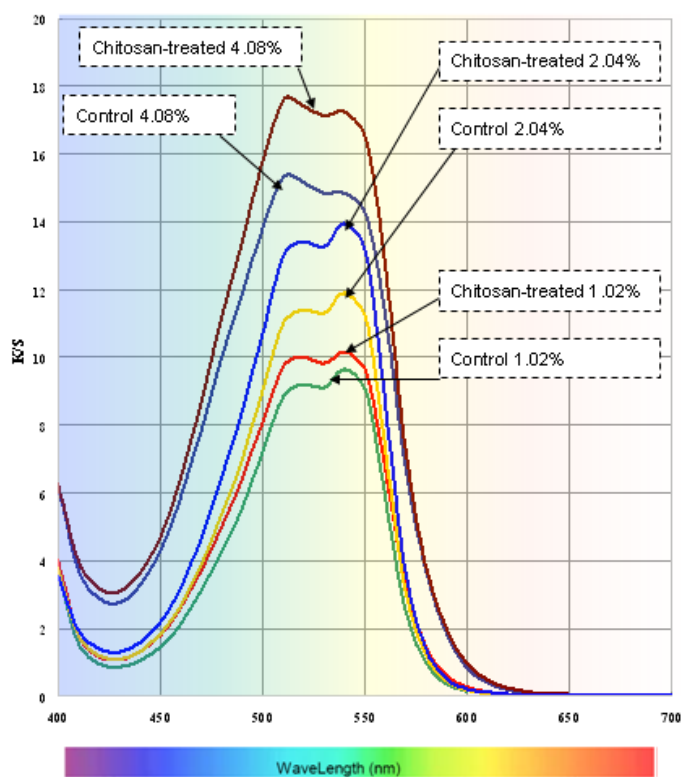


**Figure 5.26** K/S curves of fabrics dyed by Acid Red 1

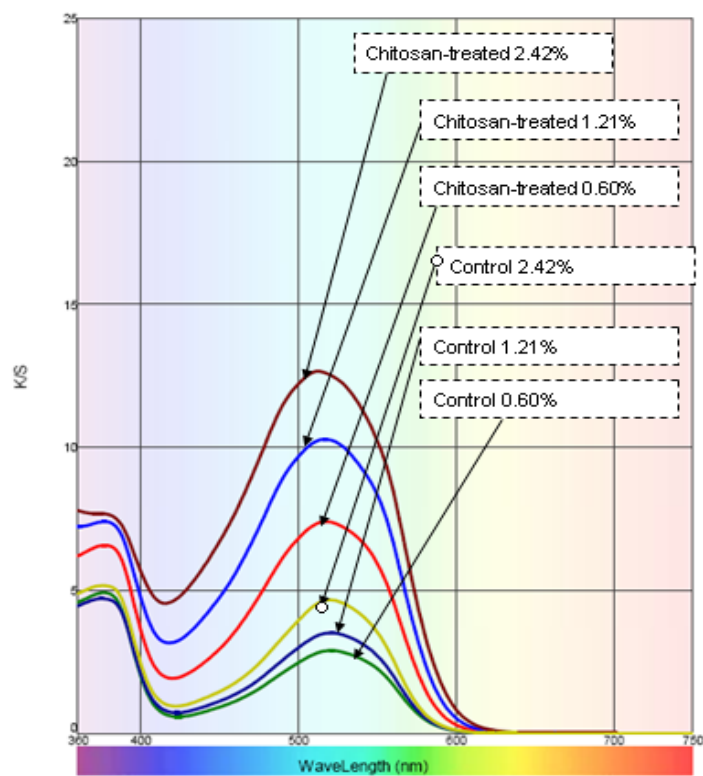


Figure 5.27 K/S curves of fabrics dyed by Acid Red 18

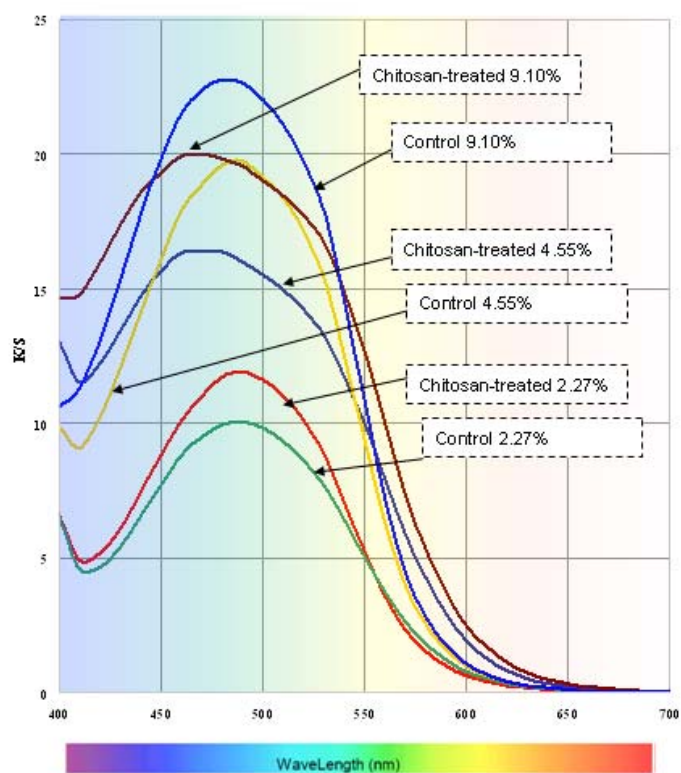
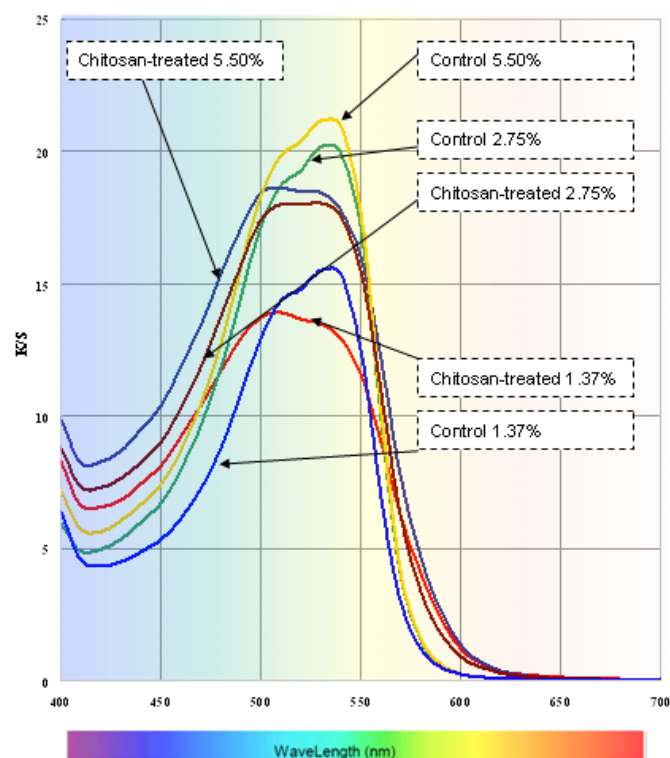
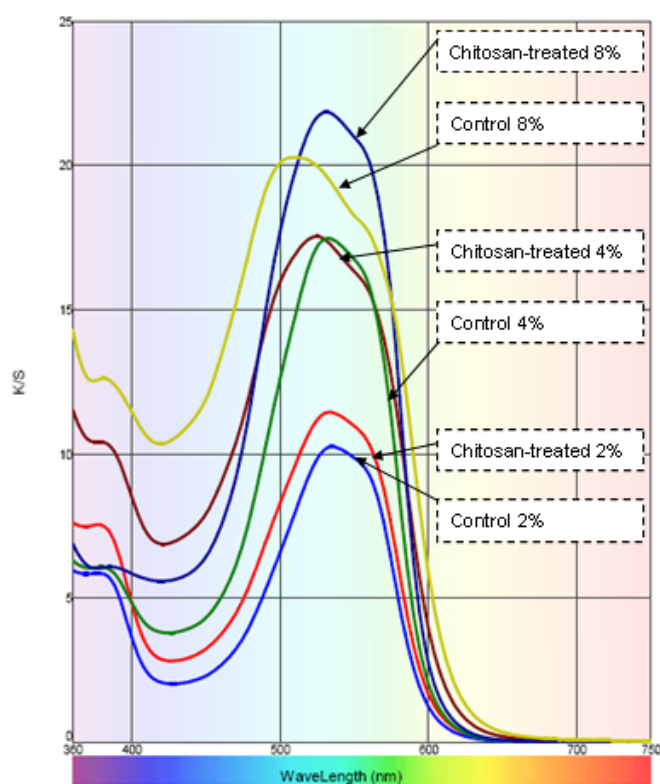


Figure 5.28 K/S curves of fabrics dyed by Sirius Brown 3RL



**Figure 5.29** K/S curves of fabrics dyed by Sirius Red F3B



**Figure 5.30** K/S curves of fabrics dyed by Telon Red M-BL

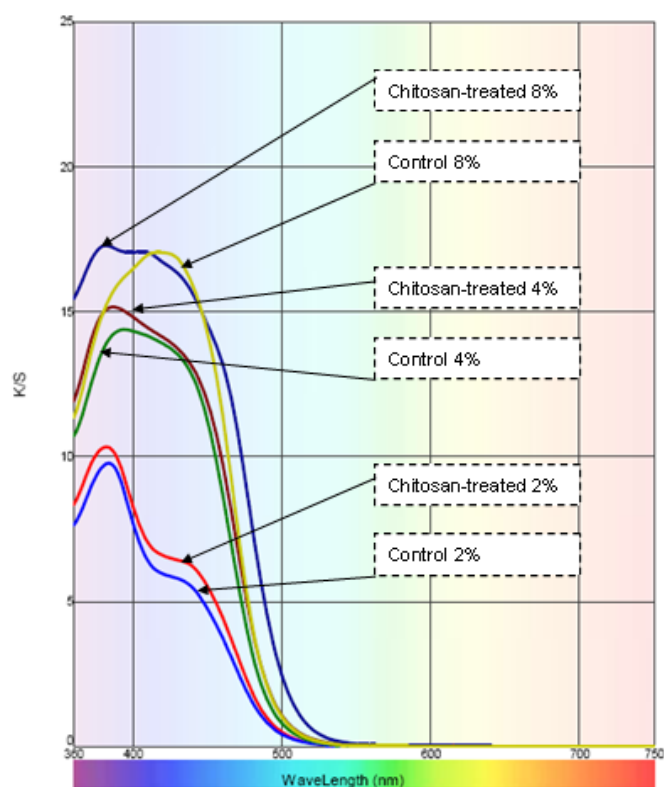


**Figure 5.31** K/S curves of fabrics dyed by Telon Yellow M-4GL

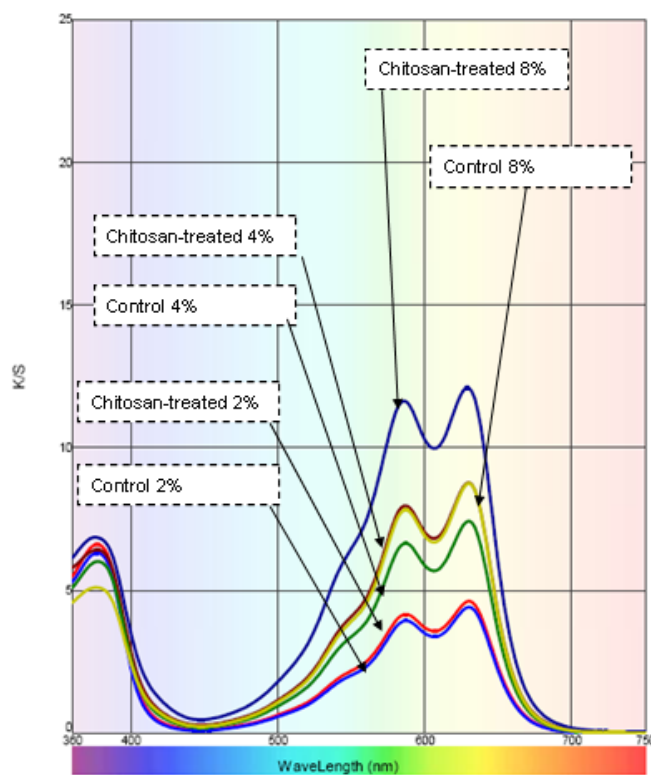


**Figure 5.32** K/S curves of fabrics dyed by Telon Blue M-RLW



**Table 5.27** K/S differences of fabrics at  $\lambda_{\max}$  at different dyeing depths

Dyes		AO7	AR 1	AR 18	SB	SR	TR	TY	TB
at $\lambda_{\max}/\text{nm}$		490	540	520	490	530	530	400	630
Depth low	Chit-treated	11.526	10.151	7.402	11.923	13.473	11.424	8.286	4.628
	Control	8.373	9.639	2.91	10.067	15.495	10.166	7.711	4.428
	Difference	37.7%	5.31%	154.4%	18.44%	-13.05%	12.4%	7.5%	4.5%
Depth middle	Chit-treated	17.464	14.851	10.271	16.001	18.025	17.450	14.814	8.784
	Control	12.683	11.904	3.531	19.722	20.18	17.457	14.326	7.439
	Difference	37.7%	24.75%	190.9%	-18.87%	-10.68%	-0.04%	3.4%	18.1%
Depth high	Chit-treated	20.003	17.242	12.543	19.563	18.427	19.707	17.045	12.094
	Control	15.49	13.942	4.681	22.615	21.16	21.852	16.472	8.755
	Difference	29.1%	23.67%	168.0%	-13.50%	-12.92%	-9.9%	3.5%	38.1%

## 5.4.14 Colorfastness

### 5.4.14.1 Colorfastness to water (ISO E05-C01:1996)

Tables 5.28-5.29 summarize the results of the colorfastness to water color (ISO E05-C01:1996) of both chitosan-treated and control fabrics. All of the ratings were within the range of 3-4 to 4-5. The results of staining on the multi-fiber fabrics of the chitosan-treated fabrics at high depths were comparatively poorer. It was because there were more dyes onto the treated fabrics at high depths. The chitosan-treated fabrics did not show much change in the colorfastness.

**Table 5.28** Colorfastness to water of fabrics dyed by Acid Orange 7, Acid Red 1, and Acid Red 18

Sample	Color Change	Staining on multi-fiber fabric					
		Wool	Polyacrylic	Polyester	nylon	Cotton	Acetate
Acid Orange 7							
1.05% chit-treated	4-5	3-4	4-5	4-5	4	4-5	4-5
1.05% control	4-5	3-4	4-5	4-5	4	4-5	4-5
2.10% chit-treated	4-5	3	4-5	4-5	3	4-5	4-5
2.10% control	4-5	3-4	4-5	4-5	3-4	4-5	4-5
4.20% chit-treated	4	3	4-5	4-5	2-3	4-5	4-5
4.20% control	4	3	4-5	4-5	2-3	4-5	4-5
Acid Red 1							
1.02% chit-treated	4	4-5	4	3-4	4-5	4-5	3-4
1.02% control	4-5	4-5	4	3-4	5	4-5	3-4
2.04% chit-treated	4-5	4-5	4	4	4-5	4	3-4
2.04% control	4-5	4	3-4	3-4	4-5	4	3-4
4.08% chit-treated	4-5	4-5	4	3-4	4	4	3
4.08% control	4-5	4	3-4	3	4	3-4	3
Acid Red 18							
0.60% chit-treated	4	4	4-5	4-5	4-5	4-5	4-5
0.60% control	4-5	4	4-5	4-5	3-4	4-5	4-5
1.21% chit-treated	3-4	3-4	4	4-5	4	4-5	4-5
1.21% control	4	4	4-5	4-5	3-4	4	4-5
2.42% chit-treated	4	3-4	4-5	4-5	3	3-4	4-5
2.42% control	4-5	4	4-5	4-5	3-4	4	4-5

**Table 5.29** Colorfastness to water of fabrics dyed by Sirius Brown 3RL, Sirius Red F3B, Telon Red M-BL, Telon Yellow M-4GL and Telon Blue M-RLW

Sample	Color Change	Staining on multi-fiber fabric					
		Wool	Polyacrylic	Polyester	nylon	Cotton	Acetate
Sirius Brown 3RL							
2.27% chit-treated	5	5	5	5	5	5	5
2.27% control	5	5	5	5	5	5	5
4.55% chit-treated	5	5	5	5	5	5	5
4.55% control	5	5	4-5	5	5	5	5
9.10% chit-treated	5	4-5	4-5	5	5	5	5
9.10% control	5	5	5	5	5	5	5
Sirius Red F3B							
1.37% chit-treated	4-5	5	5	5	5	5	4-5
1.37% control	4-5	5	4-5	5	5	5	4-5
2.75% chit-treated	4-5	5	4-5	5	5	5	4-5
2.75% control	5	5	4-5	5	5	5	4-5
5.50% chit-treated	5	5	4-5	5	5	5	4-5
5.50% control	4-5	5	4-5	5	5	5	4-5
Telon Red M-BL							
2% chit-treated	5	5	5	5	4	5	4-5
2% control	5	5	4-5	5	4	5	4-5
4% chit-treated	5	5	4-5	5	4-5	5	4-5
4% control	4-5	5	4-5	5	4	5	4-5
8% chit-treated	5	5	4-5	5	4-5	5	4-5
8% control	5	5	4-5	5	4	5	4-5
Telon Yellow M-4G							
2% chit-treated	4	4-5	5	5	4-5	5	4-5
2% control	4-5	5	5	5	4-5	4-5	4-5
4% chit-treated	4-5	4-5	5	5	4	5	4-5
4% control	5	4-5	5	5	4-5	5	4-5

**Table 5.29** Continued

Sample	Color Change	Staining on multi-fiber fabric					
		Wool	Polyacrylic	Polyester	nylon	Cotton	Acetate
Telon Yellow M-4G							
8% chit-treated	5	5	5	5	3-4	5	4-5
8% control	5	5	5	5	3-4	5	4-5
Telon Blue M-RLW							
2% chit-treated	4-5	4-5	5	5	4	5	4-5
2% control	4-5	5	4-5	5	4	5	5
4% chit-treated	5	4-5	5	5	4	5	5
4% control	5	5	5	5	4-5	5	5
8% chit-treated	5	4-5	5	4-5	3-4	5	5
8% control	4-5	4-5	4-5	4-5	3-4	5	4-5

#### 5.4.14.2 Colorfastness to washing

Tables 5.30-5.31 summarize the results of colorfastness to washing (ISO 105-C01:1989).

The color change of the fabrics was generally high. For the dyes including Acid Orange 7, Acid Red 1 and Acid Red 18, the color change was too high to be used in the commercial. But for all the other five commercial dyes, the color change which is between 3-4 and 5.

The ratings of color change at 2% depth of Telon Yellow M-4GL and Telon Blue M-RLW were around 3-4 to 4-5. However, at 4% and 8% depths, the color changes of the chitosan-treated and the control fabrics in Telon Yellow M-4GL and Telon Blue M-RLW increased. Color changes of both chitosan-treated and control fabrics in Telon Red M-BL, however, kept consistent at various depths.

In most cases, the color changes in the chitosan-treated specimens were larger than those in control specimens. It was because of the darker shade in chitosan-treated fabrics

comparing with the control fabrics. The darker of the fabric was, the more dye molecules might migrate out from the fabric during washing. Thus, the color change in chitosan-treated fabric was larger than control fabric.

**Table 5.30** Colorfastness to washing of fabrics dyed by Acid Orange 7, Acid Red 1, and Acid Red 18

Sample	Color Change	Staining on multi-fiber fabric					
		Wool	Polyacrylic	Polyester	nylon	Cotton	Acetate
Acid Orange 7							
1.05% chit-treated	3-4	5	5	5	5	5	4
1.05% control	3-4	5	5	5	5	5	5
2.10% chit-treated	2-3	5	5	5	5	5	5
2.10% control	2-3	4-5	5	5	4-5	5	5
4.20% chit-treated	2	4-5	5	5	4-5	5	5
4.20% control	1-2	5	5	5	4-5	5	5
Acid Red 1							
1.02% chit-treated	3	5	5	5	5	4-5	4-5
Acid Red 1							
1.02% control	2-3	5	5	5	5	4-5	5
2.04% chit-treated	2-3	5	5	5	5	5	5
2.04% control	2-3	5	5	5	5	5	5
4.08% chit-treated	1-2	4-5	5	5	5	5	5
4.08% control	2	5	5	5	5	5	5
Acid Red 18							
0.60% chit-treated	3	4	4-5	4-5	4-5	4-5	4-5
0.60% control	3	4	4-5	4-5	3-4	4-5	4-5
1.21% chit-treated	2-3	3-4	4	4-5	4	4-5	4-5
1.21% control	2-3	4	4-5	4-5	3-4	4	4-5
2.42% chit-treated	2	3	3-4	4-5	3	3-4	4-5
2.42% control	2	4	4-5	4-5	3-4	4	4-5

**Table 5.31** Colorfastness to washing of fabrics dyed by Sirius Brown 3RL, Sirius Red F3B, Telon Red M-BL, Telon Yellow M-4GL and Telon Blue M-RLW

Sample	Color Change	Staining on multi-fiber fabric					
		Wool	Polyacrylic	Polyester	nylon	Cotton	Acetate
Sirius Brown 3RL							
2.27% chit-treated	4-5	5	4	5	5	4-5	5
2.27% control	5	5	44-5	5	5	5	5
4.55% chit-treated	4	5	4	4-5	4-5	4-5	4-5
4.55% control	4	5	4-5	4-5	4-5	5	3-4
9.10% chit-treated	4-5	4-5	4	4-5	4-5	5	4
9.10% control	4-5	5	4-	4-5	4-5	5	4
Sirius Red F3B							
1.37% chit-treated	4-5	5	5	5	5	5	4-5
Sirius Red F3B							
1.37% control	4-5	5	4-5	5	5	5	4-5
2.75% chit-treated	4-5	5	4-5	5	5	5	4-5
2.75% control	5	5	4-5	5	5	5	4-5
5.50% chit-treated	5	5	4-5	5	5	5	4-5
5.50% control	4-5	5	4-5	5	5	5	4-5
Telon Red M-BL							
2% chit-treated	3-4	4-5	4	4	3-4	4-5	4-5
2% control	4	4-5	4-5	4-5	4	4-5	4-5
4% chit-treated	3-4	3-4	4	3-4	3	4	4
4% control	4	4-5	4-5	4-5	4	4-5	4-5
8% chit-treated	3-4	3-4	3	2-3	2-3	4	4
8% control	4	4	4	3-4	3-4	4-5	4-5
Telon Yellow M-4G							
2% chit-treated	4	4	4	4-5	4	4-5	4-5
2% control	4-5	4	4	4-5	4	4-5	4-5

**Table 5.31** Continued

Sample	Color Change	Staining on multi-fiber fabric					
		Wool	Polyacrylic	Polyester	nylon	Cotton	Acetate
Telon Yellow M-4G							
4% chit-treated	3-4	4	4	4-5	4	4-5	4-5
4% control	3	4	4	4-5	4	4-5	4-5
8% chit-treated	3-4	4	4	4-5	4	4-5	4-5
8% control	3-4	4	4	4-5	4	4-5	4-5
Telon Blue M-RLW							
2% chit-treated	4	4	4-5	4-5	4	4-5	4-5
2% control	4-5	4	4-5	4-5	4	4-5	4-5
4% chit-treated	3	4	4-5	4-5	4	4-5	4-5
4% control	3-4	4	4-5	4-5	4	4-5	4-5
8% chit-treated	3	4	4-5	4-5	4	4-5	4-5
8% control	3	4	4-5	4-5	4	4-5	4-5

## 5.5 Conclusions

Nanochitosan emulsion was prepared by the procedures as described in Section 5.3.2.1 and applied onto nylon fabrics through a pad-dry-cure method. The nanochitosan-treated and control fabrics were then dyed with eight dyes to study the enhancement of dyeability of nylon fabrics.

The rate of dyeing for the chitosan-treated fabrics was generally high and the equilibrium and final exhaustion were enhanced in chitosan-treated fabric due to the increase in the number of protonated amino group dyesites (i.e. higher saturation point). When the saturation point in control fabric was reached, the additional protonated amino groups in chitosan-treated fabric still could adsorb more dye molecules. Thus, the equilibrium and final exhaustion of chitosan-treated fabric were higher than those of the control fabric. The differences in equilibrium exhaustion at the high depth were 40.1% for Acid Orange

7, 24% for Acid Red 1, 42.5% for Acid red 18, 27.1% for Sirius Brown 3RL, 46.0% for Sirius Red F3B, 41.9% for Telon Red M-BL, 13.5% for Telon Yellow M-4GL, 46% for Telon Blue M-RLW.

The chitosan-treated fabrics not only exhausted more dye molecules than the control fabrics (higher %E), but also took a shorter period of time to achieve half dyeing (smaller  $T_{1/2}$ ). Thus, green dyeing was achieved by enhancing the exhaustion and reducing the energy needed for the dyeing process.

Color evaluations of dyed fabrics were carried out by subjective visual assessment under  $D_{65}$  and objective measurement using a VIS spectrophotometer. The CIE  $L^*a^*b^*$  data showed the chitosan-treated fabrics all had a lower  $L^*$  value than the control fabrics which meant that the former were darker than the latter. For the K/S value, the chitosan-treated fabrics had a higher K/S (i.e. more dye adsorption). The data of CIE  $L^*a^*b^*$  and K/S all showed that the dyeability of nylon fabrics was enhanced due to the additional amino groups from chitosan.

The data of colorfastness to water (ISO 105 E01:1994) and colorfastness to washing (ISO 103 C01: 1989) showed that the chitosan treatment did not greatly affect the fastness properties of the fabrics.



## **Chapter 6 Conclusions and Suggestions for Future Research**

The study mainly focused on the preparation and applications of nanochitosan. A novel dissolving-precipitating-ultrasound method has been developed for the preparation of the nanochitosan emulsion by using the ultrasound treatment. The nanochitosan was characterized by laser scanning, X-ray, FT-IR, NMR, elementary analysis, SEM, TEM, AFM and some other methods.

The prepared nanochitosan emulsion was used for dye sorption and dyeability enhancement of nylon. The capacities of nanochitosan as an adsorbent for the removal of 5 anionic dyes from aqueous solutions were studied. Similar experiments were done with microchitosan. It was found that the nanochitosan had higher sorption capacities than those of the microchitosan, especially for the dyes with large molecular sizes. The sorption kinetics of dyes onto nanochitosan and microchitosan fits the pseudo-second-order model. The Langmuir equilibrium isotherms were suitable to analyze the equilibrium data.

The nanochitosan-treated and control fabrics were dyed with eight dyes to study the enhancement of dyeability of nylon fabrics by the nanochitosan emulsion treating. The rate of dyeing for chitosan-treated fabric was enhanced and the depths of dyeing were higher. Thus, green dyeing was achieved by enhancing the exhaustion and reducing the energy needed for the dyeing process.

This project provided a simple and fast method for the preparation of nanochitosan and studied its applications. The study extended the knowledge area on chitosan nanoparticle preparation and applications. The conclusion and future work are summarized.

## **6.1 Preparation and characterization of nanochitosan emulsions**

### **6.1.1 Conclusions**

In this part, a new dissolving-precipitating-ultrasound method has been developed for the preparation of nanochitosan emulsions by using the ultrasound treatment. The optimal conditions for preparing nanochitosan emulsions with uniform nanochitosan particles were investigated by using the factorial experiment design.

The emulsions had a good stability with a zeta potential ranging from 25-40 mV because of the hydrogen bond between the amino groups and hydroxyl groups of water and chitosan molecules. Laser scanning, SEM, TEM and AFM analyses were performed to obtain the particle size and images of the particles. The particle size and molecule weight decreased with the ultrasonic duration. The DD of chitosan had no significant change after the ultrasound treatment. The crystallinity of chitosan nanoparticles was investigated using XRD. The crystallinity slightly increased with the ultrasound duration.

The methods for preparing the chitosan nanoparticles by using the ultrasound treatment did not require additional chemicals in the process. It was easy to determine the particle size in the emulsions and the emulsions were stable. By using the ultrasound treatment, we could obtain nanochitosan emulsions without additional chemicals; thus the non-toxic emulsions could find further uses in medicines and textiles.

### **6.1.2 Future research**

The mechanism of sonolysis has not been studied in my work. To explore how the nanoparticles are formed by using the ultrasonic irradiation will provide better understanding of the nanoparticle preparation and be useful in large-scale production.

## 6.2 Application of nanochitosan emulsion on dye sorption

### 6.2.1 Conclusions

In this part, the nanochitosan emulsion with particle sizes of 300 nm-400 nm was prepared by using the sonolysis method. The capacities of nanochitosan as an adsorbent for the removal of 5 anionic dyes including Acid Orange 7, Acid Red 1, Acid Red 18, Direct Red 80 and Direct Red 84 in aqueous solutions was studied. Similar experiments were done with microchitosan (180  $\mu\text{m}$ -250  $\mu\text{m}$ ). It was found that the nanochitosan had higher capacities than those of the microchitosan, especially for dyes with large molecular sizes. And the sorption is more efficient for the nanochitosan demonstrated by much shorter equilibrium time comparing with the microchitosan.

Sorption capacities of dyes onto nanochitosan and microchitosan at different temperatures were investigated. The sorption kinetics of dyes onto nanochitosan and microchitosan fit the pseudo-second-order model and the Langmuir equilibrium isotherm model were successfully used to analyze the equilibrium data. The sorption capacities of nanochitosan were 4.591 mmol/g for Acid Orange 7, 2.325 mmol/g for Acid Red 1, 1.338 mmol/g for Acid Red 18, 2.900 mmol/g for Direct Red 84, and 1.358 mmol/g for Direct Red 80 at 30 °C . The results demonstrated that comparing with the sorption capacity of microchitosan, the sorption capacity of nanochitosan increased as much as 8 times for the dyes with large molecular sizes.

The  $\Delta H$  of the sorption was obtained from the van't Hoff equation. The negative value of  $\Delta H$  suggested that the adsorption phenomenon was an exothermic reaction. The sorption studies provide both theoretical and practical values to the research area and also support the dyeing studies.

### 6.2.2 Future research

- a) To explore the affinity between dyes and chitosan thoroughly especially the affinity between direct dyes and nanochitosan which was different from that between the acid dyes and small molecular sizes;
- b) To study the sorption of other dyes onto nanochitosan besides acid dyes such as basic dyes in neutral condition or alkaline condition.

## 6.3 Application of nanochitosan emulsion on dyeing: dyeability enhancement of nylon using nanochitosan emulsion

### 6.3.1 Conclusions

In the study, the nanochitosan emulsion was applied onto nylon fabrics using a pad-dry-cure method. The nanochitosan-treated and control fabrics were dyed with eight dyes to study the enhancement of dyeability.

The rate of dyeing for the chitosan-treated fabric was increased and the dyeability of the nylon fabric was improved. The equilibrium and final exhaustion were enhanced in the chitosan-treated fabrics due to the increase of the protonated amino group dyesites (i.e. higher saturation point). The differences in equilibrium exhaustion at the high depths were 40.1% for Acid Orange 7, 24% for Acid Red 1, 42.5% for Acid red 18, 27.1% for Sirius Brown 3RL, 46.0% for Sirius Red F3B, 41.9% for Telon Red M-BL, 13.5% for Telon Yellow M-4GL, and 46% for Telon Blue M-RLW.

The chitosan-treated fabrics not only exhausted more dye molecules than the control fabrics (higher %E), but also achieved half dyeing in a shorter time (smaller  $T_{1/2}$ ). Thus,

green dyeing was achieved by enhancing the exhaustion and reducing the energy needed for the dyeing process.

Color evaluations of dyed fabrics were carried out by both the subjective visual assessment under  $D_{65}$  and objective measurement using a VIS spectrophotometer. The CIE  $L^*a^*b^*$  data showed the chitosan-treated fabrics all had darker color than the control fabrics. The data of CIE  $L^*a^*b^*$  and K/S all showed that the dyeability of nylon fabrics was enhanced due to the additional amino groups from chitosan. The data of colorfastness to water (ISO 105 E01:1994) and colorfastness to washing (ISO 103 C01: 1989) showed that the chitosan treatment did not greatly affect the fastness properties of the fabrics.

### **6.3.2 Future research**

- a) As the nanochitosan emulsion has been applied on nylon fabrics and showed improvements of dyeability, the detailed procedures and conditions including levelling agents, pH values, temperature and other conditions which could provide better dyeing results should be investigated.
- b) The nanochitosan could be applied on other fibers for dyeability improvements.

## References

- [1] Roberts, G. A. F. *Chitin Chemistry*; Macmillan Press Ltd.: London, 1992; p 1.
- [2] Kasaai, M. R. *Carbohydr. Polym.*, 2010, 79, 801-810.
- [3] Hudson, S. M.; Smith, C. Polysaccharide: chitin and chitosan: Chemistry and technology of their use as structural materials. In *Biopolymers from Renewable Resources*; Kaplan, D. L. editor.; Springer-Verlag: New York, 1998; pp 96-118.
- [4] Lim, S. H.; Hudson, S. M. *J. Macromol. Sci., Part C- Polymer Reviews*, 2003, 43, 223-269.
- [5] Majeti, N. V.; Kumar, Ravi. *Reactive & Functional Polymers*, 2000, 46, 1-27.
- [6] Marguerite, R. *Prog. Polym. Sci.*, 2006, 31, 603-632.
- [7] Cartier, N.; Domard, A.; Chanzy, H. *Int. J. Biol. Macromol.*, 1990, 12, 289-294.
- [8] Ogawa, K. *Agric. Biol. Chem*, 1991, 55, 2375-2379.
- [9] Ogawa, K.; Yui, T.; Miya, M. *Biosci. Biotech. Biochem.*, 1992, 56, 858-862.
- [10] Muzzarelli, R. A. A. *Natural Chelating Polymers*, Pergamon Press: New York, 1973; p 83.
- [11] Zikakis, J. P. *Chitin, Chitosan and Related Enzymes*; Academic Press: Orlando, 1984; p 17.
- [12] Wu, F. C.; Tseng, R. L.; Juang R. S. *Journal of Environmental Management*, 2010, 91, 798-806.
- [13] Guibal, E.; Vooren, M. V.; Dempsey, B. A.; Roussy, Jean. *Sep. Sci. Technol.*, 2006, 41, 2487-2514.
- [14] Simoncic, B.; Tomsic, B. *Textile Research Journal*, 2010, 80, 1721-1737.
- [15] Jayakumara, R.; Menona, Deepthy; Manzoora, K.; Naira, S.V.; Tamurab, H. *Carbohydr. Polym.*, 2010, 82, 227-232.
- [16] Rai, M.; Yadav, A.; Gade, A. *Biotechnology Advances*, 2009, 27, 76-83.

- [17] Madhumathi, K.; Kumar, P. T. S.; Abilash, S.; Sreeja, V.; Tamura, H.; Manzoor, K. *J. Mater. Sci.: Materials in Medicine*, 2010, 21, 807-813.
- [18] Kumar, P. T. S.; Abilash, S.; Manzoor, K.; Nair, S. V.; Tamura, H.; Jayakumar, R. *Carbohydr. Polym.*, 2010, 80, 761-767.
- [19] Pillai C. K. S.; Willi P.; Sharma, C. P. *Prog. Polym. Sci.*, 2009, 34, 641-678.
- [20] Hay, E. D. *Cell biology of extracellular matrix*; Plenum Press: NY, 1991.
- [21] Xia, W.; Chang, J. *Materials Letters*, 2007, 61, 3251-3253.
- [22] Lee, Y. M.; Kim, S. S.; Kim, S. H. *J. Mater. Sci.*, 1997, 8, 537.
- [23] Lee, E. J.; Shin, D. S.; Kim, H. E.; Kim, H. W.; Koh, Y. H.; Jang, J. H. *Biomaterials*, 2009, 30, 743-750.
- [24] Jayakumar, R.; Prabakaran, M.; Nair, S. V.; Tokura, S.; Tamura, H.; Selvamurugan, N. *Progress in Materials Science*, 2010, 55, 675-709.
- [25] Dev, A.; Binulal, N. S.; Anitha, A.; Nair, S. V.; Furuike, T.; Tamura, H. *Carbohydr. Polym.*, 2010, 80, 833-838.
- [26] Dev, A.; Mohan, J. C.; Sreeja, V.; Tamura, H.; Patzke, G. R.; Hussain, F. *Carbohydr. Polym.*, 2009, 79, 1073-1079.
- [27] Manzoor, K.; Johny, S.; Deepa, T.; Sonali, S.; Menon, D.; Nair, S. V. *Nanotechnology*, 2009, 20, 13.
- [28] Manjusha, E. M.; Mohan, J. C.; Manzoor, K.; Nair, S. V.; Tamura, H.; Jayakumar, R. *Carbohydr. Polym.*, 2010, 80, 414-420.
- [29] Higuchi, Y.; Oka, M.; Kawakami, S.; Hashida, M. *J. Controlled Release*, 2008, 125, 131-136.
- [30] McKay, G.; Blair, H.S.; Gardner, J. R. *J. Appl. Polym. Sci.*, 1989, 3043.

- [31] Crini,G.; Badot, P. M. *Prog. Polym. Sci.*, 2008, 33, 399-447.
- [32] Crini, G.; Martel, B.; Torri, G. *Int. J. Environ. Pollut.*, 2008, 33, 451-465.
- [33] Manyukova, I. I.; Safonov, V. V. *Fibre Chemistry*, 2009, 41, 169-173.
- [34] Houshyar, S.; Amirshahi, S. H. *Iranian Polymer Journal*, 2002, 11, 1026-1265.
- [35] Kitkulnumchai, Y.; Ajavakom, A.; Sukwattanasinitt, M. *Cellulose*, 2008, 15, 599-608.
- [36] Shin Y.; Yoo, D. I.; Jang, J. *J. Appl. Polym. Sci.*, 2001, 80, 2495-2501.
- [37] Giri Dev, V.R.; Venugopal, J.; Sudha, S.; Deepika, G.; Ramakrishna, S. *Carbohydr. Polym.*, 2009, 75, 646-650.
- [38] Jovic, D.; Vilchez, S.; Topalovic, T.; Navarro, A.; Jovancic, P.; Julià, M. R.; Erra, P. *Carbohydr. Polym.*, 2005, 60, 51-59.
- [39] Markey, M. L.; Bowman, M. L.; Bergamini M. V. W. *Chitin and Chitosan*; Elsevier Applied Science: London, 1989; p 13.
- [40] Jun, S. C.; Jung, E. Y.; Kang, D. H.; Kim, J. M.; Chang, U. J.; Suh, H. J. *Phytother. Res.*, 2010, 24, 1234-1241.
- [41] No, H.K.; Meyers, S. P.; Prinyawiwatkul, W.; Xu, Z. *J. Food Sci.*, 2007, 72, 87-100.
- [42] Mark, H. F.; Bikales, N .M.; Overberger, C.G.; Menges, G. *Encyclopedia of Polymer Science and Engineering*; Wiley: New York, 1985; p 20.
- [43] Huang, K.; Sheua, Y.; Chaoa, I. *Polymer-Plastics Technology and Engineering*, 2009, 48, 1239-1243.
- [44] Luo, Y. C. ; Zhang, B. C.; Cheng, W. H.; Wang, Q. *Carbohydr. Polym.*, 2010, 82, 942-951.
- [45] Haider, S.; Al-Masry, Waheed A.; Bukhari, Nausheen; Javid, Muhammad. *Polym.Eng. Sci.*, 2010, 50, 1887-1893.



- [46] Wang, Z. K.; Hu, Q. L. *Biomedical Materials*, 2010, 5.
- [47] Janes, K. A.; Alonso, M. J. *J. Applied Polym. Sci.*, 2003, 88, 2769.
- [48] Nagpal, K.; Singh, S. K.; Mishram, D. N. *Chemical & Pharmaceutical Bulletin*, 2010, 58, 1423-1430.
- [49] Li, C. B.; Hein, S.; Wang, K. *Mater. Sci. Technol.*, 2008, 24, 1088.
- [50] Muzzarelli, R.A.A.; *Natural Chelating Polymers*; Pergamon Press: New York, 1973; pp 83.
- [51] Kubota, N.; Eguchi, Y. *Polym. J.*, 1997, 29, 123-127.
- [52] Aiba, S. *Int. J. Biol. Macromol.*, 1991, 13, 40-44.
- [53] Rinaudo, M.; Domard, A. Solution properties of chitosan. In: *Chitin and chitosan: sources, chemistry, biochemistry, physical properties and applications*; Skjak-Braek, G.; Anthonsen, T.; Sandford, P., Eds.; Elsevier: London and New York, 1989; pp 71-86.
- [54] Rinaudo, M.; Pavlov, G.; Desbrières, J. *Polymer*, 1999, 40, 7029-7032.
- [55] Rinaudo, M.; Pavlov, G.; Desbrières, J. *Int. J. Polym. Anal. Charact.*, 1999, 5, 267-276.
- [56] Chenite, A.; Chaput, C.; Wang, D.; Combes, C.; Buschmann, M. D.; Hoemann, C. D. *Biomaterials*, 2000, 21, 2155-2161.
- [57] Chenite, A.; Buschmann, M.; Wang, D.; Chaput, C.; Kandani, N. *Carbohydr. Polym.*, 2001, 46, 39-47.
- [58] Molinaro, G.; Leroux, J. C.; Damas, J.; Adam, A. *Biomaterials*, 2002, 23, 2717-2722.
- [59] Cho, J.; Heuzey, M. C.; Beguin, A.; Carreau, P. J. *Biomacromolecules*, 2005, 6, 3267-3275.
- [60] Ma, G. P.; Yang, D. Z.; Zhou, Y. S.; Xiao, M.; Kennedy, J. F.; Nie, J. *Carbohydr. Polym.*, 2008, 74, 121-126.
- [61] Tao, Y.; Zhang, H. L.; Gao, B.; Guo, J.; Hu, Y.; Su, Z. *Journal of Nanomaterials*, 2011, 814606.

- [62] Zhang, H.; Wu, S.; Tao, Yi; Zang, L.; Su, Z. *Journal of Nanomaterials*, 2010, 898910.
- [63] Zhong, X.; Zhang Z. Huang, Q. Xi, T. *Chin. Pham. J.*, 2005, 40, 1823-1825.
- [64] Vårum, K. M.; Anthonsen, M. W.; Grasdalen, H.; Smidsrad, O. *Carbohydr. Res.*, 1991, 211, 17-23.
- [65] Signini, R.; Campana-Fitho, S. P. *Polym. Bull.*, 1999, 42, 159-166.
- [66] Lavertu, M.; Xia, Z.; Serreqi, A. N.; Berrada, M.; Rodrigues, A.; Wang, D.; Buschmann, M. D.; Gupta, A. *Journal of Pharmaceutical and Biomedical Analysis*, 2003, 32, 1149-1158.
- [67] Raymond, L.; Morin, F. G.; Marchessault, R. H. *Carbohydr. Res.*, 1993, 246, 331.
- [68] Duarte, M. L.; Ferreira, M. C.; Marvão, M. R.; Rocha, J. *Int. J. Biol. Macromol.*, 2002, 31, 1-8.
- [69] Yang, Z. Q.; Li, Q. X.; Song, B. Z. *Journal of Functional Polymers*, 2003, 16, 313.
- [70] Guinesi, L. S.; Cavaleiro, E. T. G. *Thermochim. Acta*, 2006, 444, 128-133.
- [71] Yu, G.; Morin, F. G.; Nobes, G. A. R.; Marchessault, R. H. *Macromolecules*, 1999, 32, 518-520.
- [72] Heux, L.; Brugnerotto, J.; Desbrières, J.; Versali, M. F.; Rinaudo, M. *Biomacromolecules*, 2000, 1, 746-751.
- [73] Sannan, T.; Kurita, K.; Ogura, K.; Iwakura, Y. *Polymer*, 1978, 19, 458.
- [74] Moore, G. K.; Roberts, G. A. F. *Int. J. Bio. Macromol.*, 1980, 2, 115.
- [75] Miya, M.; Iwamoto, R.; Yoshikawa, S. *Int. J. Bio. Macromol.*, 1980, 2, 323-324.
- [76] Domszy, J. G.; Roberts, G. A. F. *Macromol. Chem.*, 1985, 186, 1671-1677.
- [77] Baxter, A.; Dillon, M.; Taylor, K. D. A.; Roberts, A. F. *Int. J. Bio. Macromol.*, 1992, 14, 166-169.
- [78] Brugnerotto, J.; Lizardi, J.; Goycoolea, F. M.; Argüelles-Monal, W.; Desbrières, J.; Rinaudo, M. *Polymer*, 2001, 42, 3569.

- [79] Muzzarelli, R. A. A.; Rochetti, R. *Carbohydr. Polym.*, 1985, 5, 461-472.
- [80] Rathke, T. D.; Hudson, S. M. *Journal of Macromolecule Science Review Macromolmolecule ChemicalPhysics*, 1994, 34, 375-437.
- [81] Aiba, S. *Int.l J.Biol. Macromol.*, 1986, 8, 173.
- [82] Tan, S. C.; Khor, E.; Tan, T. K.; Wong, S. M. *Talanta*, 1998, 45, 713-719.
- [83] Curotto, E.; Aros, F. Q. *Anal. Biochem.*, 1993, 211, 240-241.
- [84] Prochazkova, S.; Vårum, K. M.; Stgaard, K. *Carbohydr. Polym.*, 1999, 38, 115-122.
- [85] Terayama, H. *J. Polym. Sci.*, 1952, 8, 243-253.
- [86] Ke, H.; Chen, Q. *Huaxue Tongbao*, 1990, 10, 44-46.
- [87] Tolaimate, A.; Desbrières, J.; Rhazi, M.; Alagui, A.; Vincendon, M.; Vottero, P. *Polymer*, 2000, 41, 2463-2469.
- [88] Raymond, L.; Morin, F. G.; Marchessault, R. H. *Carbohydr. Res.*, 1993, 246, 331.
- [89] Nanjo, F.; Katsumi, R.; Sakai, K. *Anal. Biochem.*, 1993, 164-167.
- [90] Niola, F.; Basora, N.; Chornet, E.; Vidal, P. F. *Carbohydr. Res.*, 1993, 238, 1-9.
- [91] Santos, Z. M. dos; Caroni, A. L. P. F.; Pereira, M. R.; Silva, D. R. da; Fonseca, J. L. C. *Carbohydr. Res.*, 2009, 344, 2591-2595.
- [92] Kim, S. S.; Kim, S. H.; Lee, Y. M. *J. Polym. Sci., Part B, Polym. Phys.*, 1999, 34, 2367-2374.
- [93] Vårum K. M., Anthonsen, M. W., Grasdalen, H., Smidsrød, O. *Carbohydr. Res.*, 1991, 217, 19-27.
- [94] Struszczyk, M. H.; Loth, F.; Peter, M. G. In *Advances in chitin science*; Domard, A.; Roberts, G. A. F.; Vårum K. M., Eds; Lyon: Jacques Andre, 1998; Vol. 1, pp 71-77.
- [95] Shigemasa, Y.; Matsuura, H.; Sashiwa, H.; Saimoto, H. *Int. J. Biol. Macromol.*, 1996, 18,

- 237-242.
- [96] Shigemasa, Y.; Matsuura, H.; Sashiwa, H.; Saimoto, H. In *Advances in chitin science*; Domard, A.; Jeuniaux, C.; Muzzarelli, R.; Roberts, G. A. F. Eds.; Lyon: Jacques Andre, 1996; Vol. 1, pp 204-209.
- [97] Sabnis, S.; Block, L. H. *Polym Bull*, 1997, 39, 67-71.
- [98] Rinaudo, M.; Milas, M.; Desbrières, J. In *Applications of chitin and chitosan*; Goosen, M. F. A. Eds.; Lancaster: Technomic, 1997; pp 89-102.
- [99] Roberts, G. A.; Domszy, J.G. *Int. J. Biol. Macromol.*, 1982, 4, 374-377.
- [100] Lee V. F. P. *Solution and shear properties of chitin and chitosan*; PhD dissotatation. University of Washington, (USA), 1974.
- [101] Rinaudo, M.; Milas, M.; Le, Dung P. *Int. J. Biol. Macromol.*, 1993, 15, 281-285.
- [102] Brugnerotto, J.; Desbrières, J.; Roberts, G.; Rinaudo, M. *Polymer*, 2001, 42, 9921-9927.
- [103] Berth, G.; Dautzenberg, H. *Carbohydr. Polym.*, 2002, 47, 39-51.
- [104] Tsaih, M. L.; Chen, R. H. *J. Appl. Polym. Sci.*, 1999, 71, 1905-1913.
- [105] Baytukalov, T. A.; Bogoslovskaya, O. A.; Olkhovskaya, I. P.; Glushchenko, N. N.; Ovsyannikova, M. N.; Lopatin, S. A.; Varlamov, V. P. *Biology Bulletin*, 2005, 32, 545-548.
- [106] Kumar, B. A. V.; Varadaraj, M. C.; Tharanathan, R. N. *Biomacromolecules*, 2007, 8, 566-572.
- [107] Prabakaran, M.; Mano, J. F. *Drug Delivery*, 2005, 12, 41-57.
- [108] Anitha, A.; Divya Rani, V. V.; Krishna, R.; Sreeja, V.; Selvamurugan, N.; Nair, S. V. et al. *Carbohydr. Polym.*, 2009, 78, 672-677.
- [109] Yamada, K.; Tamura, T.; Azaki, Y.; Kashiwada, A.; Hata, Y. Higashida, K. Nakamura, Y. *Journal of Polymers and the Environment*, 2009, 17, 95-102.

- [110] Li, B.; Liu, B.; Su, T.; Fang, Y.; Xie, G. L.; Wang, G. F.; Wang, Y. L.; Sun, G. C. *Plant Pathology Journal*, 2010, 26, 189-193.
- [111] Aly A. S.; Hashem, A.; Hussein, S. S. *Indian Journal of Fibre & Textile Research*, 2004, 29, 218-222.
- [112] Nagahama, H.; Nwe, N.; Jayakumar, R.; Koiwa, S.; Furuike, T.; Tamura, H. *Carbohydr. Polym.*, 2008, 73, 295-302.
- [113] Li, Q.; Yu, P.; Zhu, T. R.; Zhang, L.; Li, Q.; Luo, Y. B. *Desalination and Water Treatment*, 2010, 16, 304-312.
- [114] Jayakumar, R.; Nwe, N.; Tokura, S.; Tamura, H. *Int. J. Biol. Macrom.*, 2007, 40, 175-181.
- [115] Jayakumar, R.; Prabakaran, M.; Reis, R. L.; Mano, J. F. *Carbohydr. Polym.*, 2005, 62, 142-158.
- [116] Jayakumar, R.; Rajkumar, M.; Fretias, H.; Kumar, P. T. S.; Nair, S. V.; Furuike, T. et al. *Int. J. Biol. Macromol.*, 2009, 45, 135-139.
- [117] Maria, G. C.; Cerqueira, M. A.; Souza, B. W. S.; Carvalhoc, S.; Quintas, M. A. C.; Teixeira, J. A.; Vicente, A. A. *Carbohydr. Polym.*, 2010, 82, 153-159.
- [118] Tada, D. B.; Singh, S.; Nagesha, D.; Jost, E.; Levy, C. O.; Gultepe, E.; Cormack, R.; Makrigiorgos, G. M.; Sridhar, S.; *Pharm. Res.*, 2010, 27, 1738-1745.
- [119] Zhang, F. Y.; Zhou, Y. M.; Sun, Y. Q.; Chen, J.; Ye, X. Y.; Huang, J. Y. *Mater. Res. Bull.*, 2010, 45, 859-862.
- [120] Pillai, C. K. S.; Paul, W.; Sharma, C. P. *Prog. Polym. Sci.*, 2009, 34, 641-678.
- [121] Calvo, P.; Remunan-Lopez, C.; Vila-Jato, J. L.; Alonso, M. J. *J. Appl. Polym. Sci.*, 1997, 63, 125-132.
- [122] Chang, Tao-Chih; Wang, Jian-Wen; Hon, Min-Hsiung. *Macromolecular Bioscience*, 2004, 4,

- 416-420.
- [123] Banerjee, T.; Mitra, S.; Singh, A. K.; Sharma, R. K.; Maitra, A. *Int. J. Pharm.*, 2002, 243, 93-105.
- [124] Pan, Y.; Li, Y.; Zhao, H.; Zheng, J.; Xu, H.; Wei, G. *Int. J. Pharm.*, 2002, 249, 139-147.
- [125] Zhang, Y.; Yang, Y.; Tang, K.; Hu, X.; Zou, G. *J. Appl. Polym. Sci.*, 2008, 107, 891-897.
- [126] Csaba, N.; Garcia-Fuentes, M.; Alonso, M. J. *Expert. Opin.*, 2006, 3, 463-478.
- [127] Trapani, A.; Garcia-Fuentes, M.; Alonso, M. J. *Nanotechnology*, 2008, 19, 1-10.
- [128] Krauland, A. H.; Alonso, M. J. *Int. J. Pharm.*, 2007, 340, 134-142.
- [129] Maestrelli, F.; Garcia-Fuentes, M.; Mura, P.; Alonso, M. J. *Eur. J. Pharm. Biopharm.*, 2006, 63, 79-86.
- [130] Teijeiro-Osorio, D.; Remuñan-Lopez, C. Alonso, M. J. *Eur. J. Pharm. Biopharm.*, 2009, 71, 257-263.
- [131] Liu, H.; Gao, C. Y. *Polym. Adv. Technol.*, 2009, 20, 613-619.
- [132] Xing J. F.; Deng, L. D.; Dong, A. J. *J. Appl. Polym. Sci.* 2010, 117, 2354-2359.
- [133] Yang, H. C.; Hon, M. H. *Microchemical Journal*, 2009, 92, 87-91.
- [134] Dudhania, A. R.; Kosarajua, S. L. *Carbohydr. Polym.*, 2010, 81, 243-251.
- [135] Trapani, A.; Lopodota, A.; Franco, M.; Cioffi, N.; Ieva, E.; Garcia-Fuentes, M.; Alonso, M. J. *European Journal of Pharmaceutics and Biopharmaceutics*, 2010, 75, 26-32.
- [136] Huang, X. Du, Y. Z.; Yuan, H.; Hu, F. Q. *Carbohydr. Polym.*, 2009, 76, 368-373.
- [137] Grenha, A.; Gomes, M. E.; Rodrigues, M.; Santo, V. E.; Mano, J. F.; Neves, N. M.; Reis, R. L. *J. Biomed. Mater. Res. Part A*, 2010, 92, 1265-1274.
- [138] Avadi, M. R.; Sadeghi, A. M. M.; Mohammadpour, N.; PharmDc; Abedin, S.; Atyabi, P.; Dinarvand, F. R.; Rafiee-Tehrani, M.; *Nanomedicine: Nanotechnology, Biology, and Medicine*,

- 2010, 6, 58-63.
- [139] Yoksan, R.; Jirawutthiwongchai, J.; Arpo, K. *Colloids Surf. B: Biointerfaces*, 2010, 76, 292-297.
- [140] Yang, H. C.; Wang, W. H.; Huang, K. S.; Hon, M. H. *Carbohydr. Polym.*, 2010, 79, 176-179.
- [141] Cheng, D.; Xia, H. B.; Chan, H. S. O. *Langmuir*, 2004, 20, 9909. .
- [142] Cheng, D.; Xia, H.B.; Chan, H. S. O. *Nanotechnology*, 2006, 17, 1661-1667.
- [143] Xu, D.; Wu, K.; Zhang, Q.; Hu, H.; Xi, K. Chen, Q.; Yu, X. Chen, J.; Jia, X. *Polymer*, 2010, 51, 1926-1933.
- [144] Ye, W.; Xin, J. H.; Li, P. Lee, K. D.; Kwong, T. *J. Appl. Polym. Sci.*, 2006, 102, 1787-1793.
- [145] Fei, B.; Lu, H.; J Xin, J. H. *Polymer*, 2006, 47, 947.
- [146] Chang, Y. C.; Chang, S.W.; Chen, D. H. *React. Funct. Polym.*, 2006, 66, 335.
- [147] Zhu, A.; Yuan, L.; Liao, T. *Int. J. Pharm.*, 2008, 350, 361.
- [148] Chang, Y.C.; Chen, D. H. *J. Colloid Interface Sci.*, 2005, 283, 446.
- [149] Honda, H.; Kawabe, A.; Shinkai, M. Kobayashi, T. *Biochem. Eng. J.*, 1999, 3, 157.
- [150] Donadel, K.; Felisberto, M. D. V.; Fávere, V. T.; Rigoni, M.; Batistela, N. J.; Laranjeira, M. C. M. *Mater. Sci. Eng. C*, 2008, 28, 509.
- [151] Belessi, V.; Zboril, R.; Tucek, J.; Mashlan, M.; Tzitzios, V.; Petridis, D. *Chem. Mater.*, 2008, 20, 3298.
- [152] Alejandro Lopez-Cruz, Carola Barrera, Victoria L. Calero-DdelC and Carlos Rinaldi, *J. Mater. Chem.*, 2009, 19, 6870–6876.
- [153] Kavaz, D.; Odabas, S.; Güven, E.; Demirbilek, M.; Baki, E. *Journal of Bioactive and Compatible Polymers*, 2010, 25, 305-318.
- [154] Chen, L.; Subirade, M. *Biomaterials*, 2005, 26, 6041.

- [155] Lin, C. L.; Chiu, W. Y.; Lee, C. F. *Journal of Colloid Interface Sci.*, 2005, 290, 397.
- [156] Bang, J. H.; Suslick, K. S. *Adv. Mater.*, 2010, 22, 1039-1059.
- [157] Weissler, A. *J. Am. Chem. Soc.*, 1959, 81, 1077-1081.
- [158] Weissler, A. *Nature*, 1962, 193, 1070.
- [159] Anbar, M.; Pecht, I. *J. Phys. Chem.*, 1964, 68, 352-355.
- [160] Makino, K.; Mossoba, M. M.; Riesz, P. *J. Am. Chem. Soc.*, 1982, 104, 3537-3539.
- [161] Zhang, J.; Du, J.; Han, B.; Liu, Z.; Jiang, T.; Zhang, Z. *Angew. Chem. Int. Ed.*, 2006, 45, 1116-1119.
- [162] Dhas, N. A.; Raj, C. P.; Gedanken, A. *Chem. Mater.*, 1998, 10, 1446-1452.
- [163] Mizukoshi, Y.; Oshima, R.; Maeda, Y.; Nagata, Y. *Langmuir*, 1999, 15, 2733-2737.
- [164] Caruso, R. Ashokkumar, A. M. Grieser, F. *Langmuir*, 2002, 18, 7831-7836.
- [165] Su, C. H. Wu, P. L. Yeh, C. S. *J. Phys. Chem. B* 2003, 107, 14240-14243.
- [166] Nemamcha, A.; Rehspringer, J. L.; Khatmi, D. *J. Phys. Chem. B*, 2006, 110, 383-387.
- [167] Okitsu, K.; Ashokkumar, M.; Grieser, F. *J. Phys. Chem. B*, 2005, 109, 20673-20675.
- [168] Vinodgopal, K.; He, Y.; Ashokkumar, M.; Grieser, F. *J. Phys. Chem. B*, 2006, 110, 3849-3852.
- [169] Brothie, A.; Grieser, F.; Ashokkumar, M. *J. Phys. Chem. C*, 2008, 112, 10247-10250.
- [170] Anandan, S.; Grieser, F.; Ashokkumar, M. *J. Phys. Chem. C*, 2008, 112, 15102-15105.
- [171] Sánchez-Iglesias, A.; Pastoriza-Santos, I.; Pérez-Juste, J.; Rodríguez-González, B.; García de Abajo, F. J.; Liz-Marzán, L. M. *Adv. Mater.*, 2006, 18, 2529-2534.
- [172] Pastoriza-Santos, I.; Sánchez-Iglesias, A. F.; García de Abajo, J.; Liz-Marzán, L. M. *Adv. Funct. Mater.*, 2007, 17, 1443-1450.
- [173] Yu, J. C.; Yu, J.; Ho, W.; Zhang, L.; *Chem. Commun.*, 2001, 1942-1943



- [174] Qian, D.; Jiang, J. Z.; Hansen, P. L. *Chem. Commun.*, 2003, 1078-1079.
- [175] Jung, S. H.; Oh, E.; Lee, K. H.; Yang, Y.; Park, C. G.; Park, W.; Jeong, S. H. *Cryst. Growth Des.*, 2008, 8, 265-269.
- [176] Xiong, H. M.; Shchukin, D. G.; Möhwald, H.; Xu, Y.; Xia, Y. Y. *Angew. Chem. Int. Ed.*, 2009, 48, 2727-2731.
- [177] Zhang, D.; Fu, H.; Shi, L.; Pan, C.; Li, Q.; Chu, Y.; Yu, W. *Inorg. Chem.*, 2007, 46, 2446-2451.
- [178] Krishnan, C. V. C.; Chen, J. L.; Burger, C.; Chu, B. *J. Phys. Chem. B*, 2006, 110, 20182-20188.
- [179] Mao, C. J.; Pan, H. C.; Wu, X. C.; Zhu, J. J.; Chen, H. Y. *J. Phys. Chem. B*, 2006, 110, 14709-14713.
- [180] Dutta, D. P.; Sudarsan, V.; Srinivasu, P.; Vinu, A.; Tyagi, A. K. *J. Phys. Chem. C*, 2008, 112, 6781-6785.
- [181] Sivakumar, M.; Takami, T.; Ikuta, H.; Towata, A.; Yasui, K.; Tuziuti, T.; Kozuka, T.; Bhattacharya, D.; Iida, Y. *J. Phys. Chem. B*, 2006, 110, 15234-15243.
- [182] Geng, J.; Zhu, J. J.; Chen, H. Y. *Cryst. Growth Des.*, 2006, 6, 321-326.
- [183] Geng, J. Z.; Zhu, J. J.; Lu, D. J.; Chen, H. Y. *Inorg. Chem.*, 2006, 45, 8403-8407.
- [184] Geng, J.; Hou, W. H.; Lu, Y. N.; Zhu, J. J.; Chen, H. Y. *Inorg. Chem.*, 2005, 44, 8503-8509.
- [185] Dutta, D. P.; Ghildiyal, R.; Tyagi, A. K.; *J. Phys. Chem. C*, 2009, 113, 16954-16961.
- [186] Jung, S. H.; Oh, E.; Lee, K. H.; Park, W.; Jeong, S. H. *Adv. Mater.*, 2007, 19, 749-753.
- [187] Sun, X. H.; Li, C. P.; Wong, N. B.; Lee, C. S.; Lee, S. T.; Teo, B. K. *J. Am. Chem. Soc.*, 2002, 124, 14856-14857.
- [188] Li, C. P.; Teo, B. K.; Sun, X. H.; Wong, N. B.; Lee, S. T. *Chem. Mater.*, 2005, 17, 5780-5788.
- [189] Jeong, S. H.; Ko, J. H.; Park, J. B.; Park, W. *J. Am. Chem. Soc.*, 2004, 126, 15982-15983.

- [190] Viculis, L. M.; Mack, J. J.; Kaner, R. B. *Science*, 2003, 299, 1361.
- [191] Suslick, S.; Price, G. J.; *Annu. Rev. Mater. Sci.* 1999, 29, 295-326.
- [192] Suslick, K. S.; Grinstaff, M. W. *J. Am. Chem. Soc.*, 1990, 112, 7807-7809.
- [193] Grinstaff, M. W.; Suslick, K. S.; *Proc. Natl. Acad. Sci. U. S. A.*, 1991, 88, 7708-7710.
- [194] Liu, K. J.; Grinstaff, M. W.; Jiang, J.; Suslick, K. S.; Swartz, H. M.; Wang, W. *Biophys. J.*, 1994, 67, 896-901.
- [195] Suslick, K. S.; Grinstaff, M. W.; Kolbeck, K. J.; Wong, M. *Ultrason. Sonochem.*, 1994, 1, S65-S68.
- [196] Webb, A. G.; Wong, M.; Kolbeck, K. J.; Magin, R. L.; Wilmes, L. J.; Suslick, K. S.; *J. Magn. Reson. Imaging*, 1996, 6, 675-683.
- [197] Eckburg, J. J.; Chato, J. C.; Liu, K. J.; Grinstaff, M. W.; Swartz, H. M.; Suslick, K. S.; Auteri, F. *P. J. Biomech. Eng.*, 1996, 118, 193-200.
- [198] Toublan, F. J. J.; Boppart, S. K.; Suslick, S. *J. Am. Chem. Soc.*, 2006, 128, 3472-3473.
- [199] 134E. M. Dibbern, F. J.-J. Toublan, K. S. Suslick, *J. Am. Chem. Soc.* 2006, 128, 6540.
- [200] Biggs, S.; Grieser, F. *Macromolecules*, 1995, 28, 4877-4882.
- [201] Bradley, M.; Ashokkumar, M.; Grieser, F. *J. Am. Chem. Soc.*, 2003, 125, 525-529.
- [202] Kim, H. K.; Matyjaszewski, K. *J. Am. Chem. Soc.*, 1988, 110, 3321-3323.
- [203] Lenggoro, I. W.; Itoh, Y.; Okuyama, K.; Kim, T. O. *J. Mater. Res.*, 2004, 19, 3534-3539.
- [204] Xia, B.; Lenggoro, W.; Okuyama, K. *Adv. Mater.*, 2001, 13, 1579-1582.
- [205] Xia, B.; Lenggoro, I. W.; Okuyama, K. *J. Mater. Chem.*, 2001, 11, 2925-2927.
- [206] Itoh, Y.; Lenggoro, I. W.; Okuyama, K.; Mdler, L.; Pratsinis, S. E.; *Nanopart. J. Nanopart. Res.*, 2003, 5, 191-198.

- [207] Panatarani, C.; Lenggoro, I. W. Okuyama, K. *J. Nanopart. Res.*, 2003, 5, 47-53.
- [208] Itoh, Y.; Abdullah, M.; Okuyama, K.; *J. Mater. Res.*, 2004, 19, 1077-1086.
- [209] Kim, S. H.; Liu, B. Y. H.; Zachariah, M. R. *Langmuir*, 2004, 20, 2523-2526.
- [210] Jiang, X.; Brinker, C. J. *J. Am. Chem. Soc.*, 2006, 128, 4512-4513.
- [211] Zheng, T. H.; Pang, J. B.; Tan, G. He, J. B.; McPherson, G. L.; Lu, Y. F.; John, V. T.; Zhan, J. J. *Langmuir*, 2007, 23, 5143-5147.
- [212] Iskandar F., Mikrajuddin, A.; Okuyama, K. *Nano Lett.*, 2001, 1, 231-234.
- [213] Iskandar, F.; Mikrajuddin, A.; Okuyama, K. *Nano Lett.*, 2002, 2, 389-392.
- [214] Fan, H. Y.; Van Swol, F.; Lu, Y.F.; Brinker, C. J. *J. Non-Crystalline Solids*, 2001, 285, 71-78.
- [215] Suh, W. H.; Suslick, K. S. *J. Am. Chem. Soc.*, 2005, 127, 12007-12010.
- [216] Huang, H. Y.; Shieh, Y. T.; Shih, C. M.; Twu, Y. K. *Carbohydr. Polym.*, 2010, 81, 906-910.
- [217] Oliveira, B. F.; Santana, M. H. A.; Re, M. I. *Drying Technology*, 2006, 24, 373-382.
- [218] Alhalaweh, A.; Andersson, S.; Velaga, S. P. *European Journal of Pharmaceutical Sciences*, 2009, 38, 206-214.
- [219] Ochiuz, L.; Peris, J. E. *Medicinal Chemistry*, 2009, 5, 191-196.
- [220] Popa-Nita, S.; Lucas, J. M.; Ladavière, C.; David, L.; Domard, A. *Biomacromolecules*, 2009, 10, 1203-1211.
- [221] Tang, E. S. K.; Huang, M.; Lim, L. Y. *Int. J. Pharm.*, 2003, 265, 103-114.
- [222] Liu, H.; Bao, J.; Du, Y.; Zhou, X.; Kennedy, J. F. *Carbohydr. Polym.*, 2006, 64, 553-559.
- [223] Baxtera, S.; Zivanovica, S.; Weissb, J. *Food Hydrocolloids*, 2005, 19, 821-830.
- [224] Zollinger, H. *Colour Chemistry: Synthesis, Properties and Applications of Organic Dyes and Pigments*; VCH: New York, 1987; p 92.

- [225] Vaidya, A. A.; Datye, K. V. *Colorate*, 1982, 14, 3.
- [226] Easton, J. R. The dye maker's view. In Cooper, P., Ed. *Colour in Dyehouse Effluent*; Society of Dyers and Colourists: Nottingham, 1995; p 9.
- [227] Sierra, R.; Lettinga, G. *Appl. Microbiol. Biotechnol.*, 1991, 34, 544.
- [228] Ali, M.; Sreekrishnan, T. R. *Adv. Environ. Res.*, 2001, 5, 75-96.
- [229] Banat, I. M.; Nigam, P.; Singh, D.; Merchant, R.; *Bioresour. Technol.*, 1996, 58, 217-227.
- [230] Crini, G., *Bioresour. Technol.*, 1996, 97, 1061-1085.
- [231] Ramakrishna, K.; Viraraghavan, T. *Water Sci. Technol.*, 1997, 36, 189-196.
- [232] Wong, Y. C.; Szeto, Y. S.; Cheung, W. H.; McKay, G. *Langmuir*, 2003, 19, 7888-7894.
- [233] Robinson, T.; McMullan, G.; Marchant, R.; Nigam, P. *Bioresour. Technol.*, 2001, 77, 247-255.
- [234] Renganathan, S.; Thilagaraj, W. R.; Miranda, L. R.; Gautam, P.; Velan, M. *Bioresour. Technol.*, 2006, 97, 2189-2193.
- [235] Reife, A.; Freeman, H. *Environmental Chemistry of Dyes and Pigments*; John-Wiley & Sons Inc.: New York, 1996.
- [236] Crini, G. *Bioresour. Technol.*, 2006, 60, 67-75.
- [237] Arica, M.; Bayramoglu, G. *J. Hazard. Mater.*, 2007, 149, 499-507.
- [238] Aksu, Z.; Cagatay, S.S. *Separ. Purif. Technol.*, 2006, 48, 24-35.
- [239] Zhou, J. L.; Banks, C. J. *Environ. Technol.*, 1991, 12, 859-869.
- [240] Zhou, J. L.; Banks, C. J. *Chemosphere*, 1993, 27, 607-620.
- [241] Raghavacharya C. *Chem. Eng. World*, 1997, 32, 53-54.
- [242] Karthikeyan, J. Removal of colour from Industrial effluents. In *Pollution Management in Industries*; Trivedy, R. K. Eds.; Environmental Publications; Karad: India, 1995; pp 150-156.

- [243] Srinivasan, A.; Viraraghavan, T. *Journal of Environmental Management*, 2010, 91, 1915-1929.
- [244] Chiou, M. S.; Li, H. Y. *Chemosphere*, 2003, 50, 1095-1105.
- [245] Chiou, M. S.; Chuang, G. S., *Chemosphere*, 2006, 62, 731-740.
- [246] Annadurai G.; Lai Y. L.; Lee J. *J. Hazard. Mater.*, 2008, 152, 337-346.
- [247] Kamari, A.; Ngah, W. S. W.; Chong, M. Y.; Cheah, M. L. *Desalination*, 2009, 249, 1180-1189.
- [248] Hu, Z. G.; Zhang, J.; Chan, W. L.; Szeto, Y. S. *Polymer*, 2006, 47, 5838-5842.
- [249] Gibbs, G.; Tobin, J. M.; Guibal, E. *J Appl Polym Sci*, 2003, 90, 1073-1080.
- [250] Chiou, M. S, Ho, P. Y.; Li, H. Y. *Dyes and Pigments*, 2004, 60, 69-84.
- [251] Chiou, M. S.; Li, H. Y. *J. Hazard. Mater.*, 2002, B93, 248-263.
- [252] Chang, M. Y.; Juang, R. S. *Colloid Surf A, Physicochem Eng Aspects*, 2005, 269, 35-46.
- [253] Crini, G.; Gimbert, F.; Robert, C.; Martel, B.; Adam, O.; Morin-Crini, N.; De Giorgi, F.; Badot, P. M.; *J. Hazard. Mater.*, 2008, 153, 96-106.
- [254] Dutta, P. K.; Durga Bhavani, K.; Sharma, N. *Asian Textile J.*, 2001, 10, 57-63.
- [255] Annadurai, G. *Bioproc. Eng.*, 2000, 23, 451-455.
- [256] Nawi, M. A.; Sabara S.; Jawad, A. H.; Sheilatina; Wan Ngah, W. S. *Biochemical Engineering Journal*, 2010, 49, 317-325.
- [257] Kim, T. Y.; Cho, S. Y. *Korean J. Chem. Eng.*, 2005, 22, 691-696.
- [258] Wu, F. C.; Tseng, R. L.; Juang, R. S. *J. Hazard. Mater.*, 2001, 167-177.
- [259] Cheung, W. H.; Szeto, Y. S.; McKay, G. *Bioresource Technology*, 2009, 100, 1143-1148.
- [260] Chang, Y. C.; Chen D. H. *Macromolecular Bioscience*, 2005, 5, 254-261.
- [261] Bandara, J.; Mielczarski, J. A.; KiwiMolecular, J. *Langmuir*, 1999, 15, 7670-7679.
- [262] Rai, H. S.; Bhattacharyya, M. S.; Singh, J. *Critical Reviews In Environmental Science and*

- Technology*, 2005, 35, 219-238.
- [263] Sakkayawong, N.; Thiravetyan, P.; Nakbanpote, W. *J. Colloid. Int. Sci.*, 2005, 286, 36-42.
- [264] Uzun, I.; Guzel, F. *Turk. J. Chem.*, 2004, 28, 731-740.
- [265] Gibbs, G. Tobin, J. M.; Guibal, E. *Ind. Eng. Chem. Res.*, 2004, 43, 1-11.
- [266] Wong, Y. C.; Szeto, Y. S.; Cheung, W. H.; McKay, G. *Pro. Biochem.*, 2004, 39, 693-702.
- [267] Wong, Y. C.; Szeto, Y. S.; Cheung, W. H.; McKay, G. *J. Appl. Polym. Sci.*, 2004, 92, 1633-1645.
- [268] Lazaridis, N. K.; Kyzas, G. Z.; Vassiliou, A. A.; Bikiaris, D. N. *Langmuir*, 2007, 23, 7634-7643.
- [269] Shimizu, Y.; Taga, A.; Yamaoka, H. *Adsorpt. Sci. Technol.*, 2003, 21, 439-449.
- [270] Crini, G.; Martel, B.; Torri, G. *Int. J. Environment and Pollution*, 2008, 34, 451-465.
- [271] Figueiredo, S. A.; Boaventura, R. A.; Loureiro, J. M. *Purif. Technol.*, 2000, 20, 129.
- [272] Dos Anjos, F. S. C.; Vieira, E. F. S.; Cestari, A. R. *J. Colloid. Int. Sci.*, 2002, 253, 243-246.
- [273] Blackburn, R. *Environ. Sci. Technol.*, 2004, 38, 4905-4909.
- [274] Piccin, J. S.; Vieira, M. L. G.; Goncalves, J. O.; Dotto, G. L.; Pinto, L. A. A. *Journal of Food Engineering*, 2009, 95, 16-20.
- [275] Chen, A. H.; Huang, Y. Y. *J. Hazard. Mater.*, 2010, 177, 668-675.
- [276] Singh, V.; Sharma, A. K.; Tripathi, D. N.; Sanghi, R. *J. Hazard. Mater.*, 2009, 161, 955-966.
- [277] Li, C. B.; Hein, S.; Wang, K. *Mate. Sci. Technol.*, 2008, 24, 1088-1099.
- [278] Yoshida, H.; Okamoto, A.; Kataoka, T. *Chem. Eng. Sci.*, 1993, 48, 2267-2272.
- [279] Venkat, S. M.; Indra, D. M.; Vimal, C. S. *Dyes Pigm.*, 2007, 73, 269-278.
- [280] Aksu, Z.; Tezer, S. *Process Biochem.*, 2000, 36, 437-439.
- [281] Ho, Y. S.; McKay, G. *Process Biotechnol.*, 1999, 34, 451-465.
- [282] Kumar, M. N. V. R. *React. Funct. Polym.*, 2000, 46, 1-27.

- [283] Filipkowska U.; *Adsorption Science & Technology*, 2006, 24, 781-795.
- [284] Cheng, R.; Ou, S.; Xiang, B.; Li, Y.; Liao, Q. *Langmuir*, 2010, 26, 752-758.
- [285] Ho, Y. S.; McKay, G. *Chem.Eng. J.*, 1998, 70, 115-124.
- [286] Ho YS, McKay G. *Trans Chem Eng.*, 1998, 76, 183-191.
- [287] Kamel, M. M.; Youssef, B. M.; Shokry, G. M. *Dyeing of cationized cotton part II: direct dyes*.  
American Dye Stuff Reporter, 1999, 88, 28-31.
- [288] Cai, Y.; David, S. K. Pailthorpe, M. T. *Dyes and Pigments*, 2000, 45, 161-168.
- [289] Burkinshaw, S. M.; Mignanelli, M.; Froehling, P. E.; Bide, M. J. *Dyes and Pigments*, 2000, 47,  
259-267.
- [290] Kin, T. K.; Yoon, S. H.; Son, Y. A. *Dyes and Pigments*, 2004, 60, 121-127.
- [291] Gupta, D.; Haile, A. *Carbohydr. Polym.*, 2007, 69, 164.
- [292] Lin, H.; Yao, L. R.; Chen, Y. Y.; Wang, H. *Fiber Polym.*, 2008, 9, 113.
- [293] Vilchez, S.; Navarro, A.; Jocić, D.; Erra, P. In *Proceedings of 2001 International Textile  
Congress*, Terrassa, 2001; Vol. 2, pp 522-530.
- [294] Tsukada, M.; Goto, Y.; Freddi, G.; Matsumura, M.; Shiozaki, H.; Ishikawa, H. *J. Appl. Polym.  
Sci.*, 1992, 44, 2203.
- [295] Freddi, G.; Kato, H.; Tsukada, M.; Allara, G.; Shiozaki, H. *J. Appl. Polym. Sci.*, 1995, 55, 481.
- [296] Davidson, R. S.; Xue, Y. *Journal of the Society of Dyers Colourists*, 1994, 110, 24-29.
- [297] Yen, M. S. *J. Appl. Polym. Sci.*, 2001, 80, 2859-2864.
- [298] Jocić, D.; Julià, M. R.; Erra, P. *Journal of the Society of Dyers Colourists*, 1997, 113, 25-31.
- [299] Julia, M. R.; Pasual, E.; Erra, P. *J. Soc. Dyers Color.*, 2000, 116, 62-67.
- [300] Jocić, D.; Vilchez, S.; Topalovic, T.; Navarro, A.; Jovancic, P.; Julià, M. R.; Erra, P.

- Carbohydrate Polymers*, 2005, 60, 51–59.
- [301] Lu, Y. H.; Chen, Y. Y.; Lin, H.; Wang, C.; Yang, Z. D. *J. Appl. Polym. Sci.*, 2010, 117, 3362-3369.
- [302] Rattanaphani, S.; Chairat, M.; Bremner, J. B.; Rattanaphani, V. *Dyes and Pigments*, 2007, 72, 88-96.
- [303] Saxena, S.; Iyer, V.; Shaikh, A. I.; Shenai, V. A. *Colourage*, 1997, 44, 23-28.
- [304] Lim, S. H.; Hudson, S. M. *Color. Technol.*, 2004, 120, 108-113.
- [305] Nasr, H. E.; Sayyah, S. M.; Essa, D. M.; Samaha, S. H.; Rabie, A. M. *Carbohydr. Polym.*, 2009, 76, 36-45.
- [306] Houshyar, S.; Amirshahi, S. H. *Iranian Polymer Journal*, 2002, 11, 296-301.
- [307] Vakhitova, N. A.; Safonov, V. V. *Fibre Chemistry*, 2003, 1, 27-28.
- [308] Kitkulnumchai, Y.; Ajavakom, A.; Sukwattanasinitt, M. *Cellulose*, 2008, 15, 599-608.
- [309] Kim, S. H.; *Fibers and Polymers*, 2006, 7, 255-261.
- [310] Ristic, N.; Jovancic, P.; Canal, C.; Jovic, D. *Fibers and Polymers*, 2009, 10, 466-475.
- [311] Pascual, E.; Julià M. R. *J. Biotechnol.*, 2001, 89, 289-296.
- [312] Onar, N.; Sarşik M. *Fibres & Textiles in Eastern Europe*, 2005, 13, 54-59.
- [313] Ristic, N.; Jovancic, P.; Canal, C.; Jovic, D. *J. Appl. Polym. Sci.*, 2010, 117, 2487-2496.
- [314] Davarpanah, S.; Mahmoodi, N. M.; Arami, M.; Bahrami, H.; Mazaheri, F. *Appl. Surf. Sci.*, 2009, 255, 4171-4176.
- [315] Park, Y.; Koo, K.; Kim, S.; Choe, J. *J. Appl. Polym.*, 2008, 109, 160-166.
- [316] Bratskaya, S.; Marinin, D.; Nitschke, M. Pleul, D., Schwarz, S.; Simon, F. *Journal of Adhes. Sci. Technol.*, 2004, 18, 1173-1186.
- [317] Fornelli, S. *The Enzymatic Big Bang for the Textile Industry*, Sandoz Chemicals Company:



- Switzerland, 1995.
- [318] Masri, M. S.; Randal, V. G.; Pittman, A. G. Use of crosslinked chitosan in the finishing treatment of wool fabric for laundering shrinkage control. In *Proceeding of the 1<sup>st</sup> International Conference on Chitin and Chitosan*. R. A. A. Muzzarelli Ed., University of Ancona: Boston, USA, pp 306-311.
- [319] Monti P.; Freddi G.; Sampaio S.; Tsukada M.; Taddei P. *J. Mol. Struct.*, 2005, 744-747, 685-690.
- [320] Cavaco, E.; Erikson, P. A.; Karl-Erik, L.; ACS Symposium Series 687, In *Enzymes for Wool Fibre Modification*, Heine, E.; Hollfelder, B.; Lorenz, W.; Thomas, H.; Wortmann, G.; Höcker, H. Eds. Chapter 23, ISBN: 0-8412-3547-3, 1998, pp. 279-293.
- [321] Freddi, G.; Anghileri, A.; Sampaio, S.; Buchert, J.; Monti, P.; Taddei, P. *J. Biotechnol.* 2006, 125, 281-294.
- [322] Salehi, A. M.; Bahrami, H.; Arami, M. *Research Journal of Textile and Apparel*, 2005, 9, 1-11.
- [323] Sampaio, S.; Taddei, P.; Monti, P.; Buchert, J.; Freddi, G. *J. Biotechnol.*, 2005, 116, 21-33.
- [324] Bai, L.; Zhu, L.; Min, S.; Liu, L.; Cai, Y.; Yao, J. *Appl. Surf. Sci.*, 2008, 254, 2988-2995.
- [325] McPhail, D. S.; Sokhan, M.; Rees, E. E.; Cliff, B.; Eccles, A. J.; Chater, R. *J. Appl. Surf. Sci.*, 2004, 231-232, 967-971.
- [326] Lu, Y. H.; Chen, Y. Y.; Lin, H.; Wang, C.; Yang, Z. D. *J. Appl. Polym. Sci.*, 2010, 117, 3362-3369.
- [327] Lu, Y. H.; Lin, H.; Chen, Y. Y.; Wang, C.; In *Researches and Progresses of Modern Technology on Silk*, Bai L. Ed. 2007; 477-479.
- [328] Burkinshaw, S. M. *Chemical principles of synthetic fiber dyeing*, Blackie Academic & Professional, 1995.
- [329] Hawkyard, C. *Synthetic fiber dyeing*, Bradford: The Society of Dyers and Colourists, 2004;

- pp.30-33, 82-93.
- [330] Trotman, E. R. *Dyeing and chemical technology of textiles fibers*, Edward Arnold Ed., 1994.
- [331] Nunn, D. M. *The dyeing of synthetic polymer and acetate fibers*, Dyes Company Publications Trust, 1979.
- [332] Xia H.; Zhang C.; Wang Q. Q. *J. Appl. Polym. Sci.*, 2001, 80, 1130.
- [333] Ryu J. G.; Kim H. S.; Lee J. W. *Annual Technical Conference-Society of Plastics Engineers*, 2002, 60<sup>th</sup>, Vol. 2, 2240.
- [334] Louis, D.; Yves, F.; Anne, L. C. *Macromolecular Symposia*, 2000, 151, 387.
- [335] Tsaih, M. L.; Chen, R. H. *J. Appl. Polym. Sci.*, 2003, 90, 3526.
- [336] Zhou, S.; Chen, S.; Tang, W. *Pharmaceutical Journal*, 2002, 14, 5.
- [337] Zhang, Y.; Xue, C.; Xue, Y.; Gao, R.; Zhang, X. *Carbohydr. Res.*, 2005, 340, 1914-1917
- [338] Focher, B.; Beltranme, P. L.; Naggi, A.; Torri, G. *Carbohydr. Polym.*, 1990, 12, 405-418.
- [339] Kuma, A. B. V.; Varadaraj, M. C.; Lalithac, R. G.; Tharanathan, R. N. *Biochim. Biophys. Acta.*, 2004, 1670, 137-146.
- [340] Yeo G. A.; Ford T. C. *Canada Journal of Chemistry*, 1991, 69, 632.
- [341] Del Bene J. E. *J. Am. Chem. Soc.*, 1973, 95, 5460.
- [342] Stockman, P. A.; Bumgarner R. E.; Suzuki, S.; Blake, G. A. *J. Chem. Phys.*, 1992, 96, 2496.
- [343] Fraser G. T.; Suenram R. D. *Journal of Chemical Physics*, 1992, 96, 7287.
- [344] Sadle J.; Moszynski, R.; Dobrowolski, J. C.; Mazurek, A. P. *J. Phys. Chem. A*, 1999, 103, 8528.
- [345] Pearce, C. I.; Lloyd, J. R.; Guthrie, J. T.; *Dyes Pigments*, 2003, 58, 179-196.
- [346] Pokhrel, D.; Viraraghavan, T. *Sci. Total Environ.*, 2004, 333, 37-58.
- [347] Thompson, G.; Swain, J.; Kay, M.; Forster, C. F. *Bioresour. Techno.*, 2001, 77, 275-286.

- [348] Giunchedi, P.; Genta, I.; Conti, B.; Muzzarelli, R. A. A. *Biomaterials*, 1998, 19, 157-161.
- [349] Illum, L. *Pharm. Res.*, 1998, 15, 1326-1331.
- [350] Yoshida, H.; Takemori, T. *Water Sci. Technol.*, 1997, 35, 29-37.
- [351] Roberts, G. A. F. *Chitin Chemistry*, Roberts, G. A. F. Ed.; Macmillan Press Ltd.: London, 1992; pp 85–91.
- [352] Wataru, T.; Hiroyuki, Y. *Ind. Eng. Chem. Res.*, 1998, 37, 1300-1309.
- [353] Chang, X.; Chen, D.; Jiao, X. *J. Phys. Chem. B*, 2008, 112, 7721–7725.
- [354] Hadfield, H. R.; Lemin, D. R.; *Journal of the Society of Dyers and Colourists*, 1961, 77, 97-106.
- [355] Wen, G.; Rippon, J. A.; Brady, P. R.; Wang, X. G.; Liu, X.; Cookson, P. G. *Powder Technology*, 2009, 193, 200-207.
- [356] Wong, Y. C.; Szeto, Y. S.; Cheung W. H.; MaKay, G. J. *Appl. Polym. Sci.*, 2008, 109, 2232-2242.
- [357] Shore, J. In *Cellulosics Dyeing*; Shore, J., Ed.; Society of Dyers and Colourists: Bradford, 1995; Chapter 3.
- [358] Grulke, E. A. *Solubility Parameter Values*, John Wiley & Sons, 2005; 675-711.
- [359] Wong, Y. C.; Szeto, Y. S.; Cheung W. H.; MaKay, G. *Adsorption*, 2008, 14, 11-20.
- [360] Bird, J.; Brough, N.; Dixon, S.; Batchelor, S. N. *J. Phys. Chem. B.*, 2006, 110, 19557-19561.
- [361] Sueo, Kawabata. Handle and Clothing, Explanation of Key Points, *Journal of the Textile Machinery Society of Japan*, 1980, 33, 2.
- [362] Edwards, A. Collins. *Experiments in Polymer Science*, A Willey-Interscience Publication, 1973.
- [363] Parvinzadeh, M. *Color. Technol.*, 2009, 125, 228-233.
- [364] Arthur, D Broadbent. *Basic Principles of Textile Coloration*, Society of Dyers and Colorists, 2001, pp 274-275.